

EFFECT OF SYNTHESIS PARAMETERS ON STRUCTURAL PROPERTIES AND
THERMAL BEHAVIOR OF SOL-GEL SYNTHESIZED IRON OXIDE XEROGELS

A THESIS SUBMITTED TO
THE GRADUATE SCHOOL OF NATURAL AND APPLIED SCIENCES
OF
MIDDLE EAST TECHNICAL UNIVERSITY

BY

NİL EZGİ DİNÇER YILMAZ

IN PARTIAL FULFILLMENT OF THE REQUIREMENTS
FOR
THE DEGREE OF DOCTOR OF PHILOSOPHY
IN
CHEMICAL ENGINEERING

AUGUST 2018

Approval of the thesis:

**EFFECT OF SYNTHESIS PARAMETERS ON STRUCTURAL PROPERTIES
AND THERMAL BEHAVIOR OF SOL-GEL SYNTHESIZED IRON OXIDE
XEROGELS**

submitted by **NİL EZGİ DİNÇER YILMAZ** in partial fulfillment of the requirements
for the degree of **Doctor of Philosophy in Chemical Engineering Department, Middle
East Technical University** by,

Prof. Dr. Halil Kalıpçılar
Dean, Graduate School of **Natural and Applied Sciences**

Prof. Dr. Pınar Çalık
Head of Department, **Chemical Engineering**

Prof. Dr. Gürkan Karakaş
Supervisor, **Chemical Engineering Dept., METU**

Examining Committee Members:

Prof. Dr. Suna Balcı
Chemical Engineering Dept., Gazi University

Prof. Dr. Gürkan Karakaş
Chemical Engineering Dept., METU

Prof. Dr. Ayşen Yılmaz
Chemistry Dept., METU

Prof. Dr. Burcu Akata Kurç
Micro and Nanotechnology Prog., METU

Prof. Dr. Sena Yaşyerli
Chemical Engineering Dept., Gazi University

Date: 03.08.2018

I hereby declare that all information in this document has been obtained and presented in accordance with academic rules and ethical conduct. I also declare that, as required by these rules and conduct, I have fully cited and referenced all material and results that are not original to this work.

Name, Last Name: NİL EZGİ DİNÇER YILMAZ

Signature :

ABSTRACT

EFFECT OF SYNTHESIS PARAMETERS ON STRUCTURAL PROPERTIES AND THERMAL BEHAVIOR OF SOL-GEL SYNTHESIZED IRON OXIDE XEROGELS

Dinçer Yılmaz, Nil Ezgi

Ph.D., Department of Chemical Engineering

Supervisor : Prof. Dr. Gürkan Karakaş

August 2018, 231 pages

Currently used igniter system compositions are mostly based on the pyrotechnic blends of fuels and oxidizers. In this study, nanostructured metallic xerogels were synthesized by sol-gel method by using various types of proton scavengers and these metallic xerogels were used as oxidizers. In the experiments, $\text{Fe}(\text{NO}_3)_3 \cdot 9\text{H}_2\text{O}$ was used as a precursor and a wide range of proton scavengers (propylene oxide, 1,2 epoxybutane, tetrahydrofuran, tetrahydropyran, 1,4 dioxane and ammonium hydroxide) were used to start the gelation mechanisms. In order to dry the gels and to obtain xerogel structures, the room temperature drying method was utilized which was followed by low temperature direct drying method. Further, to figure out the effect of drying conditions, sequential solvent exchange (SSE) was applied to obtain xerogel structures.

The energetic compositions were prepared by mixing nanostructured Fe_2O_3 xerogel samples with metal/fuel powders. The fuels used in these energetic compositions were commercially available boron, aluminum, magnesium and 20% magnesium coated boron. The energetic properties of metal/fuel- Fe_2O_3 composites were determined and the effect

of proton scavengers, drying conditions, equivalence ratio on the textural properties and thermal behavior of the thermite mixtures were examined.

The results showed that the iron oxide xerogels dried with SSE process have exhibited intrinsic properties of aerogels with high surface area, larger than 300 m²/g, mesoporous structure with a size range of 3-4 nm and nano-scale particle sizes with 3-4 nm. It was observed that the surface area of xerogels was strongly dependent on the type of proton scavenger used. The heat output values of the fuel/iron oxide nano thermites were determined from 85 to 3285 J/g depending on the fuel-oxidant ratio, proton scavenger, drying conditions and fuel type based on DSC/TG analysis. It was shown that the type of proton scavenger, drying conditions and fuel-oxidant ratio could be used to modify the combustion performance, thermal behavior and the structural properties of nanothermites and the particle size distribution, surface area and crystallinity of the xerogels synthesized with the sol-gel synthetic route.

The structural and morphological properties of the samples were characterized by XRD, FTIR, elemental analysis and SEM. The surface area and particle size distribution of the samples were determined by BET method. The thermal behavior and combustion characteristics were characterized by using TG-DSC Instrument and Parr Bomb Calorimetry. The impact and friction sensitivity of the energetic nanocomposites were evaluated by BAM Impact and Friction Tester.

Keywords: Xerogel, Sol-Gel, Proton Scavenger, Energetic Nanocomposites, Sequential Solvent Exchange

ÖZ

SOL-JEL YÖNTEMİ İLE SENTEZLENEN DEMİR OKSİT KSEROJELLERİN YAPISAL VE TERMAL ÖZELLİKLERİ ÜZERİNE SENTEZ PARAMETRELERİNİN ETKİSİ

Dinçer Yılmaz, Nil Ezgi

Doktora, Kimya Mühendisliği Bölümü

Tez Yöneticisi: Prof. Dr. Gürkan Karakaş

Ağustos 2018, 231 sayfa

Günümüzde kullanılan ateşleyici şarjları; yakıt/metal ve oksitleyici karışımından oluşan kompozisyonlardır. Bu çalışmada, çeşitli jelleşme ajanları kullanılarak sol-jel yöntemiyle sentezlenen nano yapılı metalik kserojeller oksitleyici olarak kullanılmıştır. Deneylerde $\text{Fe}(\text{NO}_3)_3 \cdot 9\text{H}_2\text{O}$ metal başlatıcı olarak kullanılmış ve pek çok proton tutucu/jelleşme ajanı (propilen oksit, 1,2 epoksibütan, tetrahidrofur, tetrahidropiran, 1,4 dioksan ve amonyum hidroksit) metal başlatıcının jelleşme adımını gerçekleştirebilmek için kullanılmıştır. Elde edilen jel yapılı malzemeler oda koşullarında ve arkasından düşük sıcaklıklarda fırında kurutma ile kserojel haline getirilmiştir. Kurutma koşullarının malzeme üzerine etkisinin incelenmesi amacıyla, oda koşullarında birbirini izleyen çözücü uzaklaştırma yöntemi uygulanmıştır.

Nano yapılı Fe_2O_3 ile çeşitli metal tozları karıştırılarak enerjik kompozisyonlar hazırlanmıştır. Ticari olarak hazır alınan bor, alüminyum, magnezyum ve %20 magnezyum kaplı bor enerjik kompozisyonlarda metal tozu olarak kullanılmıştır. Elde edilen metal/yakıt- Fe_2O_3 kompozitlerinin enerjik özellikleri test edilmiş ve proton

tutucu/jelleşme ajanı, kurutma koşulları ve metal/yakıt miktarının kserojelin yapısal özelliklerine ve termit karışımların ısıl davranışına etkisi incelenmiştir.

Özellikle oda koşullarında çözelti-değişimi ile kurutulan kserojellerin, 300 m²/g'dan büyük yüzey alanı, 3-4 nm boyutlarındaki mezogözenekli yapısı ve 3-4 nm boyutundaki parçacık büyüklüğü ile, aerojellerin özelliklerine benzer özellikler sergilediği görülmüştür. Elde edilen sonuçlara göre kserojellerin yüzey alanı önemli oranda kullanılan proton tutucu/jelleşme ajanına bağlıdır. DSC/TG analizlerine göre metal/demir oksit nanotermitlerinin yanması sonucu açığa çıkan ısı değerinin, yakıt-oksitlerici oranına, proton tutucu/jelleşme ajanına, kurutma koşullarına ve kullanılan yakıt/metal çeşidine göre 85 ile 3285 J/g arasında değiştiği belirlenmiştir. Çeşitli jelleşme ajanları, farklı kurutma koşulları ve farklı yakıt/metal tipleri kullanılarak, sol-jel yöntemiyle sentezlenen kserojellerin parçacık boyutu dağılımının, yüzey alanının ve kristal yapısının ve kserojelin metal/yakıt ile karışımı sonrasında elde edilen nano termitlerin yanma performansının, ısıl ve yapısal özelliklerinin ayarlanması, mümkün hale gelmiştir.

Elde edilen malzemelerin yapısal ve morfolojik özellikleri XRD, FTIR, elemental analiz ve SEM ile karakterize edilmiştir. Malzemelerin yüzey alanı ve parçacık boyutu dağılımı BET metoduyla incelenmiştir. Isıl özellikler ve yanma karakteristiği TG-DSC ve Parr Bomb Kalorimetri cihazı ile incelenmiştir. Darbe ve sürtünme hassasiyeti BAM Darbe ve Sürtünme Test Cihazı ile karakterize edilmiştir.

Anahtar Kelimeler: Kserojel, Sol-Jel, Proton Tutucu, Enerjik Nanokompozitler, Çözücü Uzaklaştırma Yöntemi

To My Beloved Husband and My Family

ACKNOWLEDGMENTS

I would like to thank to my supervisor Prof. Dr. Gürkan Karakaş for his guidance, advice, criticism, encouragement and great support throughout the research project.

I am also grateful to Prof. Dr. Ayşen Yılmaz and Prof. Dr. Burcu Akata Kurç for their precious discussions and comments during the progress of this work.

I wish to express my deepest gratitude to Dr. Suzan Koç and my Manager Mr. Burç Veral for their guidance and support. My sincere gratefulness goes to pyrotechnic team of ROKETSAN for their support during the studies.

I would like to thank to the Chemical Test Laboratories Department, Physical and Metallurgical Test Laboratories Department and Pyrotechnic Systems Production Department Groups; Mrs. Mine Adıgüzel, Mr. Haluk Tansu, Mr. Yasin Ağırtopçu, Mr. Çağrı Sarıyağ, Mr. Emrah Yıldırım, Mr. Hakan Karayel, Mr. Ender Sarıkan, Mr. Hakkı Sarıyağ and Gözde Sarıtaş. I would also like to thank to other colleagues at ROKETSAN for their support throughout the project.

I am also grateful to the Department of Technology and Academic Network Management; Dr. Oğuz Menekşe and Dr. Aysu Günel for their great support and encouragement.

I would like to thank to team of METU Central Laboratory for their support throughout the analysis of samples.

ROKETSAN Missiles Industries Corporation and Undersecretariat for Defence Industries who financially support in achieving this goal are also gratefully acknowledged.

I would like to thank to my family Beliz, Burcu, Sezgi, Zehra and Murat Dinçer for their support and encouragement throughout my whole life. Thanks are not enough to explain my gratitude to them for their great love and affection.

Finally, my warmest thanks go to my beloved husband, Yusuf Yılmaz for his understanding, endless patience, love, support and encouragement throughout this research study.

“By three methods we may learn wisdom: First, by reflection, which is noblest; second, by imitation, which is easiest; and third, by experience, which is the bitterest.” – Confucius

“The good thing about science is that it’s true whether or not you believe in it.” – Neil deGrasse Tyson

“The saddest aspect of life right now is that science gathers knowledge faster than society gathers wisdom.” – Isaac Asimov

“Our true mentor in life is science” –Mustafa Kemal Atatürk

TABLE OF CONTENTS

| | |
|---|------|
| ABSTRACT..... | V |
| ÖZ..... | VII |
| ACKNOWLEDGMENTS | X |
| TABLE OF CONTENTS..... | XII |
| LIST OF TABLES..... | XV |
| LIST OF FIGURES | XVII |
| 1 INTRODUCTION | 1 |
| 1.1 MOTIVATION AND SCOPE OF THE STUDY..... | 1 |
| 1.2 ENERGETIC MATERIALS AND CONVENTIONAL METHODS FOR PREPARATION | 3 |
| 1.2.1 The Pyrotechnics..... | 4 |
| 1.2.2 Iron Oxide | 12 |
| 1.2.3 The Methods for Preparation of Pyrotechnics | 13 |
| 1.2.4 The Effect of Particle Size on Performance..... | 20 |
| 1.2.5 The Effect of Moisture on Performance | 23 |
| 1.2.6 The Effect of Binder in the Composition..... | 23 |
| 1.2.7 Nanothermites | 24 |
| 1.3 THE SENSITIVITY OF ENERGETICS | 25 |
| 1.4 THE AGEING OF PYROTECHNICS | 26 |
| 1.5 THE LITERATURE STUDIES | 27 |
| 2 EXPERIMENTAL SECTION..... | 43 |
| 2.1 MATERIALS..... | 43 |
| 2.2 EXPERIMENTAL METHODS..... | 45 |

| | |
|--|----|
| 2.2.1 Synthesis of Iron Oxide Samples | 45 |
| 2.2.2 Drying Procedure | 47 |
| 2.2.3 Preparation of Energetic Compositions | 47 |
| 2.3 MATERIAL CHARACTERIZATION | 49 |
| 2.3.1 Nitrogen Gas Adsorption Analysis | 49 |
| 2.3.2 X-Ray diffraction (XRD) | 50 |
| 2.3.3 FTIR Spectrum and Elemental Analysis | 50 |
| 2.3.4 Thermal Analysis | 50 |
| 2.3.5 The Calorific Value Tests | 51 |
| 2.3.6 Scanning Electron Microscopy Analysis | 51 |
| 2.3.7 Sensitivity tests | 52 |
| 3 RESULTS AND DISCUSSION | 53 |
| 3.1 NITROGEN GAS ADSORPTION ANALYSIS | 53 |
| 3.1.1 Effect of Proton Scavenger | 53 |
| 3.1.2 Effect of the Drying Condition | 57 |
| 3.1.3 Effect of the Concentration of Precursor Solution | 62 |
| 3.2 X-RAY DIFFRACTOMETRY (XRD) | 65 |
| 3.2.1 Effect of Proton Scavenger | 65 |
| 3.2.2 Effect of the Drying Condition | 70 |
| 3.2.3 Effect of the Concentration of Precursor Solution | 73 |
| 3.3 FTIR SPECTRUM AND ELEMENTAL ANALYSIS | 76 |
| 3.3.1 FTIR Spectrum Analysis | 76 |
| 3.3.2 Elemental Analysis | 79 |
| 3.4 PH STUDY DURING GEL FORMATION | 80 |
| 3.5 THERMAL ANALYSIS | 81 |
| 3.5.1 Effects of Drying Condition and Proton Scavenger on the Thermal Behavior of 3FR B/Fe ₂ O ₃ Thermite Compositions | 81 |
| 3.5.2 Effect of Equivalence Ratio on the Thermal Behavior | |

| | |
|--|-----|
| of B/Fe ₂ O ₃ Thermite Compositions | 89 |
| 3.5.3 Effect of Fuel Type on the Thermal Behavior of Thermite Compositions..... | 97 |
| 3.6 CALORIFIC VALUE (BOMB CALORIMETER) TEST | 107 |
| 3.6.1 Effects of Drying Condition and Proton Scavenger on Calorific Value of 3FR B/Fe ₂ O ₃ Thermite Compositions | 107 |
| 3.6.2 Effects of Equivalence Ratio on Calorific Value of B/Fe ₂ O ₃ Thermite Compositions | 110 |
| 3.6.3 Effects of Fuel Type on Calorific Value of Metal/Fe ₂ O ₃ Thermite Compositions | 123 |
| 3.6.4 Kinetic Study of SSE B/Fe ₂ O ₃ Prepared with Propylene Oxide, 1,2 Epoxybutane and Ammonium Hydroxide | 129 |
| 3.7 MORPHOLOGICAL AND STRUCTURAL ANALYSIS | 135 |
| 3.7.1 SEM Images of B/Fe ₂ O ₃ Synthesized with Ammonium Hydroxide | 135 |
| 3.7.2 SEM Images of B/Fe ₂ O ₃ Synthesized with Propylene Oxide..... | 138 |
| 3.8 SENSITIVITY TESTS..... | 140 |
| 3.9 SUMMARY | 142 |
| 4 CONCLUSIONS..... | 151 |
| REFERENCES | 155 |
| APPENDICES | 179 |
| CURRICULUM VITAE..... | 229 |

LIST OF TABLES

TABLES

| | |
|---|-----|
| Table 1.1. Possible Reaction Products of B/Fe ₂ O ₃ | 32 |
| Table 1.2. Possible Reaction Products of B/Fe ₂ O ₃ | 34 |
| Table 2.1. The Fuel and Oxidizer Content of Mg/Fe ₂ O ₃ , 20% Mg coated B/Fe ₂ O ₃ Al/Fe ₂ O ₃ and B/Fe ₂ O ₃ Compositions | 49 |
| Table 3.1. The Surface Area, Pore Size and Pore Volume of Fe ₂ O ₃ Compositions | 54 |
| Table 3.2. The Surface Area, Pore Size and Pore Volume of Fe ₂ O ₃ Compositions | 61 |
| Table 3.3 The Surface Area, Pore Size and Pore Volume of Fe ₂ O ₃ Compositions | 65 |
| Table 3.4. Crystallite Sizes on the Basis of Scherrer Analysis of (311) XRD peaks | 73 |
| Table 3.5. Mass percentage of C, H and N in Fe ₂ O ₃ samples prepared with SSE method..... | 79 |
| Table 3.6. DSC Data for 3FR B/Fe ₂ O ₃ nanothermites..... | 85 |
| Table 3.7. DSC Data for DD B/Fe ₂ O ₃ nanothermites..... | 93 |
| Table 3.8. DSC Data for 6FR Metal/Fe ₂ O ₃ xerogels synthesized with THF | 101 |
| Table 3.9. DSC Data for 6FR Metal/Fe ₂ O ₃ xerogels synthesized with THP..... | 104 |
| Table 3.10. DSC Data for 6FR Metal/Fe ₂ O ₃ xerogels synthesized with 1,4 dioxane... | 105 |
| Table 3.11. DSC Data for 6FR Metal/Fe ₂ O ₃ xerogels synthesized with propylene oxide..... | 106 |
| Table 3.12. The Calorific Values of DD and SSE 3FR B/Fe ₂ O ₃ Compositions..... | 108 |
| Table 3.13. The Calorific Values of Fuel Rich B/Fe ₂ O ₃ Compositions with an equivalence ratio of $\phi=3$, $\phi=6$ and $\phi=9$ | 113 |
| Table 3.14. The Calorific Value of Nano B/Fe ₂ O ₃ Compositions prepared by mixing of commercial powders..... | 121 |
| Table 3.15. The Calorific Values of DD 6FR metal/Fe ₂ O ₃ Compositions | 125 |
| Table 3.16. The activation energy values of SSE 3 FR B/Fe ₂ O ₃ prepared with propylene oxide, 1,2 epoxybutane and | |

| | |
|---|-----|
| ammonium hydroxide from diluted and concentrated solutions of precursor..... | 131 |
| Table 3.17. Elemental EDS Analysis of B/Fe ₂ O ₃ synthesized with ammonium hydroxide | 136 |
| Table 3.18. Elemental EDS Analysis of the combustion products of 9 FR B/Fe ₂ O ₃ synthesized with ammonium hydroxide..... | 138 |
| Table 3.19. Elemental EDS Analysis of the 9 FR B/Fe ₂ O ₃ synthesized with propylene oxide..... | 139 |
| Table 3.20. Impact and Friction Sensitivity of B/Fe ₂ O ₃ Compositions prepared with ammonium hydroxide | 140 |

LIST OF FIGURES

FIGURES

| | |
|--|----|
| Figure 1.1. Schematic Illustration of Aluminum Particle Core and Oxide Shell..... | 10 |
| Figure 1.2. Schematic Illustration of Boron Particle Core and Oxide Shell..... | 11 |
| Figure 1.3. Schematic Illustration of Aluminum Particle Surrounded with Gas in a Control Volume | 22 |
| Figure 2.1. The structure of proton scavenger molecules a. propylene oxide (C ₃ H ₆ O) b. 1,2 epoxybutane (C ₄ H ₈ O) c. tetrahydrofuran (C ₄ H ₈ O) d. tetrahydropyran (C ₅ H ₁₀ O) e. 1,4 dioxane (C ₄ H ₈ O ₂) | 44 |
| Figure 2.2. Experimental setup for gel synthesis | 45 |
| Figure 2.3. Experimental setup for gel synthesis | 46 |
| Figure 3.1. Nitrogen adsorption/desorption isotherms of Fe ₂ O ₃ xerogels synthesized by using various proton scavengers..... | 55 |
| Figure 3.2. The pore size distributions of Fe ₂ O ₃ xerogel synthesized various proton scavengers | 56 |
| Figure 3.3. The Nitrogen adsorption/desorption isotherms of a) Sequential Solvent Dried (SSE) b) Direct Dried (DD) Fe ₂ O ₃ samples synthesized with 1,2 epoxybutane, THF, THP, 1,4 dioxane, ammonium hydroxide and propylene oxide..... | 58 |
| Figure 3.4. The pore size distributions of a) Sequential Solvent Dried (SSE) b) Direct Dried (DD) Fe ₂ O ₃ samples synthesized with 1,2 epoxybutane, THF, THP, 1,4 dioxane, ammonium hydroxide and propylene oxide..... | 59 |
| Figure 3.5. Nitrogen adsorption/desorption isotherms of DD Fe ₂ O ₃ samples synthesized with 1,2 epoxybutane, THP and propylene oxide from a) concentrated b) diluted precursor solution | 63 |

| | |
|---|----|
| Figure 3.6. The pore size distributions of DD Fe ₂ O ₃ samples synthesized with 1,2 epoxybutane, THP and propylene oxide from a) concentrated b) diluted precursor solution..... | 64 |
| Figure 3.7. XRD patterns of iron oxide samples synthesized with 1,2 epoxybutane, 1,4 dioxane, THP, THF, propylene oxide and ammonium hydroxide | 66 |
| Figure 3.8. XRD patterns of iron oxide samples synthesized by 1,2 epoxybutane, THF, THP, 1,4 dioxane and propylene oxide with ICDD patterns for maghemite, γ -Fe ₂ O ₃ (no. 00-004-0755)..... | 67 |
| Figure 3.9. XRD patterns of Fe ₂ O ₃ xerogel synthesized with ammonium hydroxide with ICDD patterns of (NH ₄)(NO ₃) (no. 01-083-0520) and γ -Fe ₂ O ₃ maghemite (no. 00-004-0755)..... | 69 |
| Figure 3.10. XRD patterns of Direct Dried (DD) and Sequential Solvent Exchange (SSE) Fe ₂ O ₃ samples synthesized with a) 1,2 epoxybutane b) THF c) THP d) 1,4 dioxane e) ammonium hydroxide f) propylene oxide | 71 |
| Figure 3.11. XRD patterns of DD Fe ₂ O ₃ samples synthesized from diluted and concentrated precursor solution with a) 1,2 epoxybutane b) THP c) propylene oxide | 75 |
| Figure 3.12. FTIR spectra of SSE Fe ₂ O ₃ samples synthesized with a) 1,2 epoxybutane b) THF c) THP | 77 |
| Figure 3.13. pH change during gelation in (a) ethanol medium (b) distilled water medium & Temperature change during gelation in (a)* ethanol medium (b)* distilled water medium | 80 |
| Figure 3.14. DSC and TG plots as a function of temperature for DD 3FR B/Fe ₂ O ₃ samples synthesized with 1,2 epoxybutane, THF, THP, 1,4 dioxane and ammonium hydroxide..... | 86 |
| Figure 3.15. DSC and TG plots as a function of temperature for SSE 3FR B/Fe ₂ O ₃ samples synthesized with 1,2 epoxybutane, | |

| | |
|--|-----|
| THF, THP, 1,4 dioxane and ammonium hydroxide..... | 87 |
| Figure 3.16. DSC and TG plots as a function of temperature for DD&SSE* 3FR B/Fe ₂ O ₃ samples synthesized with 1,2 epoxybutane, THF, THP, 1,4 dioxane and ammonium hydroxide | 88 |
| Figure 3.17. DSC and TG plots as a function of temperature for 3FR, 6FR and 9FR DD B/Fe ₂ O ₃ samples synthesized with 1,2 epoxybutane, THF and THP..... | 95 |
| Figure 3.18. DSC and TG plots as a function of temperature for 3FR, 6FR and 9FR DD B/Fe ₂ O ₃ samples synthesized with 1,4 dioxane, ammonium hydroxide and 6FR and 9FR DD B/Fe ₂ O ₃ samples synthesized with propylene oxide | 96 |
| Figure 3.19. DSC and TG plots as a function of temperature at an equivalence ratio of 6 for Mg/Fe ₂ O ₃ , 20%Mg-B/Fe ₂ O ₃ , B/Fe ₂ O ₃ , Al/Fe ₂ O ₃ samples prepared by THF and THP | 102 |
| Figure 3.20. DSC and TG plots as a function of temperature at an equivalence ratio of 6 for Mg/Fe ₂ O ₃ , 20%Mg-B/Fe ₂ O ₃ , B/Fe ₂ O ₃ , Al/Fe ₂ O ₃ samples prepared by 1,4 dioxane and propylene oxide..... | 103 |
| Figure 3.21. Calorific Values of DD and SSE 3FR B/Fe ₂ O ₃ compositions..... | 108 |
| Figure 3.22. Calorific Values of B/Fe ₂ O ₃ Compositions with an equivalence ratio of A) 3 B) 6 C)9..... | 112 |
| Figure 3.23. The change in calculated mole fraction of BHO ₂ molecule with equivalence ratio of B/Fe ₂ O ₃ compositions synthesized with various proton scavengers..... | 116 |
| Figure 3.24. The change in calculated mole fraction of HBO molecule with equivalence ratio of B/Fe ₂ O ₃ compositions synthesized with various proton scavengers..... | 116 |
| Figure 3.25. The combustion products of 3FR, 6FR and 9FR B/Fe ₂ O ₃ compositions synthesized with various proton scavengers..... | 117 |
| Figure 3.26. The effect of drying conditions on 3FR, 6FR and 9FR | |

| | |
|--|-----|
| B/Fe ₂ O ₃ compositions synthesized with ammonium hydroxide..... | 119 |
| Figure 3.27. The Adiabatic Flame Temperatures of B/NH ₄ NO ₃ and B/Fe ₂ O ₃ | 120 |
| Figure 3.28. The Calorific Value of Nano B/Fe ₂ O ₃ Compositions with varying equivalence ratio prepared by physical mixing | 122 |
| Figure 3.29. The comparison of the effect of fuel type on the calorific value of DD 6 FR compositions synthesized with A) propylene oxide B) THF C) THP | 126 |
| Figure 3.30. Trend lines for calculating the activation energy of SSE 3FR B/Fe ₂ O ₃ prepared with propylene oxide from diluted solution of precursor | 132 |
| Figure 3.31. Trend lines for calculating the activation energy of SSE 3FR B/Fe ₂ O ₃ prepared with propylene oxide from concentrated solution of precursor | 133 |
| Figure 3.32. Trend lines for calculating the activation energy of SSE 3FR B/Fe ₂ O ₃ prepared with 1,2 epoxybutane from diluted solution of precursor | 133 |
| Figure 3.33. Trend lines for calculating the activation energy of SSE 3FR B/Fe ₂ O ₃ prepared with 1,2 epoxybutane from concentrated solution of precursor | 134 |
| Figure 3.34. Trend lines for calculating the activation energy of SSE 3FR B/Fe ₂ O ₃ prepared with ammonium hydroxide..... | 134 |
| Figure 3.35. SEM images of B/Fe ₂ O ₃ synthesized with ammonium hydroxide..... | 136 |
| Figure 3.36. SEM images and EDS spectrums of the combustion products of B/Fe ₂ O ₃ synthesized with ammonium hydroxide | 137 |
| Figure 3.37. SEM images and EDS spectrums of B/Fe ₂ O ₃ sample synthesized with propylene oxide..... | 139 |
| Figure 3.38. Friction sensitivity of A) 3FR SSE& DD compositions B) DD ST, 3FR & 9FR compositions & Impact sensitivity of A)* 3FR SSE& DD compositions B)* DD ST, 3FR & | |

| | |
|--|-----|
| 9FR compositions | 141 |
| Figure 3.39. The schematic results of DD 3FR B/Fe ₂ O ₃ samples prepared with THF | 143 |
| Figure 3.40. The schematic representation of the effect of drying procedure on the properties of 3FR B/Fe ₂ O ₃ samples prepared with THF..... | 144 |
| Figure 3.41. The schematic representation of the effect of equivalence ratio increasing from 3 to 9 on the properties of samples prepared with THF | 145 |
| Figure 3.42. The schematic results of DD 3FR B/Fe ₂ O ₃ samples prepared with ammonium hydroxide | 146 |
| Figure 3.43. The schematic representation of the effect of drying method on properties of samples prepared with Ammonium hydroxide..... | 147 |
| Figure 3.44. The effect of increase in fuel content with equivalence ratio from 3 to 9 on properties of samples prepared with Ammonium hydroxide | 148 |
| Figure 3.45. The effect of fuel : use of Mg instead of B with samples prepared with Ammonium hydroxide having an equivalence ratio of 9..... | 149 |

LIST OF SYMBOLS

| | |
|-----------------|---------------------------------------|
| A | Constant (independent of temperature) |
| A_s | surface area |
| B | heating rate |
| c | condensed |
| c_p | temperature-dependent heat capacity |
| C_t | Lumped thermal capacitance |
| d | dissolved |
| D | Particle diameter |
| Da | Damköhler number |
| E_a | Activation energy |
| \dot{E}_g | Thermal energy generation |
| \dot{E}_{in} | Thermal energy transport, inflow |
| \dot{E}_{out} | Thermal energy transport, outflow |
| \dot{E}_{st} | Stored energy |
| F | Acceleration reaction factor |

| | |
|----------|--|
| h | heat transfer coefficient |
| H | Heat of Reaction |
| k | reaction rates/rate constant |
| l | liquid |
| n | mole number |
| P | pressure |
| Q | gelation agent ratio |
| R | Universal gas constant |
| R_t | Resistance to convection heat transfer |
| s | substrate |
| t | time |
| t_b | total burning times |
| T | Temperature |
| T_p | Peak Temperature |
| V | volume |
| Z | pre-exponential factor |
| β | heating rate |
| θ | temperature difference |
| ϕ | equivalence ratio |

τ thermal time constant

ρ density

Abbreviations:

| | |
|------|---|
| BET | Brunauer, Emmett, Teller Method |
| BJH | Barrett-Joyner-Halenda |
| DSC | Differential Scanning Calorimeter |
| EDS | Energy Dispersive X-ray Spectroscopy |
| ESD | Electrostatic Discharge |
| FL | Fuel Lean |
| FTIR | Fourier-transform infrared spectroscopy |
| FR | Fuel Rich |
| SEM | Scanning Electron Microscopy |
| SSE | Sequential Solvent Exchange |
| TG | Thermogravimetric |
| XRD | X-Ray Diffraction |

CHAPTER 1

INTRODUCTION

1.1 Motivation and Scope of the Study

The pyrotechnic compositions used in the initiator systems are generally activated by a specific well defined electrical impulse. These initiators are used as electroexplosive devices (EEDs) which are integrated in igniters, Safe and Arm devices (SAD) and gas-generators in military systems like missiles, rockets and munitions. They can also be utilized in civil applications as micro-chip initiators, microelectromechanical systems (MEMS)-based microthruster systems for microspacecrafts and as triggering means for the inflation of automobile airbags [1, 2, 3].

The pyrotechnic compositions; especially thermites, used for nearly 100 years [4], are utilized in welding of railroad lines where the thermite reaction product molten iron flows through the joints [5, 6, 7].

The pyrotechnic compositions are prepared by physical mixing of fuel and oxidizer components. However, recently, another method called sol-gel method has been used for the synthesis of energetic materials. This method is a safe processing of energetic materials at room temperature followed by low temperature drying. It provides intimate mixing and contact of the components. In tailoring the properties of final energetic material, sol-gel method is a rather easy process compared to conventional methods.

It is possible to synthesize nano-sized energetic materials by using the sol-gel method. It is known that when the particle size decreases, materials display different properties

compared to the bulk of same material.

Another fact is that the surface to volume ratio and the interfacial contact area of the components increase when the particle size decreases to nanoscale. High surface to volume ratio and interfacial contact area lead higher energy release rate during the combustion process indicating that the particle size of the material is very important.

“Bottom-up” conceptual beginning on what later became known as nanotechnology first came up with Richard Feynman’s talk, “There’s Plenty of Room at the Bottom” at American Physical Society Meeting in 1959 [8]. The field of nanoparticles has been grown with many research studies. However, the application of nanotechnology on the energetics is relatively a new topic. The research studies show that nano-sized energetic materials will become next-generation energetics due to their controllable energy densities, particle size distributions and power/heat releases all of which can be tailored by varying fuel and oxidizer compositions. The application of nano energetics to MEMS technology may lead to size and mass reductions of the many munition subsystems in the future [3].

In the first section of this part, the literature survey is focused on detailed information about energetic materials and the methodology of xerogel synthesis. The characterization of xerogel samples are mentioned in the later sections of literature survey.

In the second part, the experimental studies and results are given in detail. The experimental procedure and the properties of both xerogels and synthesized energetic samples are explained. Comparison is made for thermal and combustion performances of the non-energetic and energetic compositions characterized by SEM, XRD, TGA, DSC and BET.

The aim of this study was to develop easily ignitable nanothermite compositions with higher heat output when properly initiated. In order to develop energetic nanocomposites, a very well-known sol-gel procedure was applied on synthesis and preparation of thermite compositions. This procedure has many advantages over conventional methods such as it lets safe processing of energetic materials at room temperature, it provides controllable parameters to tailor the properties of final energetic composition and it is possible to achieve ultrafine particle dispersion.

Furthermore, the increasing demand for longer shelf life of rocket motor systems demonstrates the necessity of development of igniter charges and pyrotechnic compositions having longer shelf life. Boron has been one of the most interesting materials, which has been used as fuel for pyrotechnic compositions not only due to its longer shelf life, but because of its higher heat of combustion and lower atomic weight with high gravimetric and volumetric energy content compared to other fuels.

In the scope of this study, in order to compare the effects of different fuels on the performance of nanocomposites; Magnesium, Aluminum and Magnesium coated Boron were used addition to Boron.

Another major objective of the study was to investigate the effects of sol-gel synthesis parameters such as proton scavenger, concentration of the precursor solution and drying conditions on the structural properties and thermal behavior of the synthesized samples.

1.2 Energetic Materials and Conventional Methods for Preparation

The energetic materials are the compositions that can store large amount of chemical energy and can release this stored energy rapidly when any proper ignition source is

introduced. The energetic materials are mainly classified into three groups: pyrotechnics, propellants and explosives.

Pyrotechnic materials burn with the velocity range of mm/s to produce special effects, propellants deflagrate with the velocity range of m/s to produce thrust and explosives detonate with supersonic velocity more than 1 km/s to produce shock.

Primary explosives are used to detonate secondary explosives by producing shock wave and they are very sensitive to shock, heat, impact and/or friction. Secondary explosives are insensitive energetic materials and more energy is needed to detonate the secondary explosives. However, they have more energy output compared to primary explosives. Lead azide, lead styphnate and DDNP (diazodinitrophenol) are some of the examples of the primary explosives. RDX (cyclotrimethylene trinitramine), PBXN-5 (polymer bonded explosive), HMX (cyclotetramethylene tetranitramine) and HNS (trans-2,2',4,4',6,6'-hexanitrostilbene) are some of the examples of secondary (high) explosives.

Propellants do not detonate or explode, they do burn. They can be double based or composite type. Double based propellants contain nitroglycerine and nitrocellulose. Composite propellants comprise oxidizer and binder.

1.2.1 The Pyrotechnics

“Pyrotechnics” is a term derived from Greek words *pyr*(πυρ) meaning fire and *techne*(τέχνη) meaning art, skill. Pyrotechnics is the science which generally deals with compositions and systems that utilize these compositions. It also deals with production and test methods of these compositions and systems.

It is important to note that the pyrotechnic compositions burn with a rate of mm/s; however, in the case of combustion in a closed space, the velocity reaches to m/s ranges and detonation can occur.

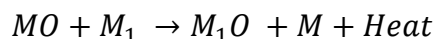
Pyrotechnic compositions contain fuel and oxidizer which react together to give necessary amount of energy in the systems such as piston actuators, gas generators for airbags, igniters for rocket propellants etc. Pyrotechnic compositions produce light, heat, smoke and sound when they burn so they can also be utilized as fireworks.

The pyrotechnic compositions can be used in granular or pellet forms depending on the application. The examples of such compositions are Magnesium-Teflon-Viton (MTV), Boron Potassium Nitrate (BPN) and Zirconium Potassium Perchlorate (ZPP). The calorific heat output value of these compositions is in the range of 4000-6750 J/g.

For a pyrotechnic composition the ignition and combustion performances are very important. That is, ignition energy and ignition time of a composition are used to specify the suitability of that composition for a particular application [9]. Regarding the nature of the combustion, the pyrotechnic compositions can be classified as flame, thermite and smoke compositions [10].

1.2.1.1 The Thermite Compositions

Thermite can be defined as a subset of pyrotechnics [11]. In thermite compositions the oxidizer can be metal oxide or oxygen-containing salt. Thermite reactions are exothermic reactions that occur by reduction of metal oxides with metals. The reactions proceed with self-sustaining oxygen content. The reactions can be represented as following,



MO : Metal oxide

M₁ : Metal

Large thermal stimulus is required for the ignition of thermites. This large thermal stimulus requirement comes from the high melting point of metal and oxidizers used in the thermites. Ignition is obtained with melting of metal and oxidizer components, so thermites are difficult to ignite compared with the other pyrotechnic compositions [9, 12].

There are some differences between the combustion mechanism of thermites and that of pyrotechnics. These differences can be summarized as follows:

- There are not any gaseous reaction products.
- The combustion reaction temperature is very high as 2000-2800°C.
- Molten slags are formed.

Thermites with a composition of Fe₂O₃/Al (2.75/1) are generally used for military purposes. The ignition temperature of thermites is about 800-1300°C. Thermites can be ignited with pyrotechnic devices such as electrical igniters and squibs [13,14]. Once they are ignited and they finally burn, the temperature rises to 3000°C.

The oxidizer used in the compositions should have a low heat of formation, a low atomic weight, sufficient oxygen content and high density for an efficient combustion of the thermite compositions. One of the following oxidizers can be used in the composition; B₂O₃, SiO₂, Cr₂O₃, MnO₂, Fe₂O₃, Fe₃O₄, CuO. In addition to oxidizers; Al, Mg or the alloys of Ca, Ti, Si and B can be utilized as the fuel (metal) [13].

Wilson et al. [11] introduced an illustration of the comparison of velocity and pressure achieved by different energetic materials. MICs have faster burning velocities than

propellants. However, they cannot reach high pressures like explosives.

It was mentioned that the explosives exhibited more gaseous products compared to MICs which cause instantaneous pressure and shock.

The Equivalence Ratio

The equivalence ratio can be defined as the ratio of the actual mass ratio of fuel to oxidizer to the stoichiometric mass ratio of fuel to oxidizer. It is calculated as;

$$\Phi = \frac{(m_{fuel}/m_{oxidizer})_{act.}}{(m_{fuel}/m_{oxidizer})_{stoich.}} \quad \text{Equation 1.1}$$

The actual fuel to oxidizer ratio is derived from the experimental values and the stoichiometric fuel to oxidizer ratio is derived from the energetic reactions. Some examples to these reactions are given below.

It should also be noted that if the equivalence ratio is larger than 1.0, the composition is defined as a fuel rich composition.

Here are some examples for thermite reactions with heat of reaction per one mole of oxidizer [5, 13, 15, 16]:

| | |
|--|---|
| $\text{Fe}_2\text{O}_3 + 2\text{Al} \rightarrow \text{Al}_2\text{O}_3 + 2\text{Fe} + 858\text{kJ}$ $3\text{MnO}_2 + 4\text{Al} \rightarrow 3\text{Mn} + 2\text{Al}_2\text{O}_3 + 1778\text{kJ}$ $\text{Cr}_2\text{O}_3 + 2\text{Al} \rightarrow 2\text{Cr} + \text{Al}_2\text{O}_3 + 544\text{kJ}$ $3\text{Fe}_3\text{O}_4 + 8\text{Al} \rightarrow 4\text{Al}_2\text{O}_3 + 9\text{Fe} + 3356\text{kJ}$ $3\text{CuO} + 2\text{Al} \rightarrow \text{Al}_2\text{O}_3 + 3\text{Cu} + 1213\text{kJ}$ | $2\text{CuO} + \text{Ti} \rightarrow \text{TiO}_2 + 2\text{Cu} + 310\text{kJ}$ $2\text{Cu}_2\text{O} + \text{Ti} \rightarrow \text{TiO}_2 + 4\text{Cu} + 297\text{kJ}$ $\text{Fe}_3\text{O}_4 + 2\text{Ti} \rightarrow 2\text{TiO}_2 + 3\text{Fe} + 197\text{kJ}$ $2\text{NiO} + \text{Ti} \rightarrow \text{TiO}_2 + 2\text{Ni} + 230\text{kJ}$ $2\text{ZnO} + \text{Ti} \rightarrow \text{TiO}_2 + 2\text{Zn} + 121\text{kJ}$ |
| $2\text{CuO} + \text{Zr} \rightarrow \text{ZrO}_2 + 2\text{Cu} + 389\text{kJ}$ $2\text{Cu}_2\text{O} + \text{Zr} \rightarrow \text{ZrO}_2 + 4\text{Cu} + 377\text{kJ}$ $\text{Fe}_3\text{O}_4 + 2\text{Zr} \rightarrow 2\text{ZrO}_2 + 3\text{Fe} + 272\text{kJ}$ $2\text{NiO} + \text{Zr} \rightarrow \text{ZrO}_2 + 2\text{Ni} + 310\text{kJ}$ $2\text{ZnO} + \text{Zr} \rightarrow \text{ZrO}_2 + 2\text{Zn} + 201\text{kJ}$ | $2\text{CuO} + \text{Hf} \rightarrow \text{HfO}_2 + 2\text{Cu} + 397\text{kJ}$ $2\text{Cu}_2\text{O} + \text{Hf} \rightarrow \text{HfO}_2 + 4\text{Cu} + 385\text{kJ}$ $\text{Fe}_3\text{O}_4 + 2\text{Hf} \rightarrow 2\text{HfO}_2 + 3\text{Fe} + 280\text{kJ}$ $2\text{NiO} + \text{Hf} \rightarrow \text{HfO}_2 + 2\text{Ni} + 318\text{kJ}$ $2\text{ZnO} + \text{Hf} \rightarrow \text{HfO}_2 + 2\text{Zn} + 209\text{kJ}$ |

Some researchers [17, 18] demonstrated that the optimum value of equivalence ratio was greater than 1.0. It was mentioned that the reactions were carried out at ambient air; therefore, oxygen was excess and the reaction of metal obtained from thermite reaction was carried out with an excess amount of oxygen. Furthermore, the increase in thermal conductivity due to the increase in metal content enhanced the combustion performance of the composition.

The characteristics of the compositions can be tailored by changing the equivalence ratio and the contents to have optimum conditions for following properties.

1. ignition temperature
2. heat release rate or heat of reaction
3. mechanical properties

4. moisture absorption
5. impact sensitivity
6. friction sensitivity
7. maximum pressure (P_{\max})
8. time to reach to P_{\max}

The heat transfer during the combustion of the pyrotechnic compositions is obtained only by heat conduction due to non-porous structure. However, for an efficient combustion, the heat transfer mechanism should not involve both conduction and convection. Therefore, porous structures are necessary for an efficient and a uniform combustion mechanism. Another parameter which affects the combustion is particle size. The heat and mass transfer length in the composition decrease when the particle size of the components reduces to nanoscale. This provides uniform combustion and higher energy release rate. The detailed information is given in following section.

The combustion mechanism of the thermite compositions is so complex that both the properties of individual components and collective properties of the mixture have to be taken in consideration. It is known that there is a relation between the physical/ structural properties of the components and the combustion mechanism. Therefore, it is extremely important to understand the phase changes and the oxidation mechanisms of the fuel/metal used in the energetic compositions [19]. It is also known that metal particles will be oxidized with air in progress of time.

1.2.1.2 The Oxidation Model for Aluminum

Aluminum is used as a fuel/metal for both pyrotechnic and thermite compositions. There is an oxide layer surrounding Al particle and this layer's melting temperature is higher

than that of Al particle core which is illustrated in Figure 1.1. The melting temperatures of Al core and oxide layer are 660°C and 2046°C , respectively [18, 20].

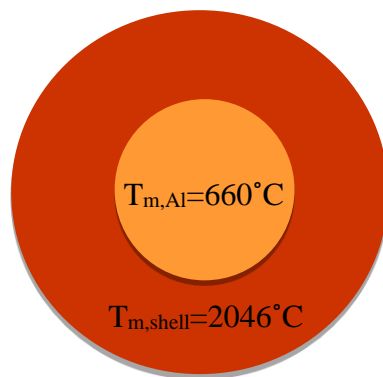


Figure 1.1. Schematic Illustration of Aluminum Particle Core and Oxide Shell

The oxidation mechanism of Aluminum has been discussed by many researchers. Proposed by Turunov et al. [21], the oxidation of Aluminum has four different stages. In the first stage, the natural amorphous oxide layer exists with a thickness of 5 nm. At this level of thickness, the metal-oxide interface stabilizes the layer at low temperatures. In addition, the rate of increase in layer thickness is controlled by diffusion of Al cations outside the core. Later on at the second stage, the shell is transformed to $\gamma\text{-Al}_2\text{O}_3$. The specific volume of $\gamma\text{-Al}_2\text{O}_3$ is lower than that of amorphous oxide. As a result of lower specific volume, the surface of aluminum is partially covered. At this stage the rate of oxidation increases and after $\gamma\text{-Al}_2\text{O}_3$ layer becomes continuous, the rate decreases. At the third stage, $\gamma\text{-Al}_2\text{O}_3$ starts to transform into $\theta\text{-Al}_2\text{O}_3$. Then at the fourth stage, this $\theta\text{-Al}_2\text{O}_3$ layer transforms to $\alpha\text{-Al}_2\text{O}_3$. This oxidation model gives an idea about diffusion mechanism through the grain boundaries [21, 22, 23, 24].

1.2.1.3 The Oxidation Layer of Boron

Similar to the other metals, oxide layer is formed over the boron particles due to exposure to air as illustrated in

Figure 1.2. The boron particle can be crystalline or amorphous depending on the production method. It is important to note that the crystal-like boron particles have more oxide shell than amorphous boron particles [25]. The oxide shell melts at lower temperatures than the boron particle core. This situation causes kinetic limitations because this oxide layer slows down the combustion of boron particle.

The melting temperatures of the B core and oxide layer are 2077°C and 450°C , respectively [26, 27]. The melting of the oxide layer before core results a different scenario for oxidation compared to aluminum particle. This scenario includes a diffusion controlled process. After oxide layer melts, it acts as a diffusive barrier covering the boron particle. If the boron particle is burned at the temperatures above the boiling point of oxide layer, which is 2065°C [26, 27], the oxide layer can be removed.

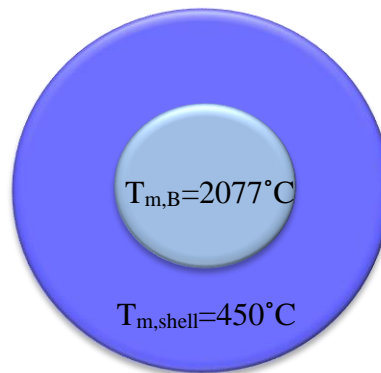


Figure 1.2. Schematic Illustration of Boron Particle Core and Oxide Shell

1.2.2 Iron Oxide

In this study the sol-gel synthesized Fe_2O_3 is used as an oxidizer for the thermite reactions. It is the most common oxidizer for the thermite compositions [28,29,30]. In addition, it has been utilized as an additive to modify/enhance burn rates of the solid propellants [31,32,33]. It has been used over many years starting with the pre-historic use in the pigments to draw on the walls of the cave which was followed by the usage in the applications of welding in the twentieth century [34]. Furthermore, recently, the Mars exploration rover Spirit has identified the iron oxide particles such as maghemite and magnetite on the surface of Mars [35]. On Earth, the iron oxide is utilized in many biological systems [36,37,38] and in addition to that, it can be employed as a catalyst, an inorganic pigment and a photoanode for photoelectron-chemical cell in many applications. Moreover, iron oxides formed by sol-gel synthesis have been extensively studied and the synthesized iron oxide samples were found to have porous structure with a high surface area [39, 40, 41, 42, 43, 44, 45].

Diebold et al.[46] define the iron oxide structure as a close-packed oxygen lattice in which Fe cations are distributed in octahedral and tetrahedral interstitial. The structure of maghemite phase of $\gamma\text{-Fe}_2\text{O}_3$ is obtained via the oxidation of Fe_3O_4 . Maghemite ($\gamma\text{-Fe}_2\text{O}_3$) preserve its spinel structure with randomly distributed octahedral Fe vacancies as schematically illustrated by Diebold et al.[46].

Maghemite has cation vacancies which affect its crystallographic structure and the magnetic properties; therefore, the researches on maghemite have received great intention [47, 48, 49, 50, 51]. The spinel structure of $\gamma\text{-Fe}_2\text{O}_3$ consists of layers of tetrahedral and octahedral positions [52, 47] and Ferguson et al. [53] indicated that the octahedral sites of maghemite involve cation vacancies. The cation vacancies are important for the thermite reactions which are based on the reduction and oxidation

mechanism between the iron oxide and the fuel used in the compositions since the existence of these cation vacancies affect the structural properties of the iron oxide xerogels [46].

1.2.3 The Methods for Preparation of Pyrotechnics

Recently modern advanced technologies have been applied to the preparation of energetic materials. These are sol-gel method, ink-jetting, vapor deposition techniques, cold spraying and arrested reactive milling. Nano energetic materials having different structures and morphologies can be produced by these advanced methods [54]. These structures can be nanofoils [55,56], core shell structures [57], nanowires [30], nanoporous particles [30] and substrates [58, 59, 60].

In general there are three main techniques for preparation of nano thermites and pyrotechnics. These are

- physical mixing
- arrested reactive milling
- sol-gel methodology

The detailed information about the mixing methods is given in following sections. It is important to mention that the rate controlling step for the combustion reaction of physically mixed energetics such as thermites and pyrotechnics is the mass diffusion between the reactants. On the other hand, for monomolecular energetics such as explosives, the rate controlling steps for combustion reaction are bond breaking and chemical kinetics between the reactants. Thermites and pyrotechnics have higher energy densities than explosives; however, they burn slower and longer than explosives because diffusion controlled reactions are slower than kinetically controlled reactions [39].

1.2.3.1 The Physical Mixing

The pyrotechnic mixtures are conventionally prepared by physical mixing of fuel and oxidizer [61]. The physical mixing is a simple and common technique. The technique is categorized in two groups, dry process and wet process. In the dry process, the components which are in granular form are mixed directly without any solvent medium.

In the wet process, the components are mixed in a volatile medium such as acetone and/or hexane to prevent the instantaneous ignition due to electrostatic discharge. At the end of mixing, the liquid phase is decanted or evaporated and the mixture is sieved.

The wet process is a simple method and it can be applied to prepare various mixtures. However, the process is labor intensive and large amount of solvent is used during the process.

1.2.3.2 The Arrested Reactive Milling (ARM)

This method is based on milling of components in a ball mill. The final particle size of the mixture depends on milling time, size and types of the milling balls. In this method, the milling time is very critical since after a certain time the milling process can lead to an inadvertent ignition due to the friction of the balls on small particle sized composition. Hence, it is very important to stop mixing at a certain time so that the resulting composition can be used as a thermite [62].

With this method, it is possible to control the degree of mixing and reactivity of the composition. However, the method has a very limited application in preparing energetics due to sensitivity issues.

An example of this method is used by Dreizin et al. [63, 64, 65, 66, 67, 68, 69] where Al/MoO₃, Al/Fe₂O₃ and Al/CuO were prepared during the studies.

The reactants were mixed in a closed container of rotary mixing machine in an appropriate solvent and under inert atmosphere such as nitrogen or argon which prevents the built up of electrostatic charge that could ignite the composition spontaneously. Moreover, the atmosphere was inert to prevent the partial oxidation of the fuel particles.

1.2.3.3 The Sol-Gel Method for Synthesis of Nanoenergetics

The importance of the particle size and intimate mixing of the components created a need for new approaches on synthesis of thermites [70]. The sol-gel method is a well-known method for producing nano-structured materials. Recently, applications of this well-known method on synthesis of nanothermites have been studied. The examples of these applications are developing self-assembled nanocomposites [71,72] and penetration of oxidizer through the silicon substrates [73, 74, 75].

The sol-gel method is the synthesis of nanoparticles by the reaction of components in a solution which is called as ‘sols’ and then linking them together in a solid matrix called as ‘gel’ with porous structure. If the liquid phase is evaporated from the pores of gel structures by controlled evaporation, dense and porous material called as xerogel is obtained. If the liquid phase is extracted by supercritical method, aerogels which have highly porous structures are obtained. The synthesized xerogels/aerogels have nanometer size particles and pores.

The application of sol-gel method on energetic materials is a new approach. This method has some advantages over conventional methods [76]:

- Safe processing of energetic materials at room temperature
- Intimate mixing of the components
- Easy control to tailor the properties of final energetic material
- Low cost compared to conventional methods
- Possibility to achieve ultrafine particle dispersion which is not possible by conventional methods

The rate controlling step that is the duration of mass diffusion between the reactants can be reduced with nano particles and consequently the reaction rate can be enhanced. So it is promising that they behave as high energy density physically mixed energetics and high power monomolecular explosives.

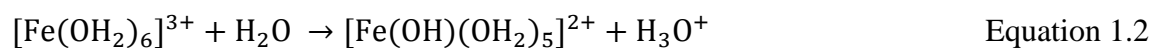
The disadvantage of the method is the possible oxidation of metal/fuel nanoparticles by water in the metal oxide gel before the removal of solvent. To prevent this situation, the oxide xerogels can be synthesized separately from the fuel and then the fuel can be added physically to the oxide xerogels. But this can reduce the interfacial contact area between the components. There is an illustrated example of the difference between the oxidizers physically mixed and sol-gel synthesized. It is mentioned by Clapsaddle et al. [77] that, this form of structure for physically mixed compositions results in particle ejection of the slower reacting SiO_2 which causes rapid burning and reaction propagation. Although SiO_2 is used as the oxidizer to slow the burning, the composition would burn rapidly which is not preferred for this type of system design with this effect of particle ejection.

1.2.3.3.1 The Gelation Mechanism

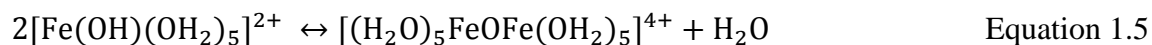
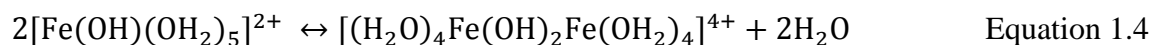
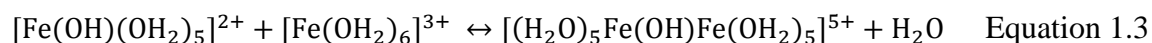
Metal alkoxides are good precursors to produce metal oxides. They easily react in hydrolysis and condensation steps. The mechanism is based on the assumption that the gelation agents are necessary for extraction of the protons to have hydrated metal complex. The gelation mechanism steps are given in following references [78, 79, 80, 81,

82, 83]. With the addition of ethanol to the iron (III) nitrate nonahydrate, $\text{Fe}(\text{NO}_3)_3 \cdot 9\text{H}_2\text{O}$, H_2O and $(\text{NO}_3)^-$ molecules release. Therefore $[\text{Fe}(\text{OH}_2)_6]^{3+}$ react readily with water as given in Equation 1.2.

Hydrolysis:

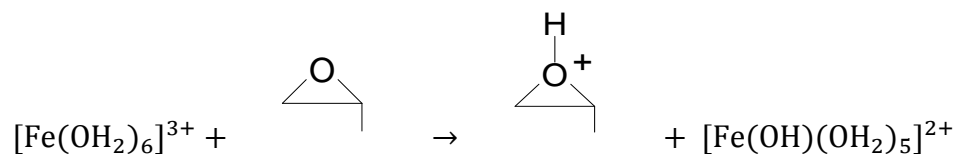


Condensation:

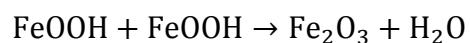


When the propylene oxide, which is a base, is added, it acts as a proton scavenger leading to irreversible ring opening and production of FeOOH shown in Equation 1.6

and Equation 1.7. So Fe_2O_3 is produced with further hydrolysis and condensation of hydrated metal.



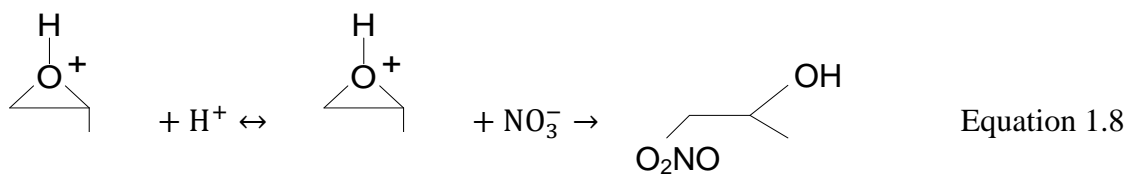
Equation 1.6



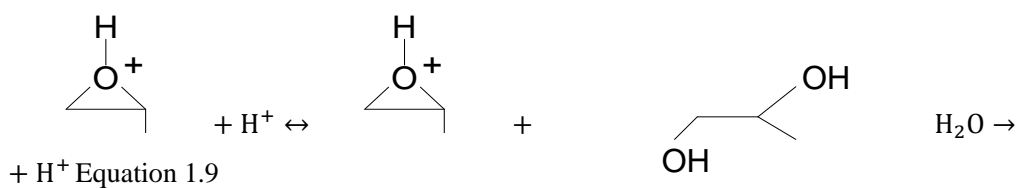
Equation 1.7

Ring Opening:

Propylene oxide:



Equation 1.8



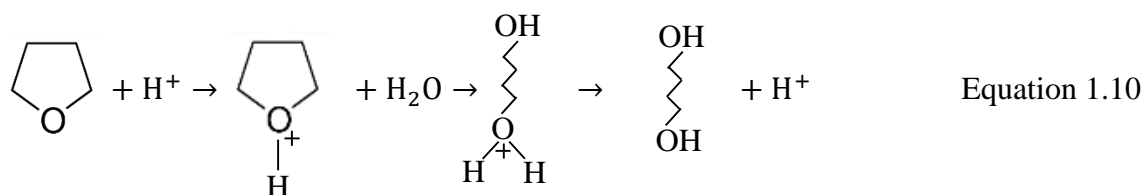
+ H⁺ Equation 1.9

It is mentioned that two different ring opening mechanisms can occur as given in Equation 1.8 and 1.9 [84]. These are ring opening with the addition of H₂O and (NO₃)⁻ molecules separately.

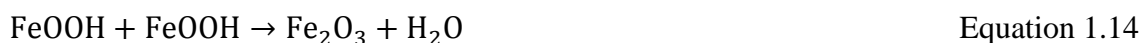
The hydronium ions are consumed by the salt anions in solution. Consequently the pH increases with time due to the decrease in hydronium ion concentration. This is shown in “pH study during gel formation” with experimental results.

Ring Opening of some proton scavengers:

THF:



In the presence of ammonium hydroxide solution instead of propylene oxide, the following reaction mechanisms occur:



In conclusion, gelation mechanism procedure is based on the phenomena of extracting of the protons by proton scavengers from the hydrated iron composites to form protonated complexes.

1.2.4 The Effect of Particle Size on Performance

The particle size, distribution, shape and specific surface area of the fuel, oxidizer and pyrotechnic compositions directly affect the burning characteristics of the materials. Decrease in particle size increases the surface area and the contact area between the components therefore increases the burning performance. As mentioned in previous sections, the thermite compositions are difficult to ignite due to high melting point of the components. However, when the particle size is decreased, the thermal properties change according to their bulk properties. This can be due to the surface effect of superfine particles [9,85].

Moreover when the particle size decreases to nano ranges, several achieved advantages can be summarized as:

- The decrease in melting temperature provides easy ignition
- The reduction in activation energy results in easy oxidation hence ignition delay lowers
- Generally higher thermal conductivity of nano - metal powders increases the heat transfer between the components accordingly enhances the burning characteristics
- The heat transfer timescales become increasingly fast due to decreases in the ratio of volume (V) to surface area (A_s) : $\tau = \frac{\rho V c_p}{h A_s}$ where τ is the thermal time constant.

Sullivan et al. [70] described the mechanism of the heat transfer through the particle. It is very difficult to heat a nanoparticle because it is a small thermal load with a very high rate of heat transfer. The transient conduction is for a solid which has a change in its thermal environment. Under this circumstance the lumped capacitance method is applied.

The main assumption of the lump capacitance method is that the solid particle has a uniform temperature which means the temperature gradients within the solid are negligible [86].

The Figure 1.3 shows the schematic illustration of Al particle surrounded by gas layer. T_P and T_G are the temperature of the particle and gas, respectively. The temperature values are equal to each other at the initial conditions. When the surrounding gas temperature increases, the heat transfer through the particle starts. To understand the heat transfer phenomenon and the relation between particle size and heating rate, the lump capacitance model is used. Firstly energy balance is introduced:

$$\dot{E}_{st} \equiv \frac{dE_{st}}{dt} = \dot{E}_{in} - \dot{E}_{out} + \dot{E}_g \quad \text{Equation 1.15}$$

$$\dot{E}_{st} = \dot{E}_{in} \quad \text{Equation 1.16}$$

$$hA_s(T_G - T) = \rho V c_p \frac{dT}{dt} \quad \text{Equation 1.17}$$

It can be concluded that when the particle size decreases, the surface area to volume ratio increases and heat transfer rate is improved.

Introducing the temperature difference:

$$\theta \equiv T_G - T \quad \text{Equation 1.18}$$

$$\frac{\rho V c_p}{h A_s} \frac{d\theta}{dt} = -\theta \quad \text{Equation 1.19}$$

$$\frac{\rho V c_p}{h A_s} \int_{\theta_P}^{\theta} \frac{d\theta}{\theta} = - \int_0^t dt \quad \text{Equation 1.20}$$

$$\theta_P \equiv T_G - T_P \quad \text{Equation 1.21}$$

$$\frac{\rho V c_p}{h A_s} \ln \frac{\theta}{\theta_P} = -t \quad \text{Equation 1.22}$$

$$\exp\left(\frac{h A_s}{\rho V c_p} t\right) = \frac{\theta}{\theta_P} = \frac{T_G - T}{T_G - T_P} \quad \text{Equation 1.23}$$

$$\tau = \left(\frac{1}{h A_s}\right) (\rho V c_p) = R_t C_t \quad \text{Equation 1.24}$$

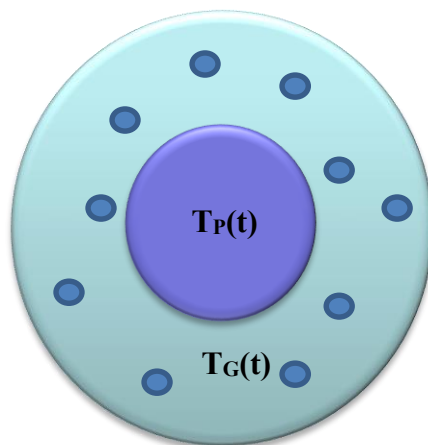


Figure 1.3. Schematic Illustration of Aluminum Particle Surrounded with Gas in a Control Volume

1.2.5 The Effect of Moisture on Performance

The hygroscopicity of the components is another factor that affects the performance and ageing of the pyrotechnics. Moisture is absorbed by many oxidizers and reacts with metals causing the formation of a metal oxide or metal hydroxide layer on the surface. So there will always be an oxide layer surrounding the active fuel.

It is vital to choose an oxidizer that can pass through this oxide layer to react with metal efficiently. The oxide layers cause changes in ignition and combustion performance negatively due to non-reactivity and this leads ageing of the composition. Therefore the shelf life of the compositions is directly dependent on the moisture content and absorption. Hence the knowledge about the moisture absorption characteristics of components and reactivity with moisture is very important. One way to protect the composition from the moisture is that it could be coated by some additives like binders. The ageing and life time of the pyrotechnics are explained in detail in “*1.4 The Ageing of Pyrotechnics*”.

1.2.6 The Effect of Binder in the Composition

Many resin types and polymers can be used as binders for pyrotechnic compositions. The binder behaves as filler between the fuel and oxidizer binding them together. At the same time it increases the mechanical strength and it modifies burning rate while desensitizing the energetic compositions. It is important to note that some of the binders with high oxygen content like unsaturated polyesters and epoxy resins improve the efficiency of combustion [13].

1.2.7 Nanothermites

One of the important parameters which affect the combustion is particle size. The heat and mass transfer length in the composition decrease when the particle size of the components reduces to nanoscale. This provides uniform combustion and higher energy release rate. The thermites that include nano oxidizer and fuel can be defined as nanocomposite thermites, metastable intermolecular/interstitial composites (MICs) or superthermites [87]. The significant changes in ignition and combustion performances are observed for the energetics with 100 nm or smaller particle size.

At this scale of the particle size, some properties like melting point may not change; however, nano-sized particles enhance the burning rates and combustion efficiency of the composite energetic materials as a consequence of intimate contact of the components and higher surface area than micron-sized particles [88,89].

As mentioned, not only the convection but also the conduction heat transfer is important for proper combustion, so if the interfacial conduct of the components increases with decreasing particle size, the conduction heat transfer can be increased. The functional groups on the surface of nanothermites also enhance the combustion. Thiruvengadathan et al. investigated the effects of functional groups of hydroxyl, methyl and methylene on the combustion with change in pressure-time characteristics. It is shown that the functional groups provide an increase in gas generation and enhance the convection heat transfer. Also it is mentioned that the convection heat transfer is dominant at lower percentages of theoretical maximum density (TMD %) while the conduction heat transfer is dominant at higher TMD % [87].

It is further stated that, the conventional mechanism based on the diffusion of aluminum and oxygen atoms in oxides is not a sufficient explanation for the fast reaction propagation of nanothermites.

The reason behind that could be the oxide shell on the melted Al nanoparticles starts to degrade physically. Different atomistic mechanisms are proposed by different researches and therefore it is important and crucial to understand how the reaction of molten metal with an oxide is initiated in picoseconds. Shimojo et al. found that a 400 m/s combustion front propagates through a 4 nm oxide shell in 10 picoseconds [90, 91].

1.3 The Sensitivity of Energetics

Sensitivity is a very important criterion for energetic materials. The sensitivity values of an energetic material give information about how it should be worked with the material during production, handling, transportation and storage. One should also know the sensitivity of a new designing pyrotechnic composition while choosing its components and production techniques. A proper energetic material should be sensitive enough to ignite and also insensitive enough to not to be initiated inadvertently during storage and handling. Sensitivity can be classified into three groups:

1. Friction sensitivity
2. Impact Sensitivity
3. Electrostatic Discharge (ESD) Sensitivity

Friction sensitivity is measured by the scraping of various weights over an energetic material and its unit is in Newtons (N). Impact sensitivity is measured by dropping weights from various heights on the energetic sample and its unit is in Joules (J).

The impact and friction sensitivity levels for energetic materials are defined in elsewhere [29,92,93]. ESD is instantaneous static electricity flow from an object to another by contact. It is tested by discharging a spark of specified energy through an

energetic sample and its unit is in millijoules (mJ). The ESD measurement is critical because the static discharge from human body is in the range between 5-20 mJ and this energy is enough to initiate very sensitive energetic materials. So, while handling these materials extra precautions must be taken. The correlation between particle size and ESD sensitivity was studied by Weir et al. [94] and it was shown that the sensitivity increased when the particle size decreased for energetic samples with Al as fuel. For Al/MoO₃ composition, ESD stimuli were measured as 0.25 mJ for 50 nm Al and 100 mJ for 20 μm Al.

1.4 The Ageing of Pyrotechnics

The service life of the pyrotechnic compositions is very important due to the explosion in different environmental and storage conditions. Particularly, the munition systems used at high altitudes are subjected to lower atmospheric pressure which causes to vaporization and sublimation, so changes in properties of the compositions. Therefore the quality of the seals of pyrotechnic systems is very important to preserve the properties of the compositions. For a reliable system, the components are tested under simulated environmental conditions such as subjecting them to different relative humidity (60%, 70%, 80%) with different temperature ranges. The reactions occurring at high temperatures can be visualized by Arrhenius equation to have some idea about the ageing mechanism of the composition. Approximate service life of the sample can be calculated with Equation 1.25 and 1.26 according to STANAG 2895 by using data from different temperature ageing tests [13, 95].

$$k = A. e^{-E_a/RT} \quad \text{Equation 1.25}$$

$$F = \frac{k_1}{k_2} = e^{\frac{-E_a}{R} \left(\frac{1}{T_1} - \frac{1}{T_2} \right)} \quad \text{Equation 1.26}$$

1.5 The Literature Studies

Both fuel/metal and oxidizer are main components of the pyrotechnics. One of the common metals is Aluminum. However, as described in section “1.2.1.2 *The Oxidation Model for Aluminum*”, it has oxide layer with high melting point therefore it causes ignition delays and slow combustion velocities. Yen et al. [96] gives the gravimetric and volumetric heats of oxidation for metals.

Boron has a very high heat of combustion and low atomic weight compared to other fuels so it is one of the highest energy density materials with high gravimetric (59 kJ/kg) and volumetric energy content (140 kJ/cm³) [97,98]. Therefore the ignition and combustion of boron particles have been of great interest.

Mačević and Semple [99] and Yeh et al. [100] proposed “two-stage” burning mechanism means that the combustion of boron takes place in two steps, the removal of oxide layer and the combustion of core of boron particle. The first step is kinetic and diffusion limited step and takes place in a large period of time with respect to combustion of boron particle. As discussed in section “*The Oxidation Layer of Boron*”, the removal of liquid oxide shell is a very important process in the ignition and combustion of boron.

Boron particle is initially at the room temperature and it is completely covered by oxide layer. Then it is suddenly surrounded by the hot gases. The initial surface chemistry is the rate controlling stage and after the oxide layer is completely consumed exothermic heterogeneous reactions are carried out at the surface of core boron particle. Detailed combustion mechanisms will be described in the following.

There is two-stage reaction of boron which includes ignition and combustion. Boron oxide layer removal is defined as first stage and “clean” boron combustion is called as second stage.

When the oxide layer is totally removed, the second stage starts. It is that the oxide layer of boron acts as an energy/heat trap [99]. Initially there is a heat up stage which leads to phase change of boron oxide from solid to liquid. Then after this point there are two different types of assumption for the first stage. Glassman et al. [101] suggested that the oxidation of boron is controlled by the diffusion of boron through the oxide layer to the oxide and oxygen interface.

On the other hand, King [102,103,104,105] suggested that oxygen, not boron, diffuses through the oxide layer to the oxide and boron core interface.

There is a heterogeneous reaction between boron and oxygen which leads to vaporization of oxide layer by producing heat. When the oxide layer becomes very thin, rapid increase in temperature of the particle is obtained. So the first stage of combustion is completed and then the second stage begins. King [102] proposed that water vapor is obtained by the reactions between boron and oxygen then water vapor reacts with boron oxide layer and forms HBO(g) species. Later on HBO(g) diffuses through the oxide layer and reacts with boron and boron oxide and forms $\text{H}_3\text{B}_3\text{O}_3(\text{g})$ at the interface of boron and oxide layer. This model is called as “first-stage” combustion model. In the second-stage the combustion is diffusion controlled and it is modelled as the combustion of clean surface boron particle [106]. There are two surface reactions which are boron particle reacting with oxygen / boron oxide to produce BO and gas phase reaction of BO and oxygen to yield boron oxide. This phenomenon is suggested by Makino and Law [107].

Some numerical models were constructed by defining the problem as ignition and combustion of isolated, single-component spherical particle covered by quiescent gases. The models involve multicomponent molecular transport in the gas phase layer, heterogeneous reactions, absorption on the interface of boron and surrounding layer.

The detailed information is given in elsewhere [108, 109]. Zhou et al. [109] classified these stages as:

1. The particle heat up
2. Removal of oxide layer
3. The combustion stage

There are two interfaces during the oxidation and ignition/combustion. These are liquid oxide/gas interface and boron/liquid oxide interface. Hence there are different reaction mechanisms.

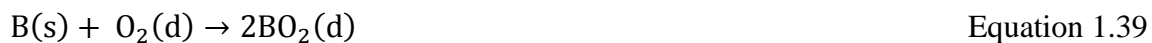
The phase change of liquid oxide layer to gaseous phase and *the liquid oxide/gas interface* kinetics model reactions are given as [108, 110]:





The model introduced by Zhou et al. [108] assumed that boron is transferred from to the oxide surface and forms suboxides as BO, BO₂, These suboxides (B₂O₂, BO, BO₂, B₂O₂) at the solid surface can be absorbed through the liquid oxide layer. H₂(g), OH(g), H₂O(g), BH(g) and O(g) are consumed at the liquid oxide/gas interface with adsorption.

The oxidation of boron particle and possible heterogeneous kinetic reactions between boron substrate and dissolved gases at the interface of boron/liquid oxide layer are given as [108]:



The species dissolved in the liquid oxide layer transport from liquid oxide/gas interface through the liquid oxide layer/boron interface and react with boron particle at this interface as given in Equation 1.38-1.45. The dissolved products of these reactions diffuse through the liquid oxide/gas interface.

All these reactions simulate the heat up of the particle and the removal of the oxide layer of boron. Zhou et al. [108] describe this model and find that especially BO_2 and HBO_2 are the main surface species at the liquid oxide layer/gas interface.

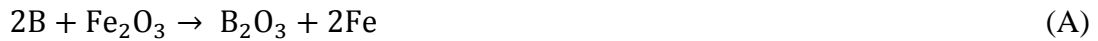
The adsorption and desorption rates are very critical and limiting steps for the removal of oxide layer.

In addition it is mentioned that the water vapor increases the rate of gasification of boron oxide layer and species with hydrogen enhances the gas-phase combustion [111,112,113,114]. However, water vapor leads to formation of HBO_2 and trapping of boron which causes less energy output [115].

In this study the reaction between boron and iron oxide is tried to be understand. The expected possible reaction products are shown in Table 1.1 and Table 1.2.

Table 1.1. Possible Reaction Products of B/Fe₂O₃

| Possible Reactions | ΔH (kcal/mol) [116,117,118] | | | | | | | | | | possible final products |
|--------------------|---|--|-------------------------------|-----|------|-------------------------------|-----------------|------------------|------------------|--------|--|
| | Fe ₂ O ₃ hematite | Fe ₃ O ₄ magnetite | B ₂ O ₃ | FeB | FeO | B ₂ O ₂ | BO ₂ | B ₂ O | ΔH_{rxn} | | |
| A | -196.8 | | -304.2 | | | | | | | -107.4 | B ₂ O ₃ , Fe, FeB, B ₂ O ₂ , B ₂ O, BO ₂ |
| B | | -267.1 | -304.2 | | | | | | | -415.5 | |
| C | | | -304.2 | | 60.0 | | | | | -484.2 | |
| D | | | | | | | | | | -9.2 | |
| E | | | | | | | | | | -108.9 | |
| F | | | | | | | | 23.0 | | 23.0 | |
| G | | | | | | | | | | -68.0 | |



Furthermore, some possible reactions between boron particles surrounded with oxide layer and ammonium nitrate which was obtained during iron oxide gelation process were also considered and given as following [25]:

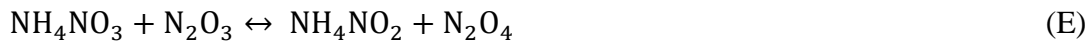
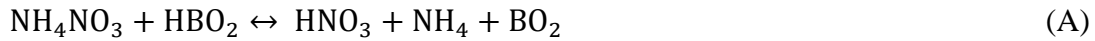


Table 1.2. Possible Reaction Products of B/Fe₂O₃

| Possible Reactions | ΔH (kcal/mol) [116,117,118] | | | | | | | | | | | | | possible final products | |
|--------------------|-------------------------------------|------------------|-------------------------------|------------------|-----------------|-----------------|------------------|-------------------------------|------------------|-------------------------------|---------------------------------|--------------------------------|------------------|-------------------------|---|
| | NH ₄ NO ₃ | HBO ₂ | B ₂ O ₃ | HNO ₃ | NH ₄ | BO ₂ | HNO ₂ | N ₂ O ₄ | H ₂ O | N ₂ O ₃ | NH ₄ NO ₂ | H ₃ BO ₃ | HBO ₂ | | ΔH_{rxn} |
| A | -87.4 | -192.2 | | -32.3 | -87.3 | -68 | | | | | | | | 91.8 | HNO ₃ , NH ₄ , BO ₂ , |
| B | | | -304.2 | -32.3 | | -18.3 | | | | | | | | -262.5 | HNO ₂ , B ₂ O ₃ , |
| C | | | | -32.3 | | -18.3 | 2.17 | -68.3 | | | | | | -15.5 | NH ₄ NO ₂ , N ₂ O ₄ , H ₂ O, |
| D | | | -304.2 | | | | 2.17 | | 20.0 | | | | | -290.7 | H ₃ BO ₃ , HBO ₂ |
| E | -87.4 | | | | | | 2.17 | | 20.0 | -61.3 | | | | 8.3 | |
| F | | | | | | | | -68.3 | | -61.3 | | | | -75.3 | |
| G | | | -304.2 | | | | | -68.3 | | | | -261.7 | | -14.3 | |
| H | | | | | | | | -68.3 | | | | -261.7 | -192.2 | 2.4 | |

The combustion process can be limited by diffusion or kinetics [106]. If the combustion rate is controlled by D^2 -law which means total burning time (t_b) is directly proportional with the square of the particle diameter, the combustion is dominated by diffusion. Mainly particles with order of 100 μm have diffusion limited combustion. And if the combustion is controlled by D^1 -law which means t_b is directly proportional with the particle diameter, the combustion is dominated by kinetics. Generally smaller than 10 μm diameter particles have kinetics controlled combustion. It can be decided by determining the Damköhler number (Da) and if it is around 1 there is a transition from diffusion controlled to kinetics controlled combustion. Da is defined as [106,119]:

$$\text{Da} = \frac{P(\text{atm})d_0(\mu\text{m})}{75} \quad \text{Equation 1.46}$$

The combustion of larger particles at high pressures is limited by diffusion and on the other hand that of smaller particles at low pressures is limited by kinetics [115].

Boron was used as an additive for Al/B/Fe₂O₃ composition prepared by sol-gel method [120]. The combustion characteristics were compared with Al/Fe₂O₃ and physical mixed Al/B/Fe₂O₃ composition. It was observed that heat of combustion of Al/B/Fe₂O₃ was higher than those of the others. Boron had an enhanced effect on the composition.

Tillotson et al. [76] synthesized nanocomposites of Al/Fe₂O₃ with using organic epoxide as gelation agent by sol-gel method. They obtained 3-10 nm sized clusters of Fe₂O₃ which is contact with 25 nm Aluminum particles. They found that Al particles have oxide layer outside with 5nm thickness which is seen as light colored ring by HRTEM images. This means the sol-gel method does not affect the metal because normally Al has similar thickness coating of oxide when the energetic material has been prepared by other methods. Their sol-gel method at low solution pH does not have any effect on oxidation of Al particle. It is mentioned that smaller particles are Fe₂O₃ xerogel clusters and

spherical particles are Aluminum which is also confirmed with selected area electron diffraction pattern (SAED).

The synthesized materials were ignited by a thermal source and their DSC thermograms with exothermic peak at nearly 500°C. The results prove that the samples are energetic. It was [121] also studied with different solvents and precursors for iron oxide xerogel synthesis.

Gash et al. [122,123] studied sol-gel synthesis of chromia from Cr(III) inorganic salts and the effects of solvents and gelation agent/salt ratio were determined. They found that these variables affected the rate of gel formation. They formed metal oxide aerogels and xerogels from their metal ion salts of Fe^{3+} , Al^{3+} , In^{3+} , Ga^{3+} , Zr^{4+} , Hf^{4+} , Ta^{5+} , Nb^{5+} and W^{6+} .

Spitzer et al. [124] prepared and compared the nano aluminum/tungsten (VI) oxide (Al/WO_3) and micron Al/WO_3 according to their sensitivity and combustion rate. It was found that nano sized Al/WO_3 (51/50nm) is more sensitive and so dangerous to handle and to work with than micron sized Al/WO_3 (1.912 $\mu\text{m}/0.724\mu\text{m}$). On the other hand, the results showed that the nano sized thermite can be used in percussion primers due to its high impact and friction sensitivity.

Poda et al.[125] studied the reaction products of $\text{Al}/\text{Fe}_2\text{O}_3$ and $\text{Al}/\text{Bi}_2\text{O}_3$ nanothermites. It was found that the particle size of the products of Bi_2O_3 was smaller than 5 μm and it included Bi and Al_2O_3 particles according to SEM, EDS, XRD analysis results. They found that the particle size of the products of $\text{Al}/\text{Fe}_2\text{O}_3$ was larger than 75 μm .

Gangopadhyay et al. [126,127] also have studies with Al/Fe₂O₃. They determined the effect of polymer loading (acrylamide-methyl cellulose acetate butyrate, AAMCAB) on the iron oxide composition. They first synthesized iron oxide by sol-gel method and surfactant templating, and then mixed with aluminum powder. The equivalence ratio was 1.4. They also used Brij76 which was non-ionic surfactant to have a template with micelles and the hydrolysis step was carried out around the micelles. They mentioned that after the removal of surfactant by drying the oxidizer with uniform pore, size distribution was obtained. They loaded polymer on matrix to have gas generation with combustion of the Al/Fe₂O₃ composition.

As expected it was found that the combustion wave speed decreased with increasing polymer loading and increasing equivalence ratio. The authors explained that the compositions should be slightly fuel rich to overcome the oxide layer around the fuel [17,126,128].

It is important to note that it was mentioned the combustion wave speed was optimum when the mixture was slightly fuel-rich because generally fuel has an oxide layer on its surface and oxidizer has impurities. To overcome these negative effects on combustion, slightly fuel-rich compositions are used. According to their study when fuel rich composition was used, there was lack of oxygen to oxidize the fuel for complete combustion.

It was also observed that when the particle size of the fuel of Al/ MoO₃ was decreased, the combustion velocities decreased [128].

Tantalum-tungsten oxide was synthesized by sol-gel method and physical mixing method by Cervantes et al [129]. They used WOCl₄ as precursor and 3,3-dimethyloxetane as gelation agent. Then the combustion properties of the compositions were compared and

it was found that the heat output of sol-gel prepared samples were 30-35 % higher than physically mixed samples.

Martirosyan et al. [3] studied with eight different compositions that were Al/Fe₂O₃, Al/Fe₃O₄, Al/MoO₂, Al/WO₃, Al/MnO₂, Al/MoO₃, Al/CuO, Al/Bi₂O₃ to develop highest peak pressure for nanoenergetic gas-generators. The highest peak pressure recorded belonged to Al/Bi₂O₃ thermite composition. The addition of carbon to mixture did not affect the peak pressure while addition of boron increased it nearly by 50 %.

Puszynski et al.[130] prepared different nanothermites with coated aluminum and applied to wet processing of percussion primers. They explained that some nanothermites which were Al/MoO₃, Al/WO₃, Al/CuO, Al/Bi₂O₃ could be used as a replacement of lead styphnate. They coated Al with organic hydrophobic materials such as oleic acid, butanedioic acid in ethanol and acetone to prevent oxidation with air and moisture and then removed solvent by drying in an oven set to temperature between 20-50°C. They also used PETN (pentaerythritol tetranitrate) and GAP (glycidyl azide polymers) as energetic additives. Then they mixed Al with Bi₂O₃ in different solvent mixtures such as polyethylene glycol trimethylnonyl ether in water, in acetone, 1-methyl-2-pyrrolidinon (NMP), by ultrasonically and placed the wet mixture into primer cup after some drying process.

Moore et al.[131] tested the deflagration of nanocomposites nano Aluminum (132nm, Technanogy) and nano molybdenum trioxide (Climax) prepared by physical mixing with 40/60 and 45/55 mass ratios. They found that deflagration wave velocity of Al/MoO₃ with ratio of 45/55 is 7% higher than that of Al/MoO₃ with ratio of 40/60. They mentioned that the results obtained are due to the higher emission of AlO by using time-resolved UV/visible emission methods.

Gash et al. [132] characterized the nanometer-sized ultra-fine grain (UFG) Aluminum/Viton A/Fe₂O₃ nanocomposite synthesized by sol-gel method. They used FeCl₃·6H₂O as precursor and Viton A as binder. They obtained nanocomposite thermites with ignition temperature of 590°C.

Clapsaddle et al. [39,77] studied the effect of SiO₂ on Al/Fe₂O₃ mixture and discussed the differences of combustion velocity between the physically mixed Al/Fe₂O₃/SiO₂ and the physically mixed Al and Fe₂O₃/SiO₂ aerogel in hexane by ultrasonic mixing. They also observed the ejection of particles from the composition which had been prepared by physically mixing of oxidizer during the combustion. They mentioned that the less exothermic reaction of SiO₂ with Al was carried out with the reaction of FeO₃ and Al due to SiO₂ particles trapped inside the sol-gel mixed composition and as a result the burning velocity decreased. They found that the combustion velocity can be controlled with the addition of SiO₂.

Shimojo et al. [90] studied molecular dynamics (MD) simulation with interatomic forces in the framework of the density functional theory (DFT) for initiation of thermite reaction of Al/Fe₂O₃. They found that redox reaction of Al/Fe₂O₃ resulted in the formation of iron metal and Al₂O₃. Al/Fe₂O₃ was initiated with the rapid formation of Al-O bonds at the interface within 1 picosecond.

Al/Co₃O₄ was synthesized on a substrate by hydrothermal method and thermal evaporation [133]. It was mentioned that the theoretical heat of reaction of Al/Co₃O₄ was larger than that of Al/Fe₂O₃ and Al/CuO. They firstly synthesized the oxidizer (Co₃O₄) on a silicon substrate then obtained penetration of Al on the oxidizer by thermal evaporation. They mainly aimed to use this energetic material network on silicon-based micro-electromechanical systems. The ignition temperature which was a critical parameter of MEMs was measured by DSC.

The ignition temperature of synthesized Al/Co₃O₄ (520°C) was lower than that of Al/Fe₂O₃ (588°C) and Al/CuO (550°C).

Pantoya et al. [18] prepared physically mixed Al/MoO₃ via sonication method and tested according to particle size, equivalence ratio and bulk density. The ignition delay time of nano Al/MoO₃ was two times more than that of micro Al/MoO₃. They mentioned that the combustion mechanisms were different from each other for nano MICs and micro MICs when they were analyzed by DSC. For the nano Al/MoO₃ the melting of Al was observed after an exothermic reaction of the components; however, for the micro Al/MoO₃ the melting of Al was observed before the exothermic reaction. The authors concluded that there was a solid state reaction for nano composition and gas-liquid reaction for micro composition. These mechanisms changed the combustion velocities of the MICs. In that study, the nano and micron size MIC pellets were pressed to a density between 6.5 to 73 % of TMD. Surprisingly the combustion velocity of nano MICs decreased as the density of pellets was increased. On the other hand the micro MIC's combustion velocity increased with increasing density. They explained this trend and concluded that as the density of micro MIC was increased, the voids which were filled by air were replaced by fuel/oxidizer particles. And if the combustion was controlled by thermal diffusivity, this situation would be the reason for increased energy transport and enhanced combustion mechanism.

Glavier et al. [134] researched the suitable oxidizer for Aluminum in nanothermite mixtures. They analyzed the burning and pressurization rate of the nanothermites of Al-Bi₂O₃, CuO, MoO₃, and micron sized Al/PTFE. The mixtures were prepared by sonication in hexane. The burning rate of Al/Bi₂O₃ was the highest with 420 m/s among the others. In addition Al/Bi₂O₃ had the highest pressure peak when 20 mg of sample was ignited in 9 mm³ closed bomb. Moreover, Al/Bi₂O₃ had the shortest time to reach the maximum pressure represented delay time which was an important parameter for ignition process.

Another study with Al/CuO nanothermite was about the investigation of the effects of non-stoichiometric mixtures on combustion performance [135]. The samples were prepared by mixing of fuel and oxidizer nano particles with sonication. 10 mg sample was ignited in 75 ml closed bomb to determine the combustion performance. According to the test results, the maximum pressure peak and pressurization rate were obtained at fuel-rich composition.

The slightly fuel rich composition had highest pressure value. The authors indicated that when the fuel rich compositions were ignited, the amount of gas produced increased. Hence heat transfer and combustion performance were enhanced.

CHAPTER 2

EXPERIMENTAL SECTION

In this chapter, the experimental method and the materials used to synthesized metallic xerogels are described. The analysis methods performed on the samples to characterize are explained.

2.1 Materials

Iron (III) nitrate nonahydrate ($\geq 99.95\%$ Sigma Aldrich) and iron (III) chloride hexahydrate ($\geq 99.0\%$ Sigma Aldrich) were used as precursors as received.

Boron powder ($\geq 98.5\%$) with an average particle size of 200 nm, magnesium powder ($> 99.0\%$) with an average particle size of 44 μm and 20 wt% Mg coated boron powder in micron size were provided by a local supplier and were used as a fuel as received. Aluminum powder (90-92%) with an average particle size of 100 nm supplied by Mach I, Inc. was used as a fuel.

Ethanol ($\geq 99.8\%$ Sigma Aldrich) was used as solvent and propylene oxide (Aldrich), 1,2 epoxybutane ($\geq 99\%$, Aldrich), ammonium hydroxide solutions (28% NH_3 in H_2O , $\geq 99.99\%$, Sigma Aldrich), tetrahydrofuran (anhydrous, $\geq 99.9\%$, Sigma Aldrich), tetrahydropyran (anhydrous, $\geq 99.0\%$, Sigma Aldrich), 1,4 dioxane (anhydrous, $\geq 99.8\%$, Sigma Aldrich) were used as gelation agent as received.

The gelation agents are very important with their proton scavenger role by reducing the amount of H_3O^+ and maintaining gelation mechanism. The chemical structures of the proton scavengers are given in Figure 2.1.

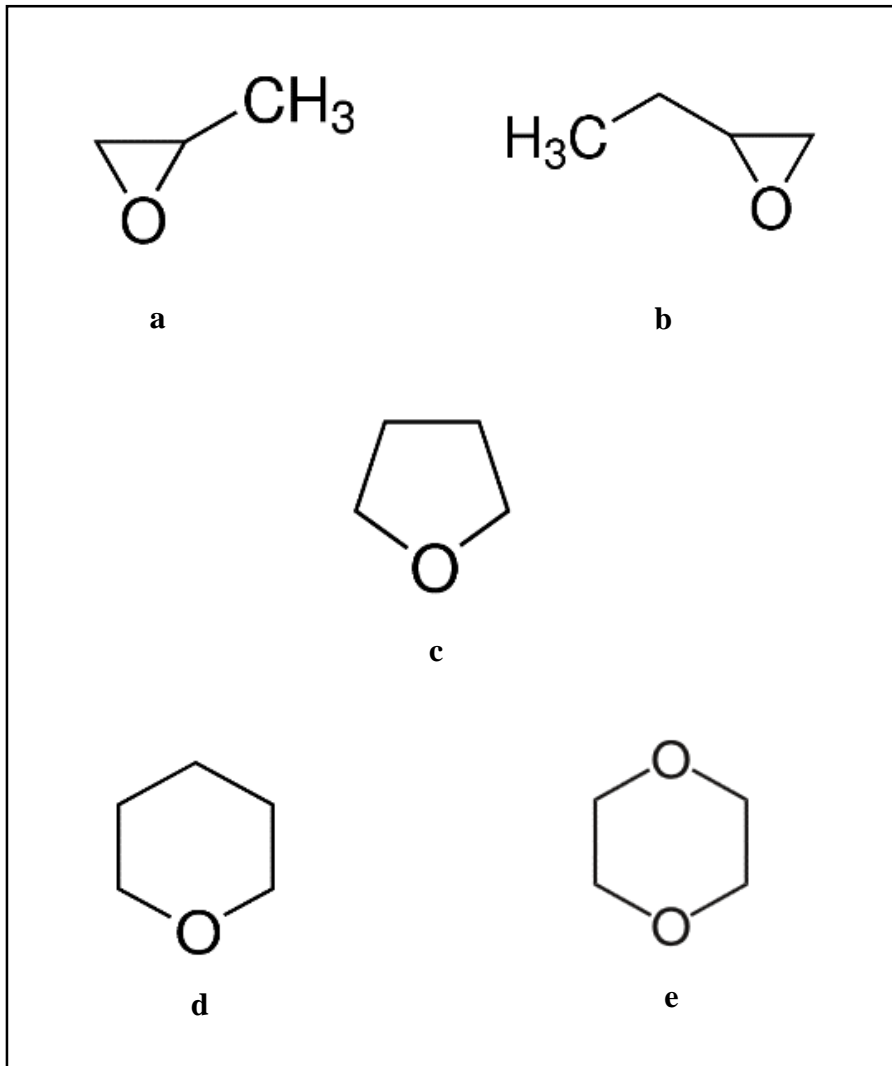


Figure 2.1. The structure of proton scavenger molecules a. propylene oxide (C_3H_6O) b. 1,2 epoxybutane (C_4H_8O) c. tetrahydrofuran (C_4H_8O) d. tetrahydropyran ($C_5H_{10}O$) e. 1,4 dioxane ($C_4H_8O_2$)

In addition to the materials mentioned above, iron (III) oxide ($< 5\mu\text{m}$, $\geq 99\%$, Aldrich) and iron (III) oxide nano powder ($< 50\text{nm}$, Aldrich) are used as oxidizers to prepare energetic compositions by physical mixing with the fuel powders.

The aim of the physical mixing of the commercially available powders is to compare the properties with those of the mixtures containing as-synthesized iron oxide samples.

2.2 Experimental Methods

2.2.1 Synthesis of Iron Oxide Samples

Iron oxide samples were synthesized by sol-gel method as shown in Figure 2.2. 4.0 g of iron nitrate nonahydrate ($\text{Fe}(\text{NO}_3)_3 \cdot 9\text{H}_2\text{O}$) was hydrolyzed in 6.4 ml of ethanol to have a clear red-orange solution in a glass beaker with constant magnetic stirring at 400 rpm by using explosion proof magnetic stirrer (2 mag magnetic motion atexMIXdrive 1) under ambient condition. 1.5 g of iron nitrate nonahydrate ($\text{Fe}(\text{NO}_3)_3 \cdot 9\text{H}_2\text{O}$) was hydrolyzed in 10.0 g of ethanol to have diluted solution to characterize the effect of concentration of precursor solution.

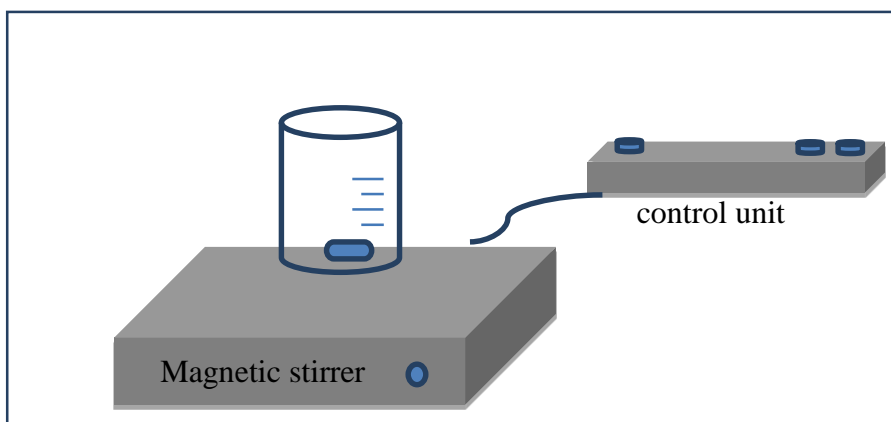


Figure 2.2. Experimental setup for gel synthesis

After the hydrolysis step, the gelation step was carried out by slow addition of the proton scavenger into the solution. The proton scavenger facilitated an exothermic

gelation reaction with a color change of solution to dark brown. In all synthesis work, the proton scavengers were added as 64.6 mmol except 1,4 dioxane (32.3 mmol) and ammonium hydroxide solution (128 mmol).

pH study during gel formation

The pH value measurements were carried out only for the synthesis of the iron oxide with propylene oxide. The pH and temperature change was measured by WTW ProfiLine pH 3110 pH meter. The experimental setup is shown in Figure 2.3.

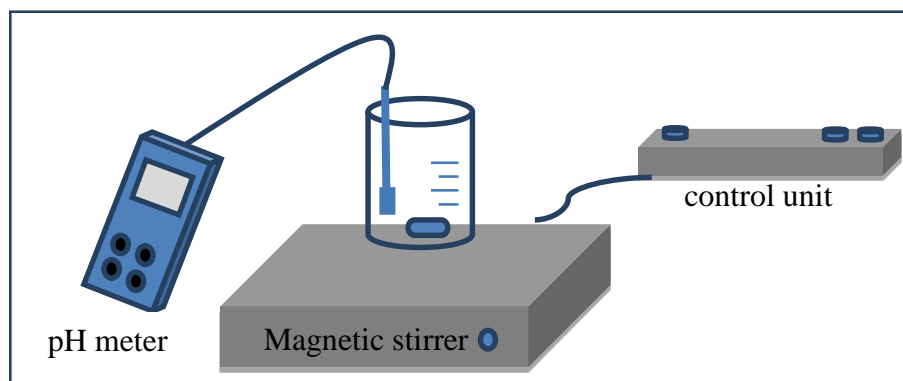


Figure 2.3. Experimental setup for gel synthesis

Two different solvents, ethanol and distilled water were used as a reaction medium to determine the effects of solvent on the gelation process. For the pH value measurement experiments 4.0 g (10 mmol) $\text{Fe}(\text{NO}_3)_3 \cdot 9\text{H}_2\text{O}$ was dissolved in 20.0 g ethanol. The first pH measurement was recorded after the dissolution of precursor. Then, the pH value was recorded at regular intervals with the addition of 4.0 g (68 mmol) propylene oxide part by part. The same procedure was performed by using distilled water as a reaction medium.

2.2.2 Drying Procedure

As synthesized iron oxide samples were dried after gelation process. Direct drying method and sequential solvent exchange (SSE) method were used. The detailed procedure is given in following sections.

2.2.2.1 Direct Drying Method

The samples were dried by conventional oven drying method at 70°C for 6 days to remove the solvent and volatiles. The small fissures or the monolith pellets were formed after drying of the samples. The direct drying process was followed by the granulation of the iron oxide samples with a mortar and pestle.

2.2.2.2 Sequential Solvent Exchange (SSE) Method

The sequential solvent exchange method was applied to remove the residual ethanol and other volatiles by successive treatment of the gel samples by series of ethanol-hexane mixtures containing 25%, 50% and 75%wt hexane. The gel samples were treated with each solvent mixture for 3 days at room temperature and the solvent was drained completely after each step. The solvent exchange process was followed by drying of the samples at 90°C for overnight. At the end of the drying process, the samples, having small fissures form, were granulated with a mortar and pestle.

2.2.3 Preparation of Energetic Compositions

B/Fe₂O₃ composites were obtained by physical mixing of specific amount of boron powder with the iron oxide samples.

The compositions have a specific mass ratio which can be described with the equivalence ratio. The equivalence ratio is the ratio of the actual mass ratio of fuel to oxidizer to the stoichiometric mass ratio of fuel to oxidizer. It is calculated by using the main chemical reaction between the fuel and the oxidizer (Equ.2.1, 2.2, 2.3) as;

$$\phi = \frac{\left(\frac{m_{fuel}}{m_{oxidizer}}\right)_{actual}}{\left(\frac{m_{fuel}}{m_{oxidizer}}\right)_{stoichiometry}}$$



For instance, according to the stoichiometric reaction (Equ.2.1, 2.2, 2.3) 2 moles of B was added to 1 mole of Fe_2O_3 or 2 moles of $Fe(NO_3)_3 \cdot 9H_2O$ for a stoichiometric composition (S.T.). The composition of 3 Fuel Rich (3FR) contains 1 mole of Fe_2O_3 and 3x stoichiometric mole numbers (3x2moles) of B. The composition of 9FR contains 1 mole of Fe_2O_3 and 9x stoichiometric mole numbers (9x2moles) of B.

The B/ Fe_2O_3 , Mg/ Fe_2O_3 , 20%Mg-B/ Fe_2O_3 and Al/ Fe_2O_3 samples were fuel rich compositions. The equivalence ratios of the samples are given in Table 2.1.

Table 2.1. The Fuel and Oxidizer Content of Mg/Fe₂O₃, 20%Mg coated B/Fe₂O₃
Al/Fe₂O₃ and B/Fe₂O₃ Compositions

| Composition | Fuel Type | Fuel Content (mmol) | Fe ₂ O ₃ Content (mmol) | Equivalence Ratio, ϕ |
|-------------|-----------|---------------------|---|---------------------------|
| 3FR | B | 6 | 1 | 3 |
| 6FR | B | 12 | 1 | 6 |
| 9FR | B | 18 | 1 | 9 |
| 6FR | Mg | 18 | 1 | 6 |
| 6FR | 20%Mg-B | 12 | 1 | 6 |
| 6FR | Al | 12 | 1 | 6 |

2.3 Material Characterization

2.3.1 Nitrogen Gas Adsorption Analysis

The textural properties of the iron oxide samples prepared by the sol-gel method were examined by N₂-BET method. The nitrogen adsorption-desorption isotherms of the samples were analyzed with Quantachrome Autosorb-6iS Instrument. The samples were degassed at 200°C for minimum 24 hours under vacuum (6.6×10^{-5} bar). The surface area, pore size distribution and pore volume were determined by the nitrogen adsorption-desorption isotherms.

2.3.2 X-Ray diffraction (XRD)

The X-ray diffraction analysis of Fe₂O₃ samples were performed at room temperature by Rigaku ULTIMA IV X-ray diffractometer using monochromatic Cu K α X-Rays with a wavelength of 0.15405 nm between 2 θ range of 3- 90° with a scan speed of 0.5 deg/min and a sampling step of 0.02. Database PDF-2 from ICDD was used to specify the lattice structures and phases.

2.3.3 FTIR Spectrum and Elemental Analysis

The iron oxide samples obtained by sequential solvent drying method were characterized with FTIR and the elemental analyzer. The FTIR spectra of the SSE iron oxide samples were recorded between 4000 and 600 cm⁻¹ with 16 scans per sample by Bruker Model Tensor 27.

The compositions of the SSE iron oxide samples were analyzed by LECO CHNS-932 elemental analyzer.

2.3.4 Thermal Analysis

Thermal analysis of the samples was carried out by NETZSCH STA 449 F3 Simultaneous TG-DSC Instrument to characterize the onset temperature and energy release of the samples. TG-DSC measurements were performed by loading 1.5-2.0 mg of energetic samples into Al₂O₃ crucibles and heated from room temperature up to 1400°C with a heating rate of 30°C/min with an accuracy of 0.0001 mg. The measurements were performed under a high purity (99.999 %) nitrogen atmosphere.

2.3.5 The Calorific Value Tests

The calorific values of the samples were determined by isoperibol operation using Isoperibol Bomb Calorimeter 6200 (Parr Instrument Company) in accordance with ASTM D3286 specification. The measurements were performed by using 0.5-1.5 gram of samples. Nickel-chromium resistance wire (Parr 45C10 34 B&S gage) with 160 μm diameter was used for the ignition of samples. The tests were carried out in air atmosphere and before the tests; the steel bomb was purged with Argon gas.

The sample was placed in a steel cup with fuse wire inside a steel vessel (combustion bomb chamber) which was suitable for measurements up to 10500 J/g. The combustion bomb chamber was submerged to the water which was in a bucket surrounded by a jacket. The jacket was held at constant temperature. The test was started by giving energy to the wire to heat and to ignite the energetic sample. Once the sample burns, the heat was released and flowed through the bomb chamber surface and water.

2.3.6 Scanning Electron Microscopy Analysis

The mixtures of boron and iron oxide xerogel synthesized with ammonium hydroxide and propylene oxide were chosen to characterize the morphological structure. The surface morphology was characterized by using QUANTA 400F high resolution field emission scanning electron microscope with magnifications of 100,000 and 400,000 operating at 30 kV.

2.3.7 Sensitivity tests

2.3.7.1 Impact sensitivity tests

The impact sensitivity response of the energetic samples was determined using BAM Impact Machine. Test procedure was applied according to “STANAG 4489 Explosives, Impact Sensitivity Tests” [93]. The tests were based on the principle of crushing the energetic sample between steel cylinders dropping weights from various heights. Drop weights were 1, 2, 5 and 10 kg and drop heights changed between 10 cm to 1 m with a logarithmic interval of 0.05. Decomposition, flash, smoke, sound ignition, crackling or explosion was considered as the response of the energetic sample. The impact sensitivity value in Joules (J) was determined by Bruceton procedure.

2.3.7.2 Friction sensitivity tests

The friction sensitivity response of the energetic samples was determined using BAM Friction Machine. Test procedure was applied according to “STANAG 4487 Explosives, Friction Sensitivity Tests” [92]. The sample was placed between porcelain peg and plate. The response of the energetic sample to the forward/backward movement of the peg loads varying from 5 to 360 N was determined. Decomposition, flash, smoke, sound ignition, crackling or explosion was considered as response. The friction sensitivity value in Newton (N) was determined by Bruceton procedure.

CHAPTER 3

RESULTS AND DISCUSSION

In this chapter, the characterization and performance test results are presented and the results are discussed in a detailed way. The effect of proton scavenger and drying conditions on the textural properties of iron oxide samples and the effect of the fuel type and stoichiometric ratio on the performance of thermite compositions have been investigated.

3.1 Nitrogen Gas Adsorption Analysis

The effect of proton scavenger, solvent exchange, drying conditions and concentration of the precursor solution on the textural properties were investigated by N₂-BET method.

3.1.1 Effect of Proton Scavenger

In the scope of this study, the effect of proton scavenger on the surface area, pore size and pore volume of the Fe₂O₃ xerogel samples were examined. The adsorption-desorption isotherms and pore size distribution of Fe₂O₃ samples are presented in Figure 3.1 and Figure 3.2.

The iron oxide samples exhibit Type IV isotherm with a hysteresis loop which indicates the mesoporous structure [136,137]. The hysteresis loops over the relative pressure of

0.5 also designate the presence of mesopores in the skeletal matrix [138].

The BET theory was applied to obtain the specific surface area and the BJH theory was applied to obtain pore volumes from nitrogen desorption isotherms. The data for the surface area, pore size and the average pore diameter are given in Table 3.1.

The specific surface area, pore volumes and average pore diameter of the iron oxide samples prepared by direct drying method vary between 67-321 m²/g, 0.02-0.88 cc/g and 1.6-9.7 nm, respectively. The wide range of the surface area can be explained by the different mechanisms, which follow through during the gelation process, depending on the proton scavenger used.

Table 3.1. The Surface Area, Pore Size and Pore Volume of Fe₂O₃ Compositions

| Proton Scavenger | Surface Area (m ² /g) | Pore Volume* (cc/g) | Average pore diameter* (nm) |
|--------------------|----------------------------------|---------------------|-----------------------------|
| Propylene oxide | 321.0 | 0.878 | 9.697 |
| THF | 109.1 | 0.087 | 3.804 |
| THP | 279.7 | 0.161 | 1.683 |
| 1,4 dioxane | 150.9 | 0.103 | 3.406 |
| 1,2 epoxybutane | 176.2 | 0.462 | 9.553 |
| Ammonium hydroxide | 67.1 | 0.022 | 1.646 |

*The pore volumes and the average pore diameter were obtained from nitrogen desorption isotherms by the BJH theory.

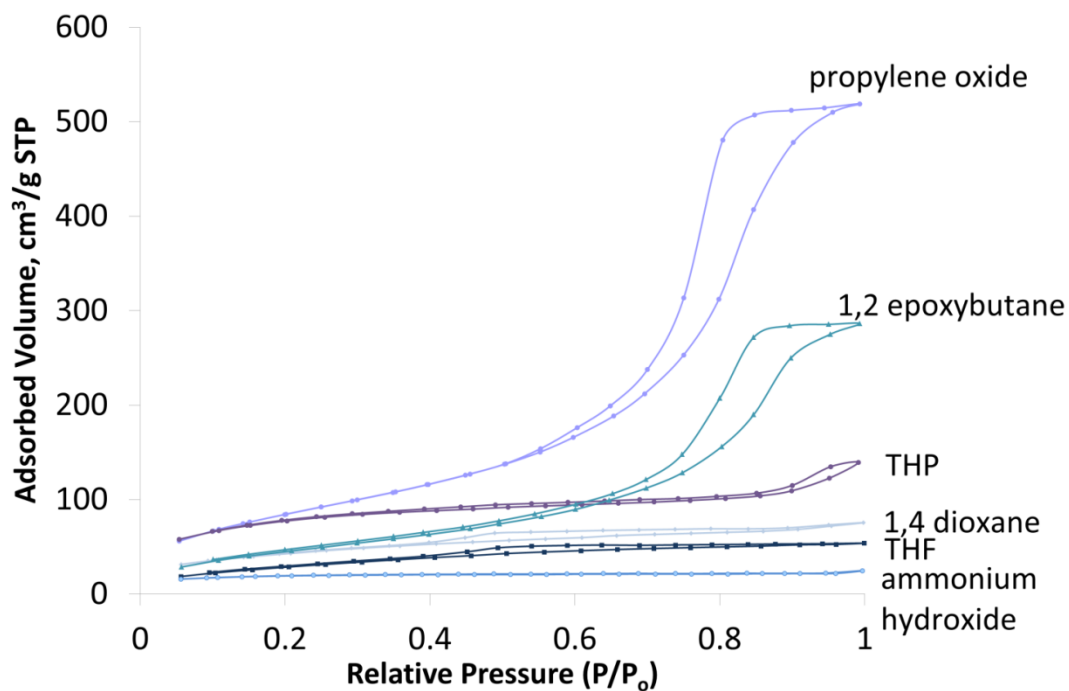


Figure 3.1. Nitrogen adsorption/desorption isotherms of Fe₂O₃ xerogels synthesized by using various proton scavengers

The sample prepared with ammonium hydroxide resulted with the smallest surface area and pore volume, because the ammonium hydroxide has stronger basicity compared to other proton scavengers. As a result, the rapid precipitation of Fe₂O₃ phase and crystallization process may lead to destruction of porous structure. However, the particle size, porosity, surface area and crystallinity of the iron oxide can be tailored by the synthesis conditions.

The samples prepared with 1,4 dioxane and THF have smaller pore size with a narrow pore size distribution as shown in Figure 3.2. Propylene oxide and THP have an enhancing effect on the surface area. The sample synthesized by propylene oxide has the

highest surface area and the sample synthesized by ammonium hydroxide has the lowest surface area.

The results show that mesoporous iron oxide xerogels with high surface area can be produced by sol-gel synthesis method and the structural properties can be tailored by changing the proton scavenger used to initiate the hydrolysis and condensation reaction of the precursor salt.

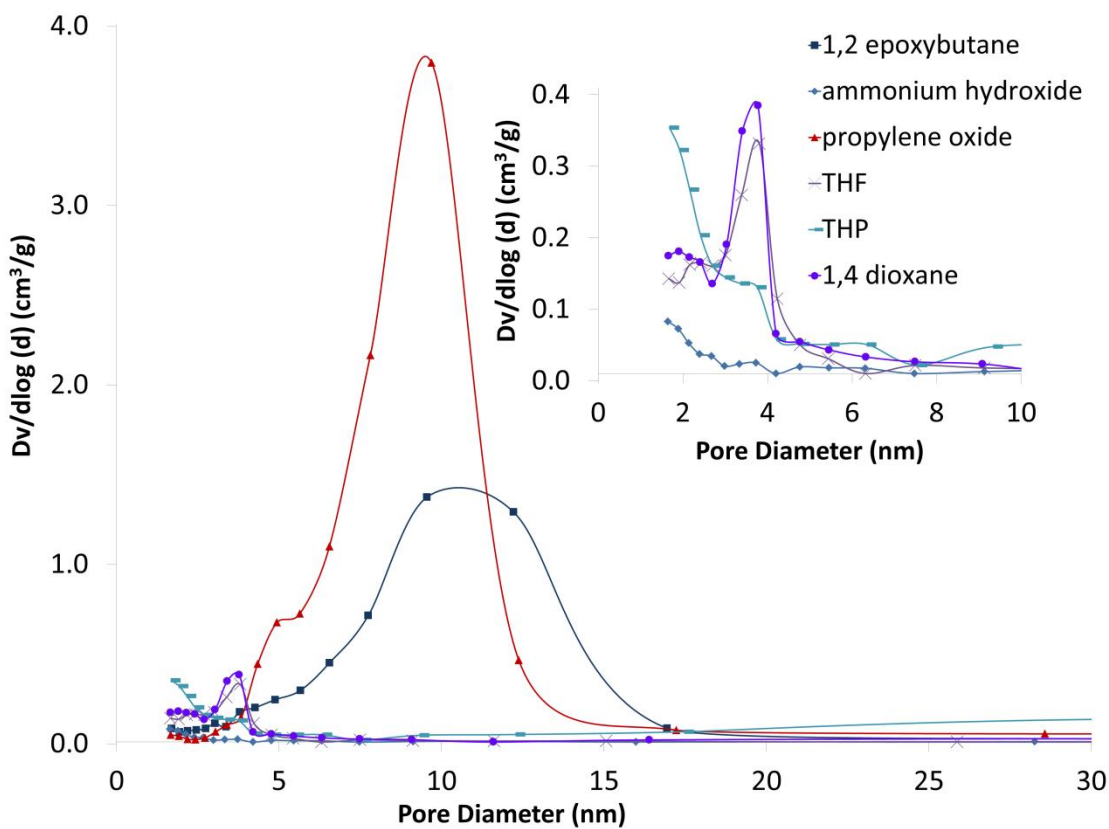


Figure 3.2. The pore size distributions of Fe_2O_3 xerogel synthesized various proton scavengers

3.1.2 Effect of the Drying Condition

In the scope of this study, the effect of solvent exchange and drying conditions on the textural properties were examined by N₂-BET method. The adsorption-desorption isotherms and pore size distribution of Fe₂O₃ samples are presented in Figure 3.3, Figure 3.4 and Table 3.2.

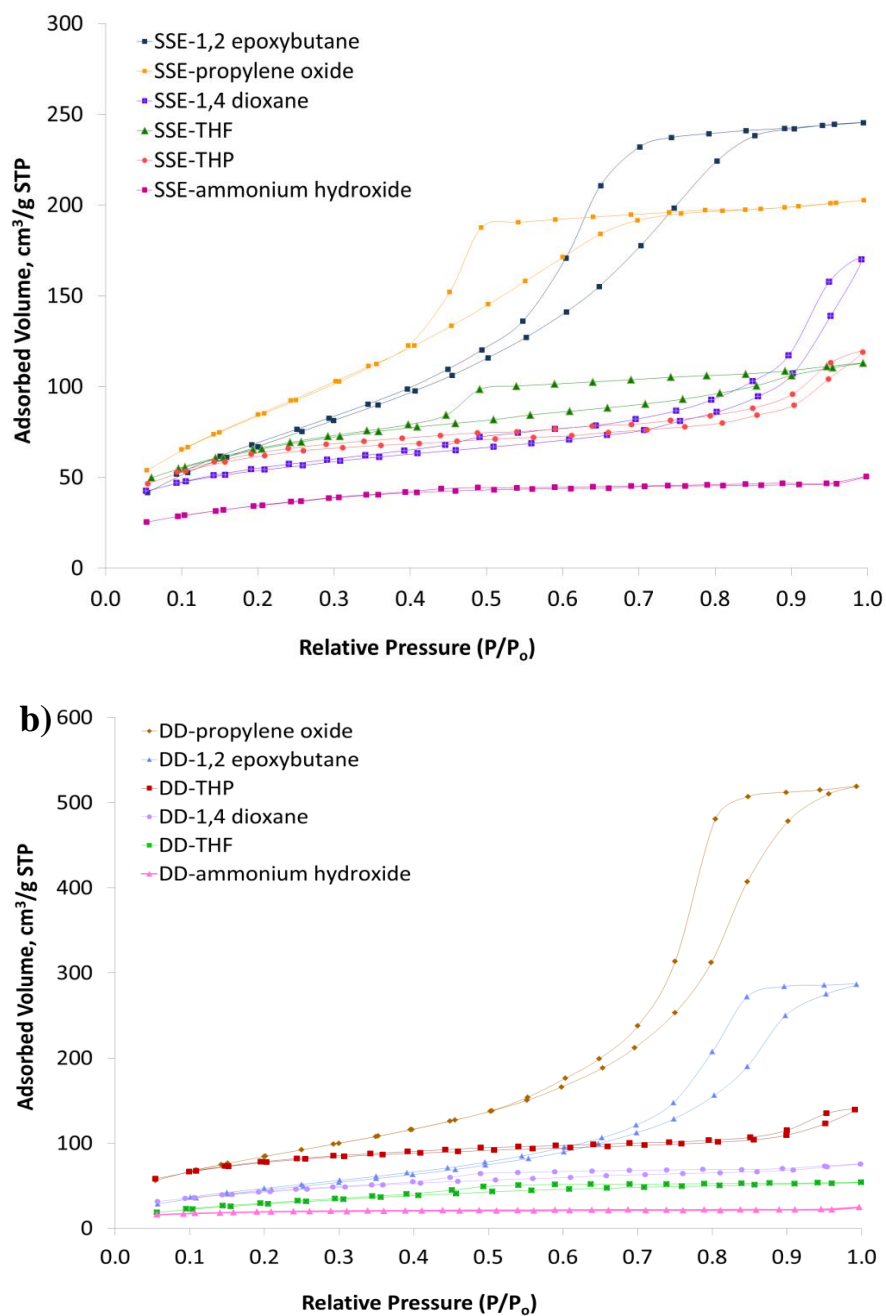


Figure 3.3. The Nitrogen adsorption/desorption isotherms of a) Sequential Solvent Dried (SSE) b) Direct Dried (DD) Fe_2O_3 samples synthesized with 1,2 epoxybutane, THF, THP, 1,4 dioxane, ammonium hydroxide and propylene oxide

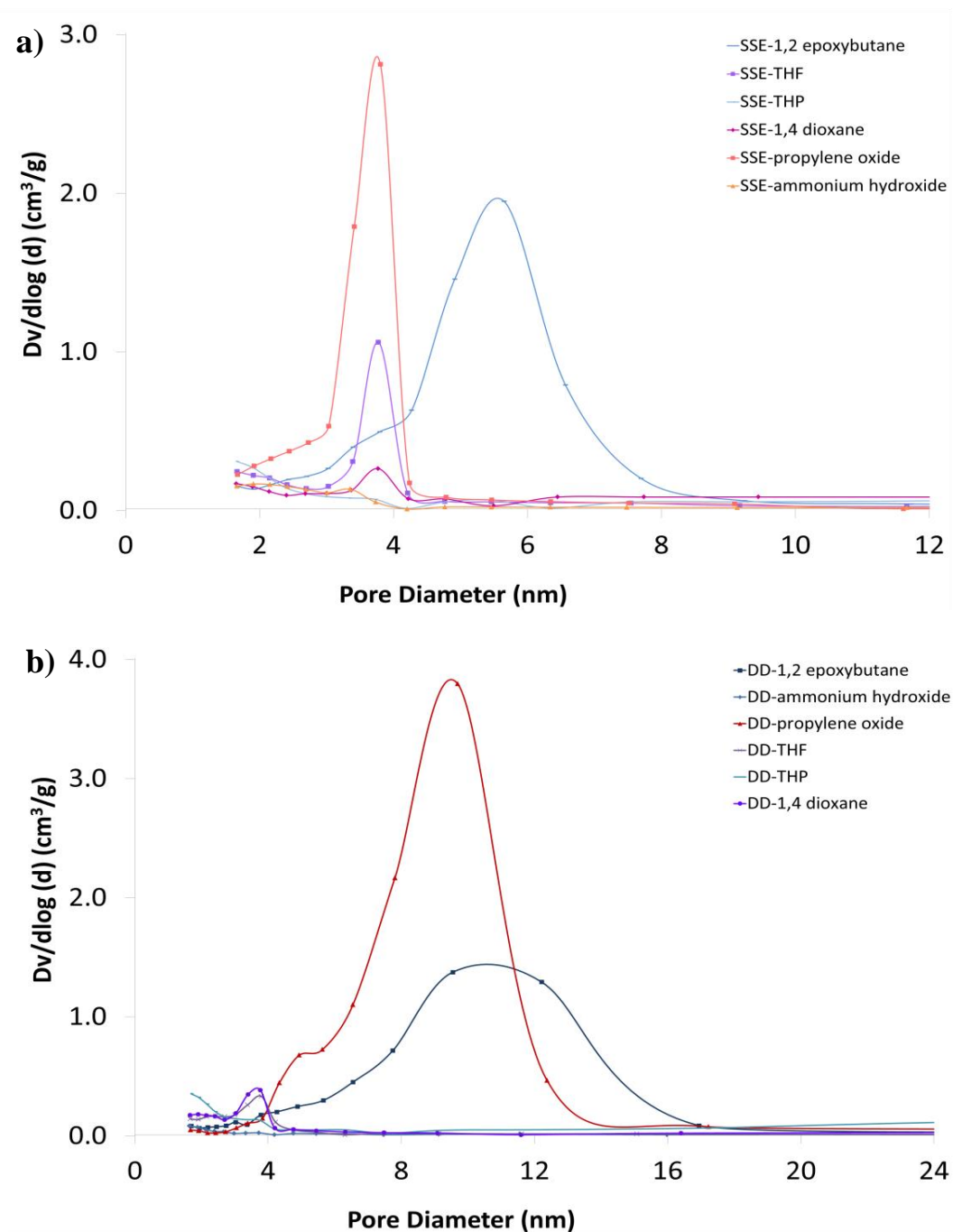


Figure 3.4. The pore size distributions of a) Sequential Solvent Dried (SSE) b) Direct Dried (DD) Fe_2O_3 samples synthesized with 1,2 epoxybutane, THF, THP, 1,4 dioxane, ammonium hydroxide and propylene oxide

The samples prepared by sequential solvent exchange method and direct drying method exhibit Type IV isotherm with a hysteresis loop which indicates the mesoporous structure [136, 137, 138]. The hysteresis loops over the relative pressure of 0.5 designate the presence of mesopores in the skeletal matrix. The hysteresis loops are observed where $0.4 < P/P_0 < 0.7$ for the samples prepared by direct drying method. For the samples prepared by sequential solvent exchange method, the loops are observed where $0.7 < P/P_0 < 0.9$. The presence of hysteresis loops in different regions of relative pressure for DD and SSE samples may be related with the differences in pore diameters of the mesoporous structures. The pore diameters of samples prepared by DD method vary between 1.6-9.7 nm while the pore diameters of samples prepared by SSE method vary between 1.6-5.6 nm.

The specific surface area, pore volumes and average pore diameter of the iron oxide samples prepared by direct drying method vary between 67-321 m^2/g , 0.022-0.878 cc/g and 1.646-9.697 nm, respectively. On the other hand, the specific surface area and the pore volume of the samples prepared by sequential solvent exchange are generally higher than the samples prepared by direct drying method. The specific surface area, pore volumes and average pore diameter of the iron oxide samples prepared by sequential solvent exchange vary between 123-330 m^2/g , 0.063-0.432 cc/g and 1.654-5.653 nm, respectively. The wide range of the surface area can be explained by the different mechanisms, which follow through during the gelation process, depending on the proton scavenger used.

Table 3.2. The Surface Area, Pore Size and Pore Volume of Fe₂O₃ Compositions

| Proton Scavenger | Surface Area (m ² /g) | | Pore Volume* (cc/g) | | Average pore diameter* (nm) | |
|--------------------|----------------------------------|-------|---------------------|-------|-----------------------------|-------|
| | DD | SSE | DD | SSE | DD | SSE |
| 1,2 epoxybutane | 176.2 | 267.6 | 0.462 | 0.432 | 9.553 | 5.653 |
| THF | 109.1 | 231.7 | 0.087 | 0.179 | 3.804 | 3.776 |
| THP | 279.7 | 214.2 | 0.161 | 0.138 | 1.683 | 1.656 |
| 1,4 dioxane | 150.9 | 190.5 | 0.103 | 0.427 | 3.406 | 1.654 |
| Ammonium hydroxide | 67.1 | 123.3 | 0.022 | 0.063 | 1.646 | 1.664 |
| Propylene oxide | 321.0 | 330.2 | 0.878 | 0.365 | 9.697 | 3.805 |

* The pore volumes and the average pore diameter were obtained from nitrogen desorption isotherms by the BJH theory.

The results show that the iron oxide samples synthesized by sol-gel method are in the xerogel form having mesoporous structures except the samples synthesized using ammonium hydroxide and subjected to direct drying method. The evaporation of the ethanol and other volatiles from the gel sample by direct drying leads to the excessive capillary forces on the gel's pore structure and these capillary forces result in shrinkage of the gel matrix. Besides, the solvent removal rate and drying is favored by the presence of non polar solvent and the porous structure is preserved after drying at 90°C.

The sample prepared with ammonium hydroxide resulted with the smallest surface area and pore volume, because the ammonium hydroxide has stronger basicity compared to other proton scavengers. As a result, the rapid precipitation of Fe_2O_3 phase and crystallization process may lead to destruction of porous structure. However, the particle size, porosity, surface area and crystallinity of the iron oxide can be tailored by the synthesis and drying conditions.

3.1.3 Effect of the Concentration of Precursor Solution

In the scope of this study, the effect of the concentration of the precursor (iron nitrate nonahydrate ($\text{Fe}(\text{NO}_3)_3 \cdot 9\text{H}_2\text{O}$)) solution on the textural properties of the iron oxide samples which were synthesized with 1,2 epoxybutane, THP and propylene oxide were examined by N_2 -BET method. The adsorption-desorption isotherms and pore size distribution of Fe_2O_3 samples are presented in Figure 3.5, Figure 3.6 and Table 3.3.

The samples prepared with diluted (1.5 g of ($\text{Fe}(\text{NO}_3)_3 \cdot 9\text{H}_2\text{O}$) in 10.0 g of ethanol) and concentrated (4.0 g of ($\text{Fe}(\text{NO}_3)_3 \cdot 9\text{H}_2\text{O}$) in 5.0 g of ethanol) precursor solution exhibit Type IV isotherm with a hysteresis loop which indicates the mesoporous structure [136, 137, 138]. The hysteresis loops over the relative pressure of 0.5 designate the presence of mesopores in the skeletal matrix. The results show that the specific surface area and the pore volume of the samples prepared with concentrated precursor solution are higher than the samples prepared with diluted precursor solution. The changes in the surface area can be explained by the gelation mechanism, which follows through during the gelation process, depending on the concentration of the precursor solution used.

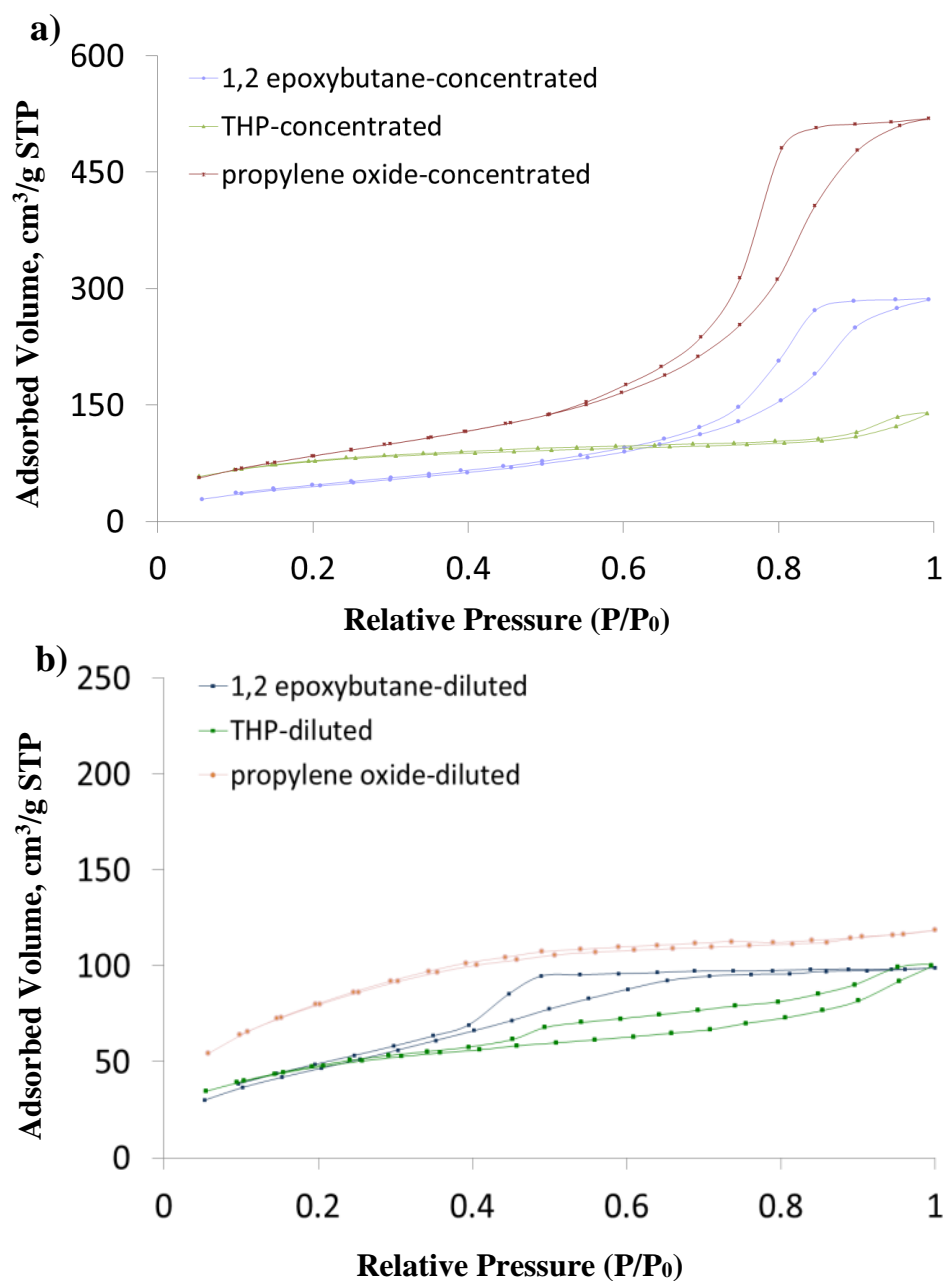


Figure 3.5. Nitrogen adsorption/desorption isotherms of DD Fe₂O₃ samples synthesized with 1,2 epoxybutane, THP and propylene oxide from a) concentrated b) diluted precursor solution

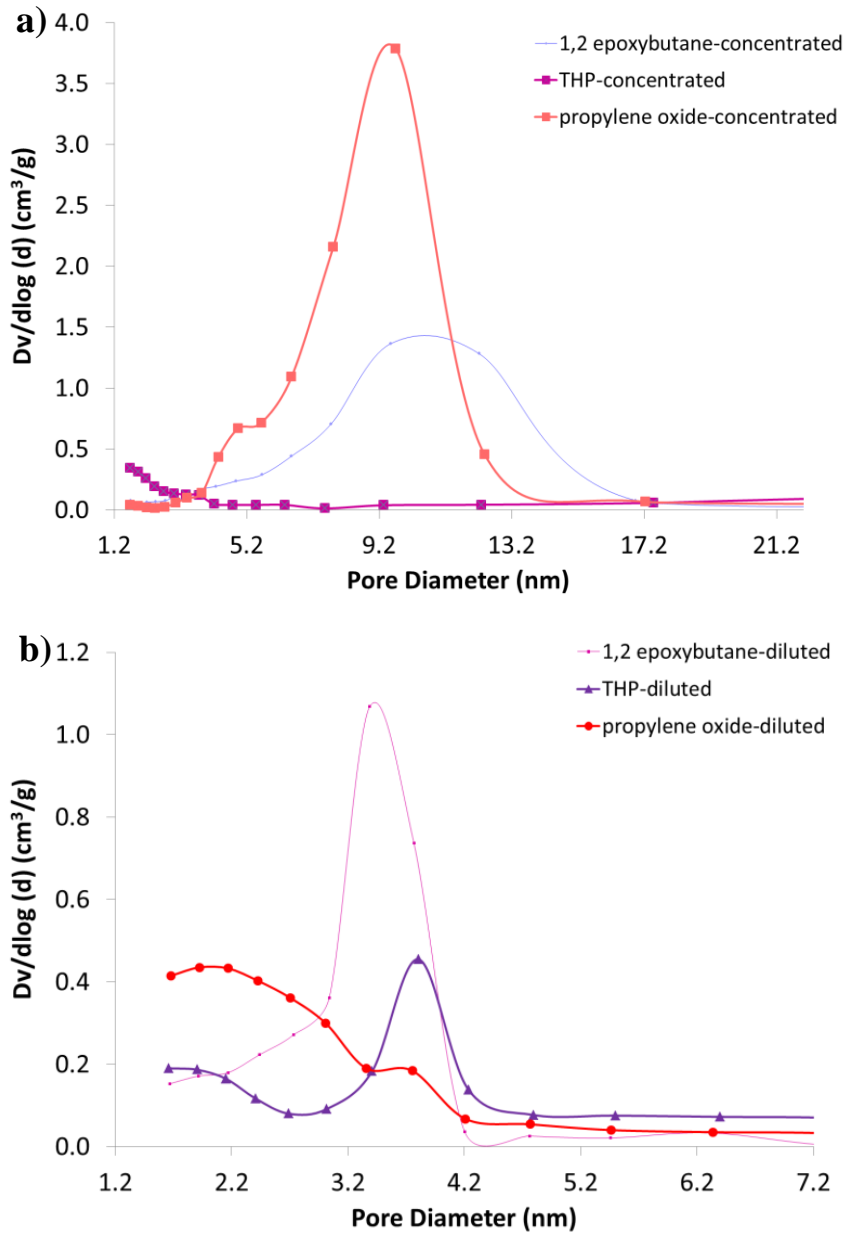


Figure 3.6. The pore size distributions of DD Fe₂O₃ samples synthesized with 1,2 epoxybutane, THP and propylene oxide from a) concentrated b) diluted precursor solution

Table 3.3 The Surface Area, Pore Size and Pore Volume of Fe₂O₃ Compositions

| Proton Scavenger | Surface Area (m ² /g) | | Pore Volume* (cc/g) | | Average pore diameter* (nm) | |
|------------------|----------------------------------|--------------|---------------------|--------------|-----------------------------|--------------|
| | diluted | concentrated | diluted | concentrated | diluted | concentrated |
| 1,2 epoxybutane | 178.9 | 176.2 | 0.169 | 0.493 | 3.388 | 9.553 |
| THP | 169.2 | 279.7 | 0.164 | 0.161 | 3.806 | 1.683 |
| Propylene oxide | 298.6 | 321.0 | 0.165 | 0.878 | 1.673 | 9.697 |

* The pore volumes and the average pore diameter were obtained from nitrogen desorption isotherms by the BJH theory.

3.2 X-ray Diffractometry (XRD)

X-ray diffraction analyses of iron oxide samples were performed to identify the effect of proton scavenger, solvent exchange, drying conditions and concentration of precursor solution on the lattice structures and the phases of iron oxide. In addition, the crystallite size was calculated based on the XRD patterns of SE and DD Fe₂O₃ samples using Scherrer equation.

3.2.1 Effect of Proton Scavenger

XRD patterns of iron oxide samples which were synthesized with various proton scavengers and were prepared by direct drying method are given in Figure 3.7.

XRD patterns of iron oxide samples synthesized with 1,2 epoxybutane, 1,4 dioxane, THP, THF and propylene oxide have broader peaks compared to those of iron oxide sample

synthesized with and ammonium hydroxide . The most intense peaks of the iron oxide samples synthesized with 1,2 epoxybutane, 1,4 dioxane, THP, THF and propylene oxide are mainly located in two broad bands of x-ray diffraction pattern. The intensity of these diffraction peaks is relatively smaller than the intensity of the diffraction peaks of iron oxide samples synthesized with ammonium hydroxide.

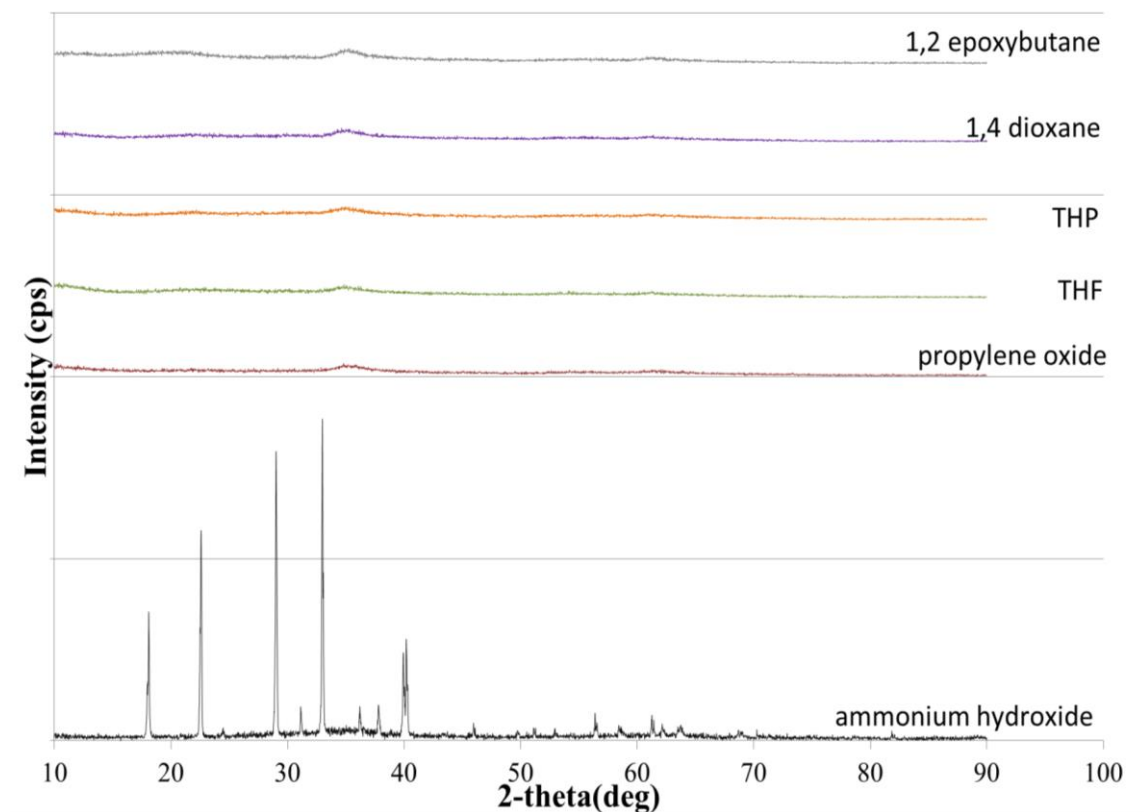


Figure 3.7. XRD patterns of iron oxide samples synthesized with 1,2 epoxybutane, 1,4 dioxane, THP, THF, propylene oxide and ammonium hydroxide

The broad peaks of the samples prepared with 1,2 epoxybutane, 1,4 dioxane, THP, THF and propylene oxide may be attributed to the structure of maghemite phase of $\gamma\text{-Fe}_2\text{O}_3$ with PDF card no 00-004-0755 of ICDD database as given in Figure 3.8.

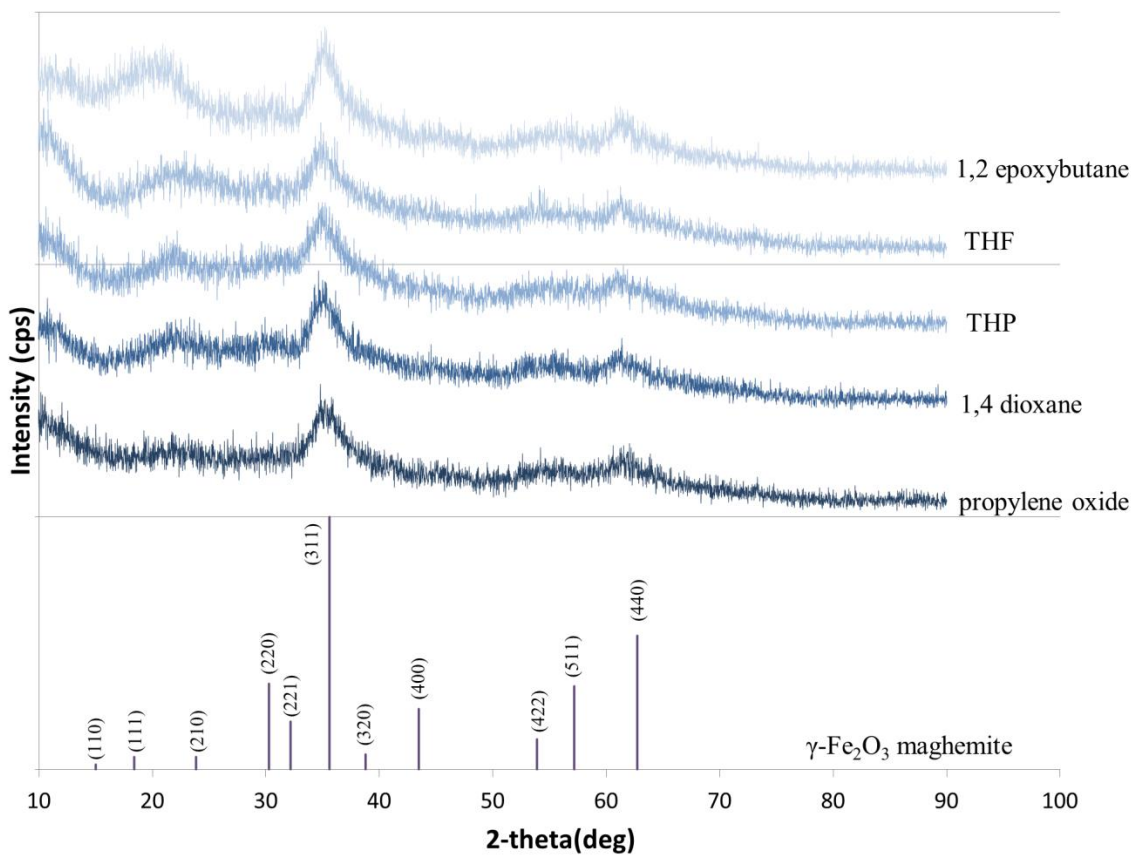


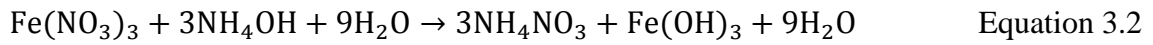
Figure 3.8. XRD patterns of iron oxide samples synthesized by 1,2 epoxybutane, THF, THP, 1,4 dioxane and propylene oxide with ICDD patterns for maghemite, $\gamma\text{-Fe}_2\text{O}_3$ (no. 00-004-0755)

Maghemite has cation vacancies which affect its crystallographic structure and the magnetic properties; therefore, the researches on maghemite have received great intention [47,48,49,50,51].

The spinel structure of $\gamma\text{-Fe}_2\text{O}_3$ maghemite consists of layers of tetrahedral and octahedral positions [47, 52] and Ferguson et al. [53] indicated that the octahedral sites of maghemite involve cation vacancies. These cation vacancies are important for the iron oxide which is used as oxidizer in the thermite compositions. The thermite reactions are based on the oxidation-reduction mechanism between the iron oxide and the fuel used in the compositions and the existence of these cation vacancies affect the structural properties of the iron oxide xerogels and as a result they also affect the thermite reaction mechanism [46]. Moreover the thermite reaction threshold is influenced by the changes in the crystal structure and the lattice defects of the iron oxide xerogel [139,140,141].

The peaks observed at $2\text{-theta}=20\text{deg}$ for samples prepared with 1,2 epoxybutane, 1,4 dioxane, THP, THF and propylene oxide (Figure 3.8) indicate super lattice structure with the ordering of cation vacancies in the maghemite crystal lattice which is specific to sol-gel synthesized samples. The intensity of these diffraction peaks was found to be relatively small presumably because of the lower crystallinity of the xerogel structure [47, 142, 143, 144, 145]. The given results above are consistent with Walker's studies [146] related with the iron oxide synthesis with weak bases such as propylene oxide and THF.

On the other hand, the XRD patterns of the sample synthesized with ammonium hydroxide are different from those of the samples synthesized with 1,2 epoxybutane, 1,4 dioxane, THP, THF and propylene oxide (Figure 3.8) as given in Figure 3.9. The sharp peaks of the sample synthesized with ammonium hydroxide may be attributed to the structure of residual ammonium nitrate, NH_4NO_3 . The presence of ammonium nitrate, $(\text{NH}_4)(\text{NO}_3)$, presumably arises from the reaction of free NO_3^- ions which are generated during the hydrolysis step of iron nitrate nonahydrate ($\text{Fe}(\text{NO}_3)_3 \cdot 9\text{H}_2\text{O}$) as given in the following equations:



The other peaks of the sample synthesized with ammonium hydroxide may be attributed to the maghemite phase of $\gamma\text{-Fe}_2\text{O}_3$ with PDF card no 00-004-0755 of ICDD database (Figure 3.9).

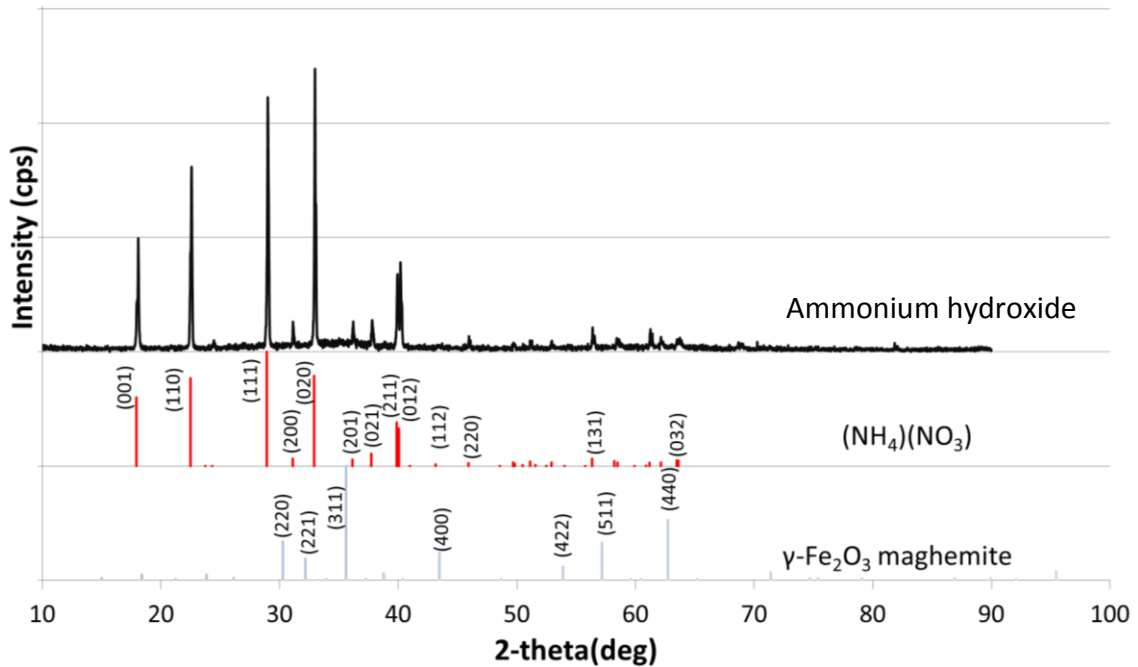


Figure 3.9. XRD patterns of Fe_2O_3 xerogel synthesized with ammonium hydroxide with ICDD patterns of $(\text{NH}_4)(\text{NO}_3)$ (no. 01-083-0520) and $\gamma\text{-Fe}_2\text{O}_3$ maghemite (no. 00-004-0755)

3.2.2 Effect of the Drying Condition

XRD patterns of iron oxide samples which were synthesized with various proton scavengers and were prepared by both direct drying and sequential solvent exchange methods are given Figure 3.10.

As mentioned in previous section, the peaks observed at $2\text{-theta}=20\text{deg}$ for samples synthesized with 1,2 epoxybutane, THF, THP, 1,4 dioxane and propylene oxide and prepared by both DD and SSE method indicate super lattice structure with the ordering of cation vacancies in the maghemite crystal lattice which is specific to sol-gel synthesized samples. The intensity of these diffraction peaks was found to be relatively small presumably because of the lower crystallinity of the xerogel structure [47, 142, 143, 143, 147].

XRD patterns of samples synthesized with ammonium hydroxide and prepared by direct drying and sequential solvent exchange method consist of similar sharp peaks attributed to the residual ammonium nitrate.

XRD patterns of samples synthesized by using 1,2 epoxybutane, THF, THP, 1,4 dioxane and propylene oxide and prepared by direct drying are very similar to those of samples obtained by sequential solvent exchange method except slight increase of peak intensity after sequential solvent exchange. It is hypothesized that the slight increase in peak intensity would be observed due to the slight growth in crystallite size as a result of Ostwald ripening phenomenon [148] during solvent exchange. Ostwald ripening can be described as the growth of the large particles on expense of the small particles in the

solution. The dissolving and deposition of small particle on the larger ones result in growth in crystallite size [148, 149].

The nano-scale structures of the iron oxide utilized as the oxidizer mean to achieve higher mass transport rate which is known as the controlling step of the combustion reactions of thermites.

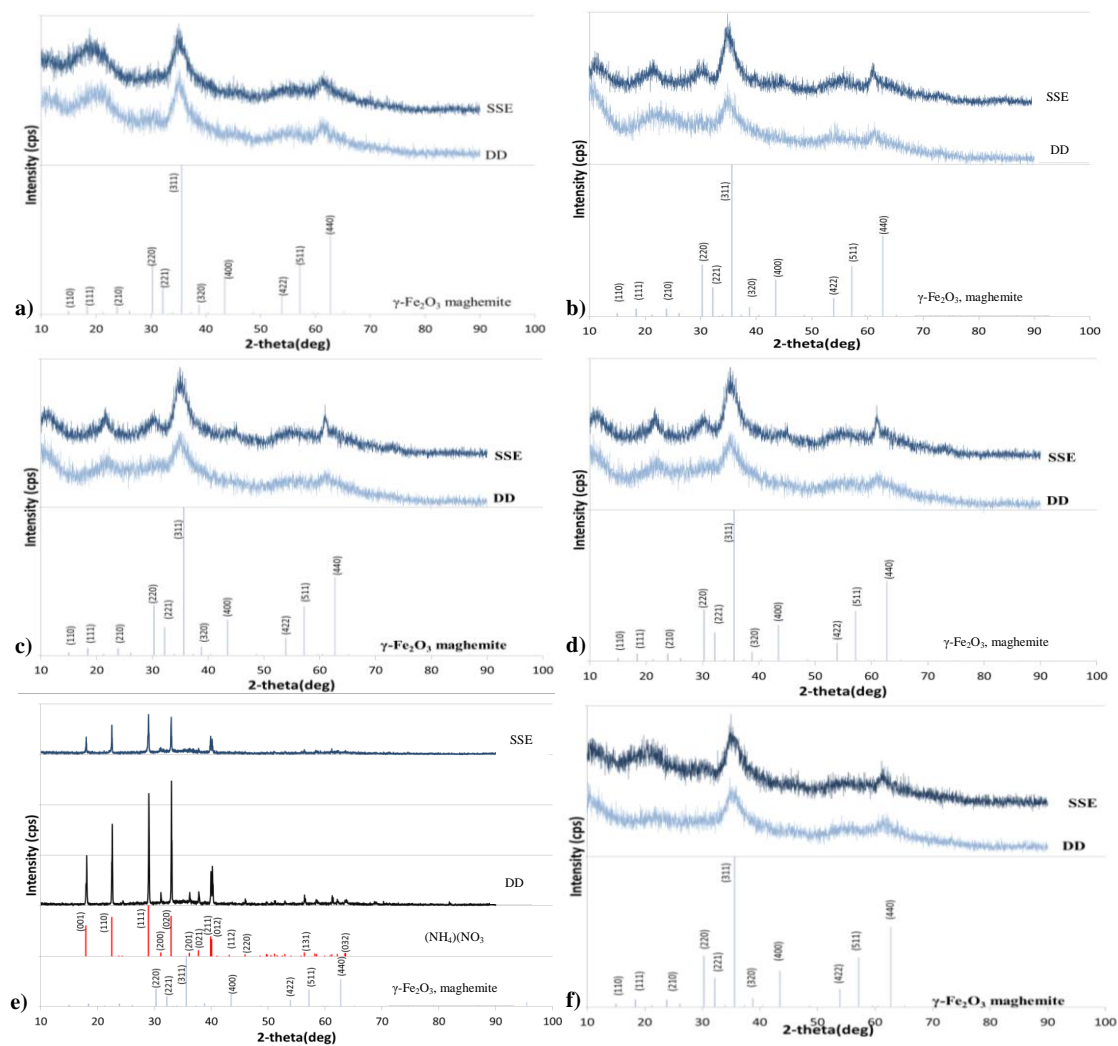


Figure 3.10. XRD patterns of Direct Dried (DD) and Sequential Solvent Exchange (SSE) Fe_2O_3 samples synthesized with a) 1,2 epoxybutane b) THF c) THP d) 1,4 dioxane e) ammonium hydroxide f) propylene oxide

Based on the XRD patterns of DD and SSE Fe₂O₃ samples synthesized with 1,2 epoxybutane, THF, THP, 1,4 dioxane and propylene oxide, the crystallite size, L, was calculated from (311) XRD peak which is common to γ -Fe₂O₃ (maghemite) using Scherrer equation [150, 151]:

$$L = \frac{K\lambda}{\beta \cos(\theta)} \quad \text{Equation 3.3}$$

where K is a constant related to crystallite shape (0.94), λ is the X-ray wavelength (0.15405 nm for CuK α), β is the full width at half maximum (FWHM) of (311) γ -Fe₂O₃ diffraction maximum in radians and θ is the diffraction angle. The calculated values on the basis of Scherrer equation were considered as preliminary measure of the crystallite sizes.

The crystallite sizes of SSE samples are slightly higher than those of DD samples according to the data evaluated by recalculating of FWHM value from the XRD patterns as given in Table 3.4. It is hypothesized that the higher peak intensity and crystallite size of SSE samples may be explained by the Ostwald ripening phenomenon [148, 149] during solvent exchange.

Table 3.4. Crystallite Sizes on the Basis of Scherrer Analysis of (311) XRD peaks

| Proton Scavenger | Crystallite Size* | | Crystallite Size | | 2θ for (311) peak (deg) | |
|------------------|-------------------|-----|------------------|-----|-------------------------|-------|
| | (nm) | | (nm) | | | |
| | DD | SSE | DD | SSE | DD | SSE |
| 1,2 epoxybutane | 3.5 | 3.6 | 3.0 | 1.1 | 35.78 | 34.66 |
| THF | 3.0 | 3.2 | 1.3 | 3.3 | 35.37 | 34.83 |
| THP | 3.0 | 3.0 | 3.2 | 3.0 | 34.75 | 34.52 |
| 1,4 dioxane | 3.5 | 3.7 | 2.9 | 3.1 | 34.94 | 35.14 |
| Propylene oxide | 2.9 | 2.9 | 2.4 | 3.0 | 35.76 | 34.94 |

* These data were evaluated by recalculating of full width at half maximum (FWHM) value from the XRD patterns rather than getting directly from the XRD measurements.

3.2.3 Effect of the Concentration of Precursor Solution

XRD patterns of DD iron oxide samples which were synthesized by 1,2 epoxybutane, THP and propylene oxide starting with diluted and concentrated precursor ($\text{Fe}(\text{NO}_3)_3 \cdot 9\text{H}_2\text{O}$) solution are given in Figure 3.11.

Similar with the results in previous section, the peaks at $2\text{-}\theta=20\text{deg}$ for samples synthesized with 1,2 epoxybutane, THP and propylene oxide starting with both diluted and concentrated precursor solution indicate super lattice structure with the ordering of cation vacancies in the maghemite crystal lattice which is specific to sol-gel synthesized samples.

The intensity of these diffraction peaks was relatively small presumably due to the lower crystallinity of the xerogel structure [47, 142, 143, 144, 152].

XRD patterns of samples synthesized by using 1,2 epoxybutane, THP and propylene oxide from diluted precursor solution are very similar to those of samples obtained from concentrated precursor solution. Slight increase of peak intensity of the samples prepared from concentrated precursor solution can be explained by Ostwald ripening phenomenon [148, 149] during gelation step.

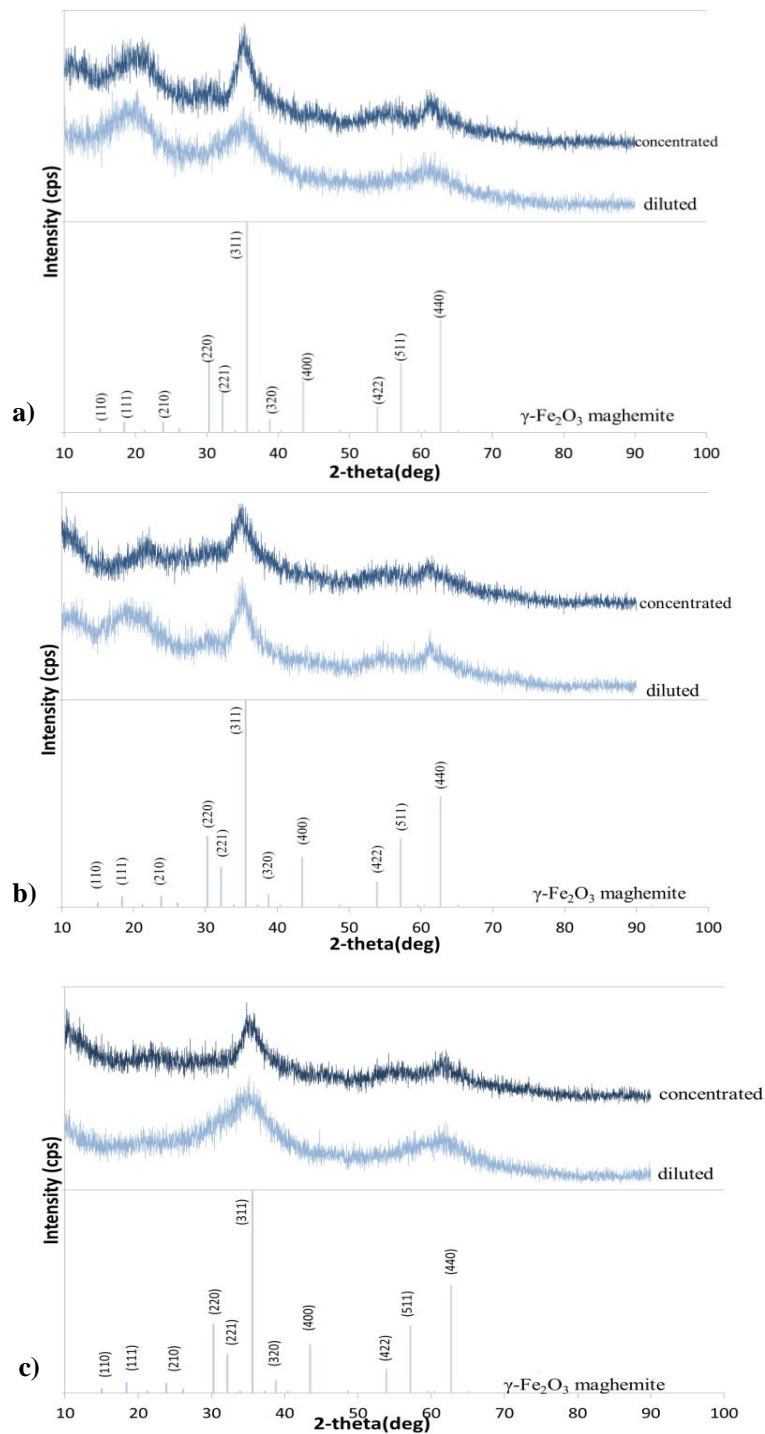


Figure 3.11. XRD patterns of DD Fe_2O_3 samples synthesized from diluted and concentrated precursor solution with a) 1,2 epoxybutane b) THP c) propylene oxide

3.3 FTIR Spectrum and Elemental Analysis

The iron oxide samples dried with sequential solvent exchange method was specifically selected and subjected to FTIR and CHN elemental analysis. The results are presented in the following sections.

3.3.1 FTIR Spectrum Analysis

FTIR spectra of Fe_2O_3 samples dried with SSE method are presented in Figure 3.12 a-f. The broad peaks of the SSE Fe_2O_3 samples, which were synthesized with 1,2 epoxybutane, THF, THP, 1,4 dioxane, propylene oxide and ammonium hydroxide, in the region of $3600\text{--}3000\text{ cm}^{-1}$ may be assigned to the stretching of surface hydroxyl groups. The peaks between $1664\text{ cm}^{-1}\text{--}1300\text{ cm}^{-1}$ may be related to the bending vibrations of H–O–H bonds and can be assigned to the water and the residuals. The peaks observed between $1124\text{--}1045\text{ cm}^{-1}$ for the samples synthesized with 1,2 epoxybutane, THF, THP, 1,4 dioxane and propylene oxide might be attributed to both stretching of the C–O bonds and bending of Fe–O bonds [153]. The bands which are in the range of 1000 cm^{-1} and 804 cm^{-1} may be assigned to the bending of –OH groups of iron oxyhydroxides. Considering the literature studies [154, 155, 156], the peaks between $670\text{--}500\text{ cm}^{-1}$ might be associated with the stretching of Fe–O bonds which may be related with iron oxides [153].

Additionally, the peaks observed between $2975\text{--}2875\text{ cm}^{-1}$ and $990\text{--}780\text{ cm}^{-1}$ for the SSE Fe_2O_3 samples synthesized with 1,2 epoxybutane and propylene oxide may be related to the stretching of C–H bonds as given in Figure 3.12 a and e. The peaks for the samples synthesized with ammonium hydroxide in the range of $3250\text{--}3000\text{ cm}^{-1}$ and $1000\text{--}800\text{ cm}^{-1}$ in Figure 3.12 f can be attributed to the NH_3 groups related with the ammonium nitrate which was generated during the hydrolysis step[157].

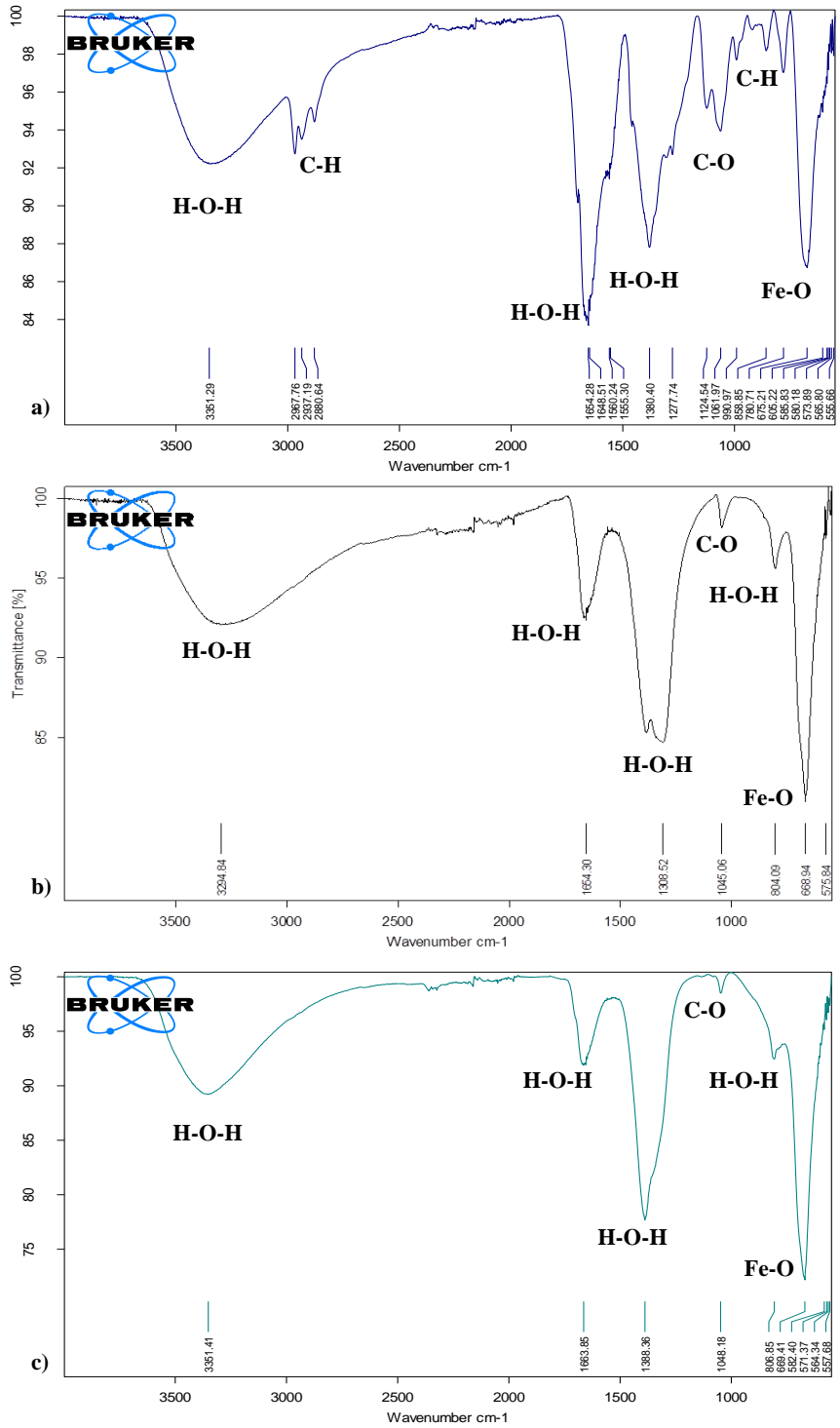


Figure 3.12. FTIR spectra of SSE Fe₂O₃ samples synthesized with a) 1,2 epoxybutane b) THF c) THP

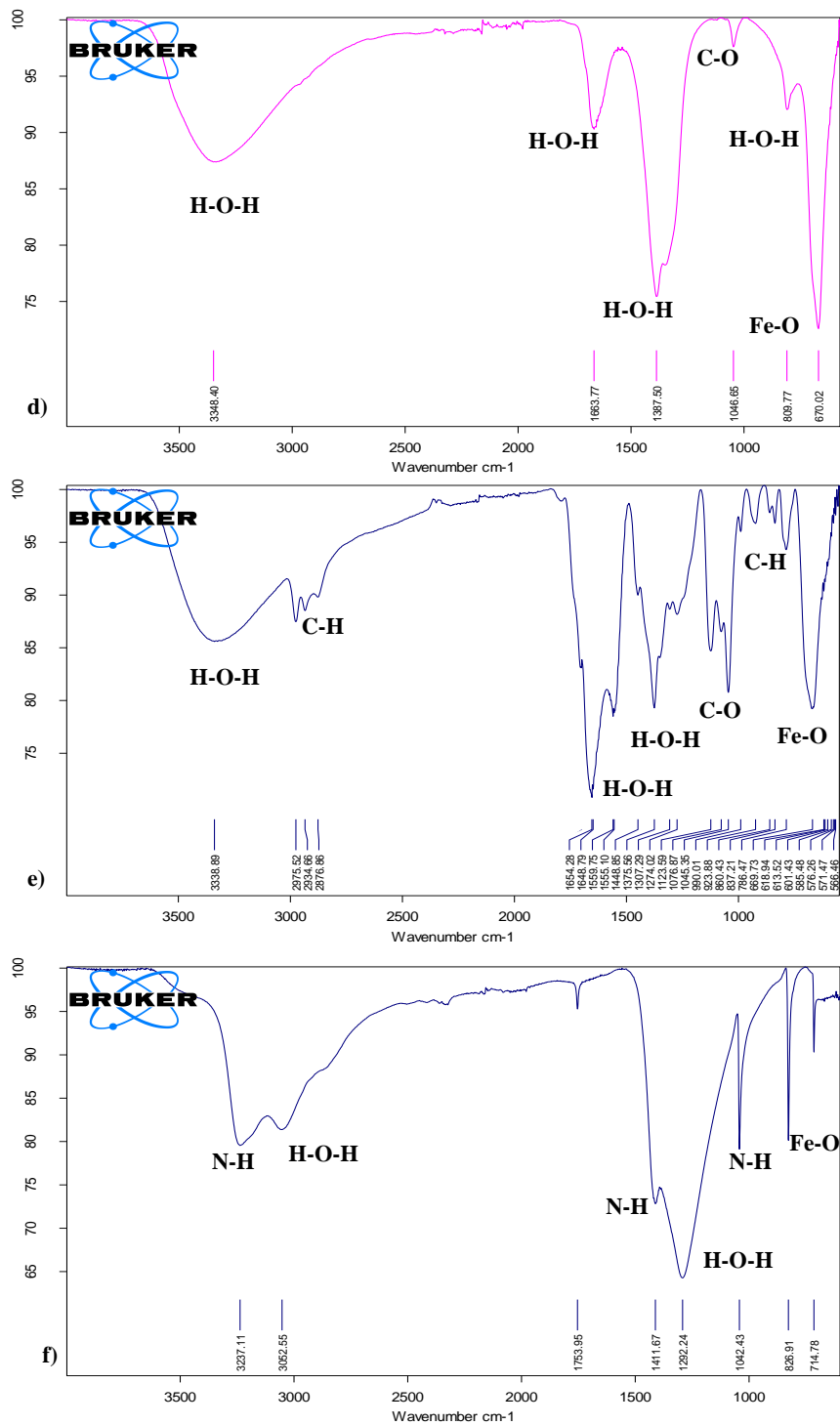


Figure 3.12 cont. FTIR spectra of SSE Fe₂O₃ samples synthesized with d) 1,4 dioxane e) propylene oxide f) ammonium hydroxide

3.3.2 Elemental Analysis

The iron oxide samples prepared with SSE method were subjected to CHN elemental analysis. The CHN elemental analysis results are presented in Table 3.5.

The elemental analysis indicates the presence of trace organic residues for SSE Fe₂O₃ samples synthesized with 1,2 epoxybutane, THF, THP, 1,4 dioxane, propylene oxide and ammonium hydroxide. The presence of N, presumably arises from the precursor, iron nitrate nonahydrate (Fe(NO₃)₃·9H₂O). In addition, Fe₂O₃ sample synthesized with ammonium hydroxide has the highest nitrogen content (wt %). It is presumably due to residual ammonium nitrate, NH₄NO₃, arises from the reaction of free NO₃⁻ ions which are generated during the hydrolysis step of iron nitrate nonahydrate (Fe(NO₃)₃·9H₂O) as given in previous sections in Equation 3.1 and 3.2.

The elemental analysis results are consistent with FTIR and TG/DSC results of SSE Fe₂O₃ samples indicating the presence of trace organic residues especially for those synthesized with propylene oxide, 1,2 epoxybutane and ammonium hydroxide.

Table 3.5. Mass percentage of C, H and N in Fe₂O₃ samples prepared with SSE method

| Proton Scavenger | C (wt%) | H (wt%) | N (wt%) |
|--------------------|---------|---------|---------|
| 1,2 epoxybutane | 15.67 | 3.39 | 1.21 |
| THF | 1.82 | 2.30 | 3.45 |
| THP | 1.68 | 2.11 | 2.89 |
| 1,4 dioxane | 1.11 | 2.26 | 3.32 |
| Propylene oxide | 20.04 | 3.93 | 0.65 |
| Ammonium hydroxide | 0.24 | 3.53 | 20.01 |

3.4 pH Study During Gel Formation

The change in pH and temperature during the gelation of Fe_2O_3 from $\text{Fe}(\text{NO}_3)_3 \cdot 9\text{H}_2\text{O}$ with propylene oxide was observed and measured in both ethanol and water medium. The change in pH during gelation process has an increasing trend in ethanol medium. It has been seen that the pH profile had a dramatic increase from 0.5 to 5.4 with time (Figure 3.13.a). It is probably explained by the addition of base (propylene oxide) and the consumption of H^+ ions formed in hydrolysis step which is explained in “1.2.3.3.1 The Gelation Mechanism”. The condensation step can be verified by the increase in temperature (Figure 3.13.a*). However, the process which was performed with distilled water has no evidence for gelation. The pH trend in Figure 3.13.b also supports this result quantitatively. The pH gradually rises from 1.0 to 1.7 and remains constant. The results given in Figure 3.13.b and b* are consistent with Gash et al. [83] and Walker’s [146] studies.

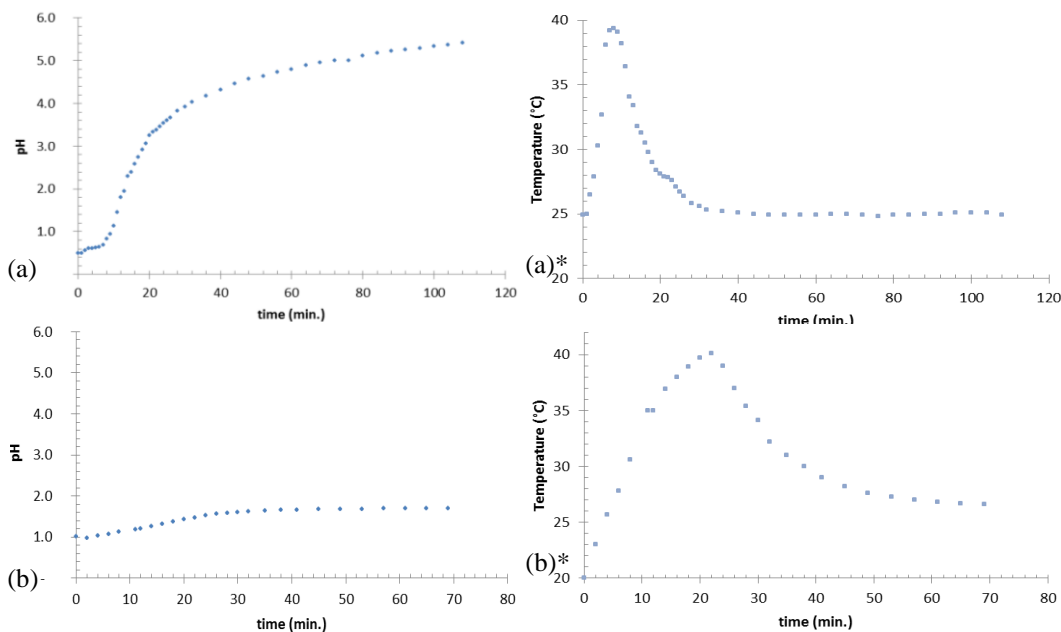


Figure 3.13. pH change during gelation in (a) ethanol medium (b) distilled water medium & Temperature change during gelation in (a)* ethanol medium (b)* distilled water medium

3.5 Thermal Analysis

The effect of proton scavenger, drying conditions, equivalence ratio and fuel type on the thermal behavior of thermite compositions were investigated.

3.5.1 Effects of Drying Condition and Proton Scavenger on the Thermal Behavior of 3FR B/Fe₂O₃ Thermite Compositions

The first exothermic events are observed above 850 °C for samples prepared by 1,2-epoxybutane. The exotherm of the SSE sample at 870 °C overlaps with an addition peak which is slightly higher than 950°C. The total heat output of DD sample is 243.3 J/g while the total heat output of SSE sample is 354.6 J/g as given in Table 3.6, Figure 3.14, Figure 3.15 and Figure 3.16.

It is observed that the first exotherm above 600°C for DD composition prepared by THF has a heat output of 166.3 J/g at 629.3°C while the first exotherm above 600°C of SSE sample has a heat output of 496.9 J/g at 667.0°C. When the results are compared for the exothermic events that take place above 600°C, it is shown that the onset temperatures of the exotherms of SSE sample are slightly higher than those of DD sample as given in Figure 3.14, Figure 3.15 and Figure 3.16. It is observed that the last exothermic event of SSE sample starts at 1188.9 °C with a heat output of 605.9 J/g and the last exothermic event of DD sample starts at 1100.7 °C with a heat output of 511.9 J/g. Another exotherm is observed which overlaps the last exothermic event for both SSE and DD samples. The onset temperature of this exotherm is 1302.6°C for SSE sample and 1203.6°C for DD sample. Similar to the results between 600-900 °C, the onset temperatures of the exothermic events above 1000 °C for SSE sample are slightly higher than those of DD sample.

The total heat output of DD sample is 967.8 J/g while the total heat output of SSE samples is 1188.7 J/g as given in Figure 3.14, Figure 3.15 and Figure 3.16.

The first exotherm above 600 °C for DD sample prepared with THP has a heat output of 316.1 J/g at 634.6 °C while the first exotherm above 600 °C of SSE sample has a heat output of 312.1 J/g at 631.6 °C. The second exotherm above 600 °C for DD sample has a heat output of 382.4 J/g at 845.7 °C while the second exotherm above 600 °C of SSE sample has a heat output of 426.4 J/g at 847.7 °C. An additional exotherm for DD sample is observed at 1078.3 °C with a heat output of 148.9 J/g. The last exothermic event of SSE sample starts at 1306.8 °C with a heat output of 553.6 J/g and the last exothermic event of DD sample starts at 1256.1 °C with a heat output of 261.0 J/g. When the results are compared for the exothermic events that take place between 800-1400 °C, it is shown that the onset temperatures of the exotherms of SSE sample are slightly higher than those of DD sample as given in Figure 3.14, Figure 3.15 and Figure 3.16. The total heat output of DD sample is 1133.5 J/g while the total heat output of SSE samples is 1311.8 J/g as given in Figure 3.14, Figure 3.15 and Figure 3.16.

The first exothermic event of DD sample prepared with 1,4-dioxane has a heat output of 185.9 J/g at 159.2 °C. It is observed that the exotherm above 600°C for DD composition has a heat output of 424.5 J/g at 867.7 °C which overlaps with the exotherm at 1046.7 °C while the first exotherm above 600°C of SSE sample has a heat output of 336.8 J/g at 639.3 °C and the second exotherm has a heat output of 329.4 J/g at 855.1 °C as given in Figure 3.14, Figure 3.15 and Figure 3.16. The total heat output of DD sample is 622.6 J/g while the total heat output of SSE samples is 718.1 J/g.

The sharp endothermic peaks are observed for DD samples prepared with ammonium hydroxide up to 250 °C as given in Figure 3.14, Figure 3.15 and Figure 3.16. The endothermic peaks between 50-150 °C correspond to the crystal transformation IV→III, III→II and II→I and the endothermic peaks above 150 °C may be related with the melting of residual ammonium nitrate [158, 159]. The ammonium nitrate phase NH_4NO_3 inside the structure may be produced during the gelation process with ammonium hydroxide according to the possible reactions given in Equation 1.13-1.15. The first exotherm is observed above 500°C for DD composition prepared by ammonium hydroxide with a heat output of 696.9 J/g at 542.7°C while the first exotherm for SSE sample is observed with a heat output of 631.6 J/g at 198.3°C. When the results are compared for the exothermic events that take place above 650°C, it is shown that the onset temperature and heat output of the exotherm of SSE sample are slightly higher than those of DD sample as given in Figure 3.14, Figure 3.15 and Figure 3.16. The last exothermic event of DD sample starts at 1095.7 °C with a heat output of 162.3 J/g which is not observed for SSE sample. The total heat output of DD sample is 961.6 J/g while the total heat output of SSE samples is 1006.7 J/g.

The onset temperatures of the SSE samples prepared by THF, THP, 1,4 dioxane and ammonium hydroxide are slightly higher than those of DD samples. Wang et al. [160] proposed that the thermite ignition is controlled by the transport of bound oxygen ions from the oxidizer and it is related with the internal structure of the oxidizer [161]. Therefore, the difference in the onset temperatures of SSE and DD iron oxide xerogels may be attributed to the slight difference in the structure, such as vacancies, defects and oxygen bonds.

The heat outputs of SSE samples are approximately 5-45% greater than the heat outputs of DD samples prepared by 1,2 epoxybutane, THF, THP, 1,4 dioxane and ammonium hydroxide as given in Table 3.6.

The enhancement of the heat output might be related with the textural properties of the samples which strongly depend on the drying conditions. Drying method affects the mechanism of extraction/evaporation of the solvent within the porous structure of gel.

The theoretical and experimental values of heat of reactions for the 3FR sequential solvent exchange and direct dried samples are shown in Table 3.6. The actual calorific values are approximately 15-65 % of the theoretical values.

It can be concluded that sequential solvent exchange method has an enhancing effect on the heat output due to the enhancement in the structure and the increase in the surface area and pore volume.

It is observed that the heat output not only depends on drying conditions but also strongly depends on the type of proton scavenger. The highest heat outputs are obtained with samples prepared by THP and THF.

Despite the lowest surface area of the sample prepared with ammonium hydroxide among the other samples, it provides enhancing effect on the heat output. It may be related with the ammonium nitrate obtained during the gelation process. It is known that ammonium

nitrate has an enhancing effect on heat output due to its behavior of strong oxidizing agent for boron powder.

On the other hand, the sample prepared with 1,2 epoxybutane has the highest surface area however 1,2 epoxybutane may inhibit the ignition conditions of the B/Fe₂O₃ by the reason of being more stable compared to other proton scavengers.

Table 3.6. DSC Data for 3FR B/Fe₂O₃ nanothermites

| Proton Scavenger | 1,2 epoxybutane | | THF | | THP | | 1,4 dioxane | | Ammonium hydroxide | |
|--------------------------------|-----------------|--------------|--------------|---------------|---------------|---------------|--------------|--------------|--------------------|---------------|
| | DD | SSE | DD | SSE | DD | SSE | DD | SSE | DD | SSE |
| Onset Temp.1 (°C) | - | - | 238.2 | - | 271.6 | 306.3 | 159.2 | - | - | 198.3 |
| Onset Temp.2 (°C) | - | - | - | - | - | - | - | - | - | 455.2 |
| Onset Temp.3 (°C) | - | - | 629.3 | 667.0 | 634.6 | 631.6 | 572.9 | 639.3 | 542.7 | 642.6 |
| Onset Temp.4 (°C) | 950.6 | 873.4 | 848.7 | 870.0 | 845.7 | 847.7 | 867.7 | 855.1 | 851.9 | 864.5 |
| Onset Temp. 5 (°C) | 1132.7 | 1117.9 | 1100.7 | 1188.9 | 1078.3 | - | 1046.7 | - | 1095.7 | - |
| Onset Temp. 6 (°C) | - | - | 1203.6 | 1302.6 | 1256.1 | 1306.8 | - | 1214.7 | - | - |
| Heat Output 1 (J/g) | - | - | 78.7 | - | 25.1 | 19.7 | 185.9 | - | - | 631.6 |
| Heat Output 2 (J/g) | - | - | - | - | - | - | - | - | - | 86.6 |
| Heat Output 3 (J/g) | - | - | 166.3 | 496.9 | 316.1 | 312.1 | 12.2 | 336.8 | 696.6 | 82.8 |
| Heat Output 4(J/g) | 12.5 | 206.5 | 210.9 | 85.9 | 382.4 | 426.4 | 424.5 | 329.4 | 102.7 | 205.7 |
| Heat Output 5 (J/g) | 230.8 | 148.1 | 511.9 | 605.9 | 148.9 | - | - | - | 162.3 | - |
| Heat Output 6 (J/g) | - | - | - | - | 261.0 | 553.6 | - | 51.9 | - | - |
| Total Heat Output (J/g) | 243.3 | 354.6 | 967.8 | 1188.7 | 1133.5 | 1311.8 | 622.6 | 718.1 | 961.6 | 1006.7 |
| Theoretical Value (J/g) | 1977 | | | | | | | | | |

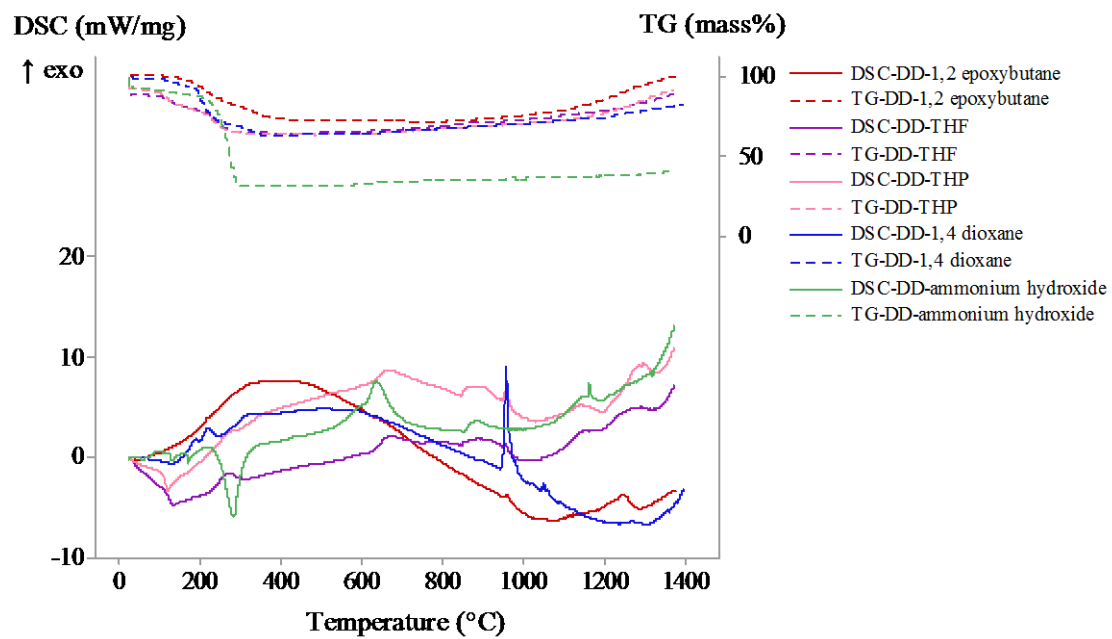


Figure 3.14. DSC and TG plots as a function of temperature for DD 3FR B/ Fe_2O_3 samples synthesized with 1,2 epoxybutane, THF, THP, 1,4 dioxane and ammonium hydroxide

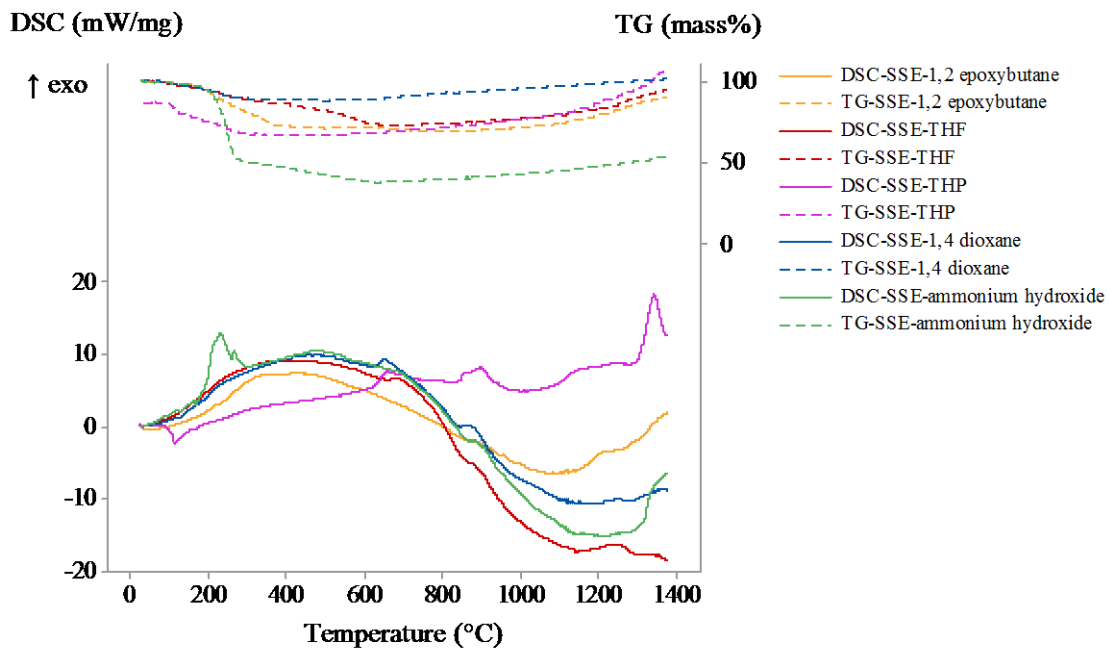


Figure 3.15. DSC and TG plots as a function of temperature for SSE 3FR B/Fe₂O₃ samples synthesized with 1,2 epoxybutane, THF, THP, 1,4 dioxane and ammonium hydroxide

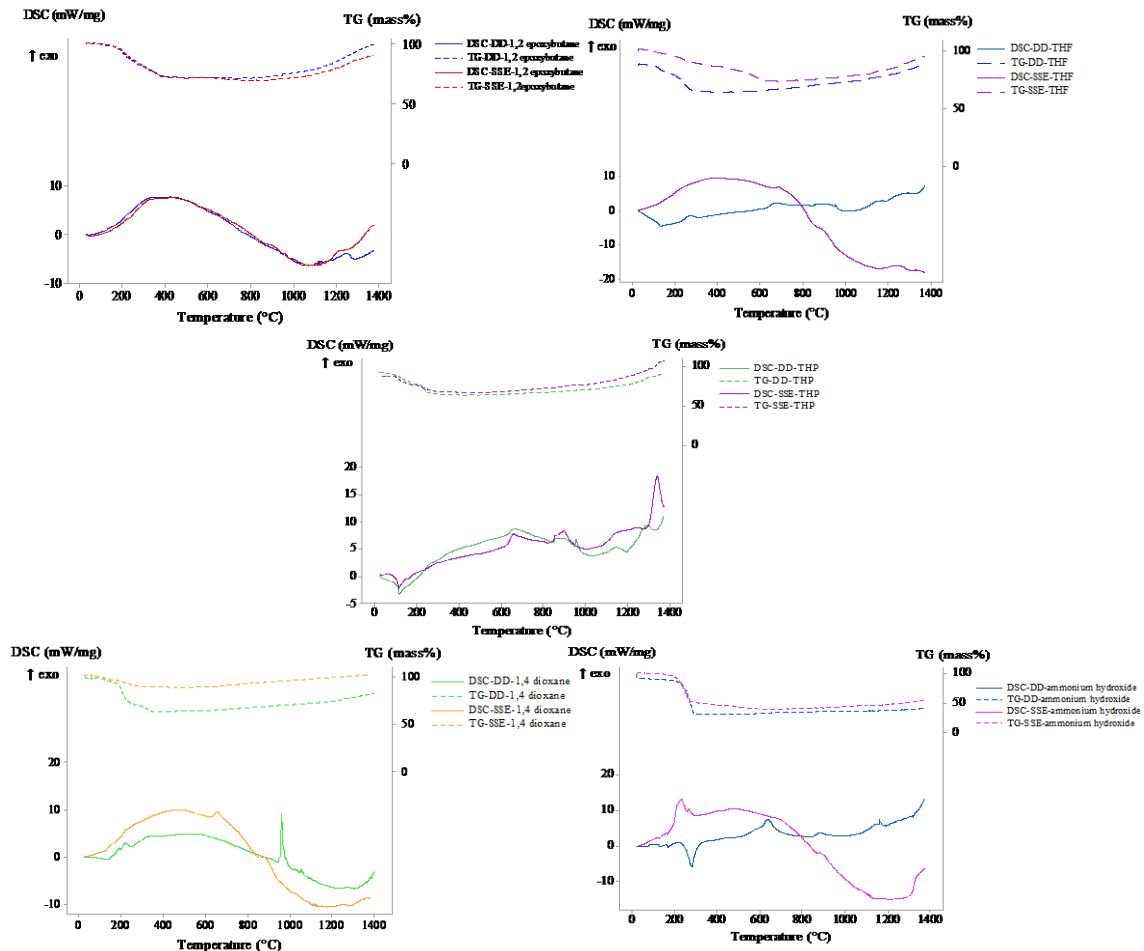


Figure 3.16. DSC and TG plots as a function of temperature for DD&SSE* 3FR B/Fe₂O₃ samples synthesized with 1,2 epoxybutane, THF, THP, 1,4 dioxane and ammonium hydroxide

3.5.2 Effect of Equivalence Ratio on the Thermal Behavior of B/Fe₂O₃ Thermite Compositions

The effect of equivalence ratio was examined by comparing the heat flow curves of B/Fe₂O₃ samples, synthesized by 1,2 epoxybutane, THF, THP, 1,4 dioxane, ammonium hydroxide and propylene oxide, where the fraction of fuel in sample (equivalence ratio) is increased from 3 (FR3) to 9 (FR9).

The samples exhibit a number of exothermic processes at a temperature range of 200-1400°C which might be associated with the oxidation reaction of B with Fe₂O₃. The observed peaks of exothermic events for these compositions are broad and weak as given in Table 3.7, Figure 3.17 and Figure 3.18. The onset temperatures of these exothermic reactions slightly increase with increasing equivalence ratio.

The broad and weak exothermic event has a heat output of 243.3 J/g with an onset temperature of 950 °C, 201.6 J/g with an onset temperature above 1200 °C, 194.2 J/g with an onset temperature above 1100 °C for 3FR, 6FR and 9FR B/Fe₂O₃ synthesized by 1,2 epoxybutane, respectively (Figure 3.17).

It is realized that the first exothermic event above 600°C for 3FR B/Fe₂O₃ synthesized by THF has a heat output of 166.3 J/g at 629.3 °C and the first exotherm above 600°C for 6FR composition has a heat output of 128.8 J/g at 630.2°C and 79.1 J/g at 631.2°C for 9FR composition (Figure 3.17). The heat output of the first exotherm of 9FR composition was found to be half of the value of 3FR composition. The heat output trend of exothermic events around 850°C of the samples is similar with the previous exothermic events; again, since the value of 9FR composition is smaller than that of 3FR composition. These

exothermic peaks of 3FR and 9FR are observed at 848.7°C and 847.3°C, respectively. The last exothermic event of 3FR composition starts at 1100.7°C overlapping with the exotherm at 1203.6 °C with a heat output of 511.9 J/g. The last exotherm of 6FR and 9FR composition starts at 1107.8°C overlapping with the exotherm at 1219.9 °C and 1159.2°C overlapping with the exotherm at 1218.1 °C, respectively, which are higher than the onset temperature of 3FR. The heat outputs of the third exotherms for 6FR and 9FR composition are 492.7 J/g and 91.5 J/g, which are smaller compared to the heat output of 3FR composition. The total energy release of the samples was determined as 967.8 J/g, 690.8 J/g and 392.8 J/g for 3FR, 6FR and 9FR compositions, respectively. As expected, lower heat release per unit mass of sample was determined for more fuel rich composition under inert atmosphere. The reaction between B and Fe₂O₃ is suggested as given in Equation 2.1. The actual calorific values are between 30-50% of the theoretical values (Table 3.7) depending on the equivalence ratio indicating the incomplete reaction.

For the samples prepared with THP, the first exothermic event above 600°C for 3FR has a heat output of 316.1 J/g at 634.6 °C and the first exotherm above 600°C for 6FR composition has a heat output of 631.7 J/g at 638.1°C and 232.8 J/g at 637.6°C for 9FR composition (Figure 3.17). The heat output of exothermic events around 850°C has a decreasing trend with increasing equivalence ratio. These exothermic peaks of 3FR, 6FR and 9FR are observed at 845.7°C, 846.3°C and 840.9°C, respectively. The last exothermic events start at 1078.3°C, 1103.8°C and 1163.9°C, with heat outputs of 148.9 J/g, 27.5 J/g and 14.8 J/g for 3FR, 6FR and 9FR. An additional exotherm is observed for 3FR composition which starts at 1256.1°C with a heat output of 261.0 J/g. The total energy release of the samples was determined as 1133.5 J/g, 940.3 J/g and 500.3 J/g for 3FR, 6FR and 9FR compositions, respectively. As expected, lower heat release per unit mass of sample was determined for more fuel rich composition under inert atmosphere. The actual calorific values are between 40-60% of the theoretical values (Table 3.7) depending on the equivalence ratio indicating the incomplete reaction.

It is observed that 3FR B/Fe₂O₃ sample prepared with 1,4 dioxane has an exothermic event at 159.2 °C with a significant heat output of 185.9 J/g compared to other samples. 6FR and 9FR compositions have very weak exotherms and the highest heat output values of 167.3 J/g and 75.6 J/g are observed at 642.8 °C and 643.6 °C (Figure 3.18). 3FR composition has a sharp exothermic peak which starts at 867.7 °C with a heat output of 424.5 J/g. It seems that the most suitable formulation for the samples prepared with 1,4 dioxane is 3FR. The total heat output of the samples was determined as 622.6 J/g, 341.1 J/g and 235.6 J/g for 3FR, 6FR and 9FR compositions, respectively. Similar to previous results, lower heat release per unit mass of sample was determined for more fuel rich composition under inert atmosphere. The actual calorific values are between 20-30% of the theoretical values (Table 3.7) depending on the equivalence ratio indicating the incomplete reaction.

The sharp endothermic peaks are observed for 3FR, 6FR and 9FR samples prepared with ammonium hydroxide up to 250 °C (Figure 3.18). The endothermic peaks between 50-150 °C correspond to the crystal transformation IV→III, III→II and II→I and the endothermic peaks above 150 °C may be related with the melting of residual ammonium nitrate [158, 159]. The first exotherm is observed above 500°C for 3FR composition with a heat output of 696.9 J/g at 542.7°C while the first exotherm for 6FR and 9FR compositions are observed with a heat output of 74.8 J/g and 44.5 J/g at 611.3 °C and 614.1 °C. When the results are compared for the exothermic events that take place above 1000°C, it is observed that the onset temperature increases with increasing equivalence ratio similar to the exotherms around 500 °C.

The total energy release of the samples was determined as 961.6 J/g, 809.6 J/g and 481.6 J/g for 3FR, 6FR and 9FR compositions. Similar to previous results, lower heat release per unit mass of sample was determined for composition with higher equivalence ratio

under inert atmosphere. The actual calorific values are between 40-50% of the theoretical values (Table 3.7) depending on the equivalence ratio indicating the incomplete reaction.

The samples prepared with propylene oxide have a broad and very weak exotherms between 500°C and 1400°C (Figure 3.18). DSC curves demonstrate two broad exothermic events which might be associated with the thermite reaction of B and Fe₂O₃ with the onset temperatures of 533.6°C and 621.0°C with a heat release of 620.0 J/g and 561.6 J/g for 6FR and 9FR compositions, respectively. The second broad exotherm starts at 1083.8 °C with a heat output of 612.9 J/g for 6FR, while the second broad exotherm of 9FR starts at 1086.0 °C with a heat output of 440.5 J/g. The total energy release of broad exotherms is found to be 1232.9 J/g and 1002.1 J/g for 6FR and 9FR compositions, respectively. The results show that 6FR composition ignited at slightly lower temperatures with a higher heat output which makes it a good candidate for the formulation of B/Fe₂O₃ nanocomposites prepared with propylene oxide. Besides, 3FR composition prepared with propylene oxide was not subjected to thermal tests due to the ignition failure during calorific value tests, which means it is not a suitable formulation for an energetic composition. Lower heat release per unit mass of sample was obtained for composition with higher equivalence ratio under inert atmosphere. The actual calorific values are about 80% of the theoretical values (Table 3.7).

Table 3.7. DSC Data for DD B/Fe₂O₃ nanothermites

| Proton Scavenger | 1,2 epoxybutane | | | THF | | | THP | | |
|-------------------------|-----------------|--------|--------|--------|--------|--------|--------|--------|--------|
| | 3FR | 6FR | 9FR | 3FR | 6FR | 9FR | 3FR | 6FR | 9FR |
| Onset Temp.1 (°C) | - | - | - | 238.2 | 213.7 | 219.4 | 271.6 | 212.4 | 264.9 |
| Onset Temp.2 (°C) | - | - | - | 629.3 | 630.2 | 631.2 | 634.6 | 638.1 | 637.6 |
| Onset Temp.3 (°C) | 950.6 | - | - | 848.7 | 848.0 | 847.3 | 845.7 | 846.3 | 840.9 |
| Onset Temp.4 (°C) | 1132.7 | - | 1113.2 | 1100.7 | 1107.8 | 1159.2 | 1078.3 | 1103.8 | 1163.9 |
| Onset Temp. 5 (°C) | - | 1223.1 | - | 1203.6 | 1219.9 | 1218.1 | 1256.1 | - | - |
| Heat Output 1 (J/g) | - | - | - | 78.7 | 66.1 | 64.8 | 25.1 | 22.8 | 48.6 |
| Heat Output 2 (J/g) | - | - | - | 166.3 | 128.8 | 79.4 | 316.1 | 631.7 | 232.8 |
| Heat Output 3 (J/g) | 12.5 | - | - | 210.9 | 3.2 | 157.4 | 382.4 | 258.3 | 204.1 |
| Heat Output 4(J/g) | 230.8 | - | 194.2 | 511.9 | 492.7 | 91.5 | 148.9 | 27.5 | 14.8 |
| Heat Output 5 (J/g) | - | 201.6 | - | - | - | - | 261.0 | - | - |
| Total Heat Output (J/g) | 243.3 | 201.6 | 194.2 | 967.8 | 690.8 | 393.1 | 1133.5 | 940.3 | 500.3 |
| Theoretical Value (J/g) | 1977 | 1549 | 1266 | 1977 | 1549 | 1266 | 1977 | 1549 | 1266 |

Table 3.7 cont. DSC Data for DD B/Fe₂O₃ nanothermites

| Proton Scavenger | 1,4 dioxane | | | Ammonium hydroxide | | | Propylene Oxide | |
|-------------------------|-------------|-------|--------|--------------------|--------|--------|-----------------|--------|
| | 3FR | 6FR | 9FR | 3FR | 6FR | 9FR | 6FR | 9FR |
| Onset Temp.1 (°C) | 159.2 | 212.5 | 234.6 | - | - | - | - | - |
| Onset Temp.2 (°C) | 572.9 | 442.3 | - | 542.7 | 611.3 | 614.1 | 533.6 | 621.0 |
| Onset Temp.3 (°C) | - | 642.8 | 643.6 | - | - | - | - | - |
| Onset Temp.4 (°C) | 867.7 | 849.4 | 847.8 | 851.9 | 847.7 | 842.8 | - | - |
| Onset Temp. 5 (°C) | 1046.7 | 924.1 | 1150.0 | 1095.7 | 1099.1 | 1103.1 | 1083.8 | 1086.0 |
| Onset Temp. 6 (°C) | - | - | - | - | 1284.2 | - | - | - |
| Heat Output 1 (J/g) | 185.9 | 40.5 | 22.3 | - | - | - | - | - |
| Heat Output 2 (J/g) | 12.2 | 43.6 | - | 696.6 | 74.8 | 44.5 | 620 | 561.6 |
| Heat Output 3 (J/g) | | 167.3 | 75.6 | - | - | - | - | - |
| Heat Output 4(J/g) | 424.5 | 23.3 | 56.7 | 102.7 | 462.5 | 274.0 | - | - |
| Heat Output 5 (J/g) | - | 66.4 | 81.0 | 162.3 | 99.8 | 163.1 | 612.9 | 440.5 |
| Heat Output 6 (J/g) | - | - | - | - | 172.5 | - | - | - |
| Total Heat Output (J/g) | 622.6 | 341.1 | 235.6 | 961.6 | 809.6 | 481.6 | 1232.9 | 1002.1 |
| Theoretical Value (J/g) | 1977 | 1549 | 1266 | 1977 | 1549 | 1266 | 1549 | 1266 |

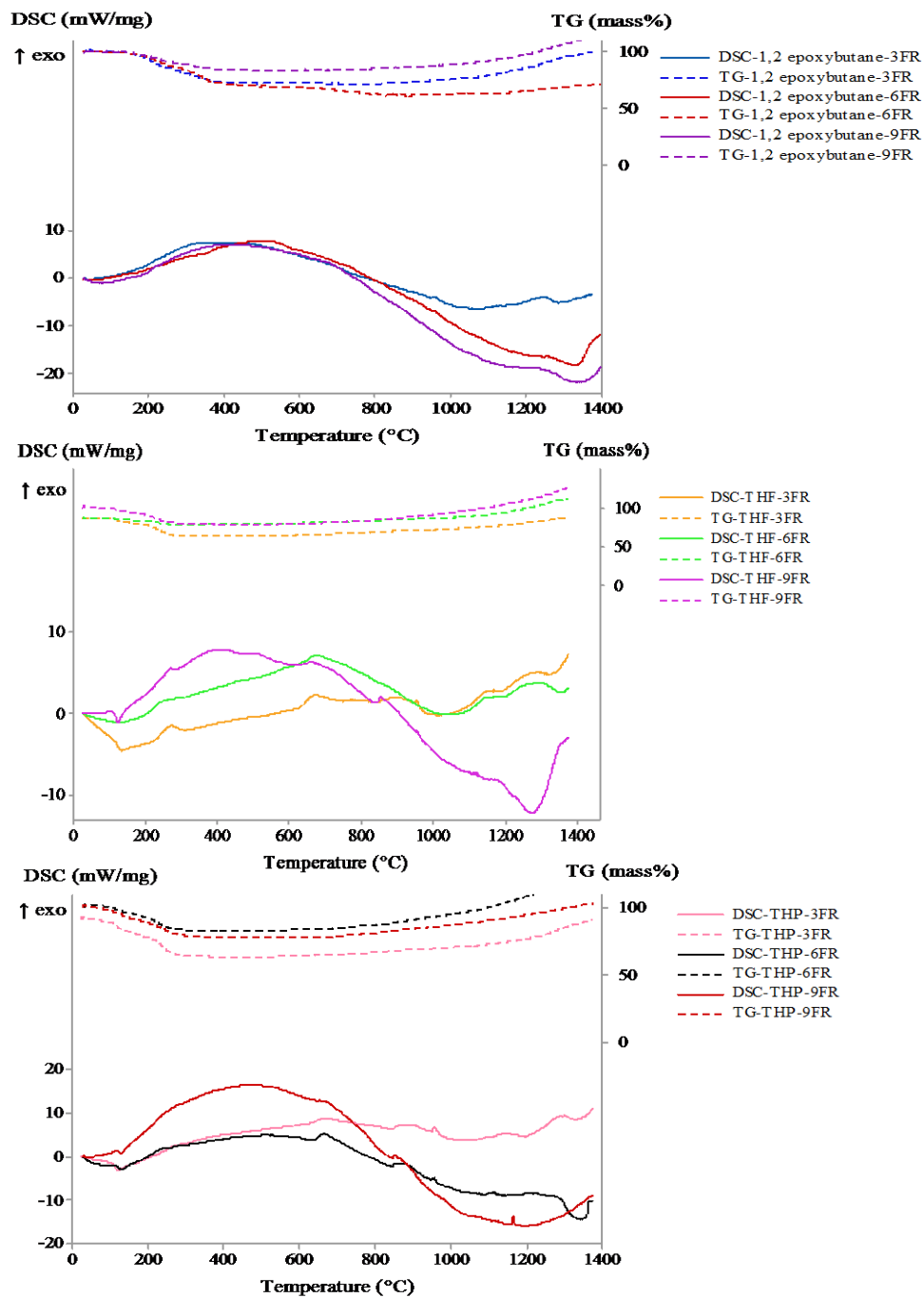


Figure 3.17. DSC and TG plots as a function of temperature for 3FR, 6FR and 9FR DD B/Fe₂O₃ samples synthesized with 1,2 epoxybutane, THF and THP

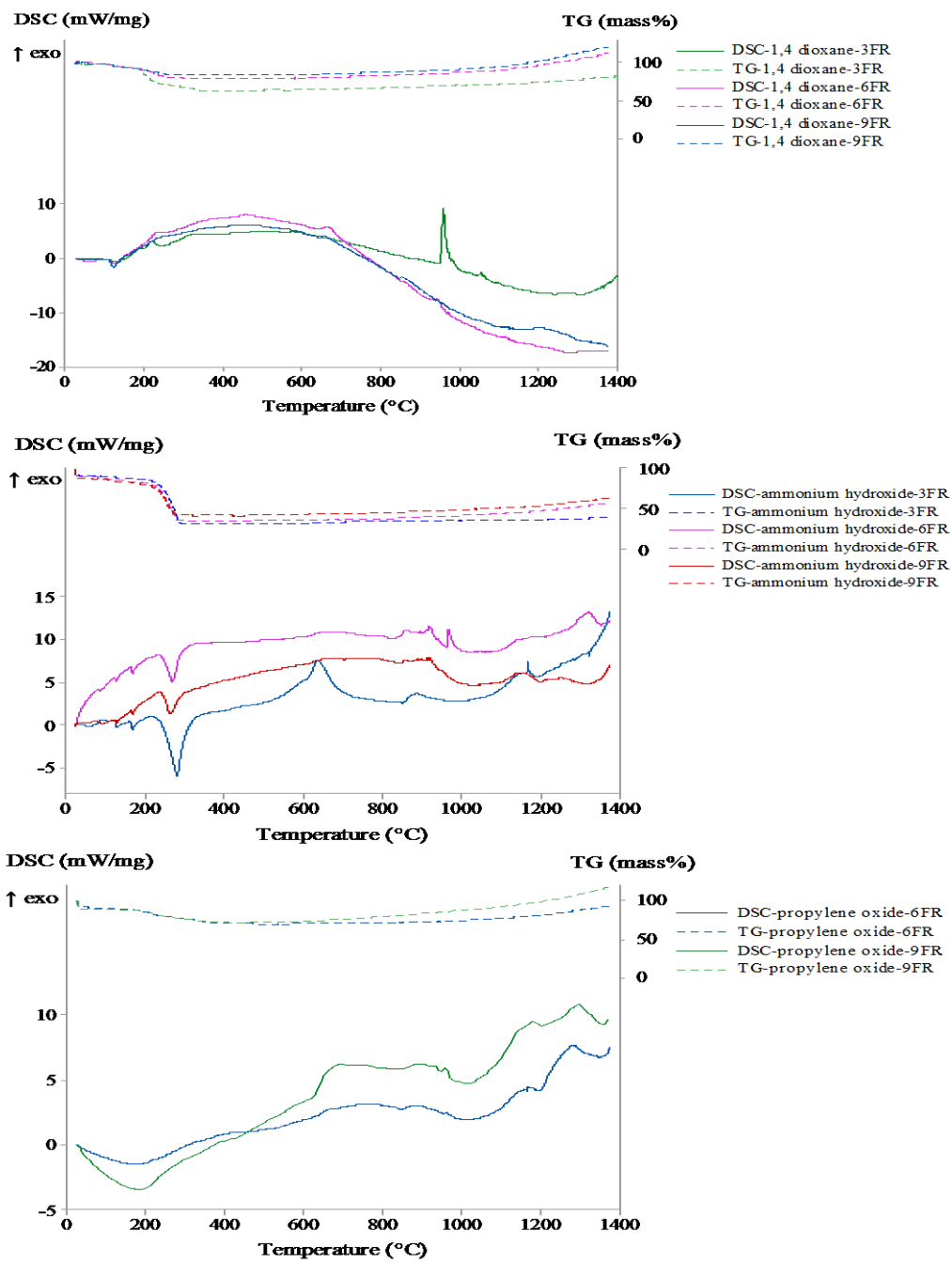


Figure 3.18. DSC and TG plots as a function of temperature for 3FR, 6FR and 9FR DD B/Fe₂O₃ samples synthesized with 1,4 dioxane, ammonium hydroxide and 6FR and 9FR DD B/Fe₂O₃ samples synthesized with propylene oxide

3.5.3 Effect of Fuel Type on the Thermal Behavior of Thermite Compositions

The scope of this part of the study is to find out the effects of the fuel type used in the formulation on the thermal behavior. For this purpose, the energetic composites, containing iron oxide samples as an oxidizer subjected to direct drying method and magnesium, aluminum, boron or 20% magnesium coated boron, were prepared with an equivalence ratio of 6 and tested. It is known that Mg, Al and 20%Mg-B powders have different volumetric and gravimetric energy content. Therefore, it is expected that the fuel type may have an effect on the thermal behavior.

The TG/DSC analysis of Mg/Fe₂O₃, 20%Mg-B/Fe₂O₃, B/Fe₂O₃ and Al/Fe₂O₃ xerogels prepared by THF with a constant equivalence ratio of 6 are given in Figure 3.19 and Table 3.8. The DSC thermogram of Mg/Fe₂O₃ nanocomposite exhibits a very sharp exothermic peak with an onset temperature of 633.0°C which is lower than the melting point of magnesium (650°C). Therefore, the oxidation reaction initiates between the solid phases of magnesium and Fe₂O₃. The mixture of Mg coated B (20%)/Fe₂O₃ seems to ignite above 750°C with a broad and weak exotherm as shown in Figure 3.19. Most probably, this particular type of thermite formulation is difficult to ignite. According to TG/DSC analysis of the 6FR B/Fe₂O₃, as given in Figure 3.19, the thermal events and mass loss up to 250°C might be associated with the evaporation of the ethanol and organic residues inside the structure. The onsets of the broad exothermic events of B/Fe₂O₃ are observed at 630.2 °C and 1107.8°C which overlaps with the peak at 1219.9°C. The thermite reaction of B/Fe₂O₃ takes place between solid phases of B and Fe₂O₃. The thermite reaction of Al/Fe₂O₃ begins above 800°C as given in Figure 3.19. The sharp endothermic peak around 650 °C can be associated with the melting of Al particles. Therefore, the thermite reaction initiates between the liquid Al and solid Fe₂O₃ phases. Highest energy release was observed for Mg/Fe₂O₃ sample (2434 J/g). The lowest heat release was utilized by 20%Mg-B/Fe₂O₃ sample (202.7 J/g). The combustion performance of Al/Fe₂O₃ (29 %) is

significantly lower than both B/Fe₂O₃ (~45 %) and Mg/Fe₂O₃ (80 %) which can be explained by poor contact between liquid Al and solid Fe₂O₃ phases.

The TG/DSC results of Mg/Fe₂O₃, 20%Mg-B/Fe₂O₃, B/Fe₂O₃ and Al/Fe₂O₃ xerogels prepared by THP are very similar to those of the samples prepared by THF as given in Figure 3.19 and Table 3.9. Mg/Fe₂O₃ sample exhibits a sharp exothermic peak starts at 638.6°C which is lower than the melting point of magnesium (650°C). Therefore, similar to the sample prepared with THF, the oxidation reaction initiates between the solid phases of magnesium and Fe₂O₃. The mixture of Mg coated B (20%)/Fe₂O₃ seems to ignite above 900°C with a weak exotherm as shown in Figure 3.19. It seems that this particular type of formulation is difficult to ignite. The thermal events and mass loss up to 250°C of B/Fe₂O₃ might be associated with the evaporation of the ethanol and organic residues inside the structure as given in Figure 3.19. The onset temperatures of the broad exothermic events of B/Fe₂O₃ are 638.2 °C, 846.3 °C and 1103.8°C. The thermite reaction of B/Fe₂O₃ takes place between solid phases of B and Fe₂O₃. The thermite reaction of Al/Fe₂O₃ begins above 750°C as given in Figure 3.19. The sharp endothermic peak around 650 °C can be related with the melting of Al particles which means the thermite reaction initiates between the liquid Al and solid Fe₂O₃ phases. Highest energy release was observed for Mg/Fe₂O₃ sample (3283.7 J/g). The lowest heat release was utilized by 20%Mg-B/Fe₂O₃ sample (216.9 J/g). The combustion performance of Al/Fe₂O₃ (50 %) is lower than B/Fe₂O₃ (60 %) which can be explained by poor contact between liquid Al and solid Fe₂O₃ phases.

The TG/DSC analysis of Mg/Fe₂O₃, 20%Mg-B/Fe₂O₃, B/Fe₂O₃ and Al/Fe₂O₃ xerogels prepared by 1,4 dioxane are given in Figure 3.20 and Table 3.10.

Similar to previous results Mg/Fe₂O₃ exhibits a sharp exothermic peak at 641.6°C which is slightly lower than the melting point of magnesium (650°C). So, the oxidation reaction initiates between the solid phases of Mg and Fe₂O₃. The mixture of Mg coated B (20%)/Fe₂O₃ seems to ignite above 850°C with a heat output of 293.0 J/g as shown in Figure 3.20. The thermal events and mass loss up to 250°C of B/Fe₂O₃ might be related with the evaporation of the ethanol and organic residues inside the structure as given in Figure 3.20. The onset temperature of the weak exothermic event of B/Fe₂O₃ is 642.8 °C with a heat release of 167.3 J/g. The thermite reaction of Al/Fe₂O₃ begins above 800°C as given in Figure 3.20. The sharp endothermic peak around 650 °C might be related with the melting of Al, which means the thermite reaction initiates between the liquid Al and solid Fe₂O₃ phases. Mg/Fe₂O₃ has the highest energy release (3078.0 J/g). 20%Mg-B/Fe₂O₃ and B/Fe₂O₃ has the lowest heat release (407.2 J/g and 341.1 J/g). The combustion performance of Al/Fe₂O₃ (30 %) is slightly higher than that of B/Fe₂O₃ (20 %).

Similar with the previous TG/DSC results, Mg/Fe₂O₃ sample prepared with propylene oxide (Figure 3.20) has a sharp exothermic peak with an onset of 641.1°C which is lower than the melting point of magnesium (650°C). Therefore, similar to Mg/Fe₂O₃ samples prepared with other proton scavengers, the oxidation reaction initiates between the solid phases of magnesium and Fe₂O₃. The mixture of Mg coated B (20%)/Fe₂O₃ seems to ignite above 1100°C with a weak exotherm as shown in Figure 3.20. It seems that this particular type of formulation is very difficult to ignite. The broad exothermic events of B/Fe₂O₃ take place between solid phases of B and Fe₂O₃ with the onset temperatures at 533.6 °C and 1083.8 °C as given in Figure 3.20. Broad and very weak exothermic event of Al/Fe₂O₃ begins above 1300°C as given in Figure 3.20. The sharp endothermic peak around 650 °C might be associated with the melting of Al, which means the exothermic event initiates between the liquid Al and solid Fe₂O₃ phases.

Highest energy release was observed for Mg/Fe₂O₃ sample (2406.0 J/g). The lowest heat release was utilized by 20%Mg-B/Fe₂O₃ (85.7 J/g) and Al/Fe₂O₃ samples (51.9 J/g). Al and 20%Mg-B are not a good candidate of fuel type for the thermite compositions containing Fe₂O₃ synthesized with propylene oxide. The combustion performance of B/Fe₂O₃ (80 %) is lower than Mg/Fe₂O₃ (80 %) when the heat output values are compared (Table 3.11).

The exothermic events initiate between the liquid Al and solid Fe₂O₃ phases, or solid B/Mg and solid Fe₂O₃ phases for all samples. Therefore, the results indicate the importance of surface free energy and wetting characteristics of fuel and oxidant which might play an important role in the combustion performance.

The measured heat outputs of the mixtures of B, Al or 20%Mg-B with Fe₂O₃ were found to be lower than the theoretical values presumably due to the incomplete thermite reaction under inert atmosphere because of the limiting oxygen which was supplied by Fe₂O₃.

Boron is a common fuel for the pyrotechnic materials with its high gravimetric and volumetric energy content but it has not been generally used for thermites. According to DSC results, Mg is a very good candidate however it is known that Mg has shelf-life issue problems due to its hygroscopic behavior. In addition, boron seems to be a good candidate for thermite compositions containing iron oxide since it has a moderate heat output and a long shelf-life compared to the other fuel types.

Table 3.8. DSC Data for 6FR Metal/Fe₂O₃ xerogels synthesized with THF

| | Mg/Fe ₂ O ₃ | 20%MgB/Fe ₂ O ₃ | B/Fe ₂ O ₃ | Al/Fe ₂ O ₃ |
|-------------------------|-----------------------------------|---------------------------------------|----------------------------------|-----------------------------------|
| Onset Temp. 1 (°C) | - | - | 213.7 | - |
| Onset Temp. 2 (°C) | 633.0 | 785.6 | 630.2 | - |
| Onset Temp. 3 (°C) | - | 876.1 | 848.0 | 812.3 |
| Onset Temp. 4 (°C) | - | - | 1107.8 | 925.2 |
| Onset Temp. 5 (°C) | - | - | 1219.9 | - |
| Heat Output 1 (J/g) | - | - | 66.1 | - |
| Heat Output 2 (J/g) | 2434.0 | 38.99 | 128.8 | - |
| Heat Output 3 (J/g) | - | 163.7 | 3.2 | 483.3 |
| Heat Output 4 (J/g) | - | - | 492.7 | 21.6 |
| Total Heat Output (J/g) | 2434.0 | 202.7 | 690.8 | 504.9 |
| Theoretical Value (J/g) | 3040 | 3178 | 1549 | 1762 |

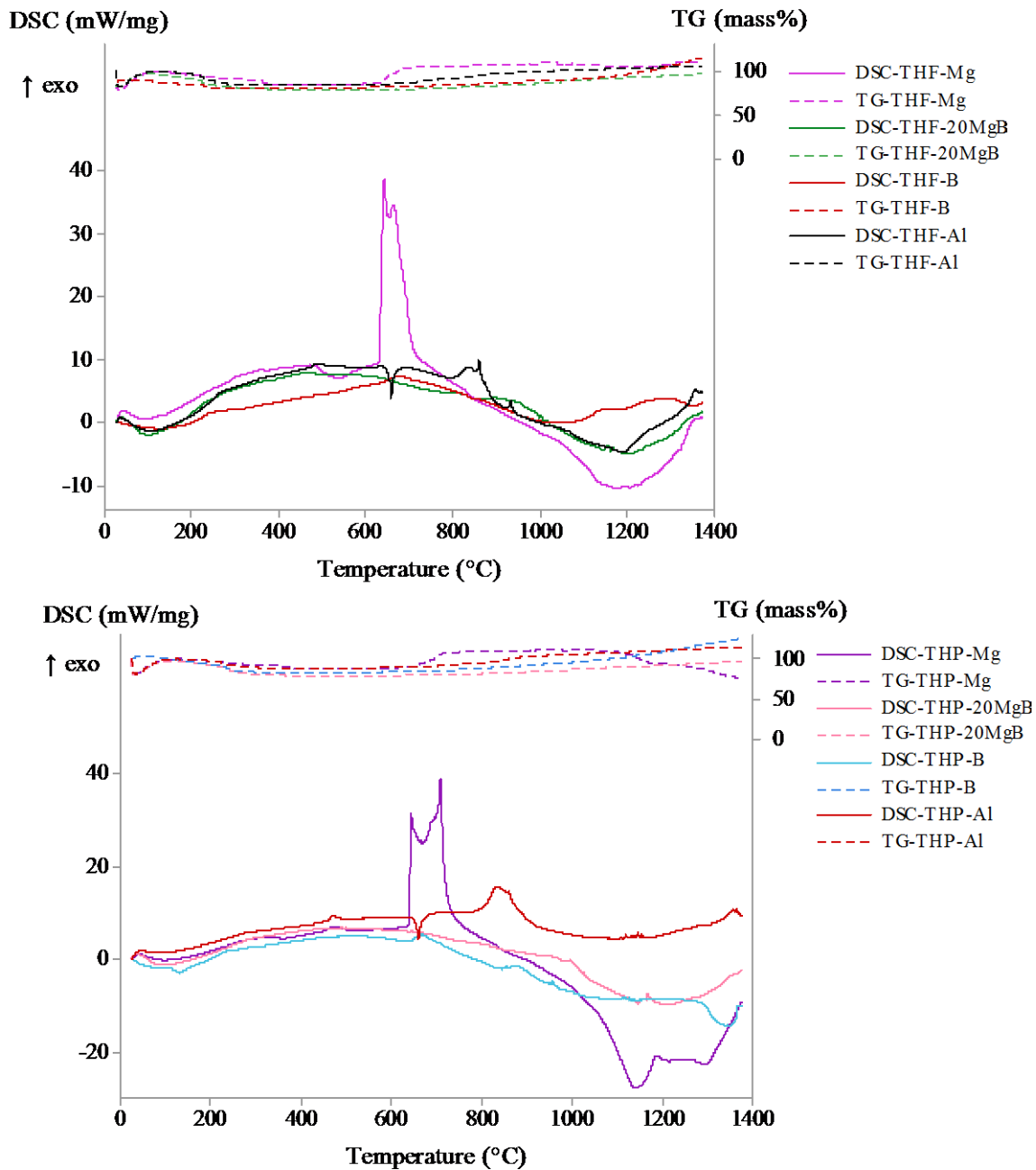


Figure 3.19. DSC and TG plots as a function of temperature at an equivalence ratio of 6 for Mg/Fe₂O₃, 20%Mg-B/Fe₂O₃, B/Fe₂O₃, Al/Fe₂O₃ samples prepared by THF and THP

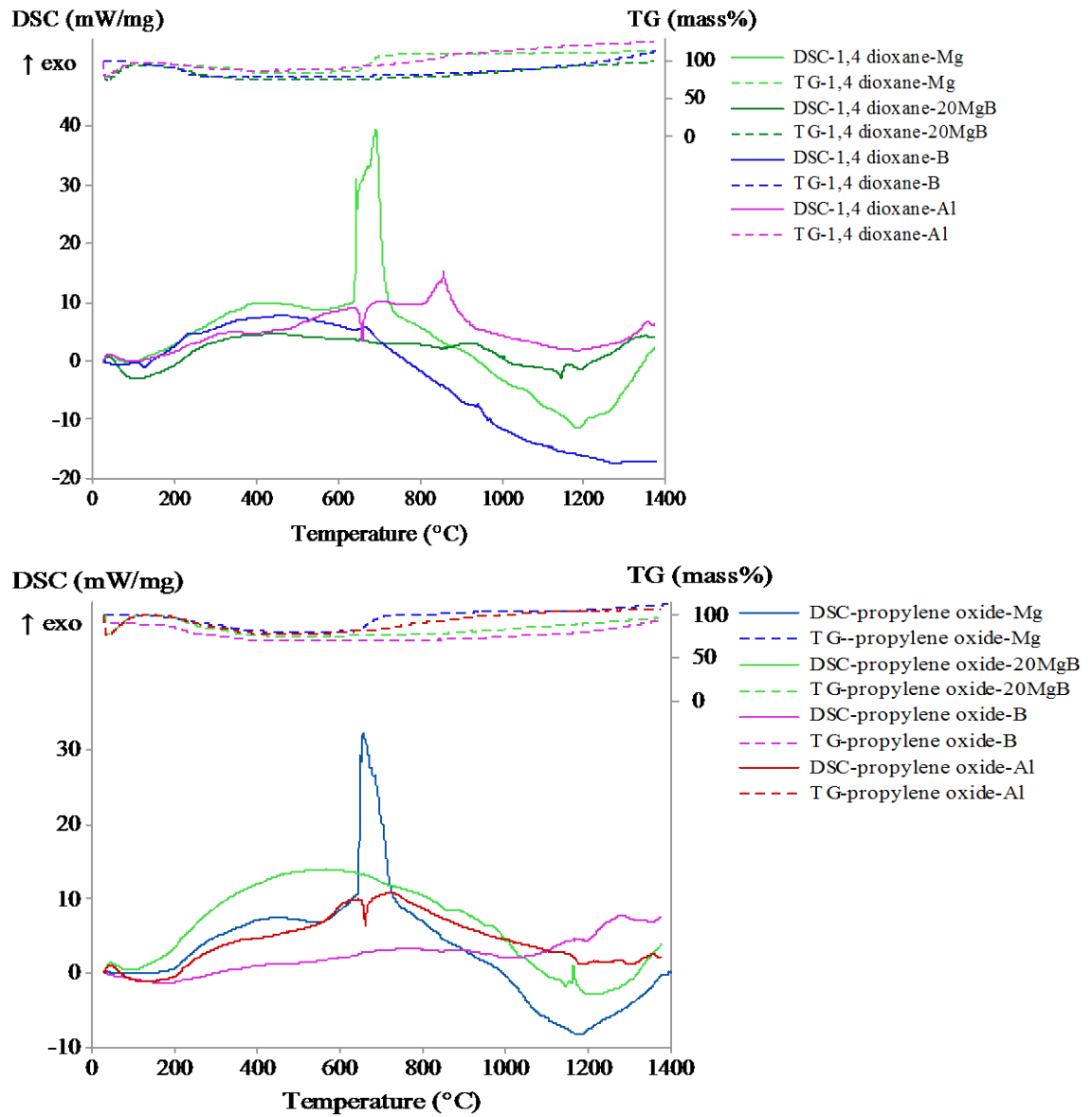


Figure 3.20. DSC and TG plots as a function of temperature at an equivalence ratio of 6 for Mg/Fe₂O₃, 20% Mg-B/Fe₂O₃, B/Fe₂O₃, Al/Fe₂O₃ samples prepared by 1,4 dioxane and propylene oxide

Table 3.9. DSC Data for 6FR Metal/Fe₂O₃ xerogels synthesized with THP

| | Mg/Fe ₂ O ₃ | 20%MgB/Fe ₂ O ₃ | B/Fe ₂ O ₃ | Al/Fe ₂ O ₃ |
|-------------------------|-----------------------------------|---------------------------------------|----------------------------------|-----------------------------------|
| Onset Temp. 1 (°C) | - | - | 212.4 | 461.4 |
| Onset Temp. 2 (°C) | 638.6 | - | 638.1 | 759.2 |
| Onset Temp. 3 (°C) | - | 938.2 | 846.3 | - |
| Onset Temp. 4 (°C) | 1163.6 | 1166.5 | 1103.8 | - |
| Heat Output 1 (J/g) | - | - | 22.8 | 41.2 |
| Heat Output 2 (J/g) | 3134.0 | - | 631.7 | 798.0 |
| Heat Output 3 (J/g) | - | 119.0 | 258.3 | - |
| Heat Output 4 (J/g) | 149.7 | 97.9 | 27.5 | - |
| Total Heat Output (J/g) | 3283.7 | 216.9 | 940.3 | 839.2 |
| Theoretical Value (J/g) | 3040 | 3178 | 1549 | 1762 |

Table 3.10. DSC Data for 6FR Metal/Fe₂O₃ xerogels synthesized with 1,4 dioxane

| | Mg/Fe ₂ O ₃ | 20%MgB/Fe ₂ O ₃ | B/Fe ₂ O ₃ | Al/Fe ₂ O ₃ |
|-------------------------|-----------------------------------|---------------------------------------|----------------------------------|-----------------------------------|
| Onset Temp. 1 (°C) | - | - | - | - |
| Onset Temp. 2 (°C) | - | - | 212.5 | - |
| Onset Temp. 3 (°C) | - | 395.3 | 442.3 | - |
| Onset Temp. 4 (°C) | 641.6 | - | 642.8 | - |
| Onset Temp. 5 (°C) | 856.0 | 865.7 | 849.4 | 810.4 |
| Onset Temp. 6 (°C) | 1038.3 | - | 924.1 | - |
| Onset Temp. 7 (°C) | 1198.3 | 1147.3 | - | - |
| Heat Output 1 (J/g) | - | - | - | - |
| Heat Output 2 (J/g) | - | - | 40.5 | - |
| Heat Output 3 (J/g) | - | 44.0 | 43.6 | - |
| Heat Output 4 (J/g) | 2852.0 | - | 167.3 | - |
| Heat Output 5 (J/g) | 116.3 | 293.0 | 23.3 | 581.0 |
| Heat Output 6 (J/g) | 67.6 | - | 66.4 | - |
| Heat Output 7 (J/g) | 42.1 | 70.2 | - | - |
| Total Heat Output (J/g) | 3078.0 | 407.2 | 341.1 | 581.0 |
| Theoretical Value (J/g) | 3040 | 3178 | 1549 | 1762 |

Table 3.11. DSC Data for 6FR Metal/Fe₂O₃ xerogels synthesized with propylene oxide

| | Mg/Fe ₂ O ₃ | 20%MgB/Fe ₂ O ₃ | B/Fe ₂ O ₃ | Al/Fe ₂ O ₃ |
|-------------------------|-----------------------------------|---------------------------------------|----------------------------------|-----------------------------------|
| Onset Temp. 1 (°C) | 641.1 | - | 533.6 | - |
| Onset Temp. 2 (°C) | - | - | 1083.8 | - |
| Onset Temp. 3 (°C) | - | 1147.2 | - | 1307.3 |
| Heat Output 1 (J/g) | 2406.0 | - | 620.0 | - |
| Heat Output 2 (J/g) | - | - | 612.9 | - |
| Heat Output 3 (J/g) | - | 85.7 | - | 51.9 |
| Total Heat Output (J/g) | 2406.0 | 85.7 | 1232.9 | 51.9 |
| Theoretical Value (J/g) | 3040 | 3178 | 1549 | 1762 |

3.6 Calorific Value (Bomb Calorimeter) Test

The calorific values of the samples were determined by the Bomb Calorimeter. In this section various parameters which affect the combustion mechanisms are discussed. These parameters are classified as drying conditions, proton scavenger, equivalence ratio and fuel type.

3.6.1 Effects of Drying Condition and Proton Scavenger on Calorific Value of 3FR B/Fe₂O₃ Thermite Compositions

3FR B/Fe₂O₃ compositions synthesized with 1,2 epoxybutane, 1,4 dioxane, ammonium hydroxide, THF and THP; and prepared by SSE and DD method were subjected to calorific value tests to determine the effects of drying conditions on the heat output.

The average of the calorific value of the DD sample prepared with 1,2 epoxybutane is 2117 J/g while the average of the calorific value results of the SSE sample is 2586 J/g. The average of the calorific value results of the DD sample prepared with 1,4 dioxane is 4230 J/g while the average of the calorific value results of the SSE sample is 6021 J/g. When the results compared for the samples prepared with ammonium hydroxide, it is observed that the average calorific value of DD sample is 3820 J/g and that of SSE sample is 5933 J/g. The average of the calorific value results of the DD sample prepared with THF is 5025 J/g while the average of the calorific value results of the SSE sample is 5138 J/g. When the calorific values of the samples prepared with THP, it is observed that DD sample has an average calorific value of 4477 J/g while SSE samples has an average calorific value of 6130 J/g.

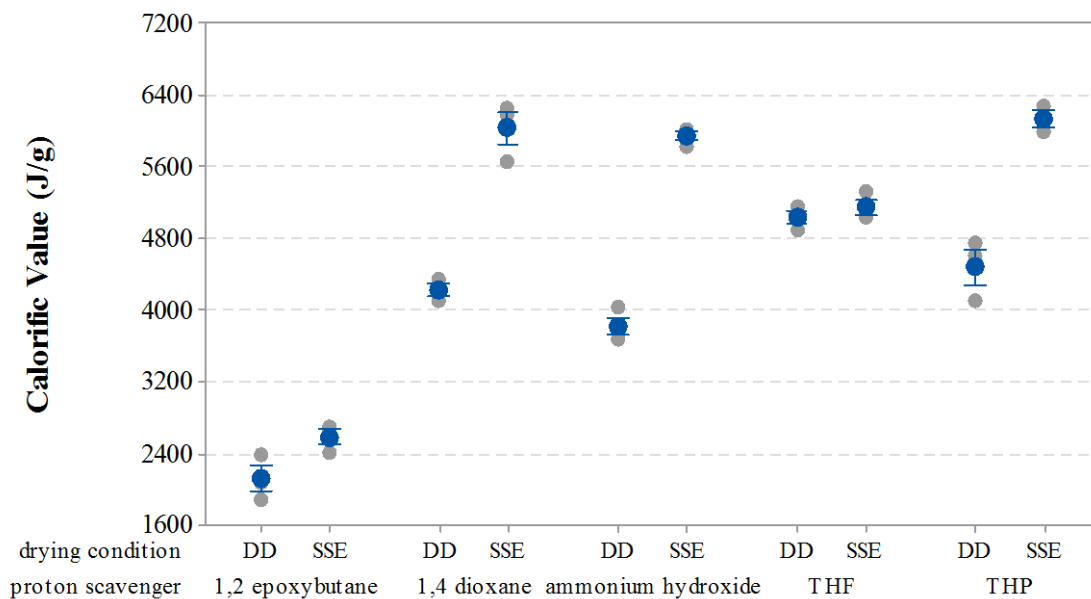


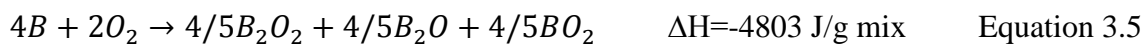
Figure 3.21. Calorific Values of DD and SSE 3FR B/Fe₂O₃ compositions

Table 3.12. The Calorific Values of DD and SSE 3FR B/Fe₂O₃ Compositions

| Proton scavenger | Average Calorific Value (J/g) | |
|--------------------|-------------------------------|------|
| | DD | SSE |
| 1,2 epoxybutane | 2117 | 2586 |
| 1,4 dioxane | 4230 | 6021 |
| Ammonium hydroxide | 3820 | 5933 |
| THF | 5025 | 5138 |
| THP | 4477 | 6130 |

The average values of the calorific heat outputs of SSE samples are approximately 2-55% greater than those of DD samples synthesized with 1,2 epoxybutane, 1,4 dioxane, ammonium hydroxide, THF and THP as given in Figure 3.21 and Table 3.12. The enhancement in the calorific values might be attributed to the textural properties of the samples which depend on the drying conditions. The reason of that could be the slow extraction/evaporation of the solvent inside the pores does not cause the contraction of the skeletal matrix which takes place in direct drying process. It is expected the high surface area and porous structure of the oxidizer may enhance the combustion propagation.

It is believed that during the calorific value tests, there was air atmosphere inside the steel closed bomb chamber of the Bomb Calorimeter. Therefore, to compare the experimental calorific values with the theoretical heat outputs, the calorific value calculations of 3FR compositions were based on the reaction of boron with iron oxide and the reaction of remaining boron with excess oxygen as given:



When the theoretical and experimental calorific values of 3FR SSE and DD samples are compared, it is observed that the actual calorific values of DD samples are approximately 30-75 % of the theoretical values and the actual calorific values of SSE samples are approximately 40-90 % of the theoretical values depending on the proton scavenger.

It is shown that the drying method directly affects the surface area of the iron oxide xerogels and the results are discussed in the section “3.1 Nitrogen Gas Adsorption Analysis”. It can be concluded that sequential solvent exchange method has an enhancing effect on the calorific values which may be related with the enhancement in the structure and the increase in the surface area and pore volume.

In addition, it is observed that the calorific values not only depends on drying conditions but also depends on the type of proton scavenger. Similar to the DSC/TG analysis, DD samples prepared with THP and THF have the highest calorific values. Furthermore, the highest calorific values can be obtained with all SSE samples prepared by 1,4 dioxane, ammonium hydroxide, THF and THP.

Despite the lowest surface area of the sample prepared with ammonium hydroxide among the other samples, ammonium hydroxide provides enhancing effect on the calorific value of B/Fe₂O₃. It may be related with the ammonium nitrate obtained during the gelation process. It is known that ammonium nitrate can improve the calorific heat output due to its behavior of strong oxidizing agent for boron powder.

3.6.2 Effects of Equivalence Ratio on Calorific Value of B/Fe₂O₃ Thermite Compositions

The effect of equivalence ratio was examined by comparing the calorific value results of B/Fe₂O₃ samples, prepared by DD method and synthesized with propylene oxide, 1,2 epoxybutane, THF, THP, 1,4 dioxane and ammonium hydroxide, where the fraction of fuel in sample (equivalence ratio) is increased from 3 (FR3) to 9 (FR9).

The calorific values for fuel rich compositions ($\phi=3$, $\phi=6$ and $\phi=9$) are shown in Figure 3.22 and the average of calorific values are presented in Table 3.13. The prepared samples are readily ignited. The samples synthesized with ammonium hydroxide and 1,4 dioxane which have an equivalence ratio of 9 have the highest heat output of 6109 J/g (average: 5979 J/g) and 6552 J/g (average: 6314 J/g), among the other compositions. On the other hand, the sample synthesized with 1,2 epoxybutane which has an equivalence ratio of 3 has the lowest calorific value of 1891 J/g (average: 2117 J/g).

For the samples having equivalence ratio of 3, the highest calorific value was obtained by THF, while for the samples having equivalence ratio of 6, the highest calorific value was obtained by ammonium hydroxide, THF, 1,4 dioxane and for the samples having equivalence ratio of 9, the highest calorific value was obtained by 1,4 dioxane and ammonium hydroxide as given in Figure 3.22 and Table 3.13.

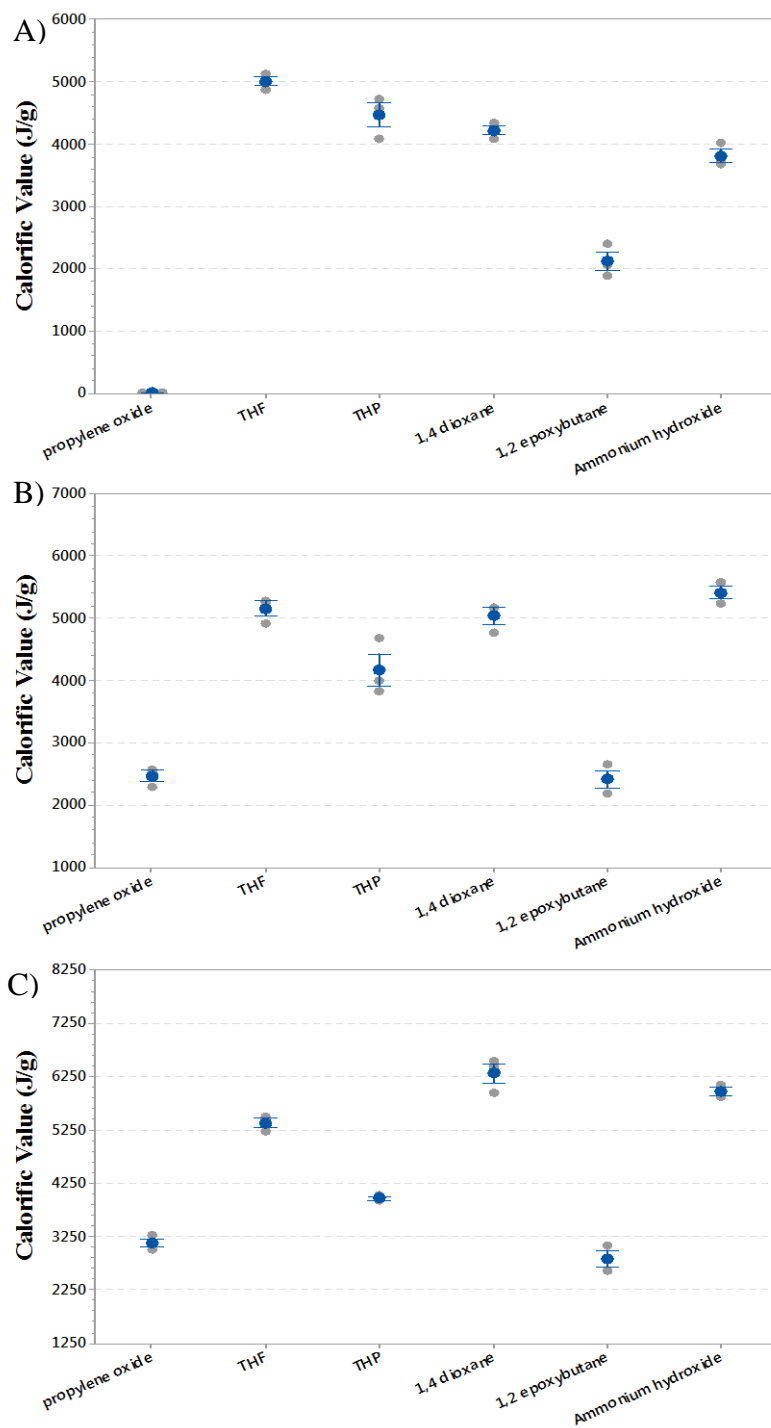


Figure 3.22. Calorific Values of B/Fe₂O₃ Compositions with an equivalence ratio of A) 3 B) 6 C) 9

Table 3.13. The Calorific Values of Fuel Rich B/Fe₂O₃ Compositions with an equivalence ratio of $\phi=3$, $\phi=6$ and $\phi=9$

| Proton scavenger | Average Calorific Value (J/g) | | |
|--------------------|-------------------------------|------|------|
| | 3FR | 6FR | 9FR |
| Propylene oxide | 0 | 2464 | 3121 |
| THF | 5025 | 5159 | 5385 |
| THP | 4477 | 4171 | 3971 |
| 1,4 dioxane | 4230 | 5042 | 6314 |
| 1,2 epoxybutane | 2117 | 2448 | 2824 |
| Ammonium hydroxide | 3820 | 5422 | 5979 |

The samples synthesized by propylene oxide with an equivalence ratio of 3 could not be ignited with the applied test protocol. However, ignitable compositions of the samples prepared by propylene oxide were obtained with higher equivalence ratios such as 6 and 9. This shows that the equivalence ratio is very critical for the ignition impetus and combustion performance of the compositions.

It is found that the characteristics of the samples prepared by THF differ from the other samples' behavior. The calorific values of the samples which are prepared by THF decrease with increasing equivalence ratio. It is observed that the optimum equivalence ratio for the formulations with THF is 6.

The calorific value increases with increasing boron content (increasing equivalence ratio). That is, the higher boron content means the higher active fuel in the energetic composition. The oxide layer around the boron particle inhibits the combustion of the fuel therefore it is possible to overcome this drawback by increasing boron content. Moreover, most probably, this change in the calorific values of fuel-rich compositions with various equivalence ratios is resulted from the differences in the oxidizing mechanism of boron particles.

Despite the lowest value of its surface area among the other xerogels due to the rapid precipitation of ammonium hydroxide during gelation step, the ammonium nitrate obtained during the gelation provides an enhancing effect on the combustion performance and calorific value. It should be noted that the nano composites derived with propylene oxide and 1, 2 epoxybutane may inhibit the ignition conditions of the pyrotechnics by the reason of being more stable despite of their high surface area.

The results showed that the calorific value strongly depends on the type of proton scavenger and the equivalence ratio. The equivalence ratio is very critical for the ignition impetus and combustion performance of the compositions.

Furthermore, the change in the calorific values of fuel-rich compositions with diverse equivalence ratios is resulted from the differences in the oxidizing mechanism of boron particles. It is outlined that the combustion of boron involves a two-stage mechanism. The first stage is the removal of oxide layer which surrounds the core of boron particle and the second stage is related with the combustion of core of boron particle [99,162,163].

The impurities of hydroxyl groups in small quantities which are resulted from the gelation process may have promoted the formation of BHO₂ molecule at the second stage of boron combustion. It is known that the formation of BHO₂ molecule is thermodynamically favored over the formation of B₂O₃ species which is related to the combustion of boron [115,164]. BHO₂ molecule acts as an energy trap of boron particle and unfortunately causes the reduction in the released energy.

In order to simulate the changes in the amount of BHO₂ molecule with equivalence ratio, NASA-GLENN Chemical Equilibrium Program CEA2 code [165, 166, 167] was used. Figure 3.23 shows the change in amount of BHO₂ molecule with equivalence ratio. It is shown that the increase in boron content of the formulation causes reduction in the amount of BHO₂. Not only BHO₂ molecule but also HBO molecule reduces the released energy. Figure 3.24 shows the change in amount of HBO molecule with equivalence ratio and it is found that the amount of HBO molecule decreases with increasing equivalence ratio. Consequently, an efficient combustion of boron particles can be achieved by increasing the equivalence ratio.

The changes in the released heat amounts of B/Fe₂O₃ compositions, prepared with various proton scavengers having the equivalence ratios of 3, 6 and 9, might be explained by analyzing the combustion products of these compositions which were obtained from NASA-GLENN Chemical Equilibrium Program CEA2 code. Figure 3.25 shows the final combustion products calculated for the energetic compositions. The products which are considered but whose mole fractions were less than 5.0×10^{-6} are given in the Appendix section.

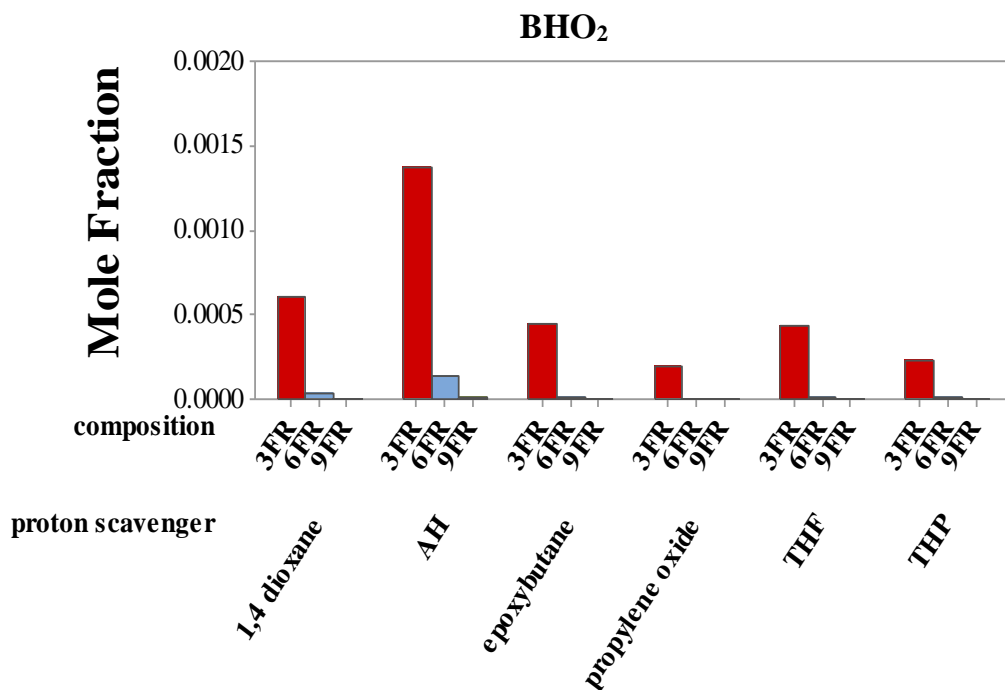


Figure 3.23. The change in calculated mole fraction of BHO₂ molecule with equivalence ratio of B/Fe₂O₃ compositions synthesized with various proton scavengers

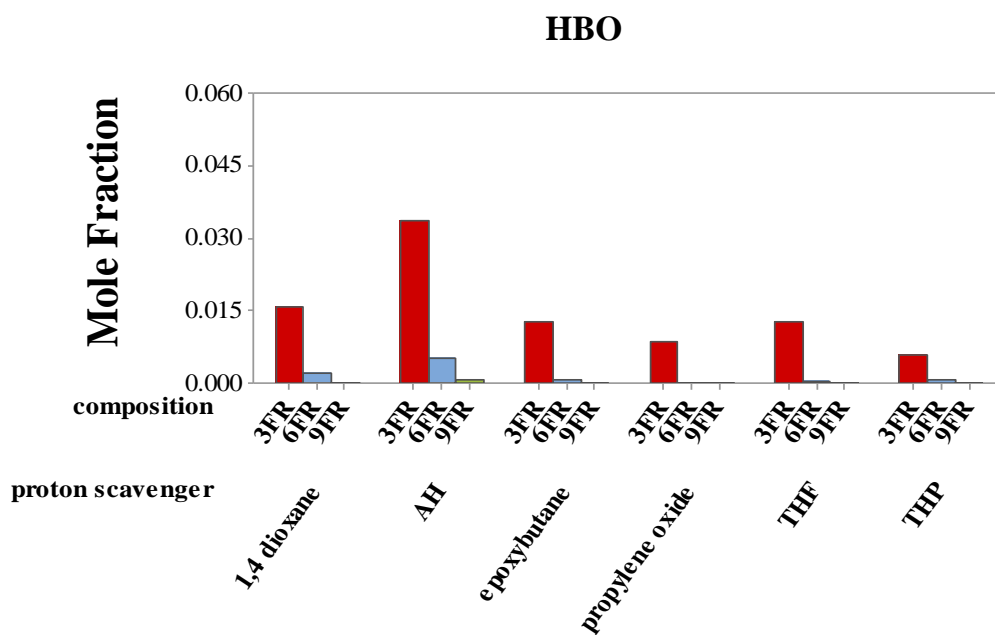


Figure 3.24. The change in calculated mole fraction of HBO molecule with equivalence ratio of B/Fe₂O₃ compositions synthesized with various proton scavengers

To conclude the results stated above, as expected, the released heat value increases with increasing B content (increasing equivalence ratio) up to a certain amount for B/Fe₂O₃ compositions. It is known that the oxide layer which surrounds the boron particle acts as a heat trap. The boron particle reacts with oxide layer to produce BO at the surface and the surface reaction gives rise to reduction in heat output [107]. It is believed that the increase in the amount of boron content lead the composition to release the energy content of boron more efficiently.

Therefore, the calorific values were found to be increased for higher equivalence ratios in air atmosphere.

3.6.2.1 B/Fe₂O₃ Compositions Prepared Ammonium Hydroxide

The iron oxide samples prepared with ammonium hydroxide were found to have the lowest surface area compared to the samples prepared with the other proton scavengers. Thus, the compositions of B and these iron oxide samples prepared by ammonium hydroxide where the fraction of fuel in sample (equivalence ratio) is increased from 3 (FR3) to 9 (FR9) were subjected to SSE method.

It was aimed to enhance both textural and energetic properties of these compositions.

The calorific value test results are given in Figure 3.26. It is observed that the SSE method has improving effect on B/Fe₂O₃ composition with ammonium hydroxide for all equivalence ratios of 3, 6 and 9. The results show that the higher surface area and porous structure enhances the combustion mechanism which is resulted with the higher calorific values.

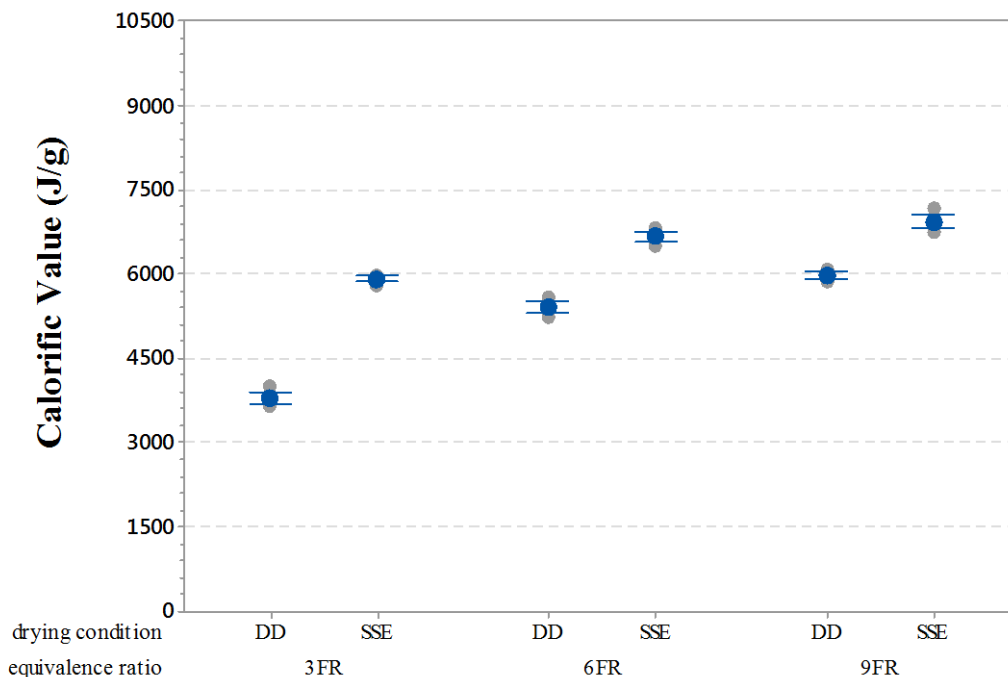


Figure 3.26. The effect of drying conditions on 3FR, 6FR and 9FR B/Fe₂O₃ compositions synthesized with ammonium hydroxide

3.6.2.1.1 Thermodynamic Model for Flame Temperature of the Samples with Ammonium Hydroxide

The samples prepared with ammonium hydroxide have lower surface area compared to samples prepared with other proton scavenger. Despite lower surface area, the calorific values are similar with the calorific values of other samples. It might be attributed to ammonium nitrate which is obtained during the gelation process. Ammonium nitrate has a positive effect on heat of combustion due to its behavior of strong oxidizing agent for boron particles.

To understand the combustion mechanisms of boron particles with ammonium nitrate and iron oxide at constant volume a computational study was carried out with “GUIPEP Thermodynamic Code” by varying the ratio of fuel to oxidizer via changing the boron content. The calculated adiabatic flame temperatures are given in Figure 3.27.

The highest adiabatic flame temperature of B/Fe₂O₃, 2269K, was reached by the composition with stoichiometric value having equivalence ratio of 1.0, while the highest adiabatic flame temperature of B/NH₄NO₃, 2821K and 2901K was reached by two different compositions having equivalence ratios of approximately 1.0 and 6.0. The maximum adiabatic flame temperature values of both compositions exceeded 2000K.

High adiabatic flame temperature improves the combustion propagation. It is observed that high adiabatic flame temperatures can be obtained by using the fuel rich compositions. The effective combustion performance of the samples prepared with ammonium hydroxide may be related with the high adiabatic flame temperatures of B/NH₄NO₃.

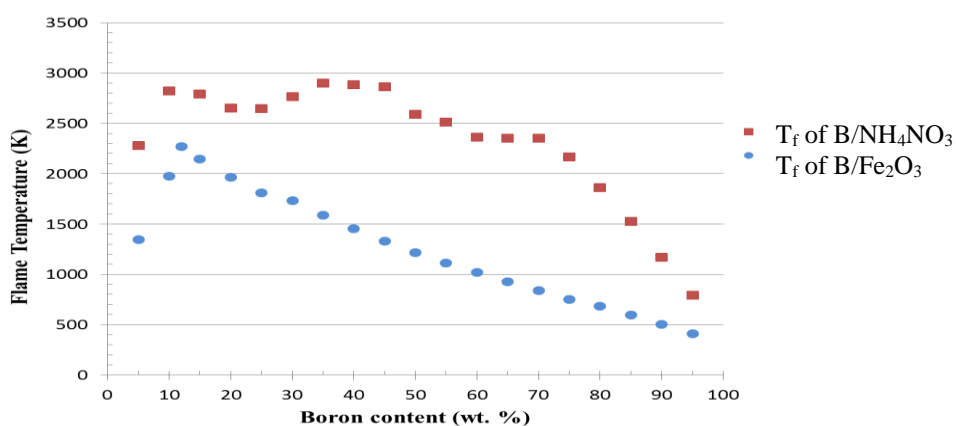


Figure 3.27. The Adiabatic Flame Temperatures of B/NH₄NO₃ and B/Fe₂O₃

3.6.2.2 *The Calorific Values of B/Fe₂O₃ Prepared Directly with Commercial Powders*

In the scope of this study, it is also aimed to find out the advantages and the superiority of the sol-gel method compared to physical mixing. Hence nano sized B/Fe₂O₃ compositions with various equivalence ratios were prepared by physical mixing of commercially available nano sized powders in ethanol medium. The data given in Figure 3.28 and Table 3.14 show the calorific value test results of physically mixed nano sized B/Fe₂O₃ compositions.

The optimum values for combustion can be achieved with the B/Fe₂O₃ compositions having equivalence ratio of 3 and 4.5. The composition with the equivalence ratio of 9 cannot be ignited. If too excess amount of fuel is used compared to the amount of oxidizer, then there will surely be a lack of oxidizer to react with the fuel. As a result, no combustion reaction can be observed.

Table 3.14. The Calorific Value of Nano B/Fe₂O₃ Compositions prepared by mixing of commercial powders

| Equivalence Ratio | Average Calorific Value (J/g) |
|-------------------|-------------------------------|
| 0.11 | - |
| 0.22 | - |
| 0.50 | - |
| 1.00 | 2360 |
| 1.50 | 2665 |
| 3.00 | 2732 |
| 4.50 | 3222 |
| 9.00 | - |
| 15.00 | - |

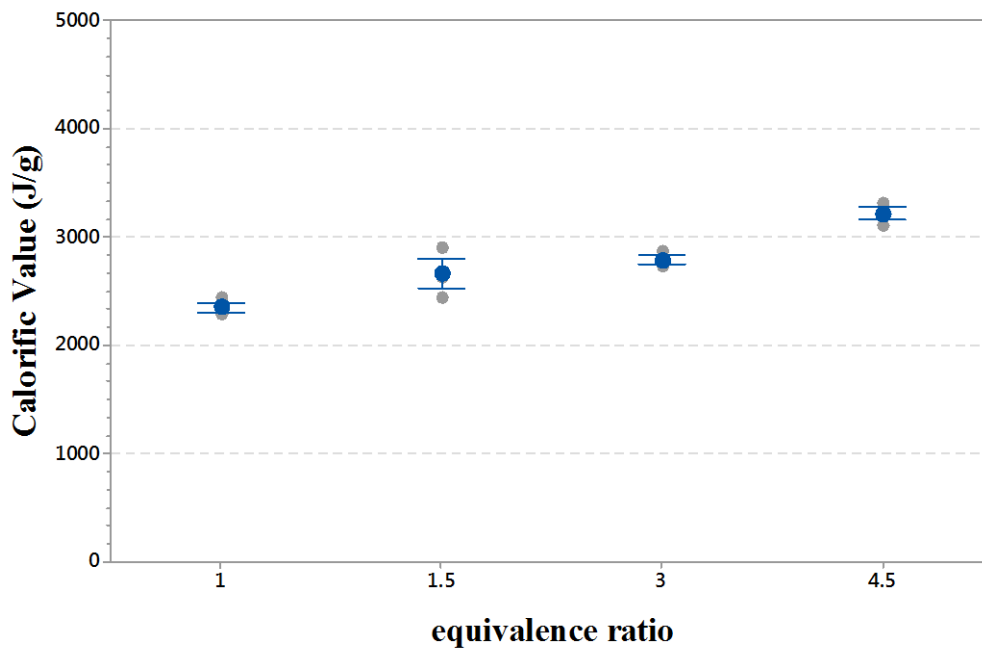


Figure 3.28. The Calorific Value of Nano B/Fe₂O₃ Compositions with varying equivalence ratio prepared by physical mixing

The slightly fuel rich compositions, having equivalence ratio of 1.5, 3 and 4.5, were readily ignited; however, the heat output values of these compositions were relatively lower than those of B/Fe₂O₃ xerogels synthesized with THF, THP, 1,4 dioxane and ammonium hydroxide.

It is observed that the calorific values of sol-gel derived samples, especially with THF, THP, 1,4 dioxane and ammonium hydroxide, are approximately 1.4-1.8 times greater than those of physically mixed nano sized compositions. The results are consistent with Shen LH et al.'s [120] results obtained with Al/B/Fe₂O₃ compositions.

They [120] showed that the heat output of sol-gel derived compositions is approximately 1.3 times greater than the heat output of physically mixed compositions.

It is concluded that the preparation method is a very important for the combustion performance of pyrotechnic materials. The sol-gel method has an enhancing effect on the heat output due to obtaining skeletal matrix structures. As a result the enhancement in the structural properties and increase in the surface area and pore volume of sol-gel synthesized compositions provide efficient combustion compared to physically mixed commercial powders.

3.6.3 Effects of Fuel Type on Calorific Value of Metal/Fe₂O₃ Thermite Compositions

The calorific value results show that the B/Fe₂O₃ samples are promising materials for pyrotechnic systems. Furthermore, in this study it is aimed to determine the effects of type of fuel on the energetic properties of the samples by using 20% Mg coated Boron and Magnesium. Another purpose of this part of the study is to compare the results with Al/Fe₂O₃ which is well-known thermite composition. The samples having an equivalence ratio of 6 were synthesized by propylene oxide, THF, THP, 1,4 dioxane and ammonium hydroxide.

B/Fe₂O₃ samples prepared with propylene oxide have generally the smallest calorific value compared to samples prepared with other proton scavengers. However, the average calorific value is increased from 2464 J/g to 5540 J/g by using magnesium instead of boron as a fuel (Figure 3.29 and Table 3.15). It is known that magnesium is relatively easy to ignite compared to other fuels. It is also used as a coating material on boron in order to make easily ignitable compositions with high calorific values. Magnesium which

surrounds the boron particle enhances the combustion by heating the boron particle and as well as keep the surface of boron clear of oxide layer as possible. On the other hand Magnesium is known with its easily humidified structure resulting shorter shelf life compared to boron containing compositions. The results indicate that the combustion characteristics of the compositions prepared with propylene oxide can be enhanced with 20%Mg coated boron and magnesium as a fuel.

Boron still is a good candidate for the compositions containing Fe_2O_3 synthesized with THF. The results show that the calorific values of the samples with THF have completely different trend than those of the samples with propylene oxide. This result indicates that the type of proton scavenger used in synthesis of iron oxide has triggered a different type of reaction mechanisms during the combustion of fuel with oxidizer.

The type of fuel is not a significant effect on the calorific values and the combustion characteristics of samples prepared by THF. Similar to the samples prepared with THP, the samples prepared with THF have the smallest calorific value when Mg coated B is used as fuel.

Magnesium has significant effect on the calorific values of the samples prepared with 1,4 dioxane and ammonium hydroxide similar to the results of the samples prepared with propylene oxide. The average calorific values of Mg/ Fe_2O_3 with 1,4 dioxane and ammonium hydroxide reach to 6858 J/g and 7740 J/g which are the highest values among the samples prepared by other proton scavengers and fuel types.

The results show that it is possible to tailor the calorific values of the thermite composition containing Fe₂O₃ xerogels by varying the proton scavengers and the fuel type.

Table 3.15. The Calorific Values of DD 6FR metal/Fe₂O₃ Compositions

| Proton scavenger | Fuel Type | | | |
|-----------------------|-----------|------|----------------|-------|
| | Al | B | 20%Mg coated B | Mg |
| Calorific Value (J/g) | | | | |
| Propylene oxide | 1674 | 2464 | 2870 | 5540 |
| THF | 5004 | 5159 | 4092 | 4556 |
| THP | 4443 | 4171 | 3816 | 4456 |
| 1,4 dioxane | 4828 | 5042 | 3904 | 6858 |
| Ammonium hydroxide | 6259 | 5422 | 6071 | 7740 |
| Theoretical | 18200 | 6351 | 7991 | 22142 |

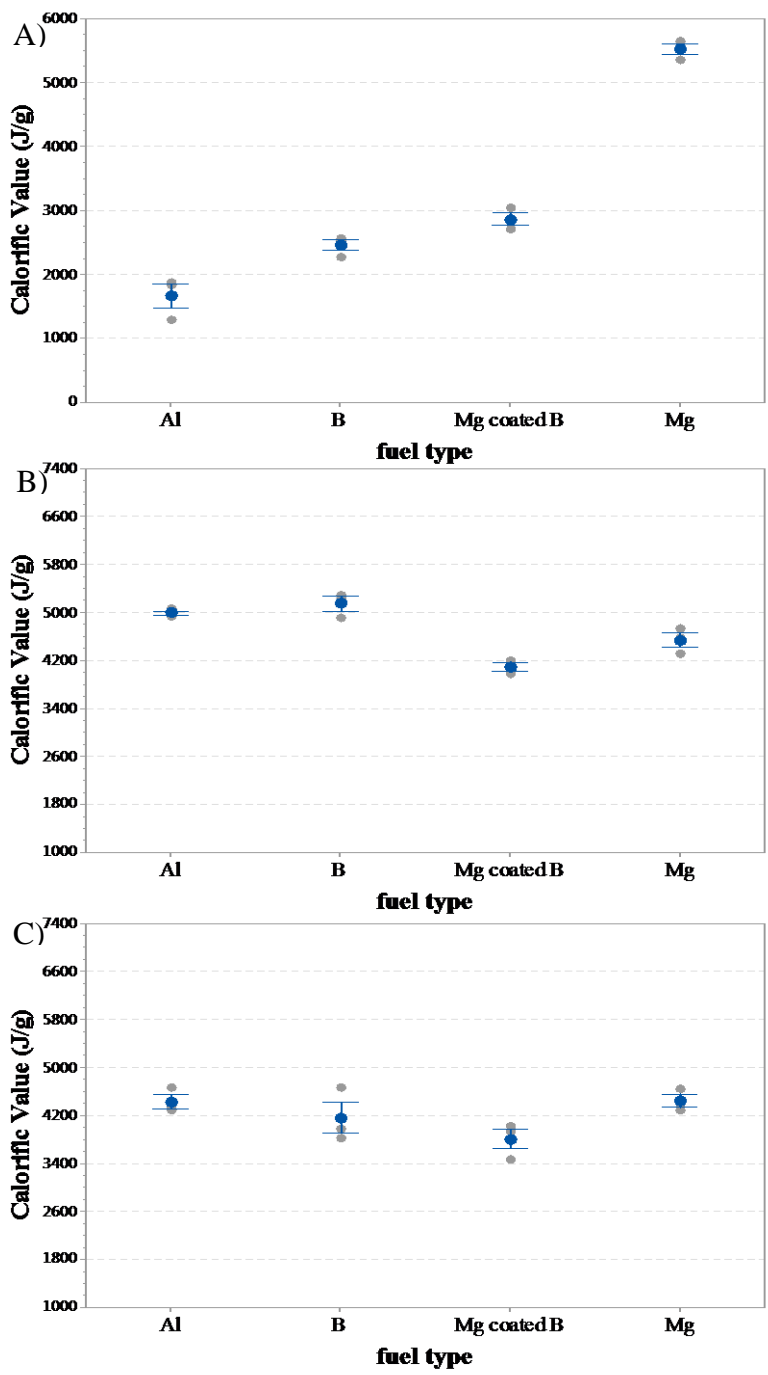


Figure 3.29. The comparison of the effect of fuel type on the calorific value of DD 6 FR compositions synthesized with A) propylene oxide B) THF C) THP

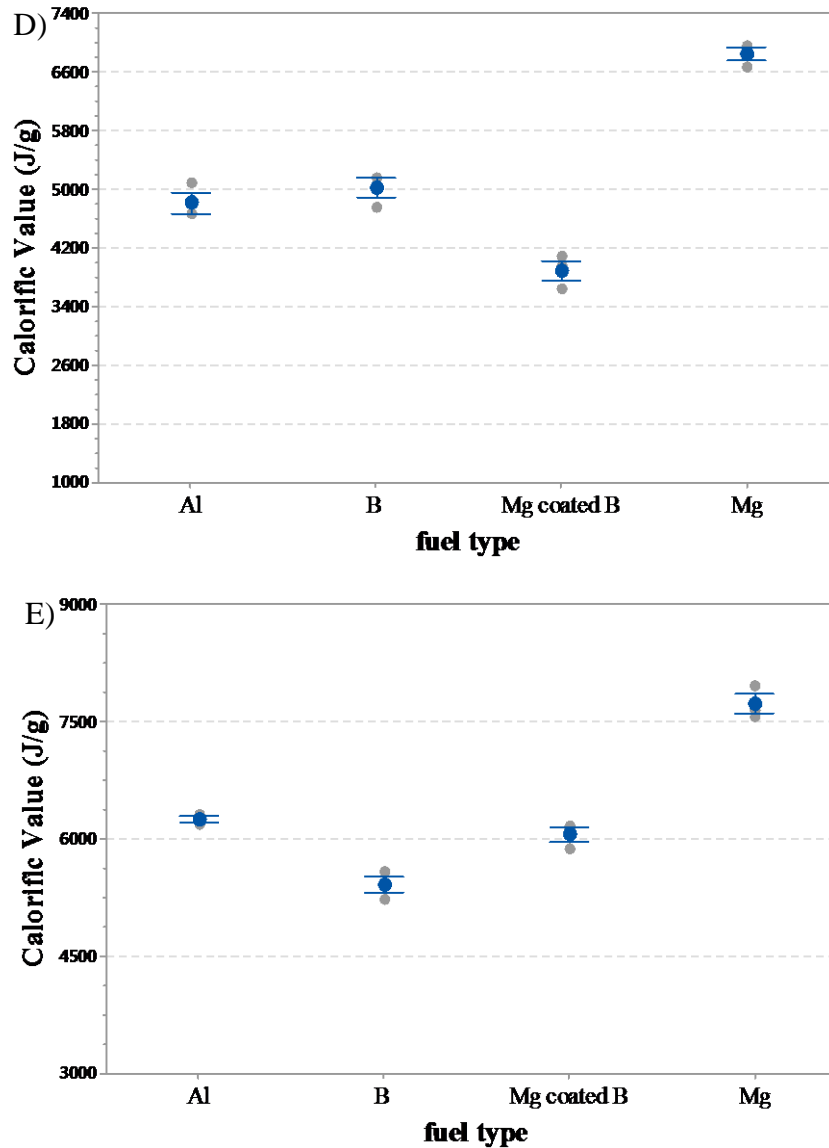


Figure 3.30. cont.’ The comparison of the effect of fuel type on the calorific value of DD 6 FR compositions synthesized with D) 1,4 dioxane E) ammonium hydroxide

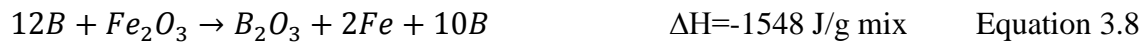
It is believed that during the calorific value tests, there was air atmosphere inside the steel closed bomb chamber of the Bomb Calorimeter. Therefore, to compare the experimental calorific values with the theoretical heat outputs, the calorific value calculations of 6FR

compositions were based on the reaction of fuels with iron oxide and the reaction of remaining fuels with excess oxygen as given:

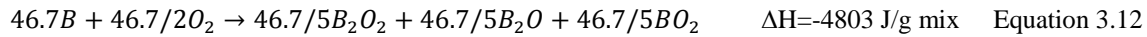
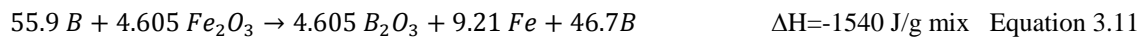
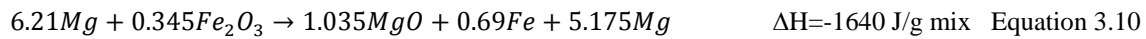
6FR Al/Fe₂O₃



6FR B/Fe₂O₃



6FR 20%Mg coated B/Fe₂O₃



6FR Mg/Fe₂O₃



3.6.4 Kinetic Study of SSE B/Fe₂O₃ Prepared with Propylene Oxide, 1,2 Epoxybutane and Ammonium Hydroxide

In this study, the effects of type of proton scavenger and concentration of precursor solution on the kinetic parameters such as activation energy, rate constant and pre-exponential factor were determined. The kinetic analysis was carried out to gain further insight into the combustion mechanism of boron and iron oxide powders. All samples were prepared by sequential solvent exchange (SSE) method. The heating rates of 10, 15 and 20°C/min. were used for DSC kinetic analysis as shown in Figure E1. Kinetic analysis of B/Fe₂O₃ combustion reaction was conducted by using Kissinger Method [168]. The stoichiometric reaction of Fe₂O₃ with B is as follows:



The activation energy, E_a (kJ/mol) were determined by plotting $\ln(\beta/T_p^2)$ as a function of $(1/T_p)$ for heating rates of 10, 15 and 20°C/min. The slope of the trend lines were used to calculate the activation energy.

The trend lines are given in Figure 3.30-Figure 3.34.

$$\ln \frac{\beta}{T_p^2} = \ln \frac{R \cdot Z}{E_a} - \frac{E_a}{R} \cdot \frac{1}{T_p} \quad \text{Equation 3.17}$$

| | | |
|-------|---|-----------------------------|
| T_p | : | peak temperature, K |
| B | : | heating rate, K/min |
| E_a | : | activation energy, kJ/mol |
| R | : | gas constant, J/mol.K |
| Z | : | pre-exponential factor, 1/s |

By using Arrhenius equation;

$$k = Z \exp\left(\frac{-E_a}{R T}\right) \quad \text{Equation 3.18}$$

the pre-exponential factor, Z was calculated. The calculated values of Z, k and activation energy values are given in Table 3.16. For example, the values for samples prepared with propylene oxide in diluted precursor solution are as following;

$$k = 9.0 \times 10^{38} \exp\left(\frac{-41026}{T}\right)$$

Table 3.16. The activation energy values of SSE 3 FR B/Fe₂O₃ prepared with propylene oxide, 1,2 epoxybutane and ammonium hydroxide from diluted and concentrated solutions of precursor

| Proton scavenger | Propylene oxide | | 1,2-epoxybutane | | Ammonium hydroxide |
|--|--|--|--|--|--|
| | diluted | conc. | diluted | conc. | - |
| Ignition temperature 1 st peak | 190°C | 190°C | 190°C | 200°C | 245°C |
| Activation energy, 1 st exotherm (kJ/mol) | 341 | 270 | 296 | 202 | 102 |
| Z | 9.0x10 ³⁸ | 3.5x10 ³⁰ | 6.3x10 ³³ | 2.7 x10 ²² | 7.8 x10 ⁹ |
| k | $9.0 \times 10^{38} \exp\left(\frac{-41026}{T}\right)$ | $3.5 \times 10^{30} \exp\left(\frac{-32562}{T}\right)$ | $6.3 \times 10^{33} \exp\left(\frac{-35596}{T}\right)$ | $2.7 \times 10^{22} \exp\left(\frac{-24341}{T}\right)$ | $7.78 \times 10^9 \exp\left(\frac{-12224}{T}\right)$ |

It is shown by the calorific value tests that 3FR samples prepared with propylene oxide cannot be ignited while samples prepared with ammonium hydroxide can easily be ignited and have high calorific values. The calorific values of samples prepared with 1,2 epoxybutane, similar to the samples prepared with propylene oxide, were found to be the smallest value among the samples prepared with other proton scavengers. This might be related with the activation energy values of these samples. As given in Table 3.16 the activation energy of samples prepared with ammonium hydroxide has the lowest value among the all samples, while the activation energy of samples prepared with propylene oxide has highest value.

The aim of this part is also to see the effect of the concentration of precursor solution. It is found that the samples prepared from diluted precursor solution have higher activation energy compared to those prepared from concentrated precursor solution. The reason of that might be the samples prepared from concentrated precursor solution have higher amount of oxidizer compared to the samples prepared from diluted precursor solution. Therefore the samples prepared from concentrated precursor solution can be easily ignited.

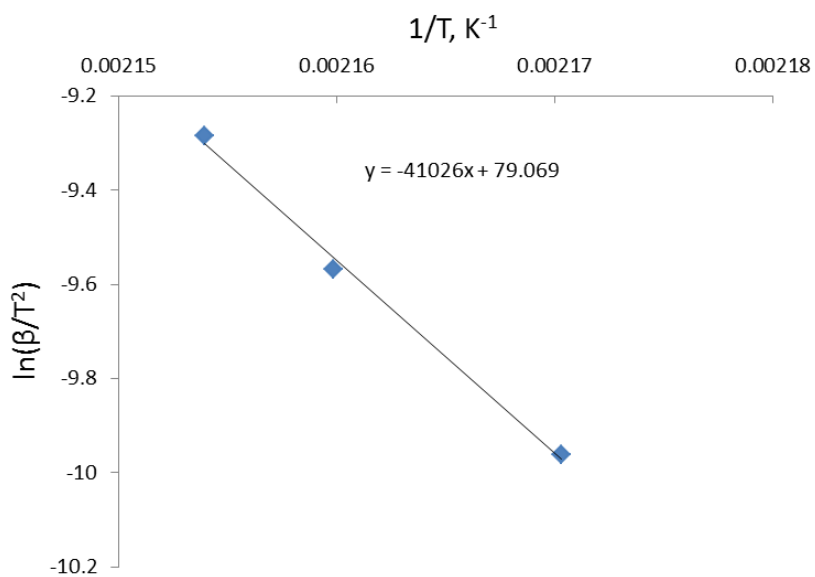


Figure 3.30. Trend lines for calculating the activation energy of SSE 3FR B/Fe₂O₃ prepared with propylene oxide from diluted solution of precursor

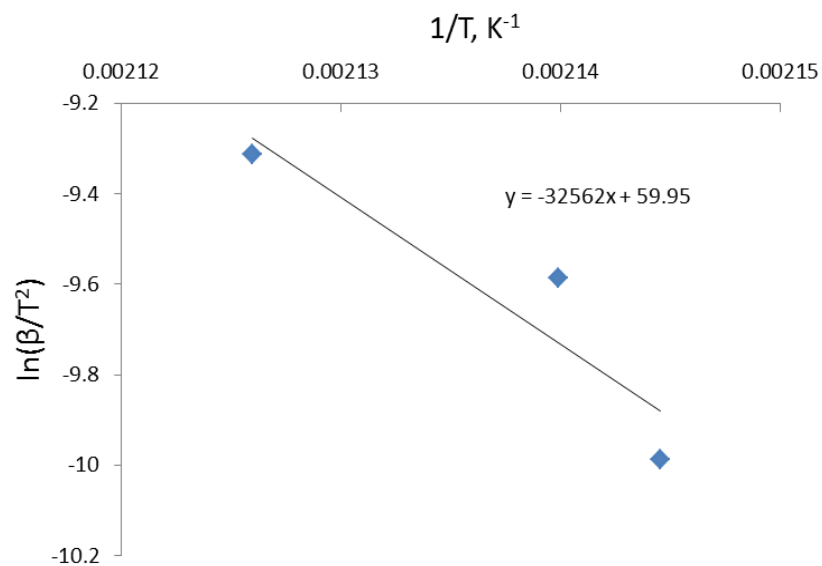


Figure 3.31. Trend lines for calculating the activation energy of SSE 3FR B/Fe₂O₃ prepared with propylene oxide from concentrated solution of precursor

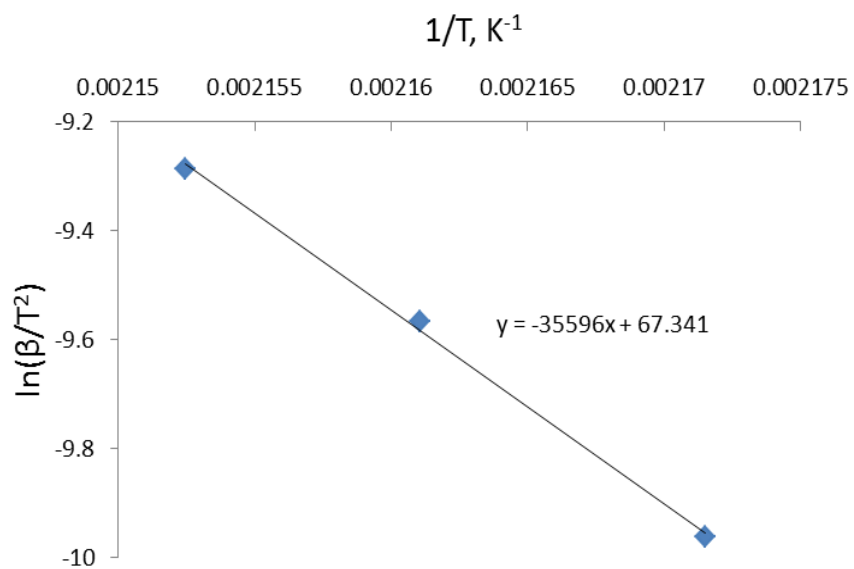


Figure 3.32. Trend lines for calculating the activation energy of SSE 3FR B/Fe₂O₃ prepared with 1,2 epoxybutane from diluted solution of precursor

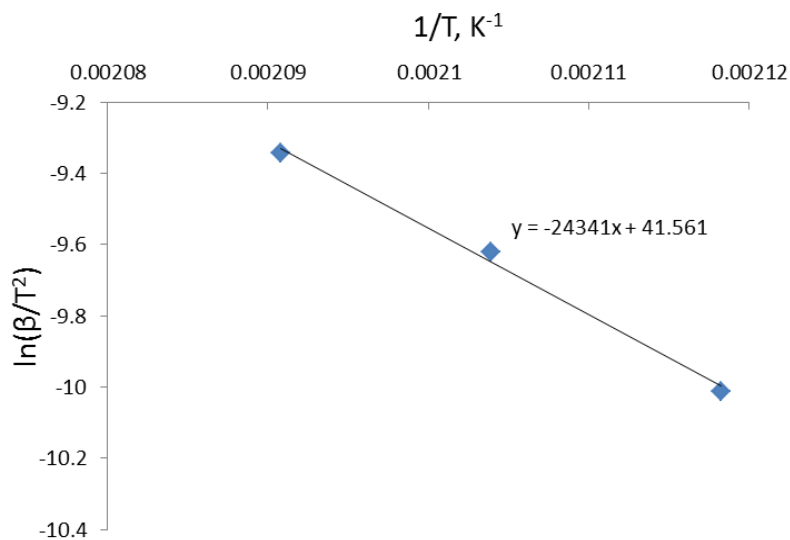


Figure 3.33. Trend lines for calculating the activation energy of SSE 3FR B/Fe₂O₃ prepared with 1,2 epoxybutane from concentrated solution of precursor

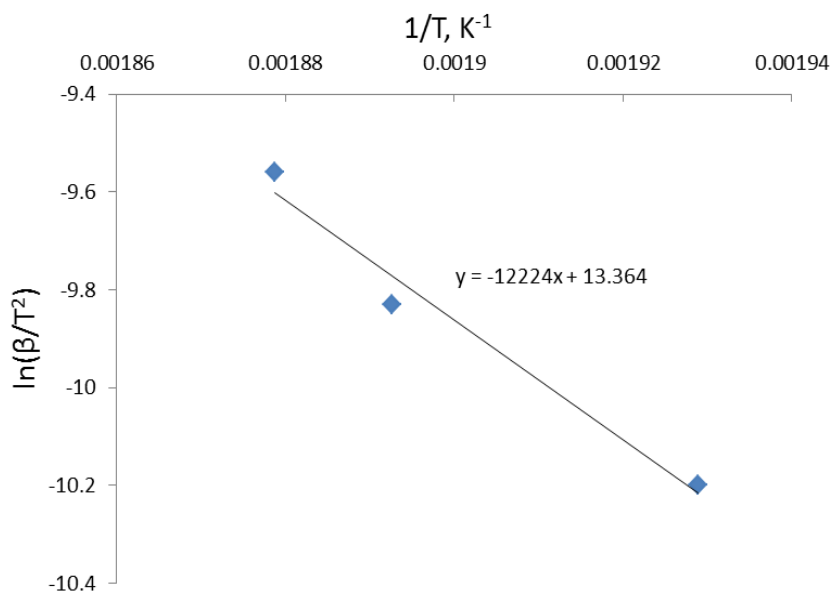


Figure 3.34. Trend lines for calculating the activation energy of SSE 3FR B/Fe₂O₃ prepared with ammonium hydroxide

3.7 Morphological and Structural Analysis

9FR compositions of B and Fe₂O₃ samples synthesized with ammonium hydroxide and propylene oxide were selected among the all xerogel samples to subject to SEM analysis and EDS (energy dispersive spectroscopy) measurements. The results are presented in the following sections.

3.7.1 SEM Images of B/Fe₂O₃ Synthesized with Ammonium Hydroxide

Figure 3.35 shows SEM images of the mixture of 9 FR B/Fe₂O₃ xerogel with magnifications of 100,000 and 400,000. The iron oxide xerogel was found to be formed as continuous phase. It is shown that the composition is well-mixed having a smooth surface (Figure 3.35).

The particles were shown to be in nano size range. In order to further analyze of the elemental constituents of the composition, EDS analysis was carried out. B, Fe, O and N contents were observed by EDS measurement as given in Table 3.17. N content shows the presence of ammonium nitrate phase NH₄NO₃ inside the structure which was produced during the gelation process according to the possible reactions given in Equation 3.1 and 3.2.

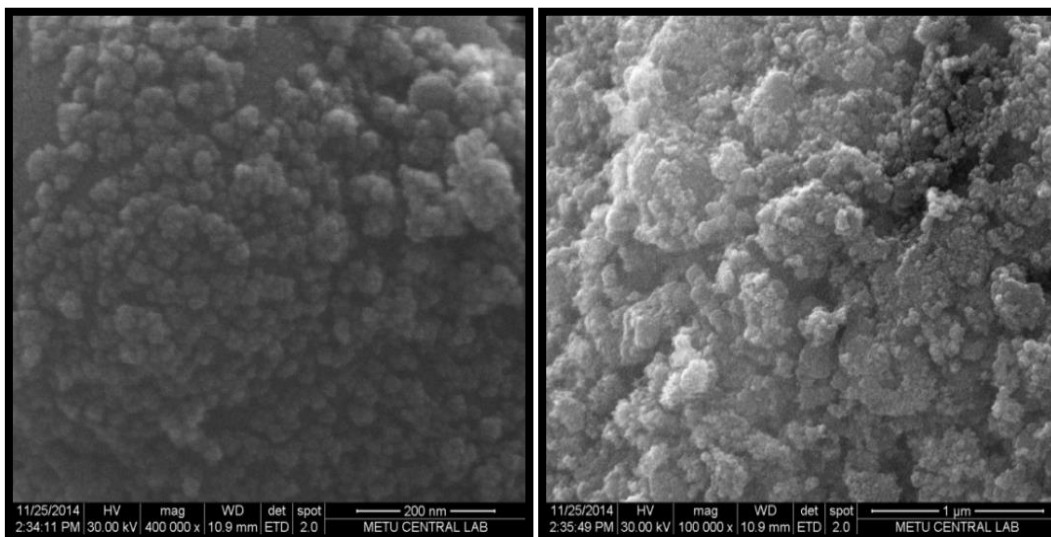


Figure 3.35. SEM images of B/Fe₂O₃ synthesized with ammonium hydroxide

Table 3.17. Elemental EDS Analysis of B/Fe₂O₃ synthesized with ammonium hydroxide

| Element | Weight % | Atomic % |
|---------|----------|----------|
| B | 75.45 | 86.43 |
| O | 10.16 | 7.86 |
| Fe | 9.28 | 2.06 |
| N | 4.02 | 3.56 |
| Au | 0.65 | 0.04 |
| Pd | 0.44 | 0.05 |

SEM Images of Combustion Products of B/Fe₂O₃

After the combustion of B/Fe₂O₃ sample with the equivalence ratio of 9, the final combustion products were also analyzed by SEM characterization and the images are shown in Figure 3.36 with the magnifications of 100,000 and 400,000. It was shown that after burning of the B/Fe₂O₃ xerogel, the morphology was completely changed. It was shown that after burning of the B/Fe₂O₃ xerogel, the morphology was completely changed. In order to further analyze of the elemental constituents of the combustion products of 9FR B/Fe₂O₃ sample, EDS analysis was carried out. B, Fe, O and N contents were observed as given in Table 3.18.

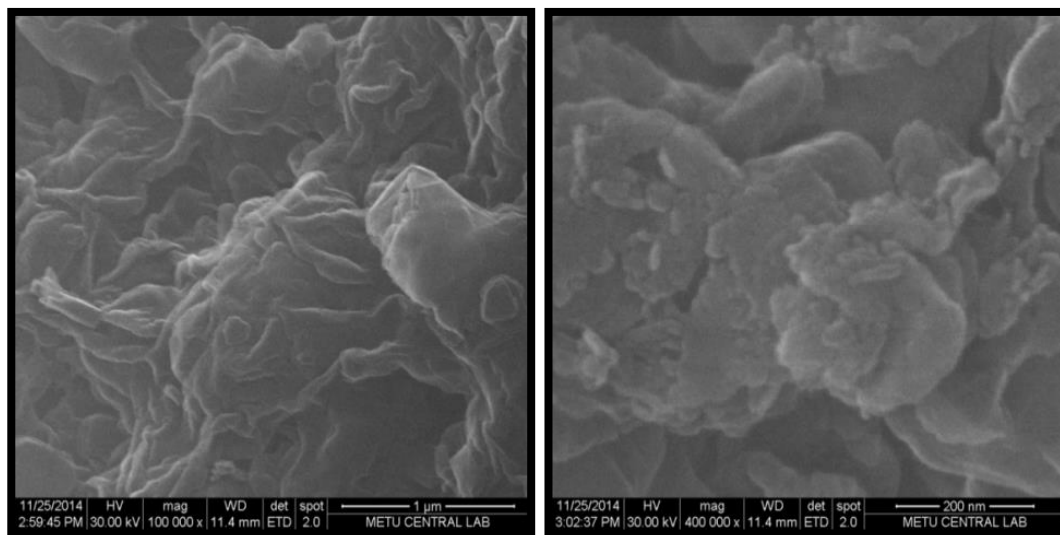


Figure 3.36. SEM images and EDS spectrums of the combustion products of B/Fe₂O₃ synthesized with ammonium hydroxide

Table 3.18. Elemental EDS Analysis of the combustion products of 9 FR B/Fe₂O₃ synthesized with ammonium hydroxide

| Element | Weight % | Atomic % |
|---------|----------|----------|
| O | 59.97 | 52.02 |
| B | 34.73 | 44.58 |
| N | 3.02 | 2.99 |
| Fe | 1.33 | 0.33 |
| Au | 0.64 | 0.05 |
| Pd | 0.31 | 0.04 |

3.7.2 SEM Images of B/Fe₂O₃ Synthesized with Propylene Oxide

9 FR B/Fe₂O₃ synthesized with propylene oxide was characterized by SEM analysis shown in Figure 3.37 with 400,000 x magnifications. The iron oxide xerogel was found to be formed as continuous phase similar to the samples prepared with ammonium hydroxide. It is shown that the composition is well-mixed having a smooth surface. The particles of the composition were shown to be in nano size range. In order to further analyze of the elemental constituents of the composition, EDS analysis was carried out. B, Fe and O contents were observed by EDS analysis as given in Table 3.19.

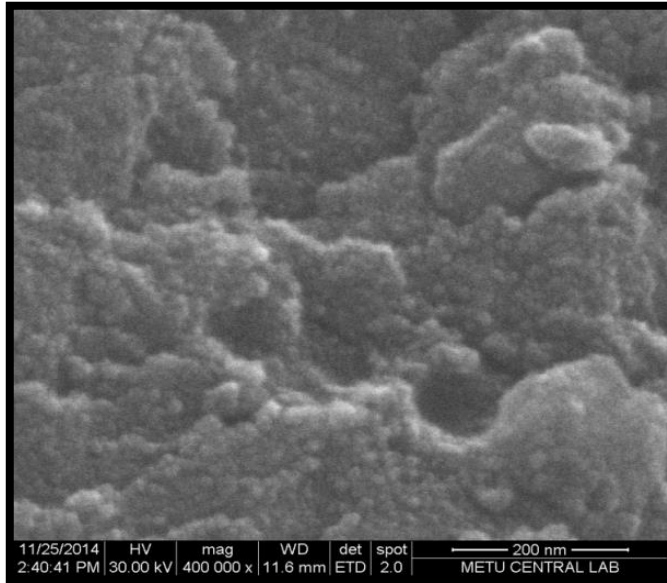


Figure 3.37. SEM images and EDS spectrums of B/Fe₂O₃ sample synthesized with propylene oxide

Table 3.19. Elemental EDS Analysis of the 9 FR B/Fe₂O₃ synthesized with propylene oxide

| Element | Weight % | Atomic % |
|---------|----------|----------|
| B | 85.16 | 90.37 |
| O | 11.84 | 8.49 |
| Fe | 1.71 | 0.35 |
| N | 0.93 | 0.76 |
| Au | 0.21 | 0.01 |
| Pd | 0.16 | 0.02 |

3.8 Sensitivity Tests

The impact and friction sensitivity tests were applied to the samples synthesized with ammonium hydroxide and prepared by DD and SSE method via the test procedure given in STANAG 4487 [92] and STANAG 4489 [93] and the results were obtained by the statistical calculations of Bruceton up and down test procedure and were given in Table 3.20 and Figure 3.38 [169, 170].

The most sensitive material to impact and friction is 3FR B/F₂O₃ sample synthesized with ammonium hydroxide and prepared by SSE method. The impact and friction stimulus of SSE 3FR sample was found to be lower than those of DD 3FR sample. DD ST, 3FR and 9FR B/F₂O₃ samples were not initiated by the maximum force of 360 N which indicated that they all were very insensitive to friction.

Table 3.20. Impact and Friction Sensitivity of B/Fe₂O₃ Compositions prepared with ammonium hydroxide

| Proton scavenger | Friction Sensitivity (N) | Impact Sensitivity (J) |
|------------------|--------------------------|------------------------|
| SSE 3FR | 216 | 3 |
| DD 3FR | > 360 | 13 |
| DD ST | > 360 | 50 |
| DD 9FR | > 360 | 3 |

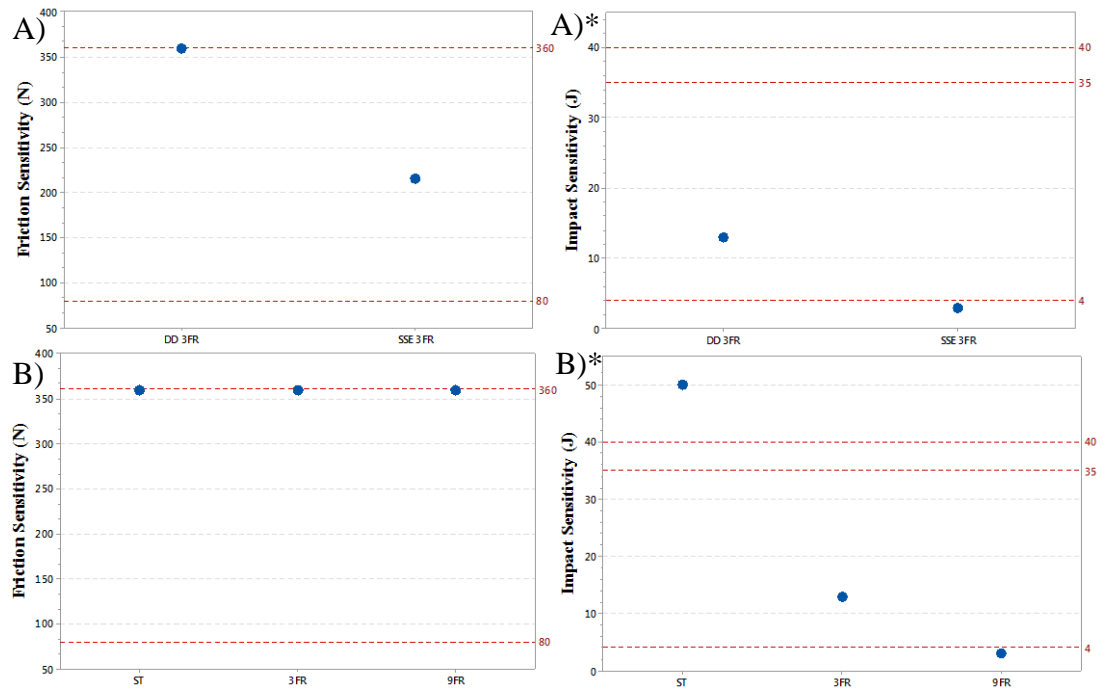


Figure 3.38. Friction sensitivity of A) 3FR SSE& DD compositions B) DD ST, 3FR & 9FR compositions & Impact sensitivity of A)* 3FR SSE& DD compositions B)* DD ST, 3FR & 9FR compositions

3.9 Summary

In this study, the major goal was to develop easily ignitable energetic nanocomposites with high heat output when properly initiated. Therefore, in order to develop nanostructured pyrotechnic materials, a very well-known sol-gel method was used for synthesis and preparation of thermite compositions.

Boron has been one of the most interesting materials, which has been used as fuel for pyrotechnic compositions not only due to its longer shelf life, but because of its higher heat of combustion and lower atomic weight with high gravimetric and volumetric energy content compared to other fuels.

Another major objective of the study was to investigate the effects of sol-gel synthesis parameters such as proton scavenger, concentration of the precursor solution and drying conditions on the structural properties and thermal behavior of the samples.

Furthermore, this study, for the first time, investigated the effects of sequential solvent exchange method on the energetic performance of the pyrotechnic compositions.

In order to investigate the effect of fuel on the combustion performance of energetic nanocomposites, as-synthesized iron oxide xerogels were mixed with Magnesium, Aluminum and Magnesium coated Boron and the results were compared with the samples containing Boron.

From the energetic characteristics point of view; tetrahydrofuran (THF) and ammonium hydroxide are realized to be the most promising proton scavengers with their enhancing effect on the combustion of energetic nanocomposites. The key findings are discussed in following lines.

Use of 1,2 epoxybutane as an alternative proton scavenger did not give any benefit for the energetic formulations of fuel/iron oxide xerogels.

Use of tetrahydrofuran as a proton scavenger to synthesize iron oxide resulted moderate surface area (Figure 3.39). The nanocomposites containing iron oxide synthesized with THF and Boron has relatively high heat output (Figure 3.40) which makes THF a very good candidate for pyrotechnic applications.

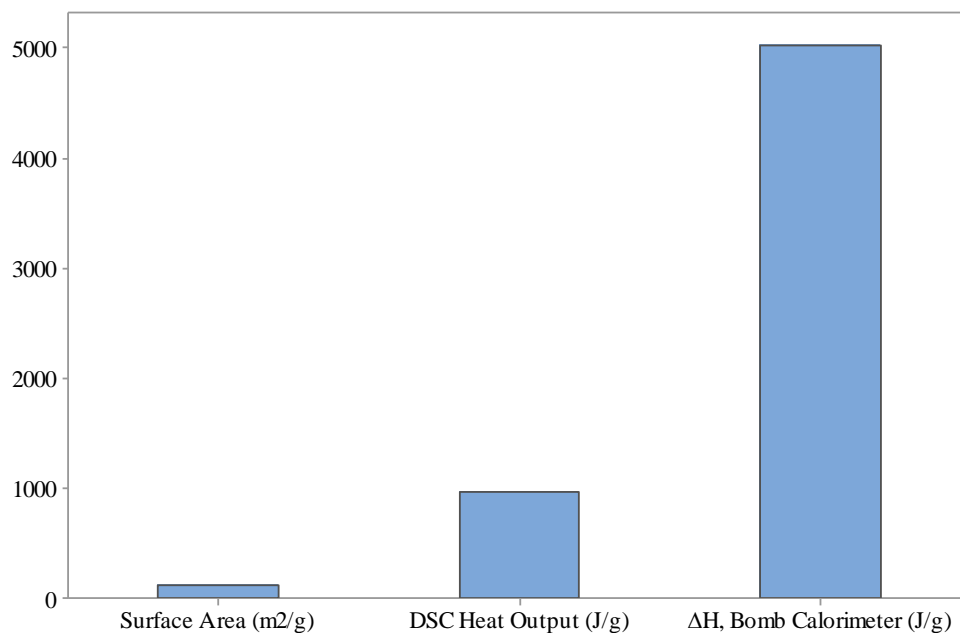


Figure 3.39. The schematic results of DD 3FR B/Fe₂O₃ samples prepared with THF

Furthermore, the application of sequential solvent exchange procedure on the iron oxide sample after synthesis steps has resulted higher surface area than the application of direct drying procedure. The solvent removal rate and drying is favored by the presence of non polar solvent and the porous structure is preserved with sequential solvent exchange method while the evaporation of the ethanol from the gel structure by direct drying leads to the excessive capillary forces on the gel's pore structure and these capillary forces result in shrinkage of the gel matrix. It can be concluded that sequential solvent exchange method has an enhancing effect on the heat output due to the enhancement in the structure and the increase in the surface area and pore volume.

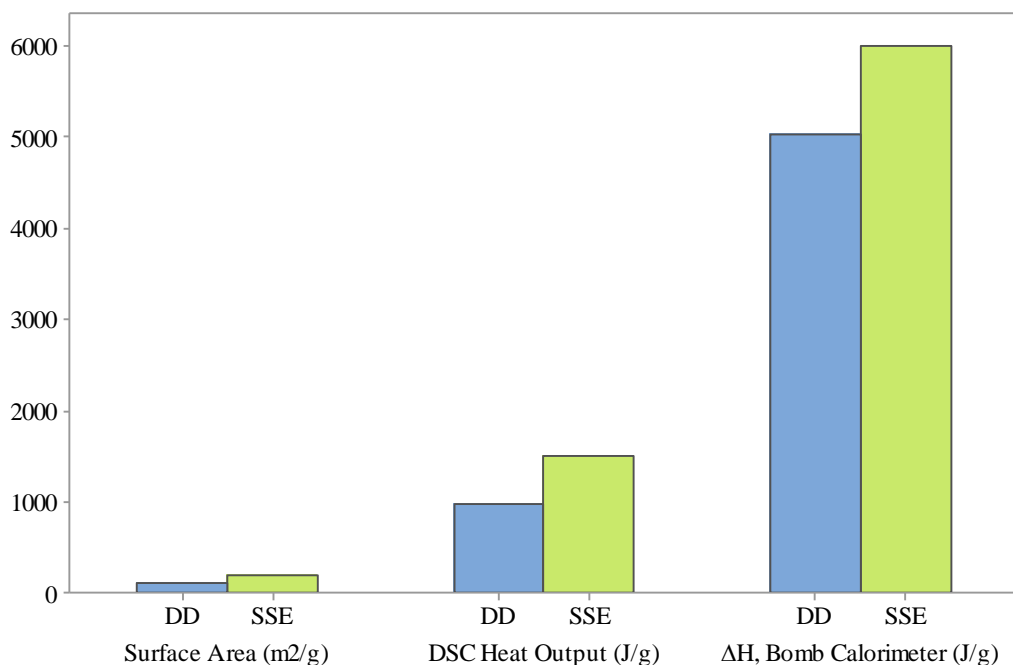


Figure 3.40. The schematic representation of the effect of drying procedure on the properties of 3FR B/Fe₂O₃ samples prepared with THF

Use of B/Fe₂O₃ formulations with more fuel content which were prepared by increasing equivalence ratio from 3 to 9 helped to achieve desired energetic performance (Figure 3.41). That is, the higher B content means the higher active fuel in the energetic composition, so excess B reacts with excess oxygen in air atmosphere. The oxide layer around the boron particle inhibits the combustion of the fuel therefore it is possible to overcome this drawback by increasing boron content.

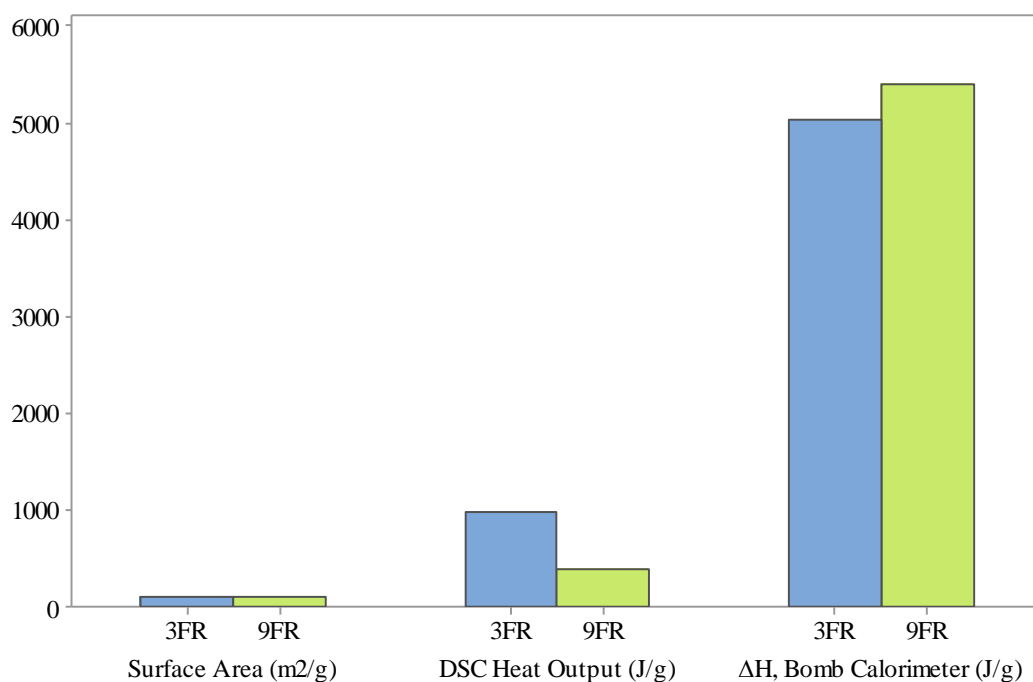


Figure 3.41. The schematic representation of the effect of equivalence ratio increasing from 3 to 9 on the properties of samples prepared with THF

As discussed above, tetrahydrofuran is the most promising one among all the other proton scavengers. Besides, based on the results, the ammonium hydroxide exhibits very different structural and thermal characteristics compared to other proton scavengers as discussed in following lines.

Use of ammonium hydroxide as a proton scavenger to synthesize iron oxide resulted the lowest surface area compared to other proton scavengers. Because the ammonium hydroxide has stronger basicity than the other proton scavengers have. As a result, the rapid precipitation of Fe_2O_3 phase and crystallization process may lead the destruction of porous structure. However, these samples were found to be reactive and easily ignitable with their high heat output as schematically illustrated in Figure 3.42. This result might be related with the less stable characteristics of ammonium hydroxide. Furthermore, it might be explained by the ammonium nitrate groups which were observed by XRD ($(\text{NH}_4)(\text{NO}_3)$ -no.01-083-0520), FTIR (NH_3 groups) and elemental analysis (N:20wt%) presented in results and discussion section. The residual ammonium nitrate, NH_4NO_3 , arises from the reaction of free NO_3^- ions which are generated during the hydrolysis step of iron nitrate nonahydrate ($\text{Fe}(\text{NO}_3)_3 \cdot 9\text{H}_2\text{O}$). The enhancement in heat output due to the ammonium nitrate can be explained by the behavior of strong oxidizing agent for boron particles.

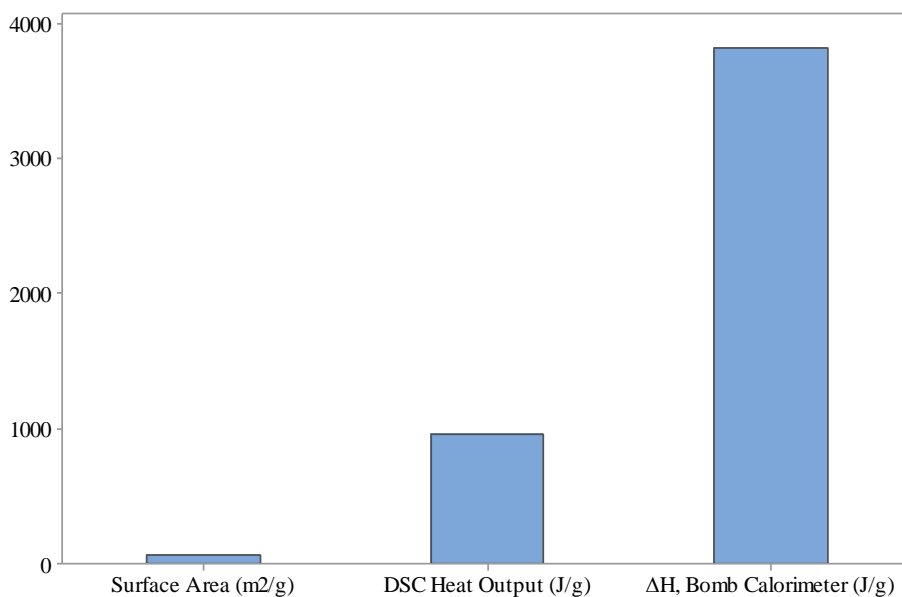


Figure 3.42. The schematic results of DD 3FR B/ Fe_2O_3 samples prepared with ammonium hydroxide

Despite its lowest surface area, it was shown that by using sequential solvent exchange method instead of direct drying method, the surface area were found to be twice as high as that obtained with direct drying method (Figure 3.43). The enhancement in the calorific values might be attributed to the textural properties of the samples which depend on the drying conditions. The reason of that could be the slow extraction/evaporation of the solvent inside the pores does not cause the contraction of the skeletal matrix which takes place in direct drying method. It is expected that the high surface area and porous structure of the oxidizer may enhance the combustion propagation.

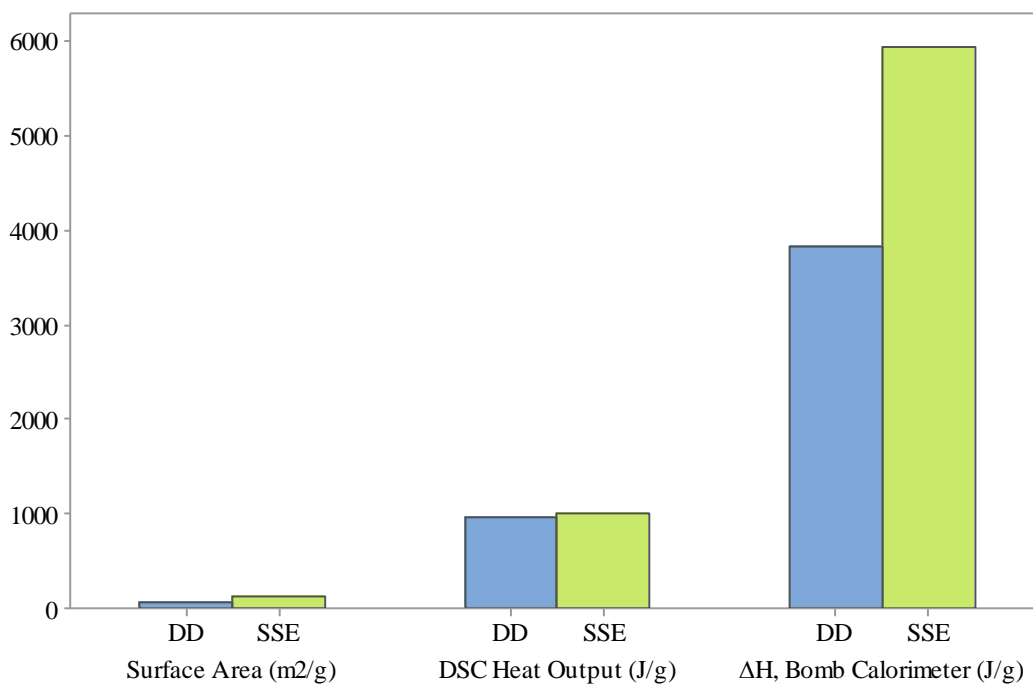


Figure 3.43. The schematic representation of the effect of drying method on properties of samples prepared with Ammonium hydroxide

Use of 9FR B/Fe₂O₃ composition instead of 3FR B/Fe₂O₃ composition prepared with ammonium hydroxide improved energetic performance in terms of heat output in air atmosphere (Figure 3.44). That is, the higher B content means the higher active fuel in the energetic composition, so excess B reacts with excess oxygen in air atmosphere. The oxide layer around the boron particle inhibits the combustion of the fuel therefore using larger amount of boron content helps to overcome this drawback.

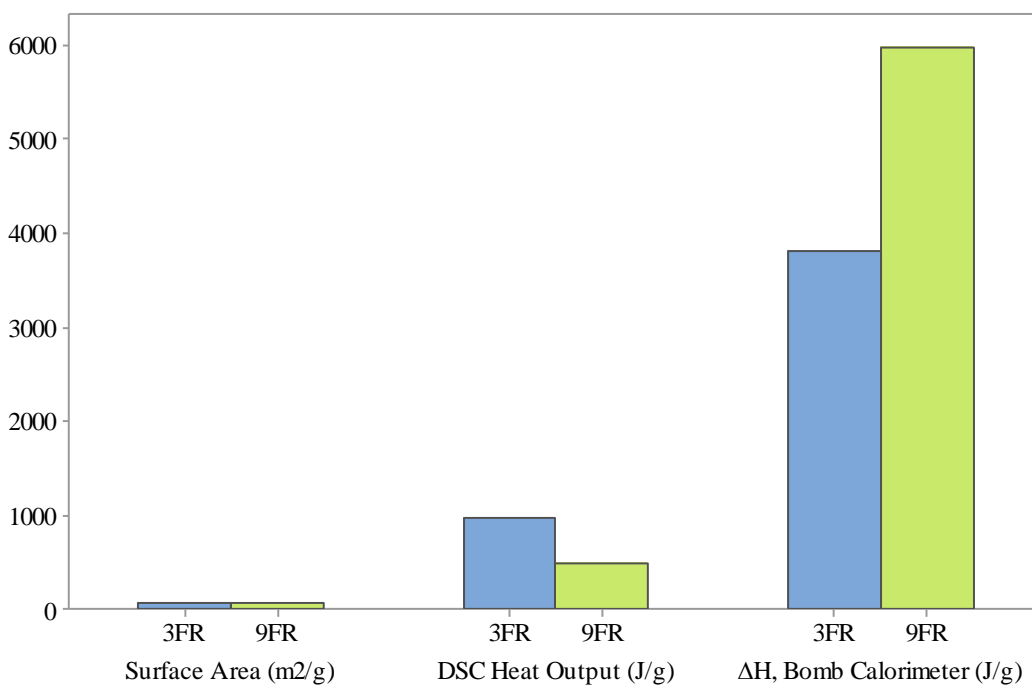


Figure 3.44. The effect of increase in fuel content with equivalence ratio from 3 to 9 on properties of samples prepared with Ammonium hydroxide

The results show that the B/Fe₂O₃ samples are promising materials for pyrotechnic systems. Furthermore, in this study it is aimed to determine the effects of type of fuel on the energetic properties of the samples. Another purpose of the study is to compare the results with Al/Fe₂O₃ which is a very well-known thermite composition.

Use of magnesium instead of boron as a fuel resulted the highest value among the samples prepared by other proton scavengers and fuel types (Figure 3.45). It is known that magnesium is relatively easy to ignite compared to other fuels. On the other hand, Magnesium is known with its easily humidified structure resulting shorter shelf life compared to boron containing compositions.

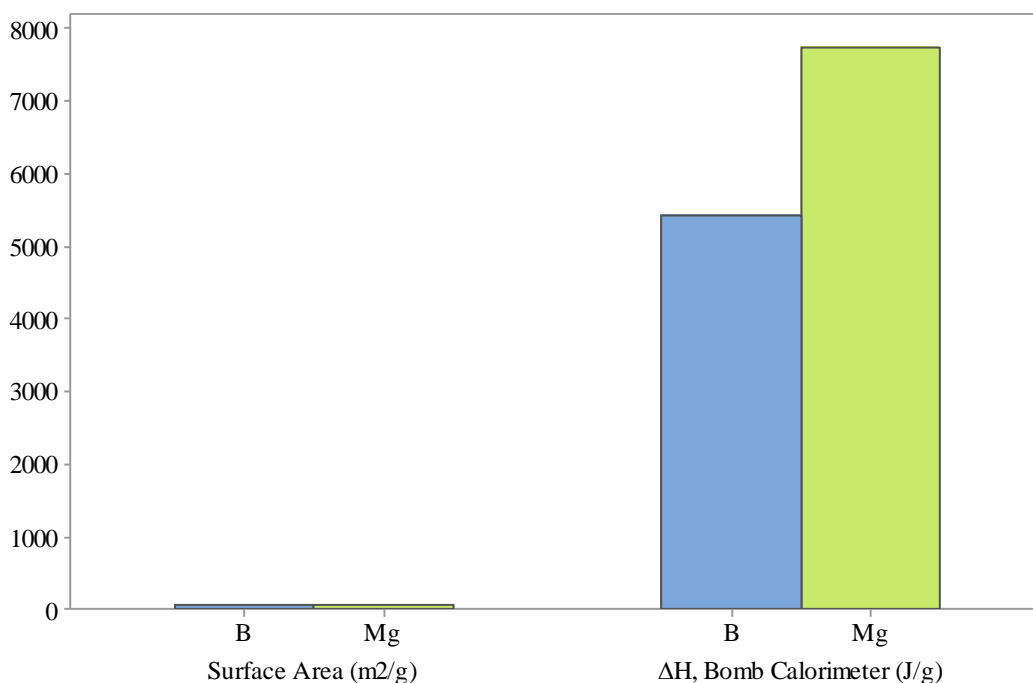


Figure 3.45. The effect of fuel : use of Mg instead of B with samples prepared with Ammonium hydroxide having an equivalence ratio of 9

CHAPTER 4

CONCLUSIONS

The energetic nanocomposites of boron and iron oxide xerogels synthesized with various proton scavengers are promising materials for thermite compositions. Moreover, the sequential solvent exchange method improves the crystallinity, textural properties of Fe_2O_3 which also enhances the combustion performance of B/ Fe_2O_3 thermites. The results indicate that the particle size, porosity, surface area and crystallinity of the iron oxide samples can be tailored by the synthesis and drying conditions. The iron oxide with mesoporous structured matrix can be derived by utilizing 1,2 epoxybutane, propylene oxide, THF, THP and 1,4 dioxane as proton scavenger. As expected, higher heat release per unit mass of B/ Fe_2O_3 sample is observed for less fuel rich composition under inert atmosphere, while higher heat release per unit mass of B/ Fe_2O_3 sample is observed for high fuel rich composition under air atmosphere. Fe_2O_3 xerogels prepared by sol-gel technique can be coupled with B, Mg, Al and Mg coated boron fuels to obtain desired heat output.

The structural and physical properties of the iron oxide xerogels are highly affected by the type of proton scavenger used in gelation process. The proton scavengers do not only affect the surface area but also the combustion mechanism of the boron / iron oxide nano composites. The lowest surface area was obtained with ammonium hydroxide. However it seems that the heat output was enhanced due to some other properties such as crystallinity and surface free energy which depend on the synthesis conditions and gelation mechanisms. Therefore, it is possible to enhance the textural properties and calorific value by changing the type of proton scavenger.

The results indicate that it is possible to tailor the properties of the nano-sized pyrotechnics by changing the fuel content of the samples. According to DSC/TG analysis, the samples with ammonium hydroxide, tetrahydrofuran (THF), tetrahydropyran (THP) which have an equivalence ratio of 3 and with propylene oxide which have an equivalence ratio of 6 have the highest calorific values of 960, 970, 1130 and 1230 J/g, respectively. In addition, the calorific values of sol-gel derived nano composites are almost 2 times greater than the calorific values of the same compositions prepared by physical mixing of commercial nano-sized raw materials based on the calorific value test results.

Consequently, different proton scavengers were found to affect different material characteristics of the synthesized nanocomposites. From the material characterization point of view; propylene oxide, tetrahydropyran (THP) and 1,2 epoxybutane are the most promising proton scavengers since they improve the structural behavior of xerogels by increasing surface area. On the other hand, from the energetic characteristics point of view; ammonium hydroxide, 1,4 dioxane and tetrahydrofuran (THF) are realized to be the most promising proton scavengers with their enhancing effect on the combustion of nano composites. The samples prepared with ammonium hydroxide, 1,4 dioxane and tetrahydrofuran (THF) were found to have lower surface area; however, their less stable characteristics made the energetic nanocomposites more reactive and easily ignitable.

In the scope of the study, the compositions containing various fuel types such as Mg, Al and 20%Mg coated B were subjected to thermal analysis and calorific value tests to investigate the effect of fuel type on the combustion characteristics of the nanocomposites. It is observed that boron is a common fuel for the pyrotechnic materials with its high gravimetric and volumetric energy content and Mg is also a good candidate for the compositions containing iron oxide xerogels.

The heat outputs of SSE samples are approximately 5-45% greater than the heat outputs of DD samples prepared by 1,2 epoxybutane, THF, THP, 1,4 dioxane and ammonium hydroxide in accordance with DSC/TG analysis. The enhancement of the heat output might be related with the textural properties of the samples which strongly depend on the drying conditions. Drying method affects the mechanism of extraction/evaporation of the solvent within the porous structure of gel.

It can be concluded that sequential solvent exchange method has an enhancing effect on the heat output due to the enhancement in the structure and the increase in the surface area and pore volume.

As a result it is possible to adjust the structural, physical and energetic properties of the iron oxide xerogels containing B, Mg, Al and Mg coated B as fuel by varying the proton scavengers, drying conditions and equivalence ratio of the formulations.

REFERENCES

- [1] Staley C. S., Morris C. J., Thiruvengadathan R., Apperson S. J., Gangopadhyay K., Gangopadhyay S., *Silicon-Based Bridge Wire Micro-Chip Initiators for Bismuth Oxide–Aluminum Nanothermite*, J. Micromech. Microeng. 21, 115015, 2011.
- [2] Zhang K.L., Choua S.K., Ang S.S., Tang X.S., *A MEMS-Based Solid Propellant Microthruster with Au/Ti Igniter*, Sensors and Actuators A 122,113–123, 2005.
- [3] Martirosyan K. S., Wang L., Vicent A., Luss D., *Nanoenergetic Gas-Generators: Design and Performance*, Propellants Explos. Pyrotech., 34, 532 – 538, 2009.
- [4] Goldschmidt H., Weil O., *Method of Manufacturing Metals*, U.S.Patent No.895,628, 1908.
- [5] Blobaum K.J., Reiss M.E., Plitzko J.M., Weihs T.P., *Deposition and Characterization of a Self-Propagating CuO_x/Al Thermite Reaction in a Multilayer Foil Geometry*, Journal of Applied Physics, 94, 2915, 2003.
- [6] Moore J.J., Feng H.J., *Combustion Synthesis of Advanced Materials: Part I. Reaction Parameters*, Progress in Materials Science, 39, 243-273, 1995.
- [7] Goldschmidt H., Lange F., *Clamping Apparatus for Clamping and Butting Railway Rails in the Welding Process*, U.S.Patent No.925,630, 1909.

[8] Feynman R.P., *There's Plenty of Room at the Bottom*, American Physical Society, Pasadena, 1959.

[9] Granier J.J., Pantoya M.L., *Laser Ignition of Nanocomposite Thermites*, *Combustion and Flame* 138, 373–383, 2004.

[10] Shidlovskiy A. A., *Principles of Pyrotechnics, Third Edition* (Revised & Enlarged, 1964), 1997.

[11] Wilson D.E., Kim K., *Combustion of Consolidated and Confined Metastable Intermolecular Composites*, 43rd AIAA Aerospace Sciences Meeting and Exhibit, Nevada, 2005.

[12] Yong L. de, Park B., Valenta F., *A Study of the Radiant Ignition of a Range of Pyrotechnic Materials Using a CO₂ Laser*, MRL Technical Report, MRL-TR-90-20, 1990.

[13] Agrawal J.P., *High Energy Materials: Propellants, Explosives and Pyrotechnics*, Wiley-VCH Verlag GmbH & Co. KGaA, Weinheim, Germany 2010.

[14] Chemical Warfare Service, *Thermite, Plain, Incendiary, C.W.S. Formula No. D-1-1*, Edgewood Arsenal, Maryland, USA, 1944.

[15] Takacs L., *Ball Milling-Induced Combustion in Powder Mixtures Containing Titanium, Zirconium, or Hafnium*, *Journal of Solid State Chemistry*, 125, 75-84, 1996.

[16] Kobaschewski O., Alcock C.B., Spencer P.J., *Materials Thermochemistry*, 6th ed. Pergamon Press, Oxford, 1993.

- [17] Plantier K.B., Pantoya M.L., Gash A.E., *Combustion Wave Speeds of Nanocomposite Al/Fe₂O₃: the Effects of Fe₂O₃ Particle Synthesis Technique*, *Combustion and Flame*, 140, (4), 299-309, 2005.
- [18] Pantoya M.L., Granier J.J., *Combustion Behavior of Highly Energetic Thermites: Nano versus Micron Composites*, *Propellants, Explosives, Pyrotechnics*, 30, No.1, 2005.
- [19] Rufino B., Boule'h F., Coulet M.V., Lacroix G., Denoyel R., *Influence of Particles Size on Thermal Properties of Aluminium Powder*, *Acta Materialia* 55, 2815-2827, 2007.
- [20] Weast R. C., *CRC Handbook of Chemistry and Physics 64th Ed.*, CRC Press, Inc. Boca Raton, FL 1984.
- [21] Trunov M. A., Schoenitz M., Dreizin E. L., *Effect of Polymorphic Phase Transformations in Alumina Layer on Ignition of Aluminium Particles*, *Combustion Theory and Modelling*, 10, (4), 603-623, 2006.
- [22] Trunov M. A., Schoenitz M., Zhu X., Dreizin E. L., *Effect of Polymorphic Phase Transformations in Al₂O₃ Film on Oxidation Kinetics of Aluminum Powders*, *Combustion and Flame*, 140, (4), 310-318, 2005.
- [23] Trunov M. A., Umbrajkar S. M., Schoenitz M., Mang J. T., Dreizin E. L., *Oxidation and Melting of Aluminum Nanopowders*, *Journal of Physical Chemistry B*, 110, (26), 13094-13099, 2006.
- [24] Levin I., Brandon D., *Metastable Alumina Polymorphs: Crystal Structures and Transition Sequences*, *Journal of the American Ceramic Society*, 81, (8), 1995-2012, 1998.

- [25] Koroban V.A., Burtsev Yu.N., Alimov F.R., Haustov A.D., Dubovik V.A., Teselkin V.A., *Thermal Decomposition Features of Ammonium Nitrate and its Boron Mixture under High Pressures*, Propellants Explos. Pyrotech., 19, 307-310, 1994.
- [26] JANAF Thermochemical Tables, third edition, 1998.
- [27] Journal of Physical and Chemical Reference Data, Volume 14, 1985.
- [28] Duraes L., Campos J., Portugal A., *Radial Combustion Propagation in Iron(III) oxide/Aluminium Thermite Mixtures*, Propellants Explos. Pyrotech., 31,42-49, 2006.
- [29] Piercey D. G., Klapötke T. M., *Nanoscale Aluminum - Metal Oxide (Thermite) Reactions for Application in Energetic Materials*, Central European Journal of Energetic Materials, 7(2), 115-129, 2010.
- [30] Prakash A., McCormick A. V., and Zachariah M. R., *Aero-Sol-Gel Synthesis of Nanoporous Iron-Oxide Particles: A potential oxidizer for Nanoenergetic Materials*, Chemistry of Materials, vol. 16, pp. 1466–1471, 2004.
- [31] Ishitha K., Ramakrishna P.A., *Studies on the Role of Iron Oxide and Copper Chromite in Solid Propellant Combustion*, Combustion and Flame, 161, 2717-2728, 2014.
- [32] Patil P.R., Krishnamurthy V.N., Joshi S.S., *Differential Scanning Calorimetric Study on HTPB Based Composite Propellants in Presence of Nano Ferric Oxide*, Propellants Explos. Pyrotech., 31,442-446, 2006.

- [33] Dey A., Athar J., Varma P., Prasant H., Sikder A.K., Chattopadhyay S., *Graphene-Iron Oxide Nanocomposite (GINC): an Efficient Catalyst for Ammonium Perchlorate (AP) Decomposition and Burn Rate Enhancer for AP Based Composite Propellant*, RSC Adv, 5, 1950, 2015.
- [34] Parkinson G. S., *Iron Oxide Surfaces*, Surf. Sci. Rep., 71(1), 272–365, 2016.
- [35] Bertelsen P., Goetz W., Madsen M.B., Kinch K.M., Hviid S.F., Knudsen J.M., Gunnlaugsson H.P., Merrison J., Nornberg P., Squyres S.W., Bell III J.F., Herkenhoff K.E., Gorevan S., Yen A.S., Myrick T., Klingelhöfer G., Rieder R., Gellert R., *Magnetic Properties Experiments on the Mars Exploration Rover Spirit at Gusev Crater*, Science, 305, 827-829, 2004.
- [36] Frankel R.B., Blakemore R.P., Wolfe R.S., *Magnetite in Freshwater Magnetotactic Bacteria*, Science, 203, 1355-1356, 1979.
- [37] Kishkinev D.A., Chernetsov N.S., *Magnetoreception Systems in Birds: a Review of Current Research*, Biol.Bull.Rev. 5, 46-62, 2015.
- [38] Kirschvink J.L., Kobayashi-Kirschvink A., Woodford B.J., *Magnetite Biomineralization in the Human Brain*, Proc.Natl.Acad.Sci., 89, 7683-7687, 1992.
- [39] Prentice D., Pantoya M. L., Clapsaddle B. J., *Synthesis and Performance Characterization of a Nanocomposite Ternary Thermite: Al/Fe₂O₃/SiO₂*, Journal of Physical Chemistry B, February 2005.
- [40] Zboril R., Mashlan M., Petridis D., *Iron(III)oxides from Thermal Processes Synthesis, Structural and Magnetic Properties*, Mössbauer Spectroscopy

Characterization, and Applications, *Chem.Mater.*, *14*, 969–982, 2002.

[41] Ennas G., Musinu A., Piccaluga G., Zedda D., Gatteschi D., Sangregorio C., Stanger J.L., Concas G., Spano G., *Characterization of Iron Oxide Nanoparticles in an Fe₂O₃-*

SiO₂ Composite Prepared By Sol-Gel Method, *Chem.Mater.*, *10*, 2, 495-502, 1998.

[42] Woo K., Lee H. J., *Synthesis and Magnetism of Hematite and Maghemite Nanoparticles*, *Journal of Magnetism and Magnetic Materials*, 272–276, 2004.

[43] Wang C.-T., Ro S.-H., *Nanocluster Iron Oxide-Silica Aerogel Catalysts for Methanol Partial Oxidation*, *Applied Catalysis A: General*, 285,(12), 196, 2005.

[44] Lin Y., Sun F. Q., Yuan X. Y., Geng B. Y., Zhang L. D., *Sol-gel Electrophoretic Deposition and Optical Properties of Fe₂O₃ Nanowire Arrays*, *Applied Physics A: Materials Science & Processing*, 78, (8), 1197, 2004.

[45] Tongpool R., Jindasuwan S., *Sol-gel Processed Iron Oxide-Silica Nanocomposite Films as Room-Temperature Humidity Sensors*, *Sensors and Actuators B: Chemical*, *B106*, (2), 523-528, 2005.

[46] Setvin M., Wagner M., Schmid M., Parkinson G.S., Diebold U., *Surface Point Defects on Bulk Oxides: Atomically-Resolved Scanning Probe Microscopy*, *Chem. Soc. Rev.*, *46*, 1772, 2017.

- [47] Serna C.J., Morales M.P., *Maghemite (γ -Fe₂O₃): A Versatile Magnetic Colloidal Material*, *Surface and Colloid Science*, 17, 27 – 81, 2004.
- [48] Yen F. S., Chen W. C., Yang J. M., Hong C. T., *Crystallite Size Variations of Nanosized Fe₂O₃ Powders During γ - to α -Phase Transformation*, *Nano Lett.*, 2, No. 3, 2002.
- [49] Gotic M., Koscec G., Music S., *Study of the Reduction and Reoxidation of Substoichiometric Magnetite*, *Journal of Molecular Structure*, 347–354, 2009.
- [50] Long J. W., Logan M. S., Rhodes C. P., Carpenter E. E., Stroud R. M., Rolison D. R., *Nanocrystalline Iron Oxide Aerogels as Mesoporous Magnetic Architectures*, *J. AM. CHEM. SOC.*, 126, 16879-16889, 2004.
- [51] Sudakar C., Subbanna G. N., Kutty T. R. N., *Synthesis of Acicular Hydrogoethite (α -FeOOH·xH₂O; 0.1<x<0.22) Particles Using Morphology Controlling Cationic Additives and Magnetic Properties of Maghemite Derived from Hydrogoethite*, *J. Mater. Chem.*, 12, 107–116, 2002.
- [52] Cornell R.M., Schwertmann U., *The Iron Oxides, Structure, Properties, Reactions, Occurrence and Uses*, VCH, Weinheim, Germany, 1996.
- [53] Ferguson A., Hass M., *Magnetic Structure and Vacancy Distribution in γ -Fe₂O₃ by Neutron Diffraction*, *Physical Review Letters* 112, 1130, 1958.

[54] Rossi J., *Two Decades of Research on Nano-Energetic Materials*, Propellants Explos. Pyrotech., 39, 323 – 327, 2014.

[55] Petrantoni M., Rossi C., Salvagnac L., Conedera V., Esteve A., Tenailleau C., *Multilayered Al/CuO Thermite Formation by Reactive Magnetron Sputtering: Nano*

Versus Micro, Journal of Applied Physics, vol. 108, 084323, 2010.

[56] Blobaum K. J., Reiss M. E., Lawrence J. M. P., and Weihs T. P., *Deposition and Characterization of a Self-Propagating CuO_x/Al Thermite Reaction in a Multilayer Foil Geometry*, Journal of Applied Physics, vol. 94, pp. 2915–2922, 2003.

[57] Prakash A., McCormick A. V., and Zachariah M. R., *Synthesis and Reactivity of a Super-Reactive Metastable Intermolecular Composite Formulation of Al/KMnO₄*, Advanced Materials, vol. 17, pp. 900-903, 2005.

[58] Piekial N. W., Churaman W. A., Morris C. J., and Currano L. J., *Combustion and Material Characterization of Porous Silicon Nanoenergetics*, 26th IEEE International Conference on Micro Electro Mechanical Systems (Mems 2013), pp. 449–452, 2013.

[59] Parimi V. S., Tadigadapa S. A., and Yetter R. A., *Control of Nanoenergetics Through Organized Microstructures*, Journal of Micromechanics and Microengineering, vol. 22, p. 055011, 2012.

[60] Currano L. J. and Churaman W. A., *Energetic Nanoporous Silicon Devices*, Journal of Microelectromechanical Systems, vol. 18, pp. 799–807, 2009.

[61] Hohmann C., Tipton B., Dutton M., *Viton's Impact on NASA Standard Initiator Propellant Properties*, NASA/TP-2000-210187, Lyndon B. Johnson Space Center Houston, Texas.

[62] Klapötke T.M., *Chemistry of High – Energy Materials*, Walter de Gruyter, 2nd Edition, Berlin, 2012.

[63] Schoenitz M., Ward T.S., Dreizin E.L., *Fully Dense Nano-Composite Energetic Powders Prepared by Arrested Reactive Milling*, Proceedings of the Combustion Institute, Vol.30(2), 2071-2078, 2005.

[64] Stamatis D., Jiang Z., Hoffmann V.K., Schoenitz M., Dreizin E.L., Fully Dense, Aluminum-Rich Al-CuO Nanocomposite Powders for Energetic Formulations Combustion Science and Technology, 181, 97-116, 2009.

[65] Shaw W.L., Dlott D.D., Williams R.A., Dreizin E.L., *Ignition of Nanocomposite Thermites by Electric Spark and Shock Wave*, Propellants Explos. Pyrotech., 39, 444 – 453, 2014.

[66] Williams R. A., Patel J. V., Ermoline A., Schoenitz M., Dreizin E. L., *Correlation of Optical Emission and Pressure Generated upon Ignition of Fully-dense Nanocomposite Thermite Powders*, Combust. Flame, 160, 734, 2013.

[67] Umbrajkar S. M., Seshadri S., Schoenitz M., Hoffmann V. K., Dreizin E. L., *Aluminum-Rich Al-MoO₃ Nanocomposite Powders Prepared by Arrested Reactive Milling*, J. Propul. Power, 24, 192, 2008.

[68] Stamatis D., Dreizin E. L., Higa K., *Thermal Initiation of Al-MoO₃ Nanocomposite Materials Prepared by Different Methods*, J. Propul. Power, 27, 1079, 2011.

[69] Dreizin E. L., Badiola C., Zhang S., Aly Y., *Particle Combustion Dynamics of Metal-Based Reactive Materials*, Int. J. Energ. Mater. Chem. Propul., 10, 22, 2011.

[70] Sullivan K.T., Kuntz J.D., Gash A.E., *The Role of Fuel Particle Size on Flame Propagation Velocity in Thermites with a Nanoscale Oxidizer*, Propellants Explos. Pyrotech., 39, 407 – 415, 2014.

[71] Malchi J. Y., Foley T. J., Yetter R. A., *Electrostatically Self-Assembled Nanocomposite Reactive Microspheres*, ACS Appl. Mater. Interf., 1, 2420–2423, 2009.

[72] Kim S. H., Zachariah M. R., *Enhancing the Rate of Energy Release from Nanoenergetic Materials by Electrostatically Enhanced Assembly*, Adv. Mater., 16, 1821–1825, 2004.

[73] Churaman W. A., Currano L. J., Becker C., *Initiation and Reaction Tuning of Nanoporous Energetic Silicon*, J. Phys. Chem. Solids, 71, 69–74, 2010.

[74] Churaman W. A., Becker C. R., Metcalfe G. D., Hanrahan B. M., Currano L. J., Stoldt C. R., *Optical Initiation of Nanoporous Energetic Silicon for Safing and Arming Technologies*, Optical Technologies for Arming, Safing, Fuzing, and Firing VI, Vol. 7795, pp. 779506-1-9, 2010.

[75] Currano L. J., Churaman W. A., *Energetic Nanoporous Silicon Devices*, Journal of Microelectromech. Sys., 18, 799–807, 2009.

[76] Tillotson T.M., Gash A.E., Simpson R.L., Hrubesh L.W., Satcher Jr. J.H., Poco J.F., *Nanostructured Energetic Materials Using Sol–Gel Methodologies*, Journal of Non-Crystalline solids 285, 338-345, 2001.

[77] Clapsaddle B. J., Zhao L., Prentice D., Pantoya M. L., Gash A. E., Satcher Jr. J. H., Shea K. J., Simpson R. L., *Formulation and Performance of Novel Energetic Nanocomposites and Gas Generators Prepared by Sol-Gel Methods*, 36th Annual Conference of ICT Karlsruhe, Germany June 28-July 1, 2005.

[78] Brinker C.J., Scherer G.W., *Sol-Gel science: The Physics and Chemistry of Sol-Gel Processing*, Academic Press, 1990.

[79] Mehendale B., Shende R., Subramanian S., Redner P., Kapoor D., Nicolich S., Gangopadhyay S., *Nanoenergetic Composite of Mesoporous Iron Oxide and Aluminum Nanoparticles*, Journal of Energetic Materials, 24, 341-360, 2006.

[80] Livage J., Henry M., Sanchez C., *Sol-Gel Chemistry of Transition Metal Oxides Progress in Solid State Chemistry*, 18, 259-341, 1988.

[81] Dobinson B., *The Determination of Epoxides*, Pergamon Press, Oxford, 1969.

[82] Shin M.S., Kim, J.K., Kim J.W., Moraes C.A.M., Kim H.S., Koo K.K., *Reaction Characteristics of Al/Fe₂O₃ Nanocomposites*, Journal of Industrial and Engineering Chemistry 18, 1768–1773, 2012.

[83] Gash A.E., Tillotson T.M., Satcher Jr. J.H., Poco J.F., Hrubesh L.W., Simpson R.L., *Use of Epoxides in the Sol-Gel Synthesis of Porous Iron (III) Oxide Monoliths from Fe(III) Salts*, Chem. Mater., 13. 999-1007, 2001.

- [84] Hao Z., Hui L., Guo B., Li H., Zhang J., Gan L., Xu Z., Chen L., *Sol-Gel Synthesis of Alumina Using Inorganic Salt Precursor*, Acta Physico-Chemica Sinica, 23, 3, 2007.
- [85] Ichinose N., Ozaki Y., Kashu S., *Superfine Particle Technology*, Springer-Verlag, London, 1992.
- [86] Incropera, F.P., Dewitt D.P., Bergman T.L., Lavine A.S., *Fundamentals of Heat and Mass Transfer, 6th edition*, John Wiley and Sons, 2007.
- [87] Thiruvengadathan R., Bezmelnitsyn A., Apperson S., Staley C., Redner P., Balas W., Nicolich S., Kapoor D., Gangopadhyay K., Gangopadhyay S., *Combustion characteristics of novel hybrid nanoenergetic formulations*, Combustion and Flame 158, 964–978, 2011.
- [88] Danen W. C., Martin J. A., *Energetic composites*, U. S. Patent No.5266132, 1993.
- [89] Son S. F., Yetter R. A., Yang V., *Introduction: Nanoscale composite energetic materails*, Journal of Propulsion and Power, 23, 643, 2007.
- [90] Shimojo F., Nakano A., Kalia R. K., Vashishta P., *Electronic Processes in Fast Thermite Chemical Reactions: A First-Principles Molecular Dynamics Study*, Physical Review E 77, 066103, 2008.
- [91] Levitas V. I., Asay B. W., Son S. F., and Pantoya M., *Melt Dispersion Mechanism for Fast Reaction of Nanothermites*, Appl.Phys. Lett. 89, 071909, 2006.
- [92] NATO Standardization Agreement (STANAG) on Explosive, *Friction Sensitivity Tests*, No. 4487, Ed. 1, Aug. 22, 2002.

- [93] NATO Standardization Agreement (STANAG) on Explosives, *Impact Sensitivity Tests*, No. 4489, Ed. 1, Sept. 17, 1999.
- [94] Weir C., Pantoya M.L., Daniels M.A., *The Role of Aluminum Particle Size in Electrostatic Ignition Sensitivity of Composite Energetic Materials*, *Combustion and Flame* 160, 10, 2013.
- [95] Standardization Agreement, *Extreme Climatic Coniditons and Derived Conditions for Use in Defining Design/Test Criteria for NATO Forces Material*, STANAG 2895, 1990.
- [96] Yen N.H., Wang L.Y. *Reactive Metals in Explosives*, *Propellants, Explosives and Pyrotechnics*, 37, 143-155, 2012.
- [97] Bellott B. J., Noh W., Nuzzo R. G., Girolami G. S., *Nanoenergetic Materials: Boron Nanoparticles from the Pyrolysis of Decaborane and Their Functionalisation*, *Chem. Communications*, 22, 3214–3215, 2009.
- [98] Dreizin E. L., *Metal-based Reactive Nanomaterials*, *Progress in Energy and Combustion Science*, 35, 141-167, 2009.
- [99] Mačević A., Semple J. M., *Combustion of Boron Particles at Atmospheric Pressure* *Combustion Science and Technology*, 1, 3, 181-191, 1969.
- [100] Yeh C.L., Hsieh W.H., Kuo K.K., Felder W., *Ignition and Combustion of Mg-Coated and Uncoated Boron Particles*, *Non-Instrusive Combustion Diagnostics*, Kuo K.K., Parr T.P., Begell House Inc., pp. 327-341, 1994.

- [101] Glassman L., Williams F.A., Antaki P., *A Physical and Chemical Interpretation of Boron Particle Combustion*, Symp. (Int'l.) on Combustion, 20,1, 2057-2064, 1985.
- [102] King, M. K., *Boron Ignition and Combustion in Air-Augmented Rocket Afterburners*, *Combustion Science and Technology*, 5, 1, 155-164, 1972.
- [103] King, M. K., *Boron Particle Ignition in Hot Gas Streams*, *Combustion Science and Technology*, 8, 5-6, 255-273, 1973.
- [104] King, M. K., *Single Particle Model Ignition Modeling*, 19th JANNAF Combustion Meeting, CPIA Publication 366, 2, 27-42, 1982.
- [105] King, M. K., *Modification of Boron Ignition Model to Include Recent Liquid Boron Oxide-Water Gas Kinetics*, 26th JANNAF Combustion Meeting, CPIA Publication, 529, 2, 203-207 1989.
- [106] Yeh C.L., Kuo K.K., *Ignition and Combustion of Boron Particles*, *Progress in Energy and Combustion Science*, 22, 511-541, 1996.
- [107] Makino A., Law C.K., *A Simplified Model for the Combustion of Uncoated Boron Particles*, *Combustion Science and Technology*, 61, 4-6, 155-168, 1988.
- [108] Zhou W., Yetter R.A., Dryer F.L., Rabitz H. Brown R.C., Kolb C.E., *Multi-Phase Model for Ignition and Combustion of Boron Particles*, *Combustion and Flame*, 117, 227-243, 1999.
- [109] Zhou W., Yetter R.A., Dryer F.L., Rabitz H. Brown R.C., Kolb C.E., *Effect of Fluorine on the Combustion of Clean Surface Boron Particles*, *Combustion and Flame*, 112, 507-521, 1998.

- [110] Zhou W., Yetter R.A., Dryer F.L., Rabitz H. Brown R.C., Kolb C.E., *A comprehensive Physical and Numerical Model of Boron Particle Ignition*, 26th Symposium (International) on Combustion/The Combustion Institute, 1909-1917, 1996.
- [111] Vovchuk Y.I., Zolotko A.N., Klyachko L.A., Polishchuk D.I., Schevchuk V.G., *Gasification of Boron Oxide*, *Combustion Explosion and Shock Waves* 10, 4, 538–540, 1974.
- [112] Turns S.R., Holl J.T., Solomon A.S.P., Faeth G.M., *Gasification of Boron Oxide Drops in Combustion Gases*, *Combustion Science and Technology* 43, 5/6, 287–300, 1985.
- [113] Yoshida T., Yuasa S., *Effect of Water Vapor on Ignition and Combustion of Boron Lumps in an Oxygen Stream*, *Proceedings of the Combustion Institute* 38, 2735–2741, 2000.
- [114] Yetter R.A., Rabitz H., Dryer F.L., Brown R.C., Kolb C.E., *Kinetics of High Temperature B/O/H/C Chemistry*, *Combustion and Flame* 83, 1, 43–62, 1991.
- [115] Young G., Sullivan K., Zachariah M.R., Yu K., *Combustion Characteristics of Boron Nanoparticles*, *Combustion and Flame* 156, 322–333, 2009.
- [116] Chase, M.W., Jr., *NIST-JANAF Thermochemical Tables, Fourth Edition*, *J.Phys. Chem. Ref. Data, Monograph 9*, 1998, 1-1951.
- [117] Cox J.D., Wagman D.D., Medvedev V.A., *CODATA Key Values for Thermodynamics*, Hemisphere Publishing Corp., New York, 1989.

[118] The NBS tables of chemical thermodynamics properties, Journal of Phys. and Chem. Ref. Data, Vol 11, 1982, Suppl. 2.

[119] Yeh, C. L., *Ignition and Combustion of Boron Particles*, Ph.D. Thesis, Department of Mechanical Engineering, The Pennsylvania State University, 1995.

[120] Shen LH, Li GP, Luo YJ, Gao K., Ge Z, *Preparation and Characterization of Al/B/Fe₂O₃ Nanothermites*, Science China Chemistry, 57, 6, 2014.

[121] Tillotson T.M., Simpson R.L., Hrubesh L.W., Gash A.E., *Method for Producing Nanostructured Metal-Oxides*, U.S.Patent No.6,986,818 B2, 2006.

[122] Gash A.E., Tillotson T.M., Satcher Jr. J.H., Hrubesh L.W., Simpson R.L., *New Sol-Gel Synthetic Route to Transition and Main-Group Metal Oxide Aerogels using Inorganic Salt Precursors*, 6th International Symposium on Aerogels, Albuquerque, NM, 22-28, 2000.

[123] Gash A.E., Tillotson T.M., Satcher Jr. J.H., Hrubesh L.W., Simpson R.L., *New Sol-Gel Synthetic Route to Transition and Main-Group Metal Oxide Aerogels using Inorganic Salt Precursors*, Journal of Non-Crystalline Solids 285, 22-28, 2001.

[124] Spitzer D., Comet M., Moeglin J.-P., Stechele E., Werner, Udo, Suma Y., *Synthesis and Investigation of the Reactivity of Nano Thermite Mixtures*, 7th Int. Ann. Conf. ICT, (Energetic Materials), 117/1-117/10, 2006.

- [125] Poda A. R., Moser R. D., Cuddy M. F., Doorenbos Z., Lafferty B. J., Weiss Jr.C. A., Harmon A., Chappell M. A., Steevens J. A., *Nano-Aluminum Thermite Formulations: Characterizing the Fate Properties of a Nanotechnology during Use*, Journal of Nanomaterials & Molecular Nanotechnology 2:1, 2013.
- [126] Bezmelnitsyn A., Thiruvengadathan R., Barizuddin S., Tappmeyer D., Apperson S., Gangopadhyay K., Gangopadhyay S., *Modified Nanoenergetic Composites with Tunable Combustion Characteristics for Propellant Applications*, Propellants Explos. Pyrotech., 35, 384 – 394, 2010.
- [127] Gangopadhyay S., Tappmeyer D., Bezmelnitsyn A., Thiruvengadathan R., Shende R., Mehendale B., Apperson S., Barizuddin S., Gangopadhyay K., *Homogeneous Mesoporous Nanoenergetic Metal Oxide Composite Fabrication Methods*, US Patent 8,512,490 B2, 2013.
- [128] Bockmon B.S., Pantoya M.L., Son S.F., Asay B.W., Mang J.T., *Combustion Velocities and Propagation Mechanisms of Metastable Interstitial Composites*, Journal of Applied Physics, 98, 064903, 2005.
- [129] Cervantes O. G., Kuntz J. D., Gash A. E., Munir Z. A., *Heat of Combustion of Tantalum–Tungsten Oxide Thermite Composites*, Combustion and Flame 157, 2326–2332, 2010.
- [130] Puszynski J.A., Bichay M.M., Swiatkiewicz J.J., *Wet Processing and Loading of Percussion Primers Based on Metastable Nanoenergetic Composites*, United States Patent Application No 20060113014, June 1, 2006.

[131] Moore D.S., Son S.F., Asay B.W., *Time-Resolved Spectral Emission of Deflagrating Nano-Al and Nano-MoO₃ Metastable Interstitial Composites*, Propellants Explos. Pyrotech., 29,2, 106-111, 2004.

[132] Gash A. E., Simpson R. L., Satcher Jr J. H., *Energetic Nanocomposites with Sol-gel Chemistry: Synthesis, Safety, and Characterization*, Lawrence Livermore National Laboratory, 29th International Pyrotechnic Seminar, Westminster, Co., July 14-19,2002.

[133] Wang J., Qiao Z., Shen J., Li R., Yang Y., Yang G., *Large-Scale Synthesis of a Porous Co₃O₄ Nanostructure and Its Application in Metastable Intermolecular Composites*, Propellants Explos. Pyrotech., 40, 1 – 5, 2015.

[134] Glavier L., Taton G., Ducéré J.M., Baijot V., Pinon S., Calais T., Estève A., Rouhani M.D., Rossi C., *Nanoenergetics as Pressure Generator for Nontoxic Impact Primers: Comparison of Al/Bi₂O₃, Al/CuO, Al/MoO₃ Nanothermites and Al/PTFE*, Combustion and Flame 162, 1813–1820, 2015.

[135] Lee K., Kim D., Shim J., Bae S., Shin D.J., Treml B.E., Yoo J., Hanrath T., Kim W.D., Lee D.C., *Formation of Cu Layer on Al Nanoparticles During Thermite Reaction in Al/CuO Nanoparticle Composites: Investigation of Off-Stoichiometry Ratio of Al and CuO Nanoparticles for Maximum Pressure Change*, Combustion and Flame 000, 1–6, 2015.

[136] Brunauer S., Deming L.S., Deming W.E., Teller E., *On a Theory of van der Waals Adsorption of Gases*, J. Am. Chem. Soc., Vol. 62, 1723, 1940.

[137] Rouquerol F., Rouquerol J., Sing K., *Adsorption by Powders and Porous Solids*, Academic Press, London, 1999.

[138] Sing K. S. W., Everett D. H., Haul R. A. W., Moscou L., Pierotti R. A., Rouquerol J., Siemieniewska T., *Reporting Physisorption Data for Gas/Solid Systems with Special Reference to the Determination of Surface Area and Porosity*, Pure & Appl. Chem., Vol. 57, No. 4, pp. 603—619, 1985.

[139] Van der Steen A.C., Verbeek H.J., Meulenbrugge J.J., *Proceeding of the 9th Symposium on Detonation*, Portland, OR, 83, 1989.

[140] Borne L., *Proceedings of the 10th Symposium on Detonation*, Boston, MA, 286, 1993.

[141] Baer M.R., *Modeling Heterogeneous Energetic Materials at the Mesoscale*, Thermochemica Acta, 384, 351-367, 2002.

[142] Morales M.P., Pecharroman C., González-Carreño T., C.J. Serna, *Structural Characterisation of Uniform γ -Fe₂O₃ Particles with Different Axial (Length/Width) Ratios*, Journal of Solid State Chemistry, 108, 158-16, 1994.

[143] Morales M.P., e Julián C., González J.M., Serna C.J., *The Effect of Vacancies Distribution on the Magnetic Properties of γ -Fe₂O₃ Particles*, J. Materials Research, 9, 135-141, 1994.

[144] Morales M.P., Serna C.J., Bødker F., Mørup S., *Spin-Canting due to Structural Disorder in Maghemite*, Journal of Physics: Condensed Matter, 9, 5461-5467, 1997.

[145] Bastow T.J., Trinchi A., Hill M.R., Harris R., Muster T.H., *Vacancy Ordering in γ - Fe_2O_3 Nanocrystals Observed by ^{57}Fe NMR*, Journal of Magnetism and Magnetic Materials, 321, 2677–2681, 2009.

[146] Walker J. D., *Exploring the Synthesis and Characterization of Nanoenergetic Materials from Sol-Gel Chemistry*, Georgia Institute of Technology, May 2007.

[147] Bastow T.J., Trinchi A., Hill M.R., Harris R., Muster T.H., *Vacancy Ordering in γ - Fe_2O_3 Nanocrystals Observed by ^{57}Fe NMR*, Journal of Magnetism and Magnetic Materials, 321, 2677–2681, 2009.

[148] Ostwald W., *Studien über die Bildung und Umwandlung fester Körper*, Zeitschrift für Physc. Chemie 22, 289-302, 1897.

[149] Threlfall T., *Structural and Thermodynamic Explanations of Ostwald's Rule*, Organic Process Research & Development, 7, 1017-1027, 2003.

[150] Scherrer P., *Bestimmung der Grösse und der inneren Struktur von Kolloidteilchen mittels Röntgenstrahlen*, Nachr. Ges. Wiss. Göttingen 26, 98 – 100, 1918.

[151] Langford J.I., Wilson A.J.C., *Scherrer after Sixty Years: A Survey and Some New Results in the Determination of Crystallite Size*, J. Appl. Cryst. 11, 102 – 113, 1978.

[152] Bastow T.J., Trinchi A., Hill M.R., Harris R., Muster T.H., *Vacancy Ordering in γ - Fe_2O_3 Nanocrystals Observed by ^{57}Fe NMR*, Journal of Magnetism and Magnetic Materials, 321, 2677–2681, 2009.

- [153] Zhao N., He C., Liu J., Gong H., An T., Xu H., Zhao F., Hu R., Ma H., Zhang J., *Dependence of Catalytic Properties of Al/Fe₂O₃ Thermites on Morphology of Fe₂O₃ Particles in Combustion Reactions*, Journal of Solid State Chemistry, 219, 2014, 67–73.
- [154] Durães L., Moutinho A., Seabra I. J., Costa B. F.O., Sousa H. C. de, Portugal A., *Characterization of Iron (III) Oxide/Hydroxide Nanostructured Materials Produced by Sol-Gel Technology Based on the Fe(NO₃)₃·9H₂O-C₂H₅OH-CH₃CHCH₂O System*, Materials Chemistry and Physics, 130, 2011, 548 – 560.
- [155] Gotić M., Dražić G., Musić S., *Hydrothermal Synthesis of α -Fe₂O₃ Nanorings with the Help of Divalent Metal Cations, Mn²⁺, Cu²⁺, Zn²⁺ and Ni²⁺*, J.Mol.Struct., 993, 2011, 167–176.
- [156] Santilli C.V., Onillon M., Bonnet J.P., *Influence of the Elaboration and Dehydration Conditions of Fe(III)Hydrous Oxides on the Characteristics of Resulting α -Fe₂O₃ Powders*, Ceram. Int., 16, 1990, 89.
- [157] Dovbeshko G.I., Gridina N.Y., Kruglova E.B., Pashchuk O.P., *FTIR Spectroscopy Studies of Nucleic Acid Damage*, Talanta, 53, 2000,233-246.
- [158] Rasulic G., Jovanovic S., Milanovic Lj., *Ammonium Nitrate Changes During Thermal Analysis*, Journal of Thermal Analysis, 30, 1985, 65-72.
- [159] Chaturvedi S., Dave P.N., *Review on Thermal Decomposition of Ammonium Nitrate*, Journal of Energetic Materials. 31, 2013, 1-26.

- [160] Wang X., Zhou W., DeLisio J.B., Egan G.C., Zachariah M.R., *Doped δ -Bismuth Oxides to Investigate Oxygen Ion Transport as a Metric for Condensed Phase Thermite Ignition*, Journal of Physical Chemistry, 121, 2017, 147-152.
- [161] Boyapati S., Wachsman E.D., Jiang N., *Effect of Oxygen Sublattice Ordering on Interstitial Transport Mechanism and Conductivity Activation Energies in Phase Stabilized Cubic Bismuth Oxides*, Solid State Ionics, 140(1), 2001, 149-160.
- [162] Mačević A., Semple J.M., *Combustion of Boron Particles at Elevated Pressures*, 13th International Symposium on Combustion, The Combustion Institute, Pittsburgh, 859-868, 1971.
- [163] Mačević A., *Combustion of Boron Particles: Experiment and Theory*, 14th International Symposium On Combustion, The Combustion Institute, Pittsburgh, 1401-1411, 1972.
- [164] Fontijn A., *Homogenous Combustion Kinetics of Boron Compounds*, AFOSR Specialists Meeting on Boron Combustion, Pittsburgh Hilton Hotel, USA, 1984.
- [165] McBride B. J., Gordon S., NASA-GLENN Chemical Equilibrium Program CEA2 code, 2004.
- [166] McBride B. J., Gordon S., NASA RP-1311, PART I, 1994.
- [167] McBride B. J., Gordon S., NASA RP-1311, PART II, 1996.

[168] Kissinger H.E., Reaction Kinetics in Differential Thermal Analysis, *Analytical Chemistry*, Vol.29, 11, 1702-1706, 1957.

[169] Dixon, W. J., F. J. Massey, *An Introduction to Statistical Analysis*, McGraw-Hill, New York, 1951.

[170] Crow., E.L., Davis F.A., Maxfield M.W., *Statistics Manual with Examples Taken from Ordnance Development*, Dover Publications, Inc., New York, 1960.

APPENDICES

A. OUTPUT FILE OF NASA-GLENN CEA2 CODE

Samples with propylene oxide, 3FR

NASA-GLENN CHEMICAL EQUILIBRIUM PROGRAM CEA2, MAY 21, 2004

BY BONNIE MCBRIDE AND SANFORD GORDON

REFS: NASA RP-1311, PART I, 1994 AND NASA RP-1311, PART II, 1996

PRODUCTS WHICH WERE CONSIDERED BUT WHOSE MOLE FRACTIONS
WERE LESS THAN 5.000000E-06 FOR ALL ASSIGNED CONDITIONS

*B BC BC2 BH BH2

BH3 BH4 BH5 *BO BOH

BO2 B(OH)2 B2 B2C B2H

B2H2 B2H3 B2H3,db B2H4 B2H4,db

B2H5 B2H5,db B2H6 B2O B2(OH)4

B3H7,C2v B3H7,Cs B3H9 B4H4 B4H10

B4H12 B5H9 *C *CH CH2

CH3 CH2OH CH3O CH4 CH3OH

CH3OOH *CO2 COOH *C2 C2H

C2H2,acetylene C2H2,vinylidene CH2CO,ketene O(CH)2O HO(CO)2OH

C₂H₃,vinyl CH₃CO,acetyl C₂H₄ C₂H₄O,ethylen-o CH₃CHO,ethanal
 CH₃COOH OHCH₂COOH C₂H₅ C₂H₆ C₂H₅OH
 CH₃OCH₃ CH₃O₂CH₃ C₂O *C₃ C₃H₃,1-propynl
 C₃H₃,2-propynl C₃H₄,allene C₃H₄,propyne C₃H₄,cyclo- C₃H₅,allyl
 C₃H₆,propylene C₃H₆,cyclo- C₃H₆O,propylox C₃H₆O,acetone C₃H₆O,propanal
 C₃H₇,n-propyl C₃H₇,i-propyl C₃H₈ C₃H₈O,1propanol C₃H₈O,2propanol
 C₃O₂ *C₄ C₄H₂,butadiyne C₄H₄,1,3-cyclo- C₄H₆,butadiene
 C₄H₆,1butyne C₄H₆,2butyne C₄H₆,cyclo- C₄H₈,1-butene C₄H₈,cis2-buten
 C₄H₈,tr2-butene C₄H₈,isobutene C₄H₈,cyclo- (CH₃COOH)₂ C₄H₉,n-butyl
 C₄H₉,i-butyl C₄H₉,s-butyl C₄H₉,t-butyl C₄H₁₀,n-butane C₄H₁₀,isobutane

 *C₅ C₅H₆,1,3cyclo- C₅H₈,cyclo- C₅H₁₀,1-pentene C₅H₁₀,cyclo-
 C₅H₁₁,pentyl C₅H₁₁,t-pentyl C₅H₁₂,n-pentane C₅H₁₂,i-pentane CH₃C(CH₃)₂CH₃
 C₆H₂ C₆H₅,phenyl C₆H₅O,phenoxy C₆H₆ C₆H₅OH,phenol
 C₆H₁₀,cyclo- C₆H₁₂,1-hexene C₆H₁₂,cyclo- C₆H₁₃,n-hexyl C₆H₁₄,n-hexane
 C₇H₇,benzyl C₇H₈ C₇H₈O,cresol-mx C₇H₁₄,1-heptene C₇H₁₅,n-heptyl
 C₇H₁₆,n-heptane C₇H₁₆,2-methylh C₈H₈,styrene C₈H₁₀,ethylbenz C₈H₁₆,1-octene
 C₈H₁₇,n-octyl C₈H₁₈,n-octane C₈H₁₈,isooctane C₉H₁₉,n-nonyl C₁₀H₈,naphthale
 C₁₀H₂₁,n-decyl C₁₂H₉,o-bipheny C₁₂H₁₀,biphenyl *Fe Fe(CO)₅
 FeO Fe(OH)₂ HCO HCCO HO₂
 HBOH HCHO, HCOOH H₂O₂ H₂BOH
 HB(OH)₂ H₃BO₃ H₃B₃O₆ (HCOOH)₂ *O
 *OH *O₂ O₃ B(L) B₂O₃(cr)
 B₃O₃H₃(cr) B₄C(L) C(gr) Fe(a) Fe(c)
 Fe(L) Fe(CO)₅(L) Fe.947O(cr) Fe.947O(L) Fe(OH)₂(cr)
 Fe(OH)₃(cr) Fe₂O₃(cr) Fe₃O₄(cr) Fe₃O₄(L) HBO₂(cr)
 HBO₂(L) H₂O(cr) H₂O(L) H₃BO₃(cr) H₃BO₃(L)

Samples with propylene oxide, 6FR

NASA-GLENN CHEMICAL EQUILIBRIUM PROGRAM CEA2, MAY 21, 2004

BY BONNIE MCBRIDE AND SANFORD GORDON

REFS: NASA RP-1311, PART I, 1994 AND NASA RP-1311, PART II, 1996

PRODUCTS WHICH WERE CONSIDERED BUT WHOSE MOLE FRACTIONS
WERE LESS THAN 5.000000E-06 FOR ALL ASSIGNED CONDITIONS

*B BC BC2 BH BH2

BH3 BH4 BH5 *BO BOH

BO2 B(OH)2 B2 B2C B2H

B2H2 B2H3 B2H3,db B2H4 B2H4,db

B2H5 B2H5,db B2H6 B2O B2O2

B2O3 B2(OH)4 B3H7,C2v B3H7,Cs B3H9

B4H4 B4H10 B4H12 B5H9 *C

*CH CH2 CH3 CH2OH CH3O

CH4 CH3OH CH3OOH *CO *CO2

COOH *C2 C2H C2H2,acetylene C2H2,vinylidene

CH2CO,ketene O(CH)2O HO(CO)2OH C2H3,vinyl CH3CO,acetyl

C2H4 C2H4O,ethylen-o CH3CHO,ethanal CH3COOH OHCH2COOH

C2H5 C2H6 C2H5OH CH3OCH3 CH3O2CH3

C2O *C3 C3H3,1-propynl C3H3,2-propynl C3H4,allene

C3H4,propyne C3H4,cyclo- C3H5,allyl C3H6,propylene C3H6,cyclo-

C3H6O,propylox C3H6O,acetone C3H6O,propanal C3H7,n-propyl C3H7,i-propyl

C3H8 C3H8O,1propanol C3H8O,2propanol C3O2 *C4
 C4H2,butadiyne C4H4,1,3-cyclo- C4H6,butadiene C4H6,1butyne C4H6,2butyne
 C4H6,cyclo- C4H8,1-butene C4H8,cis2-buten C4H8,tr2-butene C4H8,isobutene
 C4H8,cyclo- (CH3COOH)2 C4H9,n-butyl C4H9,i-butyl C4H9,s-butyl
 C4H9,t-butyl C4H10,n-butane C4H10,isobutane *C5 C5H6,1,3cyclo-
 C5H8,cyclo- C5H10,1-pentene C5H10,cyclo- C5H11,pentyl C5H11,t-pentyl
 C5H12,n-pentane C5H12,i-pentane CH3C(CH3)2CH3 C6H2 C6H5,phenyl

 C6H5O,phenoxy C6H6 C6H5OH,phenol C6H10,cyclo- C6H12,1-hexene
 C6H12,cyclo- C6H13,n-hexyl C6H14,n-hexane C7H7,benzyl C7H8
 C7H8O,cresol-mx C7H14,1-heptene C7H15,n-heptyl C7H16,n-heptane C7H16,2-
 methylh
 C8H8,styrene C8H10,ethylbenz C8H16,1-octene C8H17,n-octyl C8H18,n-octane
 C8H18,isooctane C9H19,n-nonyl C10H8,naphthale C10H21,n-decyl C12H9,o-bipheny
 C12H10,biphenyl *Fe Fe(CO)5 FeO Fe(OH)2
 *H HBO2 HCO HCCO HO2
 HBOH HCHO,formaldehy HCOOH H2O H2O2
 H2BOH HB(OH)2 H3BO3 H3B3O6 (HCOOH)2
 *O *OH *O2 O3 B(L)
 B2O3(cr) B3O3H3(cr) B4C(L) C(gr) Fe(a)
 Fe(d) Fe(L) Fe(CO)5(L) Fe.947O(cr) Fe.947O(L)
 Fe(OH)2(cr) Fe(OH)3(cr) Fe2O3(cr) Fe3O4(cr) Fe3O4(L)
 HBO2(cr) HBO2(L) H2O(cr) H2O(L) H3BO3(cr)

Samples with propylene oxide, 9FR

.....

NASA-GLENN CHEMICAL EQUILIBRIUM PROGRAM CEA2, MAY 21, 2004
 BY BONNIE MCBRIDE AND SANFORD GORDON

REFS: NASA RP-1311, PART I, 1994 AND NASA RP-1311, PART II, 1996

PRODUCTS WHICH WERE CONSIDERED BUT WHOSE MOLE FRACTIONS
WERE LESS THAN 5.000000E-06 FOR ALL ASSIGNED CONDITIONS

*B BC BC2 BH BH2

BH3 BH4 BH5 *BO BOH

BO2 B(OH)2 B2 B2C B2H

B2H2 B2H3 B2H3,db B2H4 B2H4,db

B2H5 B2H5,db B2H6 B2O B2O2

B2O3 B2(OH)4 B3H7,C2v B3H7,Cs B3H9

B4H4 B4H10 B4H12 B5H9 *C

*CH CH2 CH3 CH2OH CH3O

CH4 CH3OH CH3OOH *CO *CO2

COOH *C2 C2H C2H2,acetylene C2H2,vinylidene

CH2CO,ketene O(CH)2O HO(CO)2OH C2H3,vinyl CH3CO,acetyl

C2H4 C2H4O,ethylen-o CH3CHO,ethanal CH3COOH OHCH2COOH

C2H5 C2H6 C2H5OH CH3OCH3 CH3O2CH3

C2O *C3 C3H3,1-propynl C3H3,2-propynl C3H4,allene

C3H4,propyne C3H4,cyclo- C3H5,allyl C3H6,propylene C3H6,cyclo-

C3H6O,propylox C3H6O,acetone C3H6O,propanal C3H7,n-propyl C3H7,i-propyl

C3H8 C3H8O,1propanol C3H8O,2propanol C3O2 *C4

C4H2,butadiyne C4H4,1,3-cyclo- C4H6,butadiene C4H6,1butyne C4H6,2butyne

C4H6,cyclo- C4H8,1-butene C4H8,cis2-buten C4H8,tr2-butene C4H8,isobutene

C4H8,cyclo- (CH3COOH)2 C4H9,n-butyl C4H9,i-butyl C4H9,s-butyl

C4H9,t-butyl C4H10,n-butane C4H10,isobutane *C5 C5H6,1,3cyclo-

C5H8,cyclo- C5H10,1-pentene C5H10,cyclo- C5H11,pentyl C5H11,t-pentyl

C5H12,n-pentane C5H12,i-pentane CH3C(CH3)2CH3 C6H2 C6H5,phenyl
 C6H5O,phenoxy C6H6 C6H5OH,phenol C6H10,cyclo- C6H12,1-hexene
 C6H12,cyclo- C6H13,n-hexyl C6H14,n-hexane C7H7,benzyl C7H8

 C7H8O,cresol-mx C7H14,1-heptene C7H15,n-heptyl C7H16,n-heptane C7H16,2-
 methylh
 C8H8,styrene C8H10,ethylbenz C8H16,1-octene C8H17,n-octyl C8H18,n-octane
 C8H18,isooctane C9H19,n-nonyl C10H8,naphthale C10H21,n-decyl C12H9,o-bipheny
 C12H10,biphenyl *Fe Fe(CO)5 FeO Fe(OH)2
 *H HBO2 HCO HCCO HO2
 HBOH HCHO,formaldehy HCOOH H2O H2O2
 H2BOH HB(OH)2 H3BO3 H3B3O6 (HCOOH)2
 *O *OH *O2 O3 B(L)
 B2O3(cr) B3O3H3(cr) B4C(L) C(gr) Fe(c)
 Fe(d) Fe(L) Fe(CO)5(L) Fe.947O(cr) Fe.947O(L)
 Fe(OH)2(cr) Fe(OH)3(cr) Fe2O3(cr) Fe3O4(cr) Fe3O4(L)
 HBO2(cr) HBO2(L) H2O(cr) H2O(L) H3BO3(cr)

Samples with THF, 3FR

NASA-GLENN CHEMICAL EQUILIBRIUM PROGRAM CEA2, MAY 21, 2004

BY BONNIE MCBRIDE AND SANFORD GORDON

REFS: NASA RP-1311, PART I, 1994 AND NASA RP-1311, PART II, 1996

PRODUCTS WHICH WERE CONSIDERED BUT WHOSE MOLE FRACTIONS
 WERE LESS THAN 5.000000E-06 FOR ALL ASSIGNED CONDITIONS

*B BC BC2 BH BH2
 BH4 BH5 BOH BO2 B(OH)2
 B2 B2C B2H B2H2 B2H3
 B2H3,db B2H4 B2H4,db B2H5 B2H5,db
 B2H6 B2O B2(OH)4 B3H7,C2v B3H7,Cs
 B3H9 B4H4 B4H10 B4H12 B5H9
 *C *CH CH2 CH3 CH2OH
 CH3O CH3OH CH3OOH *CO2 COOH
 *C2 C2H C2H2,acetylene C2H2,vinylidene CH2CO,ketene
 O(CH)2O HO(CO)2OH C2H3,vinyl CH3CO,acetyl C2H4
 C2H4O,ethylen-o CH3CHO,ethanal CH3COOH OHCH2COOH C2H5
 C2H6 C2H5OH CH3OCH3 CH3O2CH3 C2O
 *C3 C3H3,1-propynl C3H3,2-propynl C3H4,allene C3H4,propyne
 C3H4,CYCLO- C3H5,ALLYL C3H6,PROPYLENE C3H6,CYCLO-
 C3H6O,PROPYLOX

 C3H6O,acetone C3H6O,propanal C3H7,n-propyl C3H7,i-propyl C3H8
 C3H8O,1propanol C3H8O,2propanol C3O2 *C4 C4H2,butadiyne
 C4H4,1,3-cyclo- C4H6,butadiene C4H6,1butyne C4H6,2butyne C4H6,cyclo-
 C4H8,1-butene C4H8,cis2-buten C4H8,tr2-butene C4H8,isobutene C4H8,cyclo-
 (CH3COOH)2 C4H9,n-butyl C4H9,i-butyl C4H9,s-butyl C4H9,t-butyl
 C4H10,n-butane C4H10,isobutane *C5 C5H6,1,3cyclo- C5H8,cyclo-
 C5H10,1-pentene C5H10,cyclo- C5H11,pentyl C5H11,t-pentyl C5H12,n-pentane
 C5H12,i-pentane CH3C(CH3)2CH3 C6H2 C6H5,phenyl C6H5O,phenoxy
 C6H6 C6H5OH,phenol C6H10,cyclo- C6H12,1-hexene C6H12,cyclo-
 C6H13,n-hexyl C6H14,n-hexane C7H7,benzyl C7H8 C7H8O,cresol-mx
 C7H14,1-heptene C7H15,n-heptyl C7H16,n-heptane C7H16,2-methylh C8H8,styrene
 C8H10,ethylbenz C8H16,1-octene C8H17,n-octyl C8H18,n-octane C8H18,isoctane

C9H19,n-nonyl C10H8,naphthale C10H21,n-decyl C12H9,o-bipheny C12H10,biphenyl

*Fe Fe(CO)5 FeO Fe(OH)2 HCO

HCCO HO2 HBOH HCHO,formaldehy HCOOH

H2O2 HB(OH)2 H3BO3 H3B3O6 (HCOOH)2

*O *OH *O2 O3 B(b)

B(L) B2O3(cr) B3O3H3(cr) B4C(L) C(gr)

Fe(a) Fe(c) Fe(L) Fe(CO)5(L) Fe.947O(cr)

Fe.947O(L) Fe(OH)2(cr) Fe(OH)3(cr) Fe2O3(cr) Fe3O4(cr)

Fe3O4(L) HBO2(cr) HBO2(L) H2O(cr) H2O(L)

H3BO3(CR) H3BO3(L)

Samples with THF, 6FR

NASA-GLENN CHEMICAL EQUILIBRIUM PROGRAM CEA2, MAY 21, 2004

BY BONNIE MCBRIDE AND SANFORD GORDON

REFS: NASA RP-1311, PART I, 1994 AND NASA RP-1311, PART II, 1996

PRODUCTS WHICH WERE CONSIDERED BUT WHOSE MOLE FRACTIONS
WERE LESS THAN 5.000000E-06 FOR ALL ASSIGNED CONDITIONS

*B BC BC2 BH BH2

BH3 BH4 BH5 *BO BOH

BO2 B(OH)2 B2 B2C B2H

B2H2 B2H3 B2H3,db B2H4 B2H4,db

B2H5 B2H5,db B2H6 B2O B2O3

B2(OH)4 B3H7,C2v B3H7,Cs B3H9 B4H4

B4H10 B4H12 B5H9 *C *CH
 CH2 CH3 CH2OH CH3O CH4
 CH3OH CH3OOH *CO *CO2 COOH
 *C2 C2H C2H2,acetylene C2H2,vinylidene CH2CO,ketene
 O(CH)2O HO(CO)2OH C2H3,vinyl CH3CO,acetyl C2H4
 C2H4O,ethylen-o CH3CHO,ethanal CH3COOH OHCH2COOH C2H5
 C2H6 C2H5OH CH3OCH3 CH3O2CH3 C2O
 *C3 C3H3,1-propynl C3H3,2-propynl C3H4,allene C3H4,propyne
 C3H4,cyclo- C3H5,allyl C3H6,propylene C3H6,cyclo- C3H6O,propylox
 C3H6O,acetone C3H6O,propanal C3H7,n-propyl C3H7,i-propyl C3H8
 C3H8O,1propanol C3H8O,2propanol C3O2 *C4 C4H2,butadiyne
 C4H4,1,3-cyclo- C4H6,butadiene C4H6,1butyne C4H6,2butyne C4H6,cyclo-
 C4H8,1-butene C4H8,cis2-buten C4H8,tr2-butene C4H8,isobutene C4H8,cyclo-
 (CH3COOH)2 C4H9,n-butyl C4H9,i-butyl C4H9,s-butyl C4H9,t-butyl
 C4H10,n-butane C4H10,isobutane *C5 C5H6,1,3cyclo- C5H8,cyclo-
 C5H10,1-pentene C5H10,cyclo- C5H11,pentyl C5H11,t-pentyl C5H12,n-pentane
 C5H12,i-pentane CH3C(CH3)2CH3 C6H2 C6H5,phenyl C6H5O,phenoxy
 C6H6 C6H5OH,phenol C6H10,cyclo- C6H12,1-hexene C6H12,cyclo-
 C6H13,n-hexyl C6H14,n-hexane C7H7,benzyl C7H8 C7H8O,cresol-mx
 C7H14,1-heptene C7H15,n-heptyl C7H16,n-heptane C7H16,2-methylh C8H8,styrene
 C8H10,ETHYLBENZ C8H16,1-OCTENE C8H17,N-OCTYL C8H18,N-OCTANE
 C8H18,ISOOCTANE

 C9H19,n-nonyl C10H8,naphthale C10H21,n-decyl C12H9,o-bipheny C12H10,biphenyl
 *Fe Fe(CO)5 FeO Fe(OH)2 *H
 HCO HCCO HO2 HBOH HCHO,formaldehy
 HCOOH H2O H2O2 H2BOH HB(OH)2
 H3BO3 H3B3O6 (HCOOH)2 *O *OH
 *O2 O3 B(L) B2O3(cr) B3O3H3(cr)

B4C(L) C(gr) Fe(a) Fe(d) Fe(L)
Fe(CO)5(L) Fe.947O(cr) Fe.947O(L) Fe(OH)2(cr) Fe(OH)3(cr)
Fe2O3(cr) Fe3O4(cr) Fe3O4(L) HBO2(cr) HBO2(L)
H2O(cr) H2O(L) H3BO3(cr) H3BO3(L)

Samples with THF, 9FR

NASA-GLENN CHEMICAL EQUILIBRIUM PROGRAM CEA2, MAY 21, 2004

BY BONNIE MCBRIDE AND SANFORD GORDON

REFS: NASA RP-1311, PART I, 1994 AND NASA RP-1311, PART II, 1996

PRODUCTS WHICH WERE CONSIDERED BUT WHOSE MOLE FRACTIONS
WERE LESS THAN 5.000000E-06 FOR ALL ASSIGNED CONDITIONS

*B BC BC2 BH BH2

BH3 BH4 BH5 *BO BOH

BO2 B(OH)2 B2 B2C B2H

B2H2 B2H3 B2H3,db B2H4 B2H4,db

B2H5 B2H5,db B2H6 B2O B2O2

B2O3 B2(OH)4 B3H7,C2v B3H7,Cs B3H9

B4H4 B4H10 B4H12 B5H9 *C

*CH CH2 CH3 CH2OH CH3O

CH4 CH3OH CH3OOH *CO *CO2

COOH *C2 C2H C2H2,acetylene C2H2,vinylidene

CH2CO,ketene O(CH)2O HO(CO)2OH C2H3,vinyl CH3CO,acetyl

C2H4 C2H4O,ethylen-o CH3CHO,ethanal CH3COOH OHCH2COOH

C2H5 C2H6 C2H5OH CH3OCH3 CH3O2CH3
 C2O *C3 C3H3,1-propynl C3H3,2-propynl C3H4,allene
 C3H4,propyne C3H4,cyclo- C3H5,allyl C3H6,propylene C3H6,cyclo-

 C3H6O,propylox C3H6O,acetone C3H6O,propanal C3H7,n-propyl C3H7,i-propyl
 C3H8 C3H8O,1propanol C3H8O,2propanol C3O2 *C4
 C4H2,butadiyne C4H4,1,3-cyclo- C4H6,butadiene C4H6,1butyne C4H6,2butyne
 C4H6,cyclo- C4H8,1-butene C4H8,cis2-buten C4H8,tr2-butene C4H8,isobutene
 C4H8,cyclo- (CH3COOH)2 C4H9,n-butyl C4H9,i-butyl C4H9,s-butyl
 C4H9,T-BUTYL C4H10,N-BUTANE C4H10,ISOBUTANE *C5 C5H6,1,3CYCLO-

 C5H8,cyclo- C5H10,1-pentene C5H10,cyclo- C5H11,pentyl C5H11,t-pentyl
 C5H12,n-pentane C5H12,i-pentane CH3C(CH3)2CH3 C6H2 C6H5,phenyl
 C6H5O,phenoxy C6H6 C6H5OH,phenol C6H10,cyclo- C6H12,1-hexene
 C6H12,cyclo- C6H13,n-hexyl C6H14,n-hexane C7H7,benzyl C7H8
 C7H8O,cresol-mx C7H14,1-heptene C7H15,n-heptyl C7H16,n-heptane C7H16,2-
 methylh
 C8H8,styrene C8H10,ethylbenz C8H16,1-octene C8H17,n-octyl C8H18,n-octane
 C8H18,isoctane C9H19,n-nonyl C10H8,naphthale C10H21,n-decyl C12H9,o-bipheny
 C12H10,biphenyl *Fe Fe(CO)5 FeO Fe(OH)2
 *H HBO2 HCO HCCO HO2
 HBOH HCHO,formaldehy HCOOH H2O H2O2
 H2BOH HB(OH)2 H3BO3 H3B3O6 (HCOOH)2
 *O *OH *O2 O3 B(L)
 B2O3(cr) B3O3H3(cr) B4C(L) C(gr) Fe(a)
 Fe(d) Fe(L) Fe(CO)5(L) Fe.947O(cr) Fe.947O(L)
 Fe(OH)2(cr) Fe(OH)3(cr) Fe2O3(cr) Fe3O4(cr) Fe3O4(L)
 HBO2(cr) HBO2(L) H2O(cr) H2O(L) H3BO3(cr) H3BO3(L)

Samples with THP, 3FR

NASA-GLENN CHEMICAL EQUILIBRIUM PROGRAM CEA2, MAY 21, 2004

BY BONNIE MCBRIDE AND SANFORD GORDON

REFS: NASA RP-1311, PART I, 1994 AND NASA RP-1311, PART II, 1996

PRODUCTS WHICH WERE CONSIDERED BUT WHOSE MOLE FRACTIONS
WERE LESS THAN 5.000000E-06 FOR ALL ASSIGNED CONDITIONS

*B BC BC2 BH BH2

BH3 BH4 BH5 *BO BOH

BO2 B(OH)2 B2 B2C B2H

B2H2 B2H3 B2H3,db B2H4 B2H4,db

B2H5 B2H5,db B2H6 B2O B2(OH)4

B3H7,C2v B3H7,Cs B3H9 B4H4 B4H10

B4H12 B5H9 *C *CH CH2

CH3 CH2OH CH3O CH3OH CH3OOH

*CO2 COOH *C2 C2H C2H2,vinylidene

CH2CO,ketene O(CH)2O HO(CO)2OH C2H3,vinyl CH3CO,acetyl

C2H4 C2H4O,ethylen-o CH3CHO,ethanal CH3COOH OHCH2COOH

C2H5 C2H6 C2H5OH CH3OCH3 CH3O2CH3

C2O *C3 C3H3,1-propynl C3H3,2-propynl C3H4,allene

C3H4,propyne C3H4,cyclo- C3H5,allyl C3H6,propylene C3H6,cyclo-

C3H6O,propylox C3H6O,acetone C3H6O,propanal C3H7,n-propyl C3H7,i-propyl

C3H8 C3H8O,1propanol C3H8O,2propanol C3O2 *C4
 C4H2,butadiyne C4H4,1,3-cyclo- C4H6,butadiene C4H6,1butyne C4H6,2butyne
 C4H6,cyclo- C4H8,1-butene C4H8,cis2-buten C4H8,tr2-butene C4H8,isobutene
 C4H8,cyclo- (CH3COOH)2 C4H9,n-butyl C4H9,i-butyl C4H9,s-butyl
 C4H9,t-butyl C4H10,n-butane C4H10,isobutane *C5 C5H6,1,3cyclo-
 C5H8,cyclo- C5H10,1-pentene C5H10,cyclo- C5H11,pentyl C5H11,t-pentyl
 C5H12,n-pentane C5H12,i-pentane CH3C(CH3)2CH3 C6H2 C6H5,phenyl
 C6H5O,phenoxy C6H6 C6H5OH,phenol C6H10,cyclo- C6H12,1-hexene
 C6H12,cyclo- C6H13,n-hexyl C6H14,n-hexane C7H7,benzyl C7H8
 C7H8O,cresol-mx C7H14,1-heptene C7H15,n-heptyl C7H16,n-heptane C7H16,2-
 methylh
 C8H8,styrene C8H10,ethylbenz C8H16,1-octene C8H17,n-octyl C8H18,n-octane
 C8H18,isoctane C9H19,n-nonyl C10H8,naphthale C10H21,n-decyl C12H9,o-bipheny
 C12H10,biphenyl *Fe Fe(CO)5 FeO Fe(OH)2
 HCO HCCO HO2 HBOH HCHO,formaldehy
 HCOOH H2O2 HB(OH)2 H3BO3 H3B3O6
 (HCOOH)2 *O *OH *O2 O3
 B(b) B(L) B2O3(cr) B3O3H3(cr) B4C(L)
 Fe(a) Fe(c) Fe(L) Fe(CO)5(L) Fe.947O(cr)
 Fe.947O(L) Fe(OH)2(cr) Fe(OH)3(cr) Fe2O3(cr) Fe3O4(cr)
 Fe3O4(L) HBO2(cr) HBO2(L) H2O(cr) H2O(L)
 H3BO3(cr) H3BO3(L)

Samples with THP, 6FR

.....
 NASA-GLENN CHEMICAL EQUILIBRIUM PROGRAM CEA2, MAY 21, 2004
 BY BONNIE MCBRIDE AND SANFORD GORDON
 REFS: NASA RP-1311, PART I, 1994 AND NASA RP-1311, PART II, 1996

PRODUCTS WHICH WERE CONSIDERED BUT WHOSE MOLE FRACTIONS
WERE LESS THAN 5.000000E-06 FOR ALL ASSIGNED CONDITIONS

*B BC BC2 BH BH2
BH3 BH4 BH5 *BO BOH
BO2 B(OH)2 B2 B2C B2H
B2H2 B2H3 B2H3,db B2H4 B2H4,db
B2H5 B2H5,db B2H6 B2O B2O3
B2(OH)4 B3H7,C2v B3H7,Cs B3H9 B4H4
B4H10 B4H12 B5H9 *C *CH
CH2 CH3 CH2OH CH3O CH3OH
CH3OOH *CO *CO2 COOH *C2
C2H C2H2,acetylene C2H2,vinylidene CH2CO,ketene O(CH)2O
HO(CO)2OH C2H3,vinyl CH3CO,acetyl C2H4 C2H4O,ethylen-o
CH3CHO,ethanal CH3COOH OHCH2COOH C2H5 C2H6
C2H5OH CH3OCH3 CH3O2CH3 C2O *C3
C3H3,1-propynyl C3H3,2-propynyl C3H4,allene C3H4,propyne C3H4,cyclo-
C3H5,allyl C3H6,propylene C3H6,cyclo- C3H6O,propylox C3H6O,acetone
C3H6O,propanal C3H7,n-propyl C3H7,i-propyl C3H8 C3H8O,1propanol
C3H8O,2propanol C3O2 *C4 C4H2,butadiyne C4H4,1,3-cyclo-
C4H6,butadiene C4H6,1butyne C4H6,2butyne C4H6,cyclo- C4H8,1-butene
C4H8,cis2-buten C4H8,tr2-butene C4H8,isobutene C4H8,cyclo- (CH3COOH)2
C4H9,n-butyl C4H9,i-butyl C4H9,s-butyl C4H9,t-butyl C4H10,n-butane
C4H10,isobutane *C5 C5H6,1,3cyclo- C5H8,cyclo- C5H10,1-pentene
C5H10,cyclo- C5H11,pentyl C5H11,t-pentyl C5H12,n-pentane C5H12,i-pentane
CH3C(CH3)2CH3 C6H2 C6H5,phenyl C6H5O,phenoxy C6H6
C6H5OH,phenol C6H10,cyclo- C6H12,1-hexene C6H12,cyclo- C6H13,n-hexyl
C6H14,n-hexane C7H7,benzyl C7H8 C7H8O,cresol-mx C7H14,1-heptene

C7H15,n-heptyl C7H16,n-heptane C7H16,2-methylh C8H8,styrene C8H10,ethylbenz
 C8H16,1-octene C8H17,n-octyl C8H18,n-octane C8H18,isooctane C9H19,n-nonyl
 C10H8,naphthale C10H21,n-decyl C12H9,o-bipheny C12H10,biphenyl *Fe
 Fe(CO)5 FeO Fe(OH)2 *H HCO
 HCCO HO2 HBOH HCHO,formaldehy HCOOH
 H2O H2O2 H2BOH HB(OH)2 H3BO3
 H3B3O6 (HCOOH)2 *O *OH *O2
 O3 B(L) B2O3(cr) B3O3H3(cr) B4C(L)
 C(gr) Fe(a) Fe(d) Fe(L) Fe(CO)5(L)
 Fe.947O(cr) Fe.947O(L) Fe(OH)2(cr) Fe(OH)3(cr) Fe2O3(cr)
 Fe3O4(cr) Fe3O4(L) HBO2(cr) HBO2(L) H2O(cr)
 H2O(L) H3BO3(cr) H3BO3(L)

Samples with THF, 9FR

NASA-GLENN CHEMICAL EQUILIBRIUM PROGRAM CEA2, MAY 21, 2004

BY BONNIE MCBRIDE AND SANFORD GORDON

REFS: NASA RP-1311, PART I, 1994 AND NASA RP-1311, PART II, 1996

PRODUCTS WHICH WERE CONSIDERED BUT WHOSE MOLE FRACTIONS
 WERE LESS THAN 5.000000E-06 FOR ALL ASSIGNED CONDITIONS

*B BC BC2 BH BH2

BH3 BH4 BH5 *BO BOH

BO2 B(OH)2 B2 B2C B2H

B2H2 B2H3 B2H3,db B2H4 B2H4,db
 B2H5 B2H5,db B2H6 B2O B2O2
 B2O3 B2(OH)4 B3H7,C2v B3H7,Cs B3H9
 B4H4 B4H10 B4H12 B5H9 *C
 *CH CH2 CH3 CH2OH CH3O
 CH4 CH3OH CH3OOH *CO *CO2
 COOH *C2 C2H C2H2,acetylene C2H2,vinylidene
 CH2CO,ketene O(CH)2O HO(CO)2OH C2H3,vinyl CH3CO,acetyl
 C2H4 C2H4O,ethylen-o CH3CHO,ethanal CH3COOH OHCH2COOH
 C2H5 C2H6 C2H5OH CH3OCH3 CH3O2CH3
 C2O *C3 C3H3,1-propynl C3H3,2-propynl C3H4,allene
 C3H4,propyne C3H4,cyclo- C3H5,allyl C3H6,propylene C3H6,cyclo-
 C3H6O,propylox C3H6O,acetone C3H6O,propanal C3H7,n-propyl C3H7,i-propyl
 C3H8 C3H8O,1propanol C3H8O,2propanol C3O2 *C4
 C4H2,butadiyne C4H4,1,3-cyclo- C4H6,butadiene C4H6,1butyne C4H6,2butyne
 C4H6,cyclo- C4H8,1-butene C4H8,cis2-buten C4H8,tr2-butene C4H8,isobutene

 C4H8,cyclo- (CH3COOH)2 C4H9,n-butyl C4H9,i-butyl C4H9,s-butyl
 C4H9,t-butyl C4H10,n-butane C4H10,isobutane *C5 C5H6,1,3cyclo-
 C5H8,cyclo- C5H10,1-pentene C5H10,cyclo- C5H11,pentyl C5H11,t-pentyl
 C5H12,n-pentane C5H12,i-pentane CH3C(CH3)2CH3 C6H2 C6H5,phenyl
 C6H5O,phenoxy C6H6 C6H5OH,phenol C6H10,cyclo- C6H12,1-hexene
 C6H12,cyclo- C6H13,n-hexyl C6H14,n-hexane C7H7,benzyl C7H8
 C7H8O,cresol-mx C7H14,1-heptene C7H15,n-heptyl C7H16,n-heptane C7H16,2-
 methylh
 C8H8,styrene C8H10,ethylbenz C8H16,1-octene C8H17,n-octyl C8H18,n-octane
 C8H18,isoctane C9H19,n-nonyl C10H8,naphthale C10H21,n-decyl C12H9,o-bipheny
 C12H10,biphenyl *Fe Fe(CO)5 FeO Fe(OH)2
 *H HBO2 HCO HCCO HO2

HBOH HCHO,formaldehy HCOOH H2O H2O2
H2BOH HB(OH)2 H3BO3 H3B3O6 (HCOOH)2
*O *OH *O2 O3 B(L)
B2O3(cr) B3O3H3(cr) B4C(L) C(gr) Fe(a)
Fe(d) Fe(L) Fe(CO)5(L) Fe.947O(cr) Fe.947O(L)
Fe(OH)2(cr) Fe(OH)3(cr) Fe2O3(cr) Fe3O4(cr) Fe3O4(L)
HBO2(cr) HBO2(L) H2O(cr) H2O(L) H3BO3(cr)
H3BO3(L)

Samples with 1,4 dioxane, 3FR

NASA-GLENN CHEMICAL EQUILIBRIUM PROGRAM CEA2, MAY 21, 2004

BY BONNIE MCBRIDE AND SANFORD GORDON

REFS: NASA RP-1311, PART I, 1994 AND NASA RP-1311, PART II, 1996

PRODUCTS WHICH WERE CONSIDERED BUT WHOSE MOLE FRACTIONS
WERE LESS THAN 5.000000E-06 FOR ALL ASSIGNED CONDITIONS

*B BC BC2 BH BH2

BH4 BH5 BOH BO2 B(OH)2

B2 B2C B2H B2H2 B2H3

B2H3,db B2H4 B2H4,db B2H5 B2H5,db

B2H6 B2O B2(OH)4 B3H7,C2v B3H7,Cs

B3H9 B4H4 B4H10 B4H12 B5H9

*C *CH CH2 CH3 CH2OH

CH3O CH3OH CH3OOH *CO2 COOH

*C2 C2H C2H2,acetylene C2H2,vinylidene CH2CO,ketene
 O(CH)2O HO(CO)2OH C2H3,vinyl CH3CO,acetyl C2H4
 C2H4O,ethylen-o CH3CHO,ethanal CH3COOH OHCH2COOH C2H5
 C2H6 C2H5OH CH3OCH3 CH3O2CH3 C2O
 *C3 C3H3,1-propynl C3H3,2-propynl C3H4,allene C3H4,propyne
 C3H4,cyclo- C3H5,allyl C3H6,propylene C3H6,cyclo- C3H6O,propylox
 C3H6O,acetone C3H6O,propanal C3H7,n-propyl C3H7,i-propyl C3H8
 C3H8O,1propanol C3H8O,2propanol C3O2 *C4 C4H2,butadiyne
 C4H4,1,3-cyclo- C4H6,butadiene C4H6,1butyne C4H6,2butyne C4H6,cyclo-
 C4H8,1-butene C4H8,cis2-buten C4H8,tr2-butene C4H8,isobutene C4H8,cyclo-
 (CH3COOH)2 C4H9,n-butyl C4H9,i-butyl C4H9,s-butyl C4H9,t-butyl
 C4H10,n-butane C4H10,isobutane *C5 C5H6,1,3cyclo- C5H8,cyclo-
 C5H10,1-pentene C5H10,cyclo- C5H11,pentyl C5H11,t-pentyl C5H12,n-pentane
 C5H12,i-pentane CH3C(CH3)2CH3 C6H2 C6H5,phenyl C6H5O,phenoxy
 C6H6 C6H5OH,phenol C6H10,cyclo- C6H12,1-hexene C6H12,cyclo-
 C6H13,n-hexyl C6H14,n-hexane C7H7,benzyl C7H8 C7H8O,cresol-mx
 C7H14,1-heptene C7H15,n-heptyl C7H16,n-heptane C7H16,2-methylh C8H8,styrene
 C8H10,ethylbenz C8H16,1-octene C8H17,n-octyl C8H18,n-octane C8H18,isooctane
 C9H19,n-nonyl C10H8,naphthale C10H21,n-decyl C12H9,o-bipheny C12H10,biphenyl
 *Fe Fe(CO)5 FeO Fe(OH)2 HCO
 HCCO HO2 HBOH HCHO,formaldehy HCOOH
 H2O2 HB(OH)2 H3BO3 H3B3O6 (HCOOH)2
 *O *OH *O2 O3 B(b)
 B(L) B2O3(cr) B3O3H3(cr) B4C(L) C(gr)
 Fe(a) Fe(c) Fe(d) Fe(CO)5(L) Fe.947O(cr)
 Fe.947O(L) Fe(OH)2(cr) Fe(OH)3(cr) Fe2O3(cr) Fe3O4(cr)
 Fe3O4(L) HBO2(cr) HBO2(L) H2O(cr) H2O(L)
 H3BO3(cr) H3BO3(L)

Samples with 1,4 dioxane, 6FR

NASA-GLENN CHEMICAL EQUILIBRIUM PROGRAM CEA2, MAY 21, 2004

BY BONNIE MCBRIDE AND SANFORD GORDON

REFS: NASA RP-1311, PART I, 1994 AND NASA RP-1311, PART II, 1996

PRODUCTS WHICH WERE CONSIDERED BUT WHOSE MOLE FRACTIONS
WERE LESS THAN 5.000000E-06 FOR ALL ASSIGNED CONDITIONS

*B BC BC2 BH BH2

BH3 BH4 BH5 *BO BOH

BO2 B(OH)2 B2 B2C B2H

B2H2 B2H3 B2H3,db B2H4 B2H4,db

B2H5 B2H5,db B2H6 B2O B2(OH)4

B3H7,C2v B3H7,Cs B3H9 B4H4 B4H10

B4H12 B5H9 *C *CH CH2

CH3 CH2OH CH3O CH4 CH3OH

CH3OOH *CO2 COOH *C2 C2H

C2H2,acetylene C2H2,vinylidene CH2CO,ketene O(CH)2O HO(CO)2OH

C2H3,vinyl CH3CO,acetyl C2H4 C2H4O,ethylen-o CH3CHO,ethanal

CH3COOH OHCH2COOH C2H5 C2H6 C2H5OH

CH3OCH3 CH3O2CH3 C2O *C3 C3H3,1-propynl

C3H3,2-propynl C3H4,allene C3H4,propyne C3H4,cyclo- C3H5,allyl

C3H6,propylene C3H6,cyclo- C3H6O,propylox C3H6O,acetone C3H6O,propanal

C3H7,n-propyl C3H7,i-propyl C3H8 C3H8O,1propanol C3H8O,2propanol

C3O2 *C4 C4H2,butadiyne C4H4,1,3-cyclo- C4H6,butadiene
 C4H6,1butyne C4H6,2butyne C4H6,cyclo- C4H8,1-butene C4H8,cis2-buten
 C4H8,tr2-butene C4H8,isobutene C4H8,cyclo- (CH3COOH)2 C4H9,n-butyl
 C4H9,i-butyl C4H9,s-butyl C4H9,t-butyl C4H10,n-butane C4H10,isobutane
 *C5 C5H6,1,3cyclo- C5H8,cyclo- C5H10,1-pentene C5H10,cyclo-
 C5H11,pentyl C5H11,t-pentyl C5H12,n-pentane C5H12,i-pentane CH3C(CH3)2CH3
 C6H2 C6H5,phenyl C6H5O,phenoxy C6H6 C6H5OH,phenol
 C6H10,cyclo- C6H12,1-hexene C6H12,cyclo- C6H13,n-hexyl C6H14,n-hexane
 C7H7,benzyl C7H8 C7H8O,cresol-mx C7H14,1-heptene C7H15,n-heptyl

 C7H16,n-heptane C7H16,2-methylh C8H8,styrene C8H10,ethylbenz C8H16,1-octene
 C8H17,n-octyl C8H18,n-octane C8H18,isoctane C9H19,n-nonyl C10H8,naphthale
 C10H21,n-decyl C12H9,o-bipheny C12H10,biphenyl *Fe Fe(CO)5
 FeO Fe(OH)2 *H HCO HCCO
 HO2 HBOH HCHO,formaldehy HCOOH H2O
 H2O2 H2BOH HB(OH)2 H3BO3 H3B3O6
 (HCOOH)2 *O *OH *O2 O3
 B(L) B2O3(cr) B3O3H3(cr) B4C(L) C(gr)
 Fe(a) Fe(d) Fe(L) Fe(CO)5(L) Fe.947O(cr)
 Fe.947O(L) Fe(OH)2(cr) Fe(OH)3(cr) Fe2O3(cr) Fe3O4(cr)
 Fe3O4(L) HBO2(cr) HBO2(L) H2O(cr) H2O(L)
 H3BO3(cr) H3BO3(L)

Samples with 1,4 dioxane, 9FR

NASA-GLENN CHEMICAL EQUILIBRIUM PROGRAM CEA2, MAY 21, 2004
 BY BONNIE MCBRIDE AND SANFORD GORDON

REFS: NASA RP-1311, PART I, 1994 AND NASA RP-1311, PART II, 1996

PRODUCTS WHICH WERE CONSIDERED BUT WHOSE MOLE FRACTIONS
WERE LESS THAN 5.000000E-06 FOR ALL ASSIGNED CONDITIONS

*B BC BC2 BH BH2

BH3 BH4 BH5 *BO BOH

BO2 B(OH)2 B2 B2C B2H

B2H2 B2H3 B2H3,db B2H4 B2H4,db

B2H5 B2H5,db B2H6 B2O B2O2

B2O3 B2(OH)4 B3H7,C2v B3H7,Cs B3H9

B4H4 B4H10 B4H12 B5H9 *C

*CH CH2 CH3 CH2OH CH3O

CH4 CH3OH CH3OOH *CO *CO2

COOH *C2 C2H C2H2,acetylene C2H2,vinylidene

CH2CO,ketene O(CH)2O HO(CO)2OH C2H3,vinyl CH3CO,acetyl

C2H4 C2H4O,ethylen-o CH3CHO,ethanal CH3COOH OHCH2COOH

C2H5 C2H6 C2H5OH CH3OCH3 CH3O2CH3

C2O *C3 C3H3,1-propynl C3H3,2-propynl C3H4,allene

C3H4,propyne C3H4,cyclo- C3H5,allyl C3H6,propylene C3H6,cyclo-

C3H6O,propylox C3H6O,acetone C3H6O,propanal C3H7,n-propyl C3H7,i-propyl

C3H8 C3H8O,1propanol C3H8O,2propanol C3O2 *C4

C4H2,butadiyne C4H4,1,3-cyclo- C4H6,butadiene C4H6,1butyne C4H6,2butyne

C4H6,cyclo- C4H8,1-butene C4H8,cis2-buten C4H8,tr2-butene C4H8,isobutene

C4H8,cyclo- (CH3COOH)2 C4H9,n-butyl C4H9,i-butyl C4H9,s-butyl

C4H9,t-butyl C4H10,n-butane C4H10,isobutane *C5 C5H6,1,3cyclo-

C5H8,cyclo- C5H10,1-pentene C5H10,cyclo- C5H11,pentyl C5H11,t-pentyl

C5H12,n-pentane C5H12,i-pentane CH3C(CH3)2CH3 C6H2 C6H5,phenyl
 C6H5O,phenoxy C6H6 C6H5OH,phenol C6H10,cyclo- C6H12,1-hexene
 C6H12,cyclo- C6H13,n-hexyl C6H14,n-hexane C7H7,benzyl C7H8
 C7H8O,cresol-mx C7H14,1-heptene C7H15,n-heptyl C7H16,n-heptane C7H16,2-
 methylh
 C8H8,styrene C8H10,ethylbenz C8H16,1-octene C8H17,n-octyl C8H18,n-octane
 C8H18,isooctane C9H19,n-nonyl C10H8,naphthale C10H21,n-decyl C12H9,o-bipheny
 C12H10,biphenyl *Fe Fe(CO)5 FeO Fe(OH)2
 *H HBO2 HCO HCCO HO2
 HBOH HCHO,formaldehy HCOOH H2O H2O2
 H2BOH HB(OH)2 H3BO3 H3B3O6 (HCOOH)2
 *O *OH *O2 O3 B(L)
 B2O3(cr) B3O3H3(cr) B4C(L) C(gr) Fe(a)
 Fe(d) Fe(L) Fe(CO)5(L) Fe.947O(cr) Fe.947O(L)
 Fe(OH)2(cr) Fe(OH)3(cr) Fe2O3(cr) Fe3O4(cr) Fe3O4(L)
 HBO2(cr) HBO2(L) H2O(cr) H2O(L) H3BO3(cr)
 H3BO3(L)

Samples with 1,2 epoxybutane, 3FR

NASA-GLENN CHEMICAL EQUILIBRIUM PROGRAM CEA2, MAY 21, 2004

BY BONNIE MCBRIDE AND SANFORD GORDON

REFS: NASA RP-1311, PART I, 1994 AND NASA RP-1311, PART II, 1996

PRODUCTS WHICH WERE CONSIDERED BUT WHOSE MOLE FRACTIONS

WERE LESS THAN 5.000000E-06 FOR ALL ASSIGNED CONDITIONS

*B BC BC2 BH BH2

BH4 BH5 BOH BO2 B(OH)2

B2 B2C B2H B2H2 B2H3

B2H3,db B2H4 B2H4,db B2H5 B2H5,db

B2H6 B2O B2(OH)4 B3H7,C2v B3H7,Cs

B3H9 B4H4 B4H10 B4H12 B5H9

*C *CH CH2 CH3 CH2OH

CH3O CH3OH CH3OOH *CO2 COOH

*C2 C2H C2H2,acetylene C2H2,vinylidene CH2CO,ketene

O(CH)2O HO(CO)2OH C2H3,vinyl CH3CO,acetyl C2H4

C2H4O,ethylen-o CH3CHO,ethanal CH3COOH OHCH2COOH C2H5

C2H6 C2H5OH CH3OCH3 CH3O2CH3 C2O

*C3 C3H3,1-propynl C3H3,2-propynl C3H4,allene C3H4,propyne

C3H4,cyclo- C3H5,allyl C3H6,propylene C3H6,cyclo- C3H6O,propylox

C3H6O,acetone C3H6O,propanal C3H7,n-propyl C3H7,i-propyl C3H8

C3H8O,1propanol C3H8O,2propanol C3O2 *C4 C4H2,butadiyne

C4H4,1,3-cyclo- C4H6,butadiene C4H6,1butyne C4H6,2butyne C4H6,cyclo-

C4H8,1-butene C4H8,cis2-buten C4H8,tr2-butene C4H8,isobutene C4H8,cyclo-

(CH3COOH)2 C4H9,n-butyl C4H9,i-butyl C4H9,s-butyl C4H9,t-butyl

C4H10,n-butane C4H10,isobutane *C5 C5H6,1,3cyclo- C5H8,cyclo-

C5H10,1-pentene C5H10,cyclo- C5H11,pentyl C5H11,t-pentyl C5H12,n-pentane

C5H12,i-pentane CH3C(CH3)2CH3 C6H2 C6H5,phenyl C6H5O,phenoxy

C6H6 C6H5OH,phenol C6H10,cyclo- C6H12,1-hexene C6H12,cyclo-

C6H13,n-hexyl C6H14,n-hexane C7H7,benzyl C7H8 C7H8O,cresol-mx

C7H14,1-heptene C7H15,n-heptyl C7H16,n-heptane C7H16,2-methylh C8H8,styrene

C8H10,ethylbenz C8H16,1-octene C8H17,n-octyl C8H18,n-octane C8H18,isoctane

C9H19,n-nonyl C10H8,naphthale C10H21,n-decyl C12H9,o-bipheny C12H10,biphenyl

*Fe Fe(CO)5 FeO Fe(OH)2 HCO

HCCO HO2 HBOH HCHO,formaldehy HCOOH

H2O2 HB(OH)2 H3BO3 H3B3O6 (HCOOH)2

*O *OH *O2 O3 B(b)

B(L) B2O3(cr) B3O3H3(cr) B4C(L) C(gr)

Fe(a) Fe(c) Fe(CO)5(L) Fe.947O(cr) Fe.947O(L)

Fe(OH)2(cr) Fe(OH)3(cr) Fe2O3(cr) Fe3O4(cr) Fe3O4(L)

HBO2(cr) HBO2(L) H2O(cr) H2O(L) H3BO3(cr)

H3BO3(L)

Samples with 1,2 epoxybutane, 6FR

NASA-GLENN CHEMICAL EQUILIBRIUM PROGRAM CEA2, MAY 21, 2004

BY BONNIE MCBRIDE AND SANFORD GORDON

REFS: NASA RP-1311, PART I, 1994 AND NASA RP-1311, PART II, 1996

PRODUCTS WHICH WERE CONSIDERED BUT WHOSE MOLE FRACTIONS

WERE LESS THAN 5.000000E-06 FOR ALL ASSIGNED CONDITIONS

*B BC BC2 BH BH2

BH3 BH4 BH5 *BO BOH

BO2 B(OH)2 B2 B2C B2H

B2H2 B2H3 B2H3,db B2H4 B2H4,db

B2H5 B2H5,db B2H6 B2O B2O3

B2(OH)4 B3H7,C2v B3H7,Cs B3H9 B4H4

B4H10 B4H12 B5H9 *C *CH
 CH2 CH3 CH2OH CH3O CH4
 CH3OH CH3OOH *CO *CO2 COOH
 *C2 C2H C2H2,acetylene C2H2,vinylidene CH2CO,ketene

 O(CH)2O HO(CO)2OH C2H3,vinyl CH3CO,acetyl C2H4
 C2H4O,ethylen-o CH3CHO,ethanal CH3COOH OHCH2COOH C2H5
 C2H6 C2H5OH CH3OCH3 CH3O2CH3 C2O
 *C3 C3H3,1-propynl C3H3,2-propynl C3H4,allene C3H4,propyne
 C3H4,cyclo- C3H5,allyl C3H6,propylene C3H6,cyclo- C3H6O,propylox
 C3H6O,acetone C3H6O,propanal C3H7,n-propyl C3H7,i-propyl C3H8
 C3H8O,1propanol C3H8O,2propanol C3O2 *C4 C4H2,butadiyne
 C4H4,1,3-cyclo- C4H6,butadiene C4H6,1butyne C4H6,2butyne C4H6,cyclo-
 C4H8,1-butene C4H8,cis2-buten C4H8,tr2-butene C4H8,isobutene C4H8,cyclo-
 (CH3COOH)2 C4H9,n-butyl C4H9,i-butyl C4H9,s-butyl C4H9,t-butyl
 C4H10,n-butane C4H10,isobutane *C5 C5H6,1,3cyclo- C5H8,cyclo-
 C5H10,1-pentene C5H10,cyclo- C5H11,pentyl C5H11,t-pentyl C5H12,n-pentane
 C5H12,i-pentane CH3C(CH3)2CH3 C6H2 C6H5,phenyl C6H5O,phenoxy
 C6H6 C6H5OH,phenol C6H10,cyclo- C6H12,1-hexene C6H12,cyclo-
 C6H13,n-hexyl C6H14,n-hexane C7H7,benzyl C7H8 C7H8O,cresol-mx
 C7H14,1-heptene C7H15,n-heptyl C7H16,n-heptane C7H16,2-methylh C8H8,styrene
 C8H10,ethylbenz C8H16,1-octene C8H17,n-octyl C8H18,n-octane C8H18,isooctane

 C9H19,n-nonyl C10H8,naphthale C10H21,n-decyl C12H9,o-bipheny C12H10,biphenyl
 *Fe Fe(CO)5 FeO Fe(OH)2 *H
 HCO HCCO HO2 HBOH HCHO,formaldehy
 HCOOH H2O H2O2 H2BOH HB(OH)2
 H3BO3 H3B3O6 (HCOOH)2 *O *OH
 *O2 O3 B(L) B2O3(cr) B3O3H3(cr)

B4C(L) C(gr) Fe(a) Fe(d) Fe(L)
Fe(CO)5(L) Fe.947O(cr) Fe.947O(L) Fe(OH)2(cr) Fe(OH)3(cr)
Fe2O3(cr) Fe3O4(cr) Fe3O4(L) HBO2(cr) HBO2(L)
H2O(cr) H2O(L) H3BO3(cr) H3BO3(L)

Samples with 1,2 epoxybutane, 9FR

NASA-GLENN CHEMICAL EQUILIBRIUM PROGRAM CEA2, MAY 21, 2004

BY BONNIE MCBRIDE AND SANFORD GORDON

REFS: NASA RP-1311, PART I, 1994 AND NASA RP-1311, PART II, 1996

PRODUCTS WHICH WERE CONSIDERED BUT WHOSE MOLE FRACTIONS
WERE LESS THAN 5.000000E-06 FOR ALL ASSIGNED CONDITIONS

*B BC BC2 BH BH2

BH3 BH4 BH5 *BO BOH

BO2 B(OH)2 B2 B2C B2H

B2H2 B2H3 B2H3,db B2H4 B2H4,db

B2H5 B2H5,db B2H6 B2O B2O2

B2O3 B2(OH)4 B3H7,C2v B3H7,Cs B3H9

B4H4 B4H10 B4H12 B5H9 *C

*CH CH2 CH3 CH2OH CH3O

CH4 CH3OH CH3OOH *CO *CO2

COOH *C2 C2H C2H2,acetylene C2H2,vinylidene

CH2CO,ketene O(CH)2O HO(CO)2OH C2H3,vinyl CH3CO,acetyl

C2H4 C2H4O,ethylen-o CH3CHO,ethanal CH3COOH OHCH2COOH

C2H5 C2H6 C2H5OH CH3OCH3 CH3O2CH3
 C2O *C3 C3H3,1-propynl C3H3,2-propynl C3H4,allene
 C3H4,propyne C3H4,cyclo- C3H5,allyl C3H6,propylene C3H6,cyclo-
 C3H6O,propylox C3H6O,acetone C3H6O,propanal C3H7,n-propyl C3H7,i-propyl
 C3H8 C3H8O,1propanol C3H8O,2propanol C3O2 *C4
 C4H2,butadiyne C4H4,1,3-cyclo- C4H6,butadiene C4H6,1butyne C4H6,2butyne

 C4H6,cyclo- C4H8,1-butene C4H8,cis2-buten C4H8,tr2-butene C4H8,isobutene
 C4H8,cyclo- (CH3COOH)2 C4H9,n-butyl C4H9,i-butyl C4H9,s-butyl
 C4H9,t-butyl C4H10,n-butane C4H10,isobutane *C5 C5H6,1,3cyclo-
 C5H8,cyclo- C5H10,1-pentene C5H10,cyclo- C5H11,pentyl C5H11,t-pentyl
 C5H12,n-pentane C5H12,i-pentane CH3C(CH3)2CH3 C6H2 C6H5,phenyl
 C6H5O,phenoxy C6H6 C6H5OH,phenol C6H10,cyclo- C6H12,1-hexene

 C6H12,cyclo- C6H13,n-hexyl C6H14,n-hexane C7H7,benzyl C7H8
 C7H8O,cresol-mx C7H14,1-heptene C7H15,n-heptyl C7H16,n-heptane C7H16,2-
 methylh
 C8H8,styrene C8H10,ethylbenz C8H16,1-octene C8H17,n-octyl C8H18,n-octane
 C8H18,isoctane C9H19,n-nonyl C10H8,naphthale C10H21,n-decyl C12H9,o-bipheny
 C12H10,biphenyl *Fe Fe(CO)5 FeO Fe(OH)2
 *H HBO2 HCO HCCO HO2
 HBOH HCHO,formaldehy HCOOH H2O H2O2
 H2BOH HB(OH)2 H3BO3 H3B3O6 (HCOOH)2
 *O *OH *O2 O3 B(L)
 B2O3(cr) B3O3H3(cr) B4C(L) C(gr) Fe(a)
 Fe(d) Fe(L) Fe(CO)5(L) Fe.947O(cr) Fe.947O(L)
 Fe(OH)2(cr) Fe(OH)3(cr) Fe2O3(cr) Fe3O4(cr) Fe3O4(L)
 HBO2(cr) HBO2(L) H2O(cr) H2O(L) H3BO3(cr)
 H3BO3(L)

Samples with ammonium hydroxide, 3FR

NASA-GLENN CHEMICAL EQUILIBRIUM PROGRAM CEA2, MAY 21, 2004

BY BONNIE MCBRIDE AND SANFORD GORDON

REFS: NASA RP-1311, PART I, 1994 AND NASA RP-1311, PART II, 1996

PRODUCTS WHICH WERE CONSIDERED BUT WHOSE MOLE FRACTIONS
WERE LESS THAN 5.000000E-06 FOR ALL ASSIGNED CONDITIONS

*B BH BH2 BH3 BH4

BH5 BH3NH3 BN BOH BO2

B(OH)2 B2 B2H B2H2 B2H3

B2H3,db B2H4 B2H4,db B2H5 B2H5,db

B2H6 B2O B2(OH)4 B3H7,C2v B3H7,Cs

B3H9 B3N3H6 B4H4 B4H10 B4H12

B5H9 FeO Fe(OH)2 HNO HNO2

HNO3 HO2 HBOH H2O2 H2BOH

HB(OH)2 H3BO3 H3B3O6 *N *NH

NH2 NH3 NH2OH *NO NO2

NO3 N2H2 NH2NO2 N2H4 N2O

N2O3 N2O4 N2O5 N3 N3H

*O *OH *O2 O3 B(L)

BN(L) B2O3(cr) B3O3H3(cr) Fe(a) Fe(c)

Fe(d) Fe.947O(cr) Fe.947O(L) Fe(OH)2(cr) Fe(OH)3(cr)

Fe2O3(cr) Fe3O4(cr) Fe3O4(L) HBO2(cr) HBO2(L)

H2O(cr) H2O(L) H3BO3(cr) H3BO3(L)

Samples with ammonium hydroxide, 6FR

NASA-GLENN CHEMICAL EQUILIBRIUM PROGRAM CEA2, MAY 21, 2004

BY BONNIE MCBRIDE AND SANFORD GORDON

REFS: NASA RP-1311, PART I, 1994 AND NASA RP-1311, PART II, 1996

PRODUCTS WHICH WERE CONSIDERED BUT WHOSE MOLE FRACTIONS
WERE LESS THAN 5.000000E-06 FOR ALL ASSIGNED CONDITIONS

*B BH BH2 BH3 BH4

BH5 BH3NH3 BN BOH BO2

B(OH)2 B2 B2H B2H2 B2H3

B2H3,db B2H4 B2H4,db B2H5 B2H5,db

B2H6 B2O B2(OH)4 B3H7,C2v B3H7,Cs

B3H9 B3N3H6 B4H4 B4H10 B4H12

B5H9 *Fe FeO Fe(OH)2 HNO

HNO2 HNO3 HO2 HBOH H2O

H2O2 H2BOH HB(OH)2 H3BO3 H3B3O6

*N *NH NH2 NH3 NH2OH

*NO NO2 NO3 *N2 N2H2

NH2NO2 N2H4 N2O N2O3 N2O4

N2O5 N3 N3H *O *OH

*O2 O3 B(L) BN(L) B2O3(cr)

B3O3H3(cr) Fe(a) Fe(c) Fe(d) Fe.947O(cr)

Fe.947O(L) Fe(OH)2(cr) Fe(OH)3(cr) Fe2O3(cr) Fe3O4(cr)
Fe3O4(L) HBO2(cr) HBO2(L) H2O(cr) H2O(L)
H3BO3(cr) H3BO3(L)

Samples with ammonium hydroxide, 9FR

NASA-GLENN CHEMICAL EQUILIBRIUM PROGRAM CEA2, MAY 21, 2004
BY BONNIE MCBRIDE AND SANFORD GORDON
REFS: NASA RP-1311, PART I, 1994 AND NASA RP-1311, PART II, 1996

PRODUCTS WHICH WERE CONSIDERED BUT WHOSE MOLE FRACTIONS
WERE LESS THAN 5.000000E-06 FOR ALL ASSIGNED CONDITIONS

*B BH BH2 BH3 BH4

BH5 BH3NH3 BN *BO BOH

BO2 B(OH)2 B2 B2H B2H2

B2H3 B2H3,db B2H4 B2H4,db B2H5

B2H5,db B2H6 B2O B2O3 B2(OH)4

B3H7,C2v B3H7,Cs B3H9 B3N3H6 B4H4

B4H10 B4H12 B5H9 *Fe FeO

Fe(OH)2 *H HNO HNO2 HNO3

HO2 HBOH H2O H2O2 H2BOH

HB(OH)2 H3BO3 H3B3O6 *N *NH

NH2 NH3 NH2OH *NO NO2

NO3 *N2 N2H2 NH2NO2 N2H4

N2O N2O3 N2O4 N2O5 N3

N3H *O *OH *O2 O3

B(L) BN(L) B2O3(cr) B3O3H3(cr) Fe(a)

Fe(d) Fe(L) Fe.947O(cr) Fe.947O(L) Fe(OH)2(cr)

Fe(OH)3(cr) Fe2O3(cr) Fe3O4(cr) Fe3O4(L) HBO2(cr)

HBO2(L) H2O(cr) H2O(L) H3BO3(cr) H3BO3(L)

B. NITROGEN GAS ADSORPTION ANALYSIS

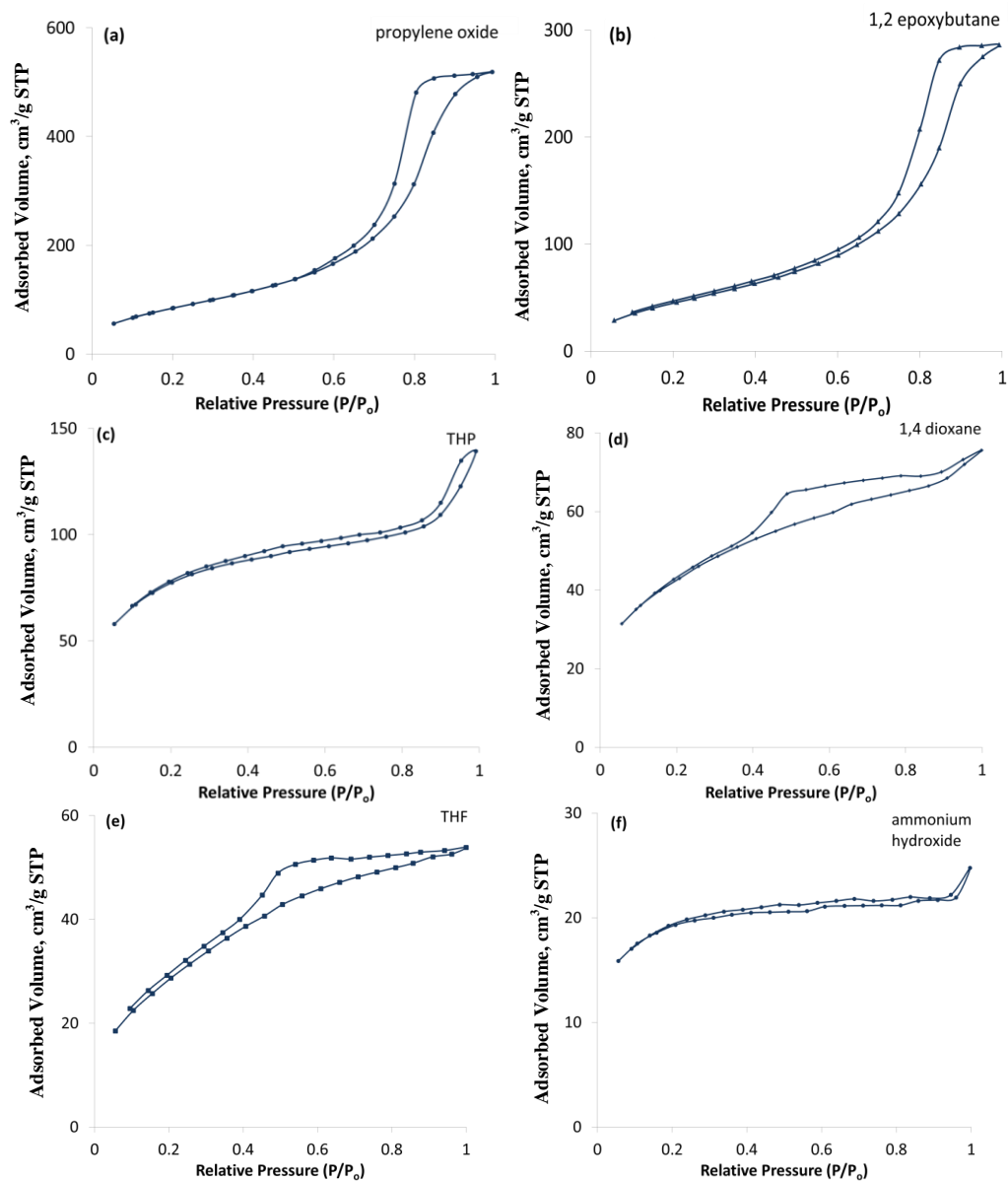


Figure B.1. Nitrogen adsorption/desorption isotherms of Fe_2O_3 xerogels synthesized by using (a) propylene oxide (b) 1,2 epoxybutane (c) THP (d) 1,4 dioxane (e) THF (f) ammonium hydroxide

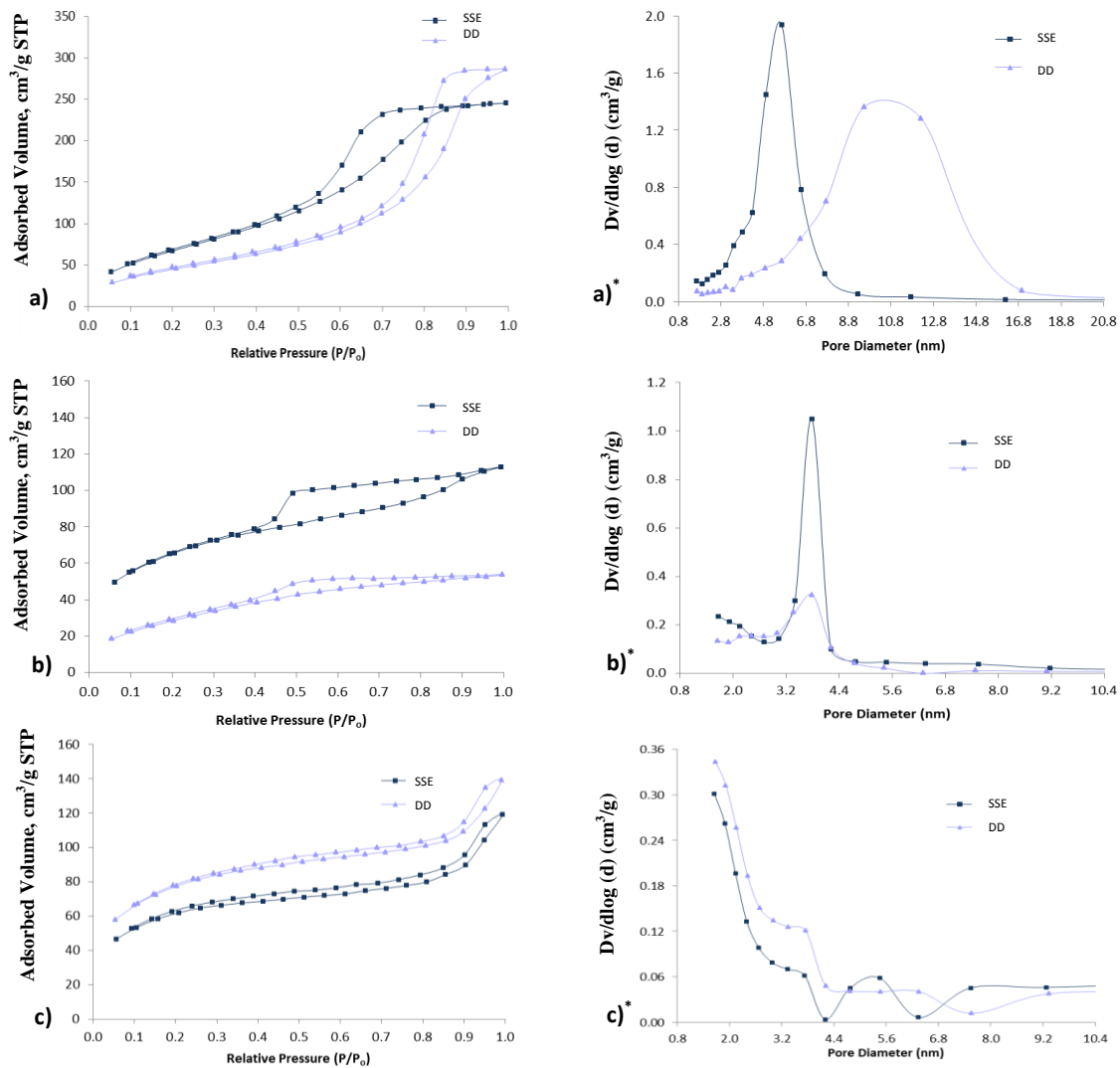


Figure B.2. The Nitrogen adsorption/desorption isotherms of Direct Dried (DD) and Sequential Solvent Dried (SSE) Fe_2O_3 samples synthesized with a) 1,2 epoxybutane b) THF c) THP & The pore size distributions of Fe_2O_3 samples synthesized with a)* epoxybutane b)* THF c)* THP

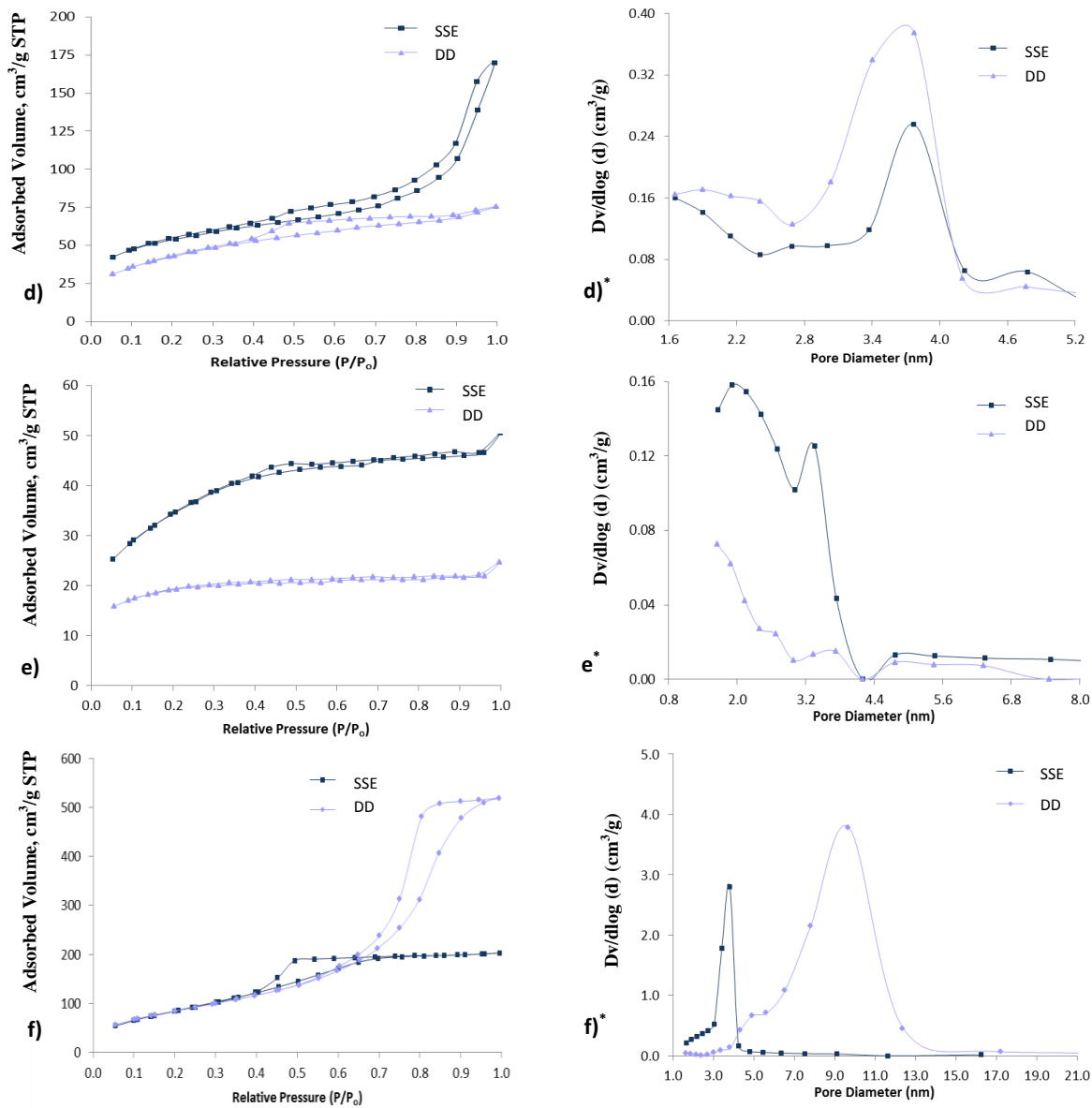


Figure B.2. cont. The Nitrogen adsorption/desorption isotherms of Direct Dried (DD) and Sequential Solvent Dried (SSE) Fe₂O₃ samples synthesized with d) 1,4 dioxane e) ammonium hydroxide f) propylene oxide & The pore size distributions of Fe₂O₃ samples synthesized with d)* 1,4 dioxane e)* ammonium hydroxide f)* propylene oxide

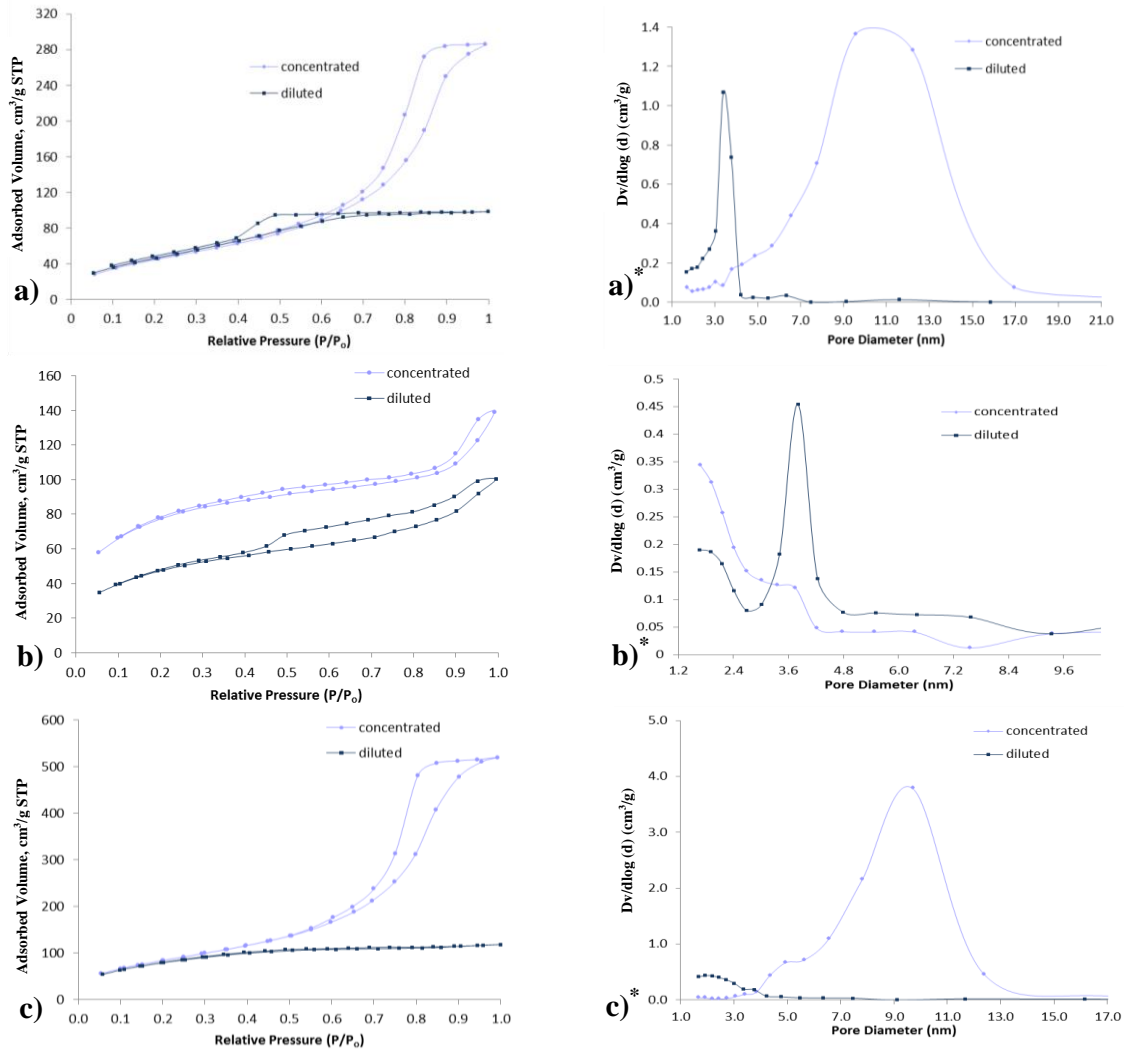


Figure B.3. Nitrogen adsorption/desorption isotherms of DD Fe₂O₃ samples synthesized from diluted and concentrated precursor solution with a) epoxybutane b) THP c) propylene oxide & The pore size distributions of DD Fe₂O₃ samples synthesized from diluted and concentrated precursor solution with a)* epoxybutane b)* THP c)* propylene oxide

C. THERMAL ANALYSIS

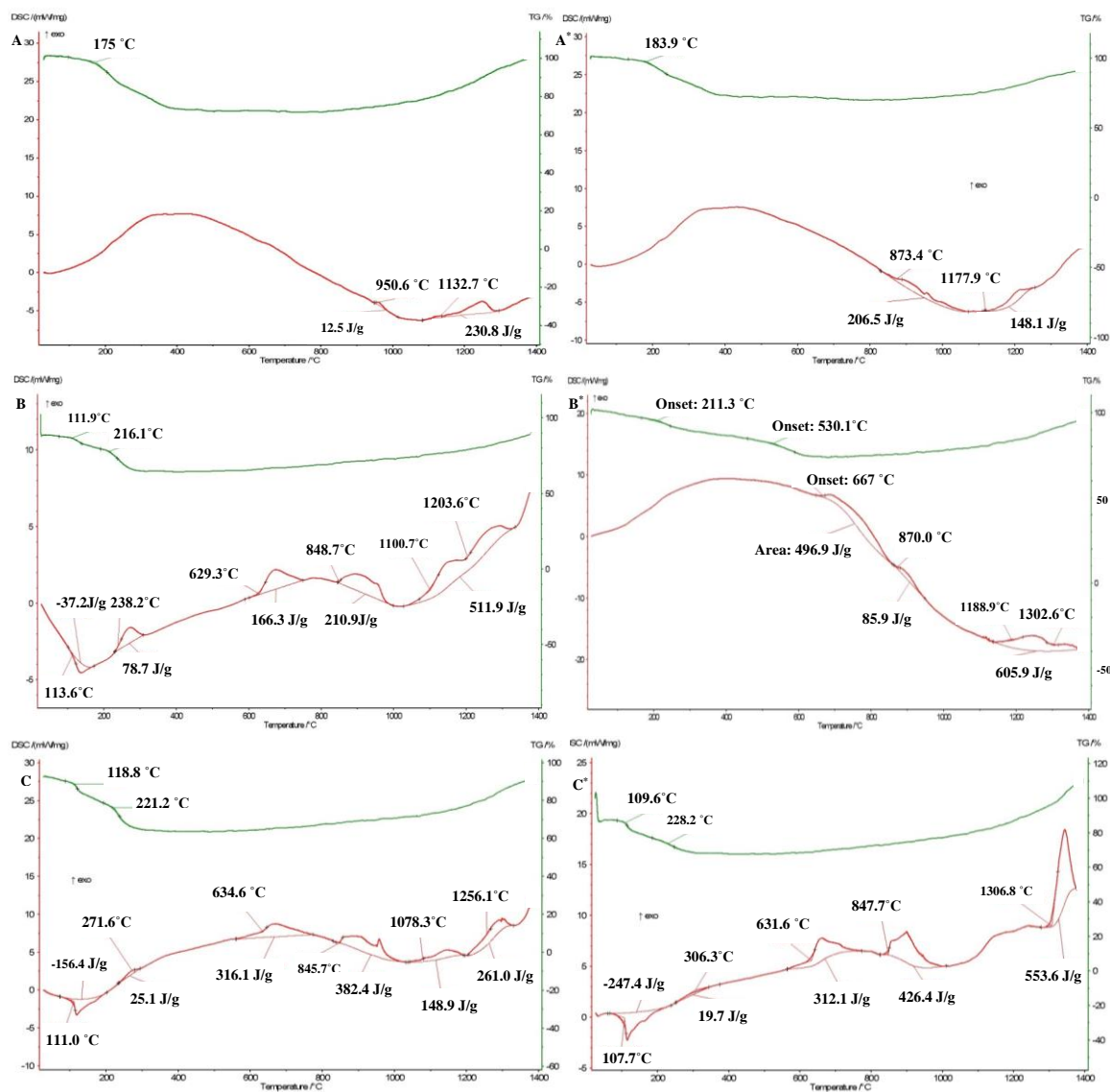


Figure C.1. DSC and TG plots as a function of temperature for DD & SSE* 3FR B/Fe₂O₃ samples synthesized with a) 1,2 epoxybutane b) THF c) THP

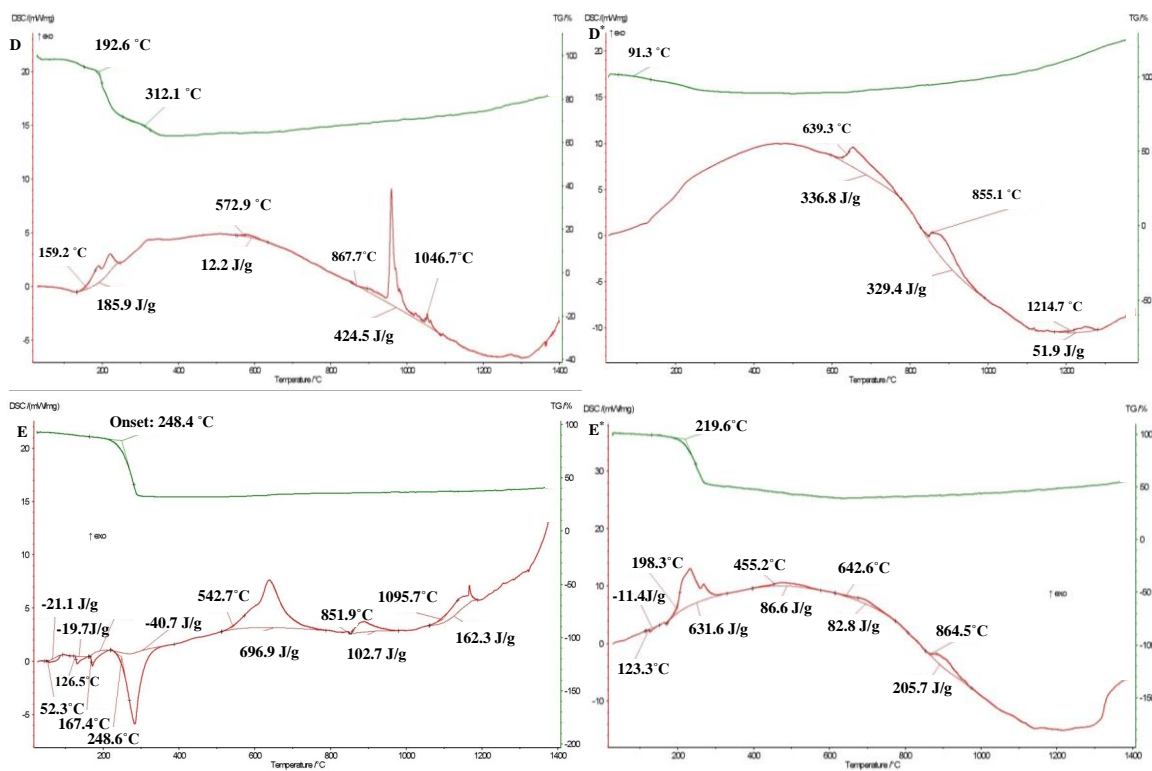


Figure C.1. cont. DSC and TG plots as a function of temperature for DD & SSE* 3FR B/Fe₂O₃ samples synthesized with d) 1,4 dioxane e) ammonium hydroxide

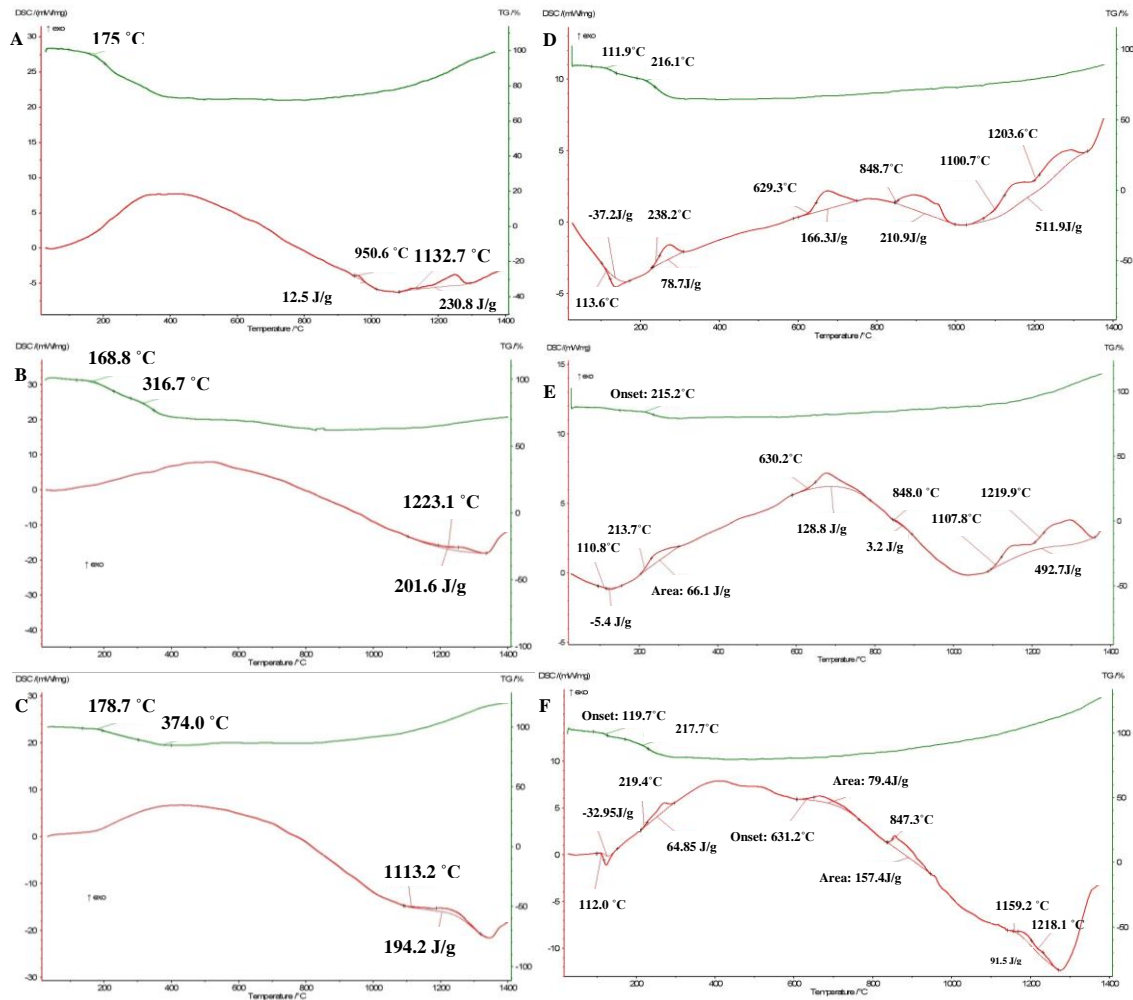


Figure C.2. DSC and TG plots as a function of temperature for DD B/Fe₂O₃ samples synthesized with 1,2 epoxybutane a) 3FR b) 6FR c) 9FR and synthesized with THF d) 3FR e) 6FR f) 9FR

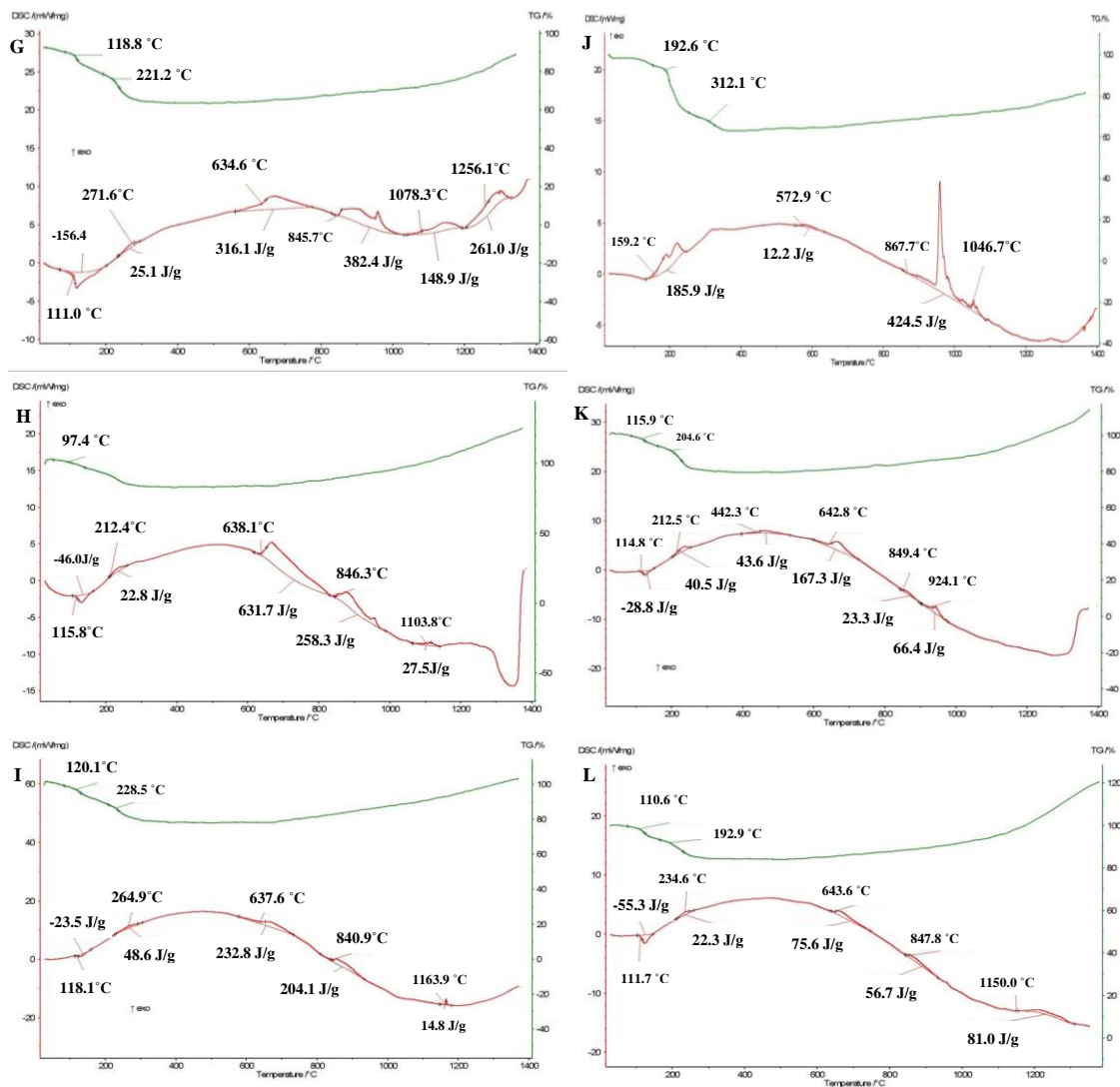


Figure C.2. cont. DSC and TG plots as a function of temperature for DD B/Fe₂O₃ samples synthesized with THP g) 3FR h) 6FR i) 9FR and synthesized with 1,4 dioxane j) 3FR k) 6FR l) 9FR

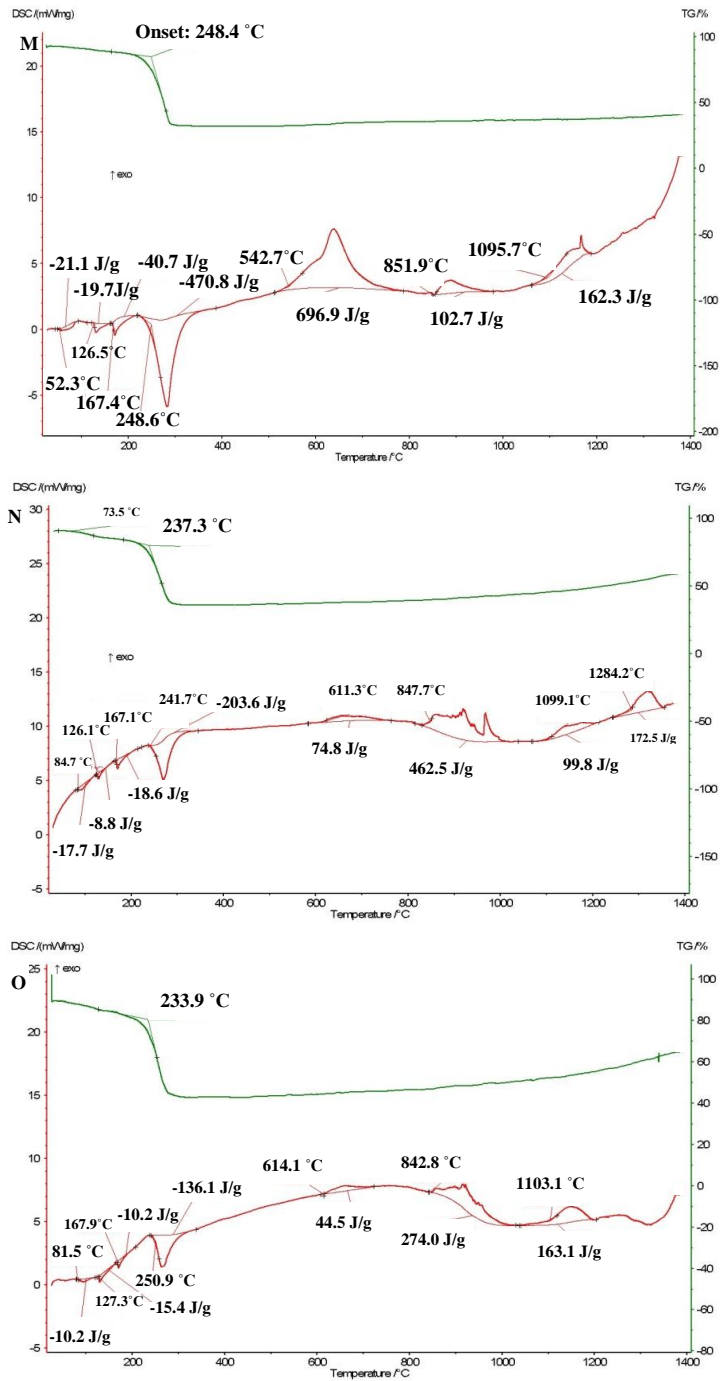


Figure C.2. cont. DSC and TG plots as a function of temperature for DD B/Fe₂O₃ samples synthesized with ammonium hydroxide m)3FR n)6FR o)9FR

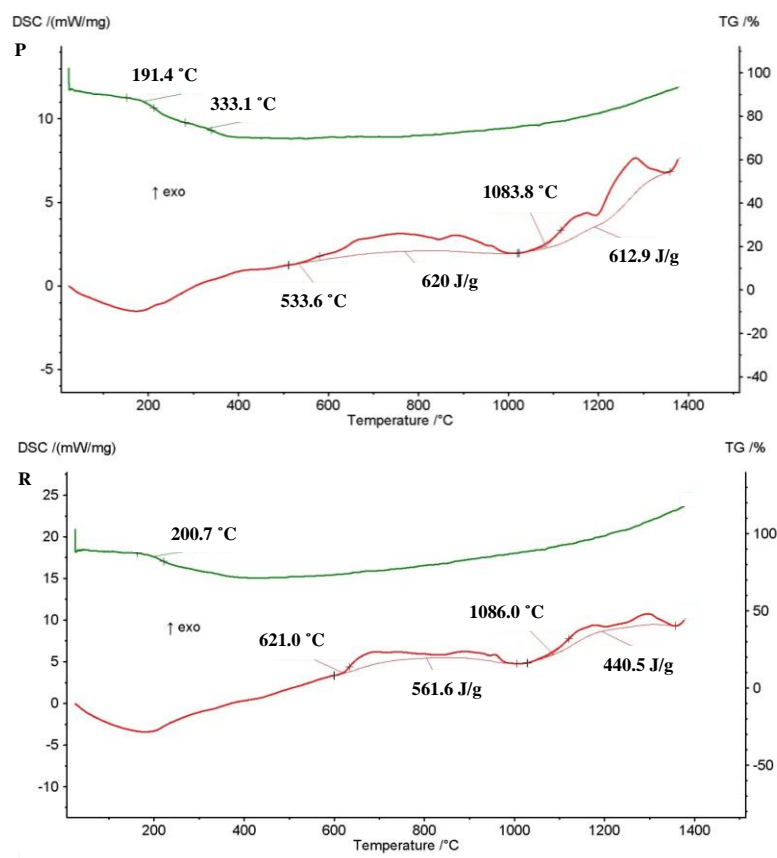


Figure C.2. cont. DSC and TG plots as a function of temperature for DD B/Fe₂O₃ samples synthesized with propylene oxide p) 6FR r) 9FR

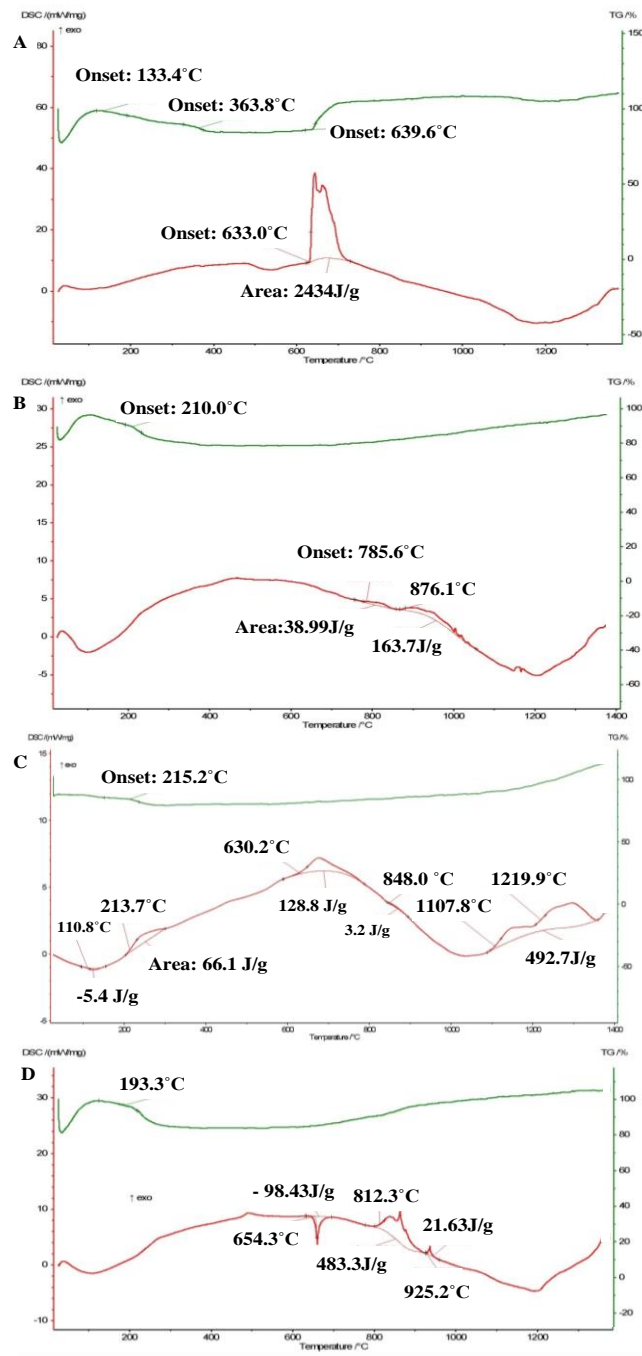


Figure C.3. DSC and TG plots as a function of temperature at an equivalence ratio of 6 for A. Mg/Fe₂O₃ samples B. 20% Mg-B/Fe₂O₃ samples C. B/Fe₂O₃ samples D. Al/Fe₂O₃ samples prepared by THF

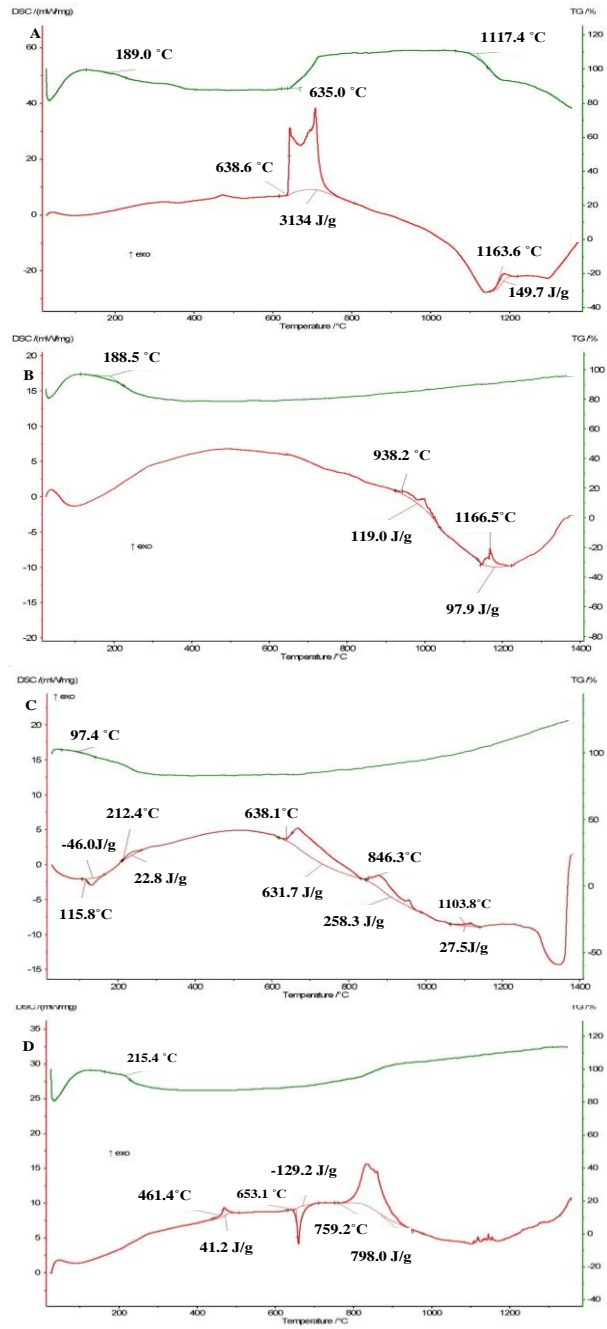


Figure C.4. DSC and TG plots as a function of temperature at an equivalence ratio of 6 for A. Mg/Fe₂O₃ samples B. 20%Mg-B/Fe₂O₃ samples C. B/Fe₂O₃ samples D. Al/Fe₂O₃ samples prepared by THP

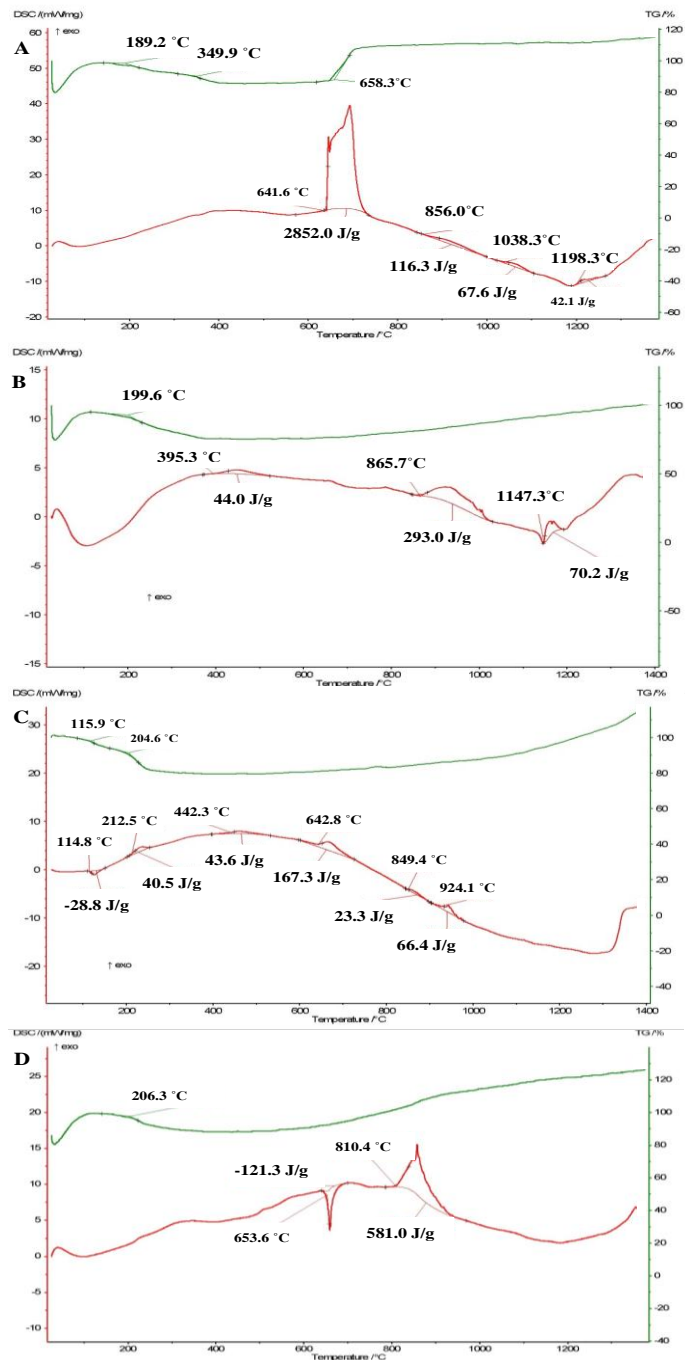


Figure C.5. DSC and TG plots as a function of temperature at an equivalence ratio of 6 for A. Mg/Fe₂O₃ samples B. 20% Mg-B/Fe₂O₃ samples C. B/Fe₂O₃ samples D. Al/Fe₂O₃ samples prepared by 1,4 dioxane

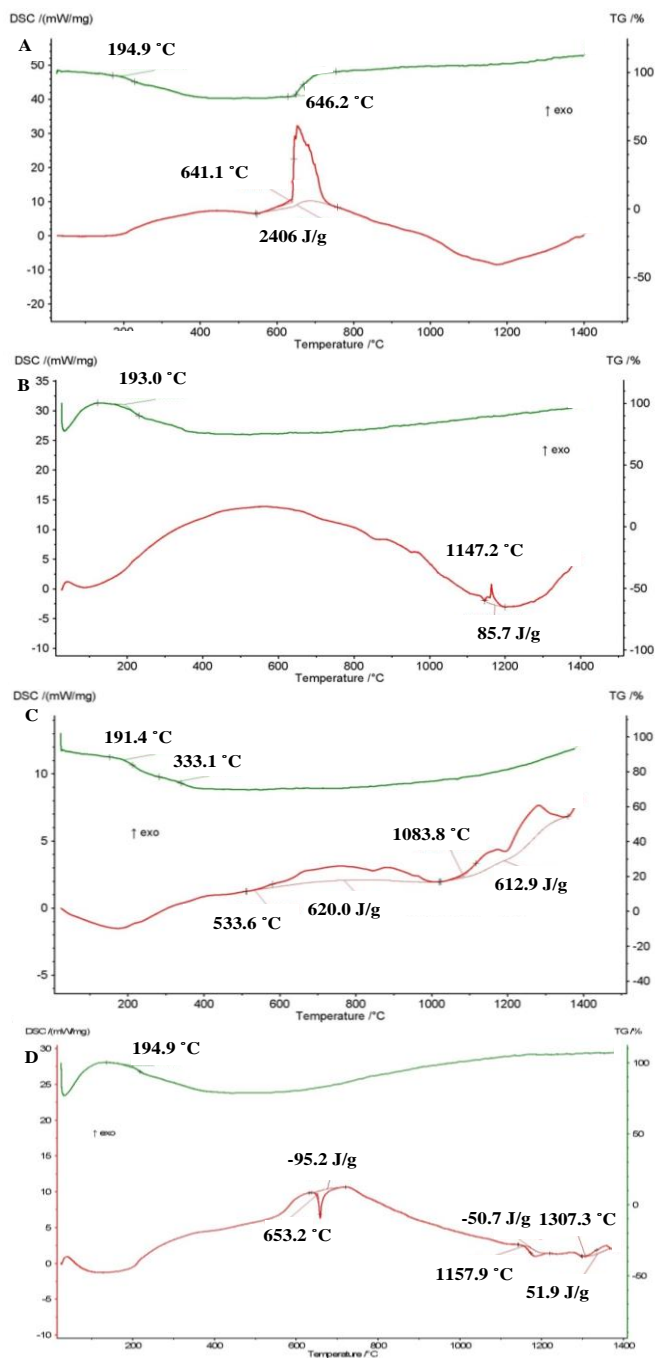


Figure C.6. DSC and TG plots as a function of temperature at an equivalence ratio of 6 for A. Mg/Fe₂O₃ samples B. 20%Mg-B/Fe₂O₃ samples C. B/Fe₂O₃ samples D. Al/Fe₂O₃ samples prepared by propylene oxide

D. EDS ANALYSIS

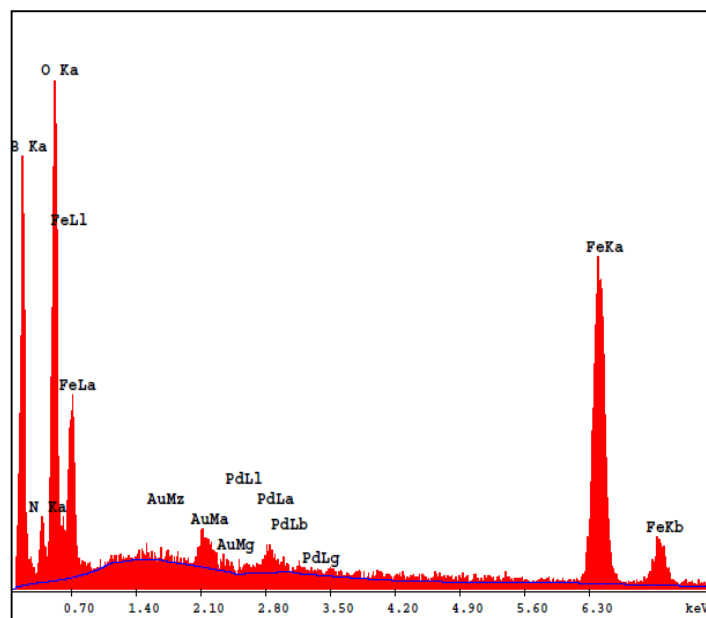


Figure D.1. EDS spectrum of 9 FR B/Fe₂O₃ synthesized with ammonium hydroxide

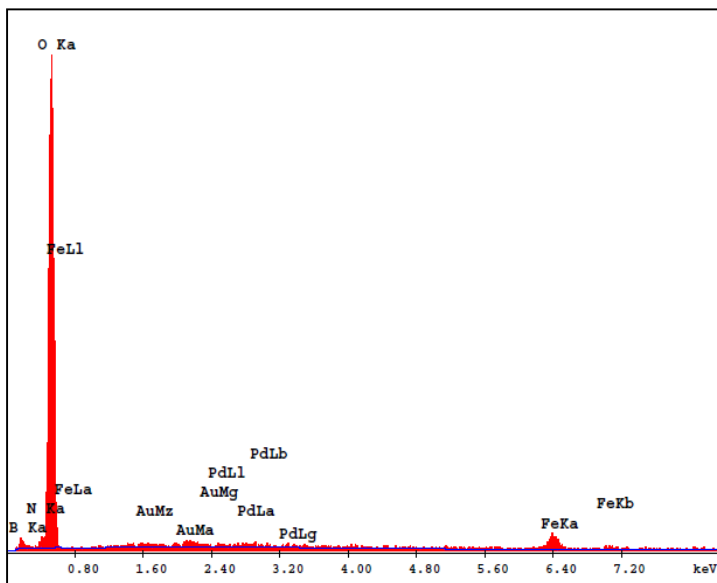


Figure D.2. EDS spectrum of combustion products of 9 FR B/Fe₂O₃ synthesized with ammonium hydroxide

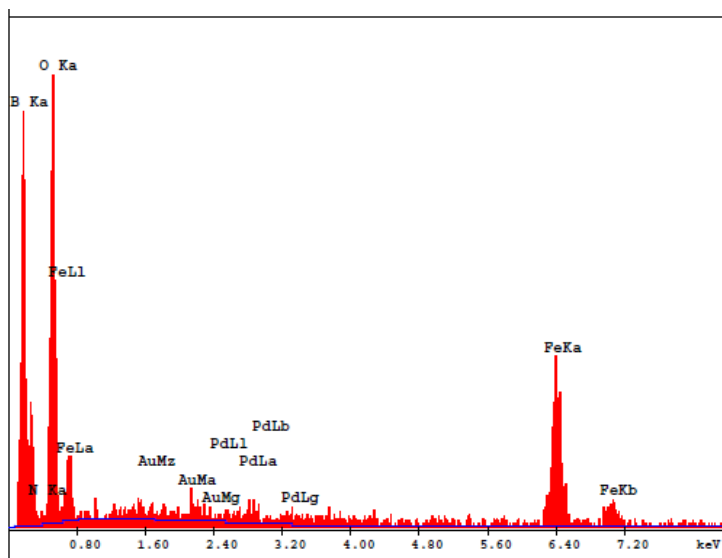


Figure D.3. EDS spectrum of 9 FR B/Fe₂O₃ synthesized with propylene oxide

E. KINETIC STUDY

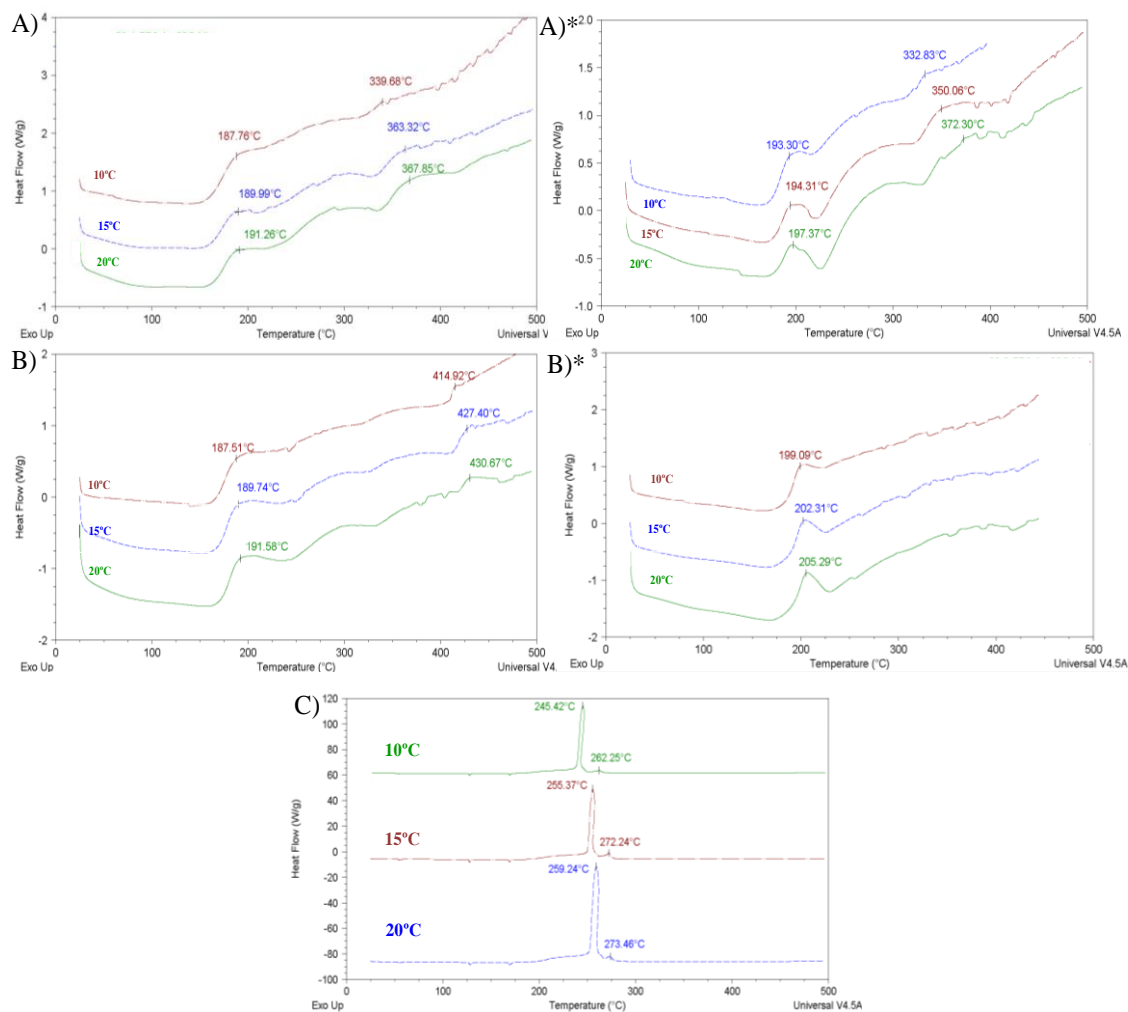


Figure E1. DSC Thermograms of SSE 3FR B/Fe₂O₃ prepared with A) propylene oxide from diluted solution of precursor A)* propylene oxide from concentrated solution of precursor B) 1,2 epoxybutane from diluted solution of precursor B)* 1,2 epoxybutane from concentrated solution of precursor C) ammonium hydroxide

CURRICULUM VITAE

PERSONAL INFORMATION

Surname, Name: DİNÇER YILMAZ, Nil Ezgi

Nationality: Turkish (TC)

Date and Place of Birth: 04-09-1986, Artvin

Marital Status: Married

Phone: + 90 312 860 4454

email: e183488@metu.edu.tr / edincer@roketan.com.tr

EDUCATION

| Degree | Institution | Year of Graduation |
|--------|---|--------------------|
| MS | KOÇ UNIVERSITY, Chemical and Biological Engineering | 2010 |
| BS | HACETTEPE UNIVERSITY, Chemical Engineering | 2008 |

WORK EXPERIENCE

| Year | Place | Enrollment |
|--------------|---|----------------------------|
| 2016-Present | ROKETSAN | Design Leader |
| 2014-2016 | ROKETSAN | Senior Engineer |
| 2010-2014 | ROKETSAN | Design Engineer |
| 2008-2010 | KOÇ UNIVERSITY, Chemical and Biological Engineering | Research Assistant |
| 2006 August | TUBITAK-MAM | Intern Engineering Student |
| 2006 July | TAI | Intern Engineering Student |

PUBLICATIONS

Journal Articles

1. Koç S., Ulaş A. and Dinçer Yılmaz N.E., “Characterization of BPN Pyrotechnic Composition Containing Micro- and Nanometer-Sized Boron Particles”, *Propellants, Explosives and Pyrotechnics*, Volume 40, Issue 5, 735-742, 2015
2. Dinçer N.E. and Erkey C., “Measurement and thermodynamic modeling of partition coefficients in N,N-Dimethylacetamide – water – carbon dioxide system” *J. Supercrit. Fluids.*, Volume 55, 690-695, 2010.

Conference and Symposium Proceedings

1. Dinçer Yılmaz N.E., Karakaş G. “Effect of Proton Scavengers on the Textural Properties and Performance of Fe₂O₃ Xerogels for Boron Containing Pyrotechnics”, 53rd AIAA Propulsion and Energy Forum and Exposition, 2017.
2. Koç S., Dinçer Yılmaz N.E., Eroğul F. and Ulaş A., “Comparison of BPN Igniter Compositions Containing Micron- and Nano-Sized Boron Particles”, 51th AIAA Propulsion and Energy Forum and Exposition, Orlando, Florida, USA, July 2015.
3. Dinçer N.E. “Yeni Nesil Piroteknik Malzemeler: Nanopiroteknikler”, II. Enerjik Malzemeler Çalıştayı (2nd Energetic Materials Symposium), Ankara, Turkey, November 2013.
4. Dinçer N.E. and Erkey C. “Phase Behaviour Measurements and Thermodynamic Modelling of N,N-Dimethylacetamide - Carbon Dioxide - Water System”, 9th Conference on Supercritical Fluids and Their Applications, Sorrento (Napoli), Italy, September 2010.

5. Dinçer N.E. and Erkey C. “Polar Organiklerin Süperkritik Karbondioksit ile Su Arasındaki Dağılım Katsayıları ve Termodinamik Modellemeleri”, 9. Ulusal Kimya Mühendisliği Kongresi (9th National Chemical Engineering Conference), Ankara, Turkey, June 2010.